Defining the genetic and molecular basis of inherited eye diseases present in Pakistan

Submitted by Ilaria D'Atri to the University of Exeter as a thesis for the degree of Doctor of Philosophy in Medical Studies, January 2020.

I certify that all material in this thesis which is not my own work has been identified and that no material has previously been submitted and approved for the award of a degree by this or any other University.

……

ACKNOWLEDGMENTS

I would like to acknowledge my supervisors Prof. Andrew Crosby, Dr. Emma Baple, and a special thanks goes to Dr. John Chilton for his invaluable support and supervision thought out my degree.

I also have to acknowledge Dr. Asami Oguro-Ando and Dr. Rosie Bamford for their technical support and discussions.

I would like to thank my family, in particular my parents, who always supported me during these years.

These years wouldn’t have been the same without the support of colleagues and friends. In particular, Dr. Barry Chioza who patiently answered all my questions, Dr. Serene Lin who constantly supported me during these three years with a flux of donuts and cakes while listening to all my rants about failed experiments. I also need to acknowledge my imaginary friend Isabella Provenzale for her friendship and advise.

Finally, a thanks goes to all the people at the RILD who made these years the most memorable.

ABSTRACT

Human Mendelian genetics aims to define the link between the phenotypical manifestations of a disease, and the identity of the gene that when mutated causes disease. Rare ocular genetic disorders are typically difficult to manage due to an incomplete understanding of their genetic causes and clinical outcomes. However, in the last few years rapid advancements in high throughput genomic sequencing techniques has paved the way for the discovery of new genes causing inherited diseases, and provided new insights into the breadth of phenotypical manifestations associated with pathogenic variants in genes already known to be linked with ocular disease. The discovery of new disease-associated genes provides important diagnostic benefits for patients, and also aids scientific understanding of how the biological processes within cells work. In turn, this drives the development of new treatments and therapies.

Chapter three documents a comprehensive series of genetic studies leading to the discovery of a novel founder mutation in the *CLCC1* gene, associated with an autosomal recessive form of retinitis pigmentosa in families from Pakistan, as well as the characterisation of *CLCC1* in zebrafish and mouse retina. Moreover, the chapter details extensive molecular studies to discover the functional role of CLCC1 in the cells. This includes the localisation of CLCC1 within the endoplasmic reticulum, the identification of CLCC1 binding partners, and the exploration of a possible role of CLCC1 in endoplasmic reticulum stress and calcium signalling. This section also describes the generation of a *CLCC1* knockout cell line using CRISPR-Cas9, to enable future more extensive studies of CLCC1 molecular function.

Chapter four of this thesis entails a comprehensive investigation by way of genetic studies, and literature review, of novel and known genetic variants associated with a wide range of inherited retinal dystrophies in families from Pakistani. This data provides the most comprehensive repository of information available for designing molecular diagnostic testing approaches in the region.

TABLE OF CONTENTS

LIST OF FIGURES

CHAPTER 4

LIST OF TABLES

LIST OF ACCOMPANYING MATERIAL

This thesis is accompanied by a CD containing Appendix E (Media 1 to 6).

PUBLICATIONS RELATING TO THE WORK IN THIS THESIS

Mutation in the intracellular chloride channel CLCC1 associated with autosomal recessive retinitis pigmentosa (2018) *Li L, *Jiao X, ***D'Atri I**, Ono F, Nelson R, Chan CC, Nakaya N, Ma Z, Ma Y, Cai X, Zhang L, Lin S, Hameed A, Chioza BA, Hardy H, Arno G, Hull S, Khan MI, Fasham J, Harlalka GV, Michaelides M, Moore AT, Coban Akdemir ZH, Jhangiani S, Lupski JR, Cremers FPM, Qamar R, Salman A, Chilton J, Self J, Ayyagari R, Kabir F, Naeem MA, Ali M, Akram J, Sieving PA, Riazuddin S, Baple EL, Riazuddin SA, Crosby AH, Hejtmancik JF. *PLoS Genetics* 14(8):e1007504 DOI:10.1371/journal.pgen.1007504 * joint first author

Genetic spectrum of inherited retinal dystrophies in Pakistan (2020) D'Atri I, Lin S, Shakil M, Saleha S, Khan J, Akbar A, Arshad MW, Jiao X, Riazuddin SA, Ma Y, Chornobai M, Vendra VPR, Ma Z, Wang X, Hu H, Li J, Shoshany N, Norman CS, O'Gorman L, Ennis S, Hassan MJ,Tahir R, Nadeem R, Naeem MA, Shahzad M, Ali MH, Ullah MI, Harlalka GV, Kiran U, Mahmood S, Gul A, Shabbir MI, Riazuddin S, Self JE, Hejtmancik JF, Crosby AH, Baple EL. *currently under review with Human Mutation*

ABBREVIATIONS

17-N-Allylamino-17-demethoxygeldanamycin	17-AAG
2-DG	2-Deoxy-D-Glucose
aa	Amino acid
ACHM	Achromatopsia
ALMS	Alström syndrome
AMD	Age-related macular degeneration
ANOVA	Analysis of variance
APS	Ammonium persulphate
ATP	Adenosine triphosphate
BAM	Binary SAM format
BBA	Binding buffer
BBS	Bardet-Biedl syndrome
BCA	Bicinchoninic acid
BCS	Bovine calf serum
BMP	Bone morphogenic protein
bp	Base pair
BSA	Bovine serum albumin
BWA	Burrows-Wheeler aligner
bZIP	Basic leucine zipper
°C	°Centigrade
C-	Carboxy-terminus
cc	Coiled coil
Ca^{2+}	Calcium ion

CD	Cone dystrophy
cDNA	Complementary deoxyribonucleic acid
CHO	Chinese hamster ovary cells
CO_2	Carbon dioxide
Co-IP	Co-immunoprecipitation
CLB	Cell lysis buffer
CLCC1	Chloride channel CLCC-like 1
CLZ	C-terminal leucine zipper domain of cyclic nucleotide-gated channels.
CMV	Cytomegalovirus
CNG	Cyclic nucleotide channel
cNMP_binding	Cyclic nucleotide-binding domain
CRAC	Ca^{2+} release-activated Ca^{2+} channel
CRALBP	Cellular retinaldehyde binding protein
CRBP	Cellular retinoid binding protein
CRD	Cone rod dystrophy
CSNB	Congenital stationary night blindness
CWS	Column wash solution
D-V	Dorso-ventral
DAPI	4'6-diamidino-2-phenylindole dihydrochloride
dd.H_20	Double distilled water
DHA	Docosahexaenoic acid
DIDS	4,49-diisothiocyanatostilbene-2,29-disulfonate
DM	Disease-causing mutation
DM?	Disease-causing mutation?
DMEM	Dulbecco’s modified eagle medium

DMSO	Dimethyl sulfoxide
DNA	Deoxyribonucleic acid
dNTP	Deoxyribonucleotide triphosphate
DTT	Dithiothreitol
E	Embryonic day
EDTA	Ethylene diamine tetraacetic acid
EEM	Ectodermal dysplasia, ectrodactyly, and macular dystrophy
EGFP	Enhanced green fluorescent protein
eIF2α	Eukaryotic translation initiation factor-2α
EMC	ER membrane protein complex
EOIRD	Early-onset inherited retinal dystrophy
EORP	Early-onset retinitis pigmentosa
ER	Endoplasmic reticulum
ERAD	Endoplasmic reticulum-associated degradation
ERG	Electroretinogram
EtOH	Ethanol
ExAC	Exome Aggregation Consortium
FA	Fundus albipunctatus
FACS	Fluorescence-activated cell sorting
FDR	False discovery rate
g	grams
GAF	cGMP-specific phosphodiesterases, adenylyl cyclases and FhlA
GC	Guanine cytosine
GCAP	Guanylyl cyclase activating protein

GCL	Ganglion cell layer
GFP	Green fluorescent protein
GO	Gene ontology
gnomAD	Genome Aggregation Database
GPCR	G-protein coupled receptor
GRK1	Rhodopsin kinase
gRNA	guide RNA
HBSS	Hank's balanced salt solution
HCl	Hydrochloric acid
HEK	Human embryonic kidney
HEPES	4-(2-hydroxyethyl)piperazine-1-ethanesulphonic acid
hESC	Human embryonic stem cells
HH	Hamburger Hamilton
HI	Heat-inactivated
HiFBS	Heat inactivated foetal bovine serum
hiPSC	Human induced pluripotent stem cells
HRP	Horseradish peroxidase
HTA	Human tissue authority
ICC	Immunocytochemistry
ID	Identifier
Ion_tran	Ion channel transmembrane domain
INL	Inner nuclear layer
IP	Immunoprecipitated
IP_3R	Inositol-1,4,5-triphosphate receptor
IPL	Inner plexiform layer

IRBP	Inter photoreceptor retinoid binding protein
IRD	Inherited retinal dystrophy
IRE1	Inositol requiring enzyme 1
JBTS	Joubert syndrome
kb	Kilobases
kDa	Kilodalton
KEGG	Kyoto Encyclopedia of Genes and Genomes
KO	Knockout
KPK	Khyber Pakhtunkhwa
KSS	Kearns-Sayre syndrome
LB	Luria Bertani
LC	Lamina cribrosa
LCA	Leber congenital amaurosis
LC-MS/MS	Liquid chromatography tandem-mass spectrometry
LRAT	Lecithin retinol acyltransferase
M	Molar
mA	Milliamps
MAM	Mitochondria associated membrane
MAF	Minor allele frequency
MCLC	Mid-1- related chloride channel
MELAS	Mitochondrial encephalomyopathy, lactic acidosis, stroke-like episodes
MeOH	Methanol
mg	Milligrams
Mg^{2+}	Magnesium ion

$MgCl_2$	Magnesium chloride
min	Minutes
MKS	Meckel-Gruber syndrome
ml	Millilitre
mm	Millimeter
mM	Millimolar
MM-MO	Mismatch morpholino
MO	Morpholino
MORM	Mental retardation, truncal obesity, retinal dystrophy, and micropenis
MTT	(3-(4,5-dimethylthiazol-2-yl)-2,5-diphenyltetrazolium bromide
MW	Molecular weight
nm	Nanometer
N-	Amino-terminus
NA	Not available
NaCl	Sodium chloride
NaOH	Sodium hydroxide
NARP	Neuropathy, ataxia, retinitis pigmentosa
ng	Nanograms
NGS	Next-generation sequencing
OCT	Optical coherence tomography
ON	Optic nerve
ONL	Outer nuclear layer
OPL	Outer plexiform layer
OV	Optic vesicle

PBS	Phosphate-buffered saline
PCR	Polymerase chain reaction
P-D	Proximal-distal
PDE	Cyclic nucleotide (cGMP) phosphodiesterase
PDL	Poly-D-lysine
PERK	Protein kinase RNA-activated (PKR)-like ER kinase
PFA	Paraformaldehyde
PG	Paraformaldehyde-glutaraldehyde
pH	Potential of hydrogen
PM	Plasma membrane
PMSF	phenylmethylsulfonyl fluoride
PVDF	polyvinylidene difluoride
QC	Quality control
RDH5	11-cis retinol dehydrogenase
RGC	Retinal ganglion cell
RNase	Ribonuclease
ROH	Runs of homozygosity
RP	Retinitis pigmentosa
RPE	Retinal pigment epithelium
rpm	Revolutions per minute
RT	Room temperature
RyR	Ryanodine receptor
s	Seconds
SAM	Sequence alignment map
SAP	Shrimp alkaline phosphatase

SD	Standard deviation
SDS	Sodium dodecyl sulphate
SDS-PAGE	Sodium dodecyl sulphate polyacrylamide gel electrophoresis
SE	Surface ectoderm
SEM	Standard error of the mean
SERCA	Sarcoplasmic–endoplasmic reticulum Ca2+ - ATPase
SLS	Senior-Løken syndrome
SNP	Single nucleotide polymorphism
SOC	Super optimal broth with catabolite repression
SOCE	Store-operated Ca2+ entry
SRP	Signal recognition particle
STIM1	Stromal interaction molecule 1
sXBP1	Spliced X-box binding protein 1
TAD	Transcriptional activation domain
TAE	Tris[hydroxymethyl]-amino-methane-acetate-EDTA
TALEN	Transcription activator–like effector nuclease
TBS	Tris[hydroxymethyl]-amino-methane-buffered saline
TBS-T	Tris[hydroxymethyl]-amino-methane-buffered saline + Tween-20
TCA	Tricarboxylic acid
TEMED	N,N,N',N'-tetramethylethane-1,2-diamine

TM	Transmembrane domains
Tris	Tris[hydroxymethyl]-amino-methane
U	Units
UK	United Kingdom
UPR	Unfolded protein response
USA	United States of America
USH	Usher syndrome
usXBP1	Unspliced X-box binding protein 1
V	Volts
VCF	Variant call file
v/v	Volume per volume
WB	Western blotting
WES	Whole exome sequencing
WGS	Whole genome sequencing
WT	Wild type
w/v	Weight per volume
YFP	Yellow florescent protein
µg	Microgram
µL	Microlitre
µm	Micrometer
µM	Micromolar

CHAPTER 1

INTRODUCTION

CHAPTER 1 INTRODUCTION

1.1 Developmental origins of the eye

The organogenesis of the eye is a multi-step process occurring in the ventral forebrain during the final stages of neuronal tube formation. After gastrulation, the eye primordium is specified in the medial anterior neural plate. In mice, the first structure indicating eye organogenesis is visible at embryonic (E) day 8.0 and is named optic sulcus, while in humans the optic primordia appear at Carnegie Stage 10. Eye field specification happens though the expression and regulation of eye field transcription factors *Rx1/Rax, Pax6, Six3, Lhx2, tll/Tlx, Optx2/Six6* and *ET/Tbx* (Fig. 1.1) [2]. Mutation of any of these genes and many of their molecular pathway partners may be associated with developmental defects of the eye [3, 4].

Eye organogenesis begins with the evagination of the neuroepithelium, at E8.5-9.0 of mouse development, forming bilateral optic vesicles. The optic vesicle is patterned in the dorso-ventral (D-V) and proximal-distal (P-D) axes, and regionalised in neural retina and retinal pigmented epithelium (RPE). Each compartment of the optic vesicle expresses specific sets of transcription factors important for the development of different types of cell. The D-V axis is established by the hedgehog-family gene *Shh*, which drives expression of the ventralising homeodomain transcription factors *Vax1* and *Vax2*. *Shh* also drives the P-D patterning, regulating the localisation of *Pax2* and *Pax6* expression, which in turn maintains the P-D axis of the optic vesicle/optic cup boundary. The dorsal identity of the optic vesicle requires the induction of *Tbx5* by bone morphogenetic protein 4 (*BMP4*) [2, 5].

The earliest gene expressed in the eye field, upstream to the above genetic interactions, is LIM homeobox transcription factor *Lhx2;* required for expression of *Mitf* and for retinal determinants in the optic vesicle [1]. Subsequent to this at E10.5 the optic vesicles invaginate giving rise to the optic cup. This invagination is induced by the contact between the distal portion of the optic vesicles with the overlaying ectoderm. From the optic cup two types of tissues generate different classes of retinal cell. The presumptive neural retina develops from the distal optic vesicle and becomes the inner layer of the optic cup; whilst the presumptive RPE derives from the proximal optic vesicle, forming the outer layer of the optic cup. An additional invagination occurs in the ventral optic vesicle, generating the optic fissure [5-8]. The presumptive RPE is specified by the TGFβ signalling from the extraocular mesenchyme, in particular, TGFβ induces the expression of bHLH transcription factor, *Mitf,* and *Otx2* in the distal optic vesicle. As the optic vesicle approaches the surface ectoderm, *Vsx2* expression initiated from FGFs signals, coming from the ectoderm surface which specifies the D-V patterning of the optic vesicle as neural retina. *Vsx2* represses *Mitf* allowing the distal optic vesicle to develop into neural retina [2, 9, 10]. Retinoic acid (via its receptors) and BMP signalling are involved in the maintenance of RPE in the ventral optic cup [6]. Wnt/β-catenin pathway also controls differentiation of the RPE in the optic cup; the activation of the Wnt/β-catenin pathway results in cytoplasmic stabilisation of β-catenin, ultimately converting TCF/LEF transcription factors from repressors into activators [6].

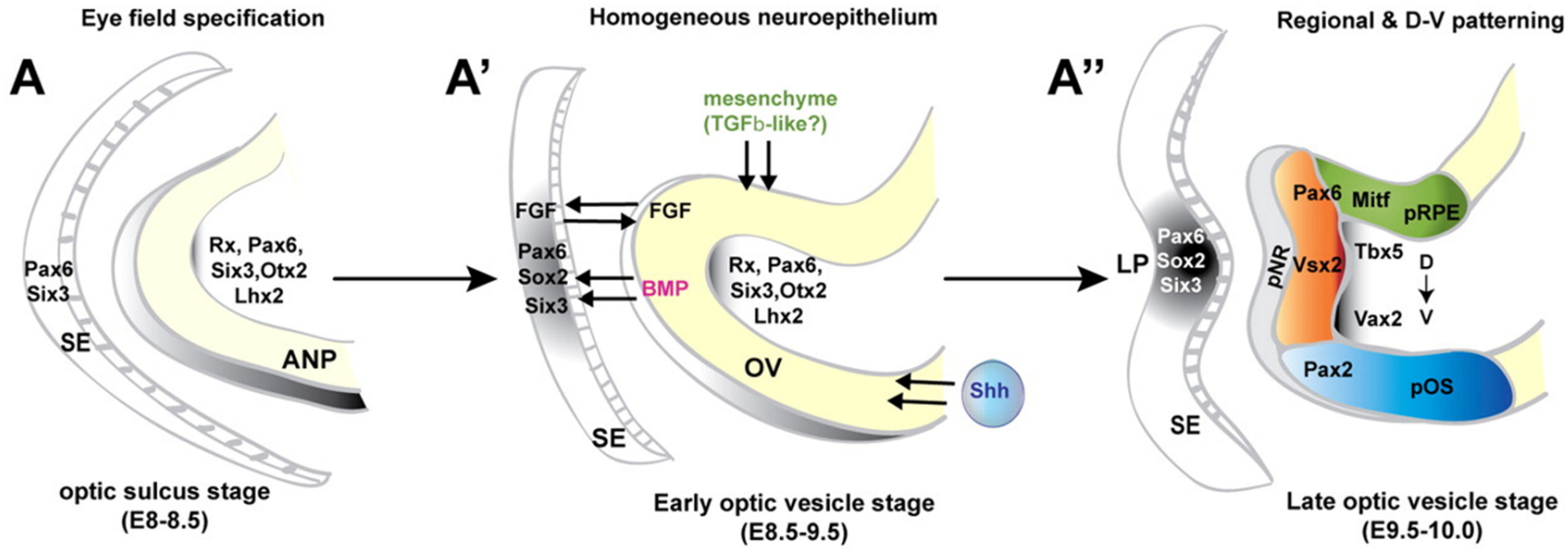

Figure 1.1 Formation of the optic vesicle (A) *The anterior neural plate expresses Rx, Pax6, Otx2, Six3, and Lhx2; while lens-forming region of the surface ectoderm (SE) expresses Pax6 and Six3 at the optic sulcus stage at E8-8.5.* ***(A'-A'')*** *At E8.5 the optic vesicle (OV) evaginates, and Shh drives the dorso-ventral (D-V) and proximal-distal (P-D) patterning, regulating the localisation of Pax2 and Pax6 expression. The dorsal identity of the optic vesicle requires the induction of Tbx5 by BMP, while the ventral domain express Vax2. The presumptive RPE (pRPE) is specified by TGFβ though the expression of Mitf, whilst the presumptive neural retina (pNR) is specified by Vsx2. LP, lens placode; pOS, presumptive optic stalk; pNR, presumptive neural retina; pRPE, presumptive retinal pigmented epithelium. Image adapted from Yun et al., 2009 [1].*

The maturation of the neural retina gives rise to the retinal progenitor cells, which differentiate into all the classes of postmitotic neuronal and glial cells that will form the retina [11, 12]; the RPE instead gives rise to the pigmented epithelium cells [8]. Peripheral structures such as the iris epithelium and ciliary body originate from the margin between the RPE and the neural retina. The lens vesicle separates from the surface ectoderm and differentiates into the mature lens [6, 7].

The neural retina is patterned along the D-V axis and the nasal-temporal (N-T) axis. The axons of the retinal ganglion cells enter into the optic stalk at E11.5. The optic nerve derives from the optic stalk, and its placement depends on the D-V signals of *Vax1* and *Vax2* in the optic stalk and ventral retina, between E9.5 and E11.5. The N-T patterning of the optic cup ensures that the axons of the retinal ganglion cells reach their targets in the Geniculate Nucleus [5].

1.2 Anatomy of the eye.

The eye (Fig. 1.2) is a fluid-filled sphere enclosed by three layers of tissue. Externally, the sclera forms a tough white fibrous tissue which becomes the cornea at the front of the eye. The cornea is a transparent, non-vascularised, layer which refracts the light onto the lens.

The second layer is the choroid, a capillary-rich tissue containing melanin that absorbs excess of light. In the anterior part of the eye the lens is attached to the choroid through the ciliary body. The lens is a transparent biconvex structure, which refracts the incoming light and focuses it on the retina. Behind the cornea there is a ring-like structure, the iris, with a central opening though which the light enters in the eye, the pupil. The lumen between the cornea and iris, also called the anterior chamber, is filled with aqueous humor, a watery fluid rich in

nutrients, produced by the ciliary processes in the posterior chamber, the region between the lens and the iris. The inner chamber of the eye is filled with vitreous humor, a gel-like substance that helps to maintain the shape of the eye. The third layer of tissue, the inner one, is the retina. The serrated junction marking the transition between the retina and the ciliary body is called ora serrata. The retina is composed of different types of neurons sensitive to light. The internal surface of the retina presents an oval yellow spot at the back of the eye called the macula lutea, which supports high visual acuity. At the centre of the macula a small depression, called the fovea comprising the area of greatest visual acuity, supported by high density of cone photoreceptors in the fovea and one-to-one relationship with bipolar and ganglion cells [13]. Blood vessels and the optic nerve leave the eye though the optic disc.

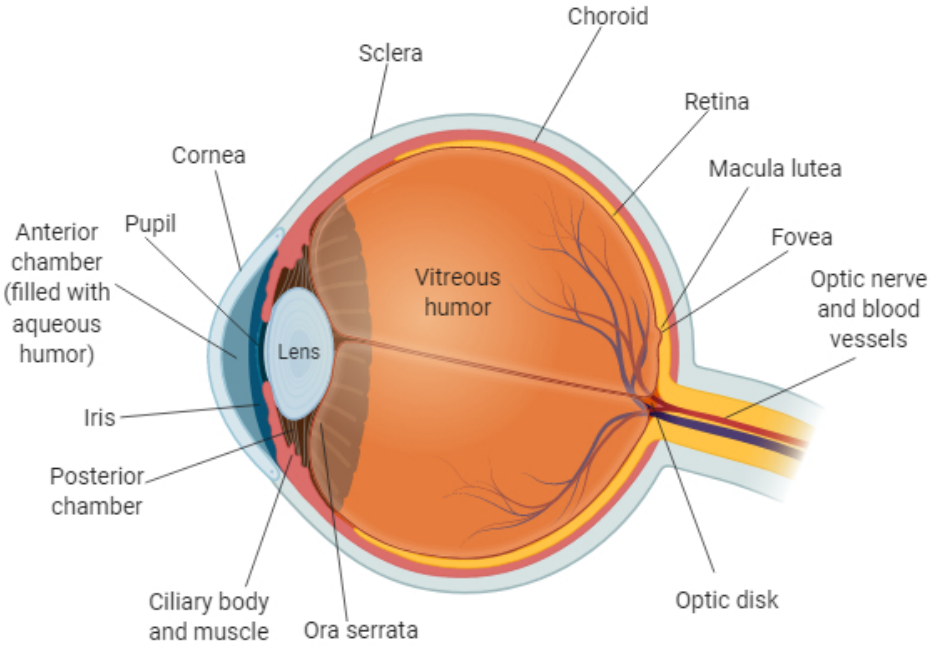

Figure 1.2 Diagram showing the anatomy of the eye. *Image created with BioRender.*

1.3 Fundamentals of retina lamination

The retina is a layered tissue responsible for light processing. To fulfil its function, at the cellular level the retina is highly organised, allowing fast and precise delivery of visual information. Vertebrates have an inverted retina, meaning that the light-sensitive cells are situated proximally to the choroid, so the light has to pass through the different layers before reaching the photoreceptors. Neuronal circuits in the retina are arranged following a layered pattern, where cell bodies and synapses are compartmentalised in different layers of tissue, disruption of which leads to impairment of the organ function [14]. The organisation and neuronal migration in the retina were firstly acknowledged by Ramon y Cajal in 1893.

The retina is composed of five classes of neurons: photoreceptors, horizontal cells, amacrine cells, bipolar cells and ganglion cells; and a single class of glial cells, the Müller glia. Most of these cells have multiple subtypes, based on morphology and transcription profile, it has been estimated that over 55 types of cells are present in the retina [15].

Seven layers of tissue compose the retina [14, 16-18] (Fig. 1.3):

1. The retinal pigmented epithelium (RPE) consists of a single layer of hexagonal cells, the retinal pigmented cells, separating the choroid from the retina. The cells contain melanin, a pigment, which absorbs reflected light.
2. The outer segment layer hosts the membranous disks of the photoreceptor cells, rods and cones.
3. The outer nuclear layer (ONL) is formed by the cell bodies of the photoreceptors.

4. The outer plexiform layer (OPL) harbours the synapses that the photoreceptors make with bipolar and horizontal cells.

Horizontal cells provide inhibitory feedback to photoreceptors, while bipolar cells connect the photoreceptors with the ganglion cells. In this layer light stimuli are converted into electrochemical signals by modulation of tonic glutamate release from photoreceptors [15, 19].

5. In the inner nuclear layer (INL) there are amacrine, bipolar, horizontal and Muller glia cell bodies.
6. The inner plexiform layer (IPL) presents the synapse of axon of amacrine cells, bipolar cells and ganglion cells [14].

The amacrine cells refine the input delivered to the ganglion cells from the bipolar cells.

7. The ganglion cell layer (RGL) contains ganglion cell, bearing the visual signal into the optic nerve.

Among all these classes of cell, photoreceptors, cones and rods, are specialised for different aspects of vision. The shape of the outer segment gives the name to the respective cell type. Both types of cells contain visual pigments in the outer segment, a modified cilium formed by stacks of membrane disks in continuum with the plasma membrane. In rods, the visual pigment is rhodopsin (spectral peak sensitivity at 500 nm), while the cones embody three types of opsin: red-sensitive (564 nm; L cones), green-sensitive (533 nm; M cones), and blue-sensitive (437 nm; S cones). Photoreceptors have the ability to respond differently to light intensities. Rods are very sensitive to light, mediating dim light vision (also called scotopic vision) with low spatial resolution; while the cones are relatively insensitive to the light, working in bright environment (photopic

vision), and mediating the colour vision. Differences in transduction mechanisms contribute to the ability of the photoreceptors to respond differently to the light. Visual responses can be elicited in rods by a single photon, whereas more than 100 photons are necessary to activate the same responses in cones. Photoreceptors differ also in terms of number; there are 4.6 million cones, 100,000 cones are packed in the foveola- the centre of the fovea- allowing visual acuity, while there are 92 million rods, spread over the rest of the retina [13, 20, 21].

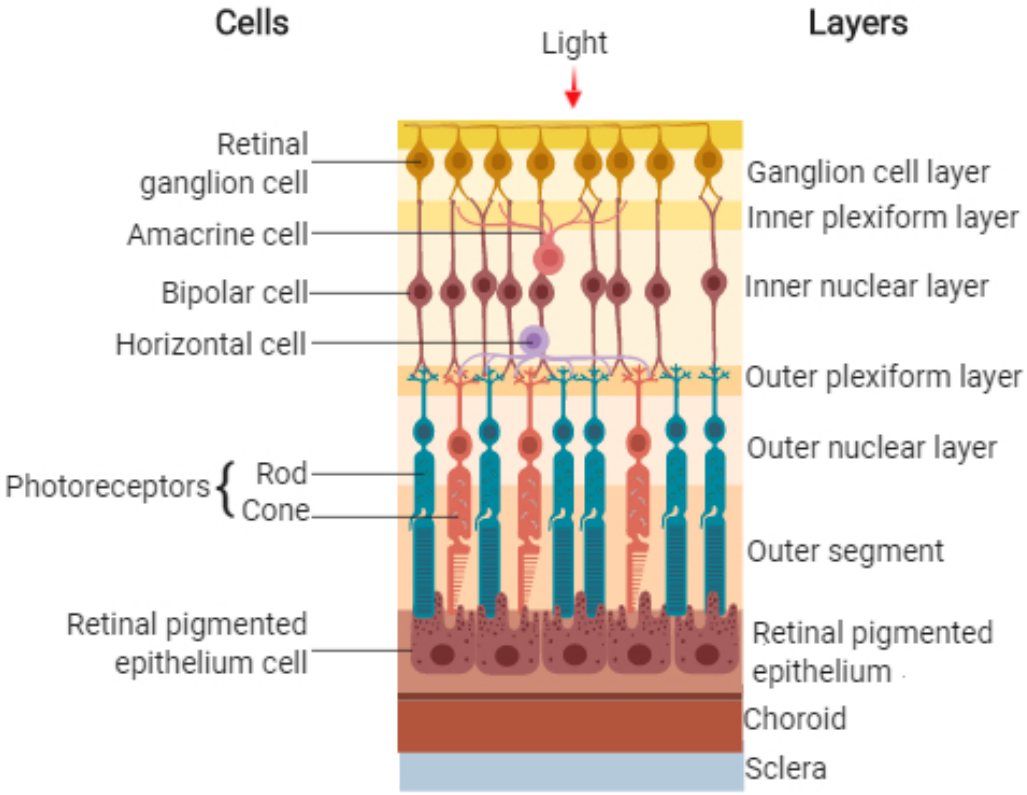

Figure 1.3 The visual sense organ. *The retina is laminated. The nuclei of the photoreceptors constitute the outer nuclear layer (ONL). The nuclei of the bipolar cells, amacrine cells and horizontal cells are found in the inner nuclear layer (INL), and the nuclei of ganglion cells form the ganglion cell layer (GCL). The outer plexiform layer (OPL) contains the processes and synaptic terminals of photoreceptors, horizontal cells, and bipolar cells. The inner plexiform layer (IPL) contains the processes and terminals of bipolar cells, amacrine cells, and ganglion cells. Image created with BioRender.*

1.4 Mechanism of vision

The mechanism of vision can be divided in two processes: the phototransduction, and the retinoid cycle.

1.4.1 Phototransduction

Phototransduction (Fig. 1.4) is the process by which photons captured in the photoreceptor's OS are converted into a visual impulse. In the membranous disks, the combination of opsin, a light-sensitive seven-transmembrane-domain G-protein coupled receptor (GPCR), with 11-*cis*-retinal, a chromophore, forms the rhodopsin. Light initiates the isomerization of the 11-*cis*-retinal into all-*trans*-retinal (also called R* or metarhodopsin II) which activates the heterotrimeric G protein transducin, by catalysing the exchange of GDP for GTP. The transducin Gα-subunit dissociates from the Gβγ subunit, and activates cGMP-phosphodiesterase (PDE), which hydrolyses cytoplasmic cGMP into 5'GMP. The decrease of cytoplasmic cGMP concentration causes the dissociation of the cGMP from the cGMP-gated cation channels, causing their closure. This results in the reduction of the intracellular concentration of Ca^{2+} and Na^{+}, and the hyperpolarisation of the membrane [22]. The phototransduction cascade is truncated when the photoactivated rhodopsin is inactivated by phosphorylation from the rhodopsin kinase GRK1 [23], and the subsequent binding of arrestin, to cap its catalytic activity [24]. At the end of the cascade the all-*trans*-retinal becomes all-*trans*-retinol, which detaches from the opsin and diffuses in the cytosol. Here, the chaperone inter photoreceptor retinoid binding protein (IRBP) transports the all-*trans*-retinol into the pigmented epithelium. At the same time the all-*trans*-retinol undergoes a series of enzymatic reactions, leading to the regeneration of 11-*cis*-retinal for the next visual cycle [20, 25].

Different levels of illumination give rise to different responses from the photoreceptors (Fig 1.4), the process is known as light adaptation. In the dark the cGMP binds the cGMP-gated channel, allowing the Ca^{2+} to enter the cells. At the same time the intracellular Ca^{2+} is removed by Ca^{2+}/Na^{+} exchangers present on the plasma membrane, and the potassium exits the cell, inducing depolarisation. In bright light all the channels are closed and the levels of cytoplasmic Ca^{2+} are low, even though the Ca^{2+}/Na^{+} exchanger operates independently [4]. S-modulin/recoverin and guanylyl cyclase activating protein (GCAPs) detect the concentration of Ca^{2+} and shorten the life of all-*trans*-retinal accelerating the synthesis of cGMP [25].

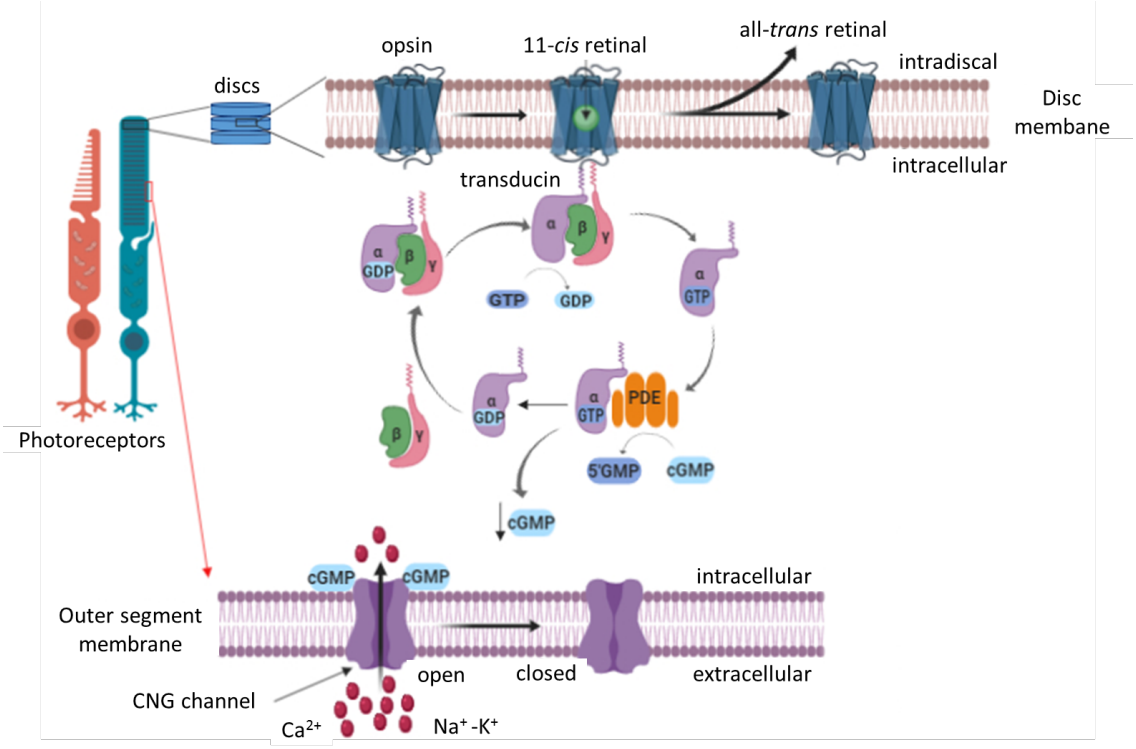

Figure 1.4 Phototransduction *Opsins contained in rod and cone photoreceptor's discs absorb photons, resulting in the opsins activation and inducing the activation of G protein, transducin, through the exchange of GDP to GTP. The Gα subunit dissociates from the Gβγ and binds and activates PDE (cyclic nucleotide phosphodiesterase), which breaks the cGMP in 5' GMP. The decrease of cGMP concentration causes the closure of cyclic nucleotide channel (CNG) on the outer segment membrane, decreasing the Na^+ current and inducing hyperpolarisation of the photoreceptors. Figure made with BioRender.*

1.4.2 Retinoid cycle

The retinoid cycle (Fig. 1.5) allows the reconstitution of the 11-*cis*-retinal after the phototransduction. All-*trans*-retinal released from the activated opsin into the lipid leaflet bi-layer of the optic disc is pumped into the photoreceptors cytoplasm by the transporter ABCA4 [26]. The dehydrogenases RHD8 and RHD12 reduce all-*trans*-retinal into all-*trans*-retinol (vitamin A), in a NADPH-dependent reaction [27], which diffuses in the RPE cells though the binding of IRBP [28-31]. After entering the RPE, all-*trans*-retinol is transferred to the cellular retinoid binding protein (CRBP) [32] and delivered to the lecithin retinol acyltransferase (LRAT) which esterifies all-*trans*-retinol into retinyl esters [33]. RPE65 isomerises and hydrolyses the retinyl esters into 11-*cis*-retinol [34-37], which binds the cellular retinaldehyde binding protein (CRALBP) [38], allowing the delivery to the enzyme 11-*cis* retinol dehydrogenase (RDH5) [39, 40]. RDH5 oxidises 11-*cis*-retinol into 11-*cis*-retinal, using NAD as cofactor. 11-*cis*-retinal then diffuses back out of the RPE cell into the photoreceptor though IRBP [28, 31, 41, 42], where it recombines with opsin ready for stimulation.

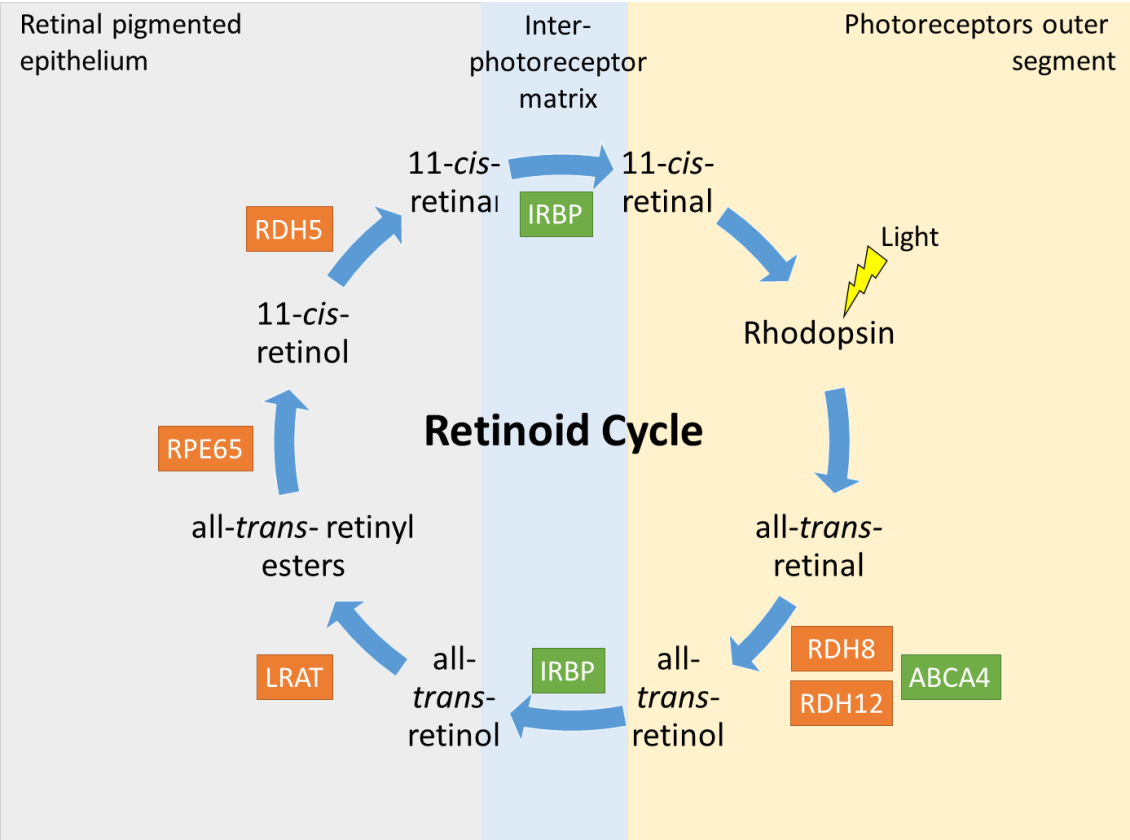

Figure 1.5 Retinoid cycle. *Once the all-trans-retinal dissociates from the rhodopsin, it is transported into the photoreceptor cytoplasm by the transporter ABCA4. Here, the enzymes RHD8 and RDH12 reduce all-trans-retinal into all-trans-retinol, which is pumped by IRBP into the retinal pigmented epithelium. All-trans-retinol is esterified by LRAT into all-trans-retinyl esters, and converted into 11-cis-retinol by RPE65. RHD5 oxidases 11-cis-retinol into 11-cis-retinal, which is pumped back into the photoreceptor outer segment, ready for the next cycle. Transporters, in green; enzymes, in orange.*

1.5 Inherited retinal dystrophies

Inherited retinal dystrophies (IRDs) are a heterogeneous group of ocular diseases characterised by the loss of sight due to the death or dysfunction of photoreceptors, and their contacts with the RPE [43]. Collectively, Mendelian forms of retinal dystrophy have an estimated incidence of 1:2000 [44].

To date, a total of 260 disease genes (RetNet Retinal Information Network https://sph.uth.edu/RetNet/) have been identified as causing such diseases. Most are specifically involved in the visual cascade of photoreceptors and RPE, while others encode transcription factors regulating the progenitors cell fate such as *OTX2* and *CRX* [45] (see Appendix A). Variants in the same gene may give rise to different clinical outcomes (Fig. 1.6), with phenotypes of variable severity, mode of inheritance, and progression, even between affected members of the same family. Therefore, a definite diagnosis may not always be straightforward.

The clinical and genetic heterogeneity of IRD makes the classification of these conditions problematical. IRD is typically categorised based on the course of the disease (progressive or stationary), mode of inheritance (autosomal dominant (AD), recessive (AR), or X-linked), phenotype (rod-dominant, cone-dominant, macular), or whether it can be found as part of a wider syndromic presentation (non-syndromic forms of IRD, exclusively affect the eye, or syndromic forms if associated with additional systemic symptoms). One important differential diagnosis for IRDs is retinal degeneration caused by injury. The most common injuries associated with retinal degeneration are laser-induced retinal degeneration and retinal degeneration which occurs as result of side-effects of drugs. One example is hydroxychloroquine, used for the treatment of rheumatoid arthritis and systemic lupus erythematosus, accumulates in tissues

with high melanin content as RPE and induces loss of central vision and irreversible macula changes [46].

1.5.1 Non-syndromic inherited retinal dystrophies

Non-syndromic IRDs may be classified based on the progression or on the type of cells involved. Here, IRDs are classified based on the cell-type involved.

1.5.1.1 Rod-dominant IRDs

Amongst IRDs, non-syndromic retinitis pigmentosa (RP) (MIM: 268000) is the most common with a worldwide prevalence of ~1 in 4000 [44]. The term 'retinitis pigmentosa' was coined by the Dutch ophthalmologist F.C. Donders in the mid-1800s. Non-syndromic RP is typically inherited as autosomal recessive in 15-20% of the cases, autosomal dominant in the 20-25% of the cases, or X-linked (5-15%) [44, 47], depending on the particular community or geographical region. The clinical presentation of RP is highly variable, however the classical pattern that is observed is typified by the presence of bone spicules inside the retina (retinal pigmented epithelium cells migrated into the neural retina caused by photoreceptors death [48]), night blindness, difficulties in dark adaptation, narrowing of blood vessels, and tunnel vision in young adulthood. While the age of onset of the symptoms can range between early childhood to adulthood, the disease typically progresses to the loss of central vision around the age of 60 years. The loss of colour vision is characteristic of advanced RP. Patients affected by RP also show a reduction or absence of electroretinogram (ERG) amplitudes due to the loss of rod and cone photoreceptors. Over 70 genes and loci have been reported as causative of RP on RetNet, most of which are involved in the photoreceptor's phototransduction cascade and visual cycle or connecting structures (Appendix A).

The genetics of RP is complicated, and clear genotype-phenotype correlations are often not possible. Moreover, mutations in the same gene may cause differing phenotypes, including variability within the same family. A striking example is mutations in the *RHO* gene, encoding for rhodopsin which encompasses 26.5% of cases of adRP [47, 49]. The disease-associated variant p.Pro23His represents a founder mutation in North America [50] in individuals with western-European ancestry (about 10% of adRP cases) [51], and it is the most studied [52]. Mutations in *RHO* may also cause arRP, in particular the variants p.Glu150Lys, p.Met253Ile, p.Trp161*, and p.Glu249*; while other five variants in *RHO* have been associated with adCSNB [52]. Another common cause of adRP involves sequence alterations in *PRPF31*, encoding a pre-mRNA splicing factor, which accounts for 1-8% of cases worldwide, a higher prevalence of *PRPF31* associated RP has been found in the USA [53]. Similarly, another two splicing factors *PRPF3* and *PRPF8* have been found to account for 1% and 3% of adRP cases respectively [53]. *RP1*, a gene encoding a microtubule-associated protein involved in the maintenance of the photoreceptors outer segment, has been found associated with adRP in 5-10% of cases, half of which due to p.Arg677* [47, 49, 53, 54].

The most common gene associated with autosomal recessive RP is *USH2A,* estimated to account for ~10% of cases*,* and shown to be causative of around 6-9% of arRP in the Chinese population [55, 56], and Spanish population, where mutations in *USH2A* have also been associated with cone-rod dystrophy [47]. Mutations in *CRB1* are responsible for ~6.5% of cases [53]; while mutations in *PDE6B* and *CEP290* have also been commonly associated with arRP [47]. A study of a cohort of patients in Jerusalem (Israel) highlighted that the most common genes associated with arRP are *DHDDS*, *FAM161A* and *EYS*

[57]. The high prevalence of pathogenic variants in these disease-associated genes, which are very rare in western populations, indicated that this relatively genetically-isolated population has its own genetic make-up.

X-linked RP accounts for 10-15% of RP inheritance pattern; patients display a more severe phenotype at early stages compared to adRP and arRP. Additionally, a mild phenotype may be present in carrier females due to skewed X chromosome inactivation. Six loci have been associated with this mechanism of disease, although to date mutations in only two genes have been established. *RPGR*-associated X-linked RP explains ~74% of cases [53], in which ~ 60% of all *RPGR* disease-associated alterations reside in a specific RPGR isoform (RPGR-ORF15) [58]. Sequence alterations in *RP2* explain ~15% of cases [53]; this protein is a GTPase-activating protein (GAP) involved in trafficking between the Golgi and the ciliary membrane.

Although RP is generally considered a monogenic disease, digenic inheritance has also been described. The first report of a digenic disease in humans was in 1994, in which three families affected by RP segregated with variants in *PRPF2* and *ROM1* [59]. Since then multiple diseases, especially syndromic RP, have been shown to follow this pattern. Despite many genes discovered causing RP, in ~20-30% of (mostly isolated or 'sporadic') cases a genetic cause of the disease remains to be determined. *De novo* mutations, deep intronic variants of uncertain significance, or incomplete penetrance could explain some of those cases.

Leber congenital amaurosis (LCA) was first described by Theodore Leber in 1869, and defines a group of severe recessively inherited, early infantile onset rod–cone dystrophies. LCA affects 2-3 people in every 100,000 worldwide. The

visual impairment starts during infancy and is usually associated with photophobia, nystagmus, hyperopia, reduced reactions of the pupil, and keratoconus. The fundus may appear abnormal, and the ERG is undetectable or severely abnormal. In rare cases, delayed development and intellectual disability have also been reported in people affected by more clinically complex forms of LCA, including *CEP290 and AIPL1* [60, 61]. Out of 260 genes reported on RetNet as causative of retinal diseases, 25 have been associated with LCA (Appendix A). These genes typically have a highly restricted expression pattern within retinal cells [62], and together underlie approximately 70% of LCA cases [63]. The most common causes of LCA involve sequence variants in *GUCY2D* (accounting for 10-20% of cases)*, CEP290* (15-20% of cases), *CRB1* (10% of cases)*, RDH12* (10% of cases) and *RPE65* (accounting for 5-10% of cases); some of these genes show specific phenotypic features [62]. Patients with *GUCY2D* mutation have poor vision in early life, poor responses to visual stimuli, photophobia and nystagmus, whilst patients affected by mutation of *RPE65* show night blindness as the most common feature, nystagmus, and poor vision. Cataract and myopia are also often associated with mutations in the *RPE65* gene [64].

Congenital stationary night blindness (CSNB) is a group of non-progressive retinal disorders characterised by night blindness, decreased visual acuity, nystagmus, myopia, and strabismus. A meta-analysis reported that X-linked CSNB accounts for 50-60% of cases, autosomal recessive and sporadic CSNB accounted for 40% including 23.6% with a fundus abnormality, and the remaining 2.1% of cases had autosomal dominant CSNB [65]. Mutations in genes encoding for proteins involved in the phototransduction cascade (e.g. *GNAT1* encodes for α-subunit of transducin, *PDE6B* encodes for γ-subunit of

PDE) and signal transmission from photoreceptors to bipolar cells (e.g. *CACNA1F* encodes the α1-subunit of an L-type voltage-dependent Ca2+ channel) are often the cause of this disease (Appendix A) [65].

1.5.1.2 Cone-dominant IRDs

Cone dystrophy (CD) or cone-rod dystrophy (CRD) (MIM: 615973) is a heterogeneous group of progressive retinal dystrophies affecting primarily the cone photoreceptors however, rod degeneration may also present in later stages of the disease. It affects 1 in 30,000 people, and clinical signs are absence of photopic ERG responses, decreased visual acuity, photophobia, loss of colour vision and peripheral vision, and night blindness. The inheritance pattern is mainly autosomal recessive, but it can also present as autosomal dominant, and rarely as X-linked forms. Sequence alterations in 35 genes have been described as associated with this disease (Appendix A) including the transcription factor *CRX* (~5-10% of autosomal dominant CRD cases). Sequence alterations in the transporter *ABCA4*, involved in retinoid metabolism (see Fig.1.4 and Fig. 1.5) and also associated with Stargardt disease and RP, encompass 30-60% of the autosomal recessive CRD cases. X-linked CRD is most often caused by mutation in the GTPase regulator *RPGR* (also associated with X-linked RP), expressed in the cilium of the photoreceptors. RPGR interacts with another protein expressed in the cilium, RPGRIP1, which is also associated with CRD and LCA [66-68].

Achromatopsia (ACHM) is an autosomal recessive form of non-progressive cone dystrophy, affecting 1:30,000 people, consisting in partial or complete absence of colour vision, due to the degeneration of cone photoreceptors. Affected individuals also experience photophobia, nystagmus, and low visual acuity. Six genes have been identified as causative of this disease (Appendix

A). *CNGA3 [69, 70], CNGB3 [69],* are subunits of the cone photoreceptor CNG channel; *GNAT2 [71, 72]* encodes for the cone-specific alpha subunit of transducin*; ATF6 [73-75]* is a transcription factor involved in endoplasmic reticulum stress*; PDE6C [76], PDE6H [77]* encode for the photoreceptor's phosphodiesterase (see Fig. 1.4 and 1.5).

1.5.1.3 Macular dystrophies

The most common macular dystrophy, a rare condition involving the degeneration of the macula, is Stargardt disease, an autosomal recessive progressive inherited disease cause by alteration in *ABCA4* gene which has > 900-reported disease-associated variants. Stargardt disease has a prevalence of 1:8000-1:10,000 with a carrier frequency of aa high as 1:20. Clinical signs, which present during childhood or early adulthood, are macular atrophy, loss of central vision, and yellow-white flakes at the level of RPE [78]. Loss of function mutations usually give rise to a severe and early onset disease, while missense mutations have been associated with late-onset and milder phenotype. Variants in *ABCA4* are also associated with RP and CRD, however allelic heterogeneity makes genotype-phenotype correlations challenging [78].

1.5.2 Syndromic inherited retinal dystrophies

1.5.2.1 Usher syndrome

The most common form of syndromic RP is Usher syndrome (USH), first described by the Scottish ophthalmologist Charles Usher in 1914, in which hearing loss combines with visual loss, and occasional balance problems. It has a prevalence of 1-4 per 25,000 people [44, 79, 80]. USH can be classified in three types, based on the clinical symptoms. USH type I (USH1) (MIM: 276900) patients are defined as having congenital severe-to-profound deafness, vestibular areflexia and onset of RP within the first decade of life. Six genes

have been associated with Usher syndrome type I, *MYO7A* [81-83], *USH1C* [82, 84-86], *PCDH15* [87-89], *CDH23* [90-92], *USH1G* [93, 94], *CIB2* [95], *ESPN* [96]. USH2 (MIM: 276901, 611383, 605472) patients display congenital moderate-to-severe hearing loss, normal vestibular function and onset of RP within the second decade of life. The most common gene mutated is *USH2A* [97-99] however, it may be also caused by mutation in *ADGRV1* [100], and *DFNB31* [101]. Patients affected by USH3 (MIM: 276902, 614504) have hearing loss, vestibular dysfunction, with variable onset of RP [102]. Mutations in genes *CLRN1* [103] and *HARS* [104] have been associated with this disease, as well as mutation in *ABDH12* which has also been associated with PHARC (neurodegenerative disease involving polyneuropathy, hearing loss, ataxia, retinitis pigmentosa and cataract) and USH3 [105, 106]. Mutation in *CEP250* [107] and *CEP78* [108] genes were reported as causing atypical USH. Most of the genes involved in the development of Usher syndrome encode for cilia components (Fig. 1.6) (Appendix A).

1.5.2.2 Ciliopathies

Ciliopathies are a group of disorders involving genes encoding for components of the primary cilia, which can manifest with a variety of features including retinal, renal, and cerebral abnormalities. Bardet-Biedl syndrome (BBS) was firstly described by Georges Bardet and Arthur Biedl in the early 1920s. BBS (MIM: 209900) is the second most common form of syndromic RP with an estimated prevalence of 1:100,000 people, which tends to be higher in populations with a high degree of consanguinity. It is a heterogeneous autosomal recessive ciliopathy characterised by RP, obesity, kidney dysfunction, polydactyly, behavioural dysfunction, and hypogonadism. These symptoms may also be associated with developmental delay, hypertension,

speech disorders, anosmia, strabismus, and dental anomalies. Twenty-one genes are associated with this group of diseases: *BBS1* [109], *BBS2* [110, 111], *ARL6* [112, 113], *BBS4* [114], *BB5* [115, 116], *MKKS* [117, 118], *BBS7* [119], *TTC8* [120], *BBS9* [121], *BBS10* [122, 123], *TRIM32* [124], *BBS12* [125], *MKS1* [126], *CEP290* [126], *WDPCP* [127], *SDCCAG8* [128], *LZTFL1* [129], *BBIP1* [130], *IFT27* [131], *IFT172* [132], *CEP19* [133], and *C8orf37* [134, 135] (Appendix A). The majority of these genes encode for components of the BBSome, an octameric protein complex, part of the basal body, involved in the cargo trafficking to the primary cilium [136]. In some patients more complex inheritance patterns have been indicated involving the interaction of multiple mutations and distinct BBS loci, in particular it has been proposed that *BBS1*, *BBS4* and *MKKS* loci contributes to the triallelic inheritance [137-139], which modify the severity of phenotype and the age of onset of BBS [140]. Additionally, the hypomorphic variant p.Cys470Tyr in the *CCDC28B* gene has been shown to modify the severity of BBS primarily due to mutations in other BBS-associated genes [141]. Similarly, sequence alterations in *MKS1*, *TMEM67*, and *WDPCP* [127] genes, involved in ciliogenesis, may also modify the expression of BBS phenotypes.

Alström syndrome (ALMS) is a recessive disease with a similar manifestation of BBS however, in ALMS progressive sensorineural hearing loss is often present alongside cone-rod dystrophy, nystagmus, photophobia, cardiomyopathy, insulin resistance and type 2 diabetes, progressive renal disease, and hypogonadism. Mutations in *ALMS1,* a gene encoding a centrosomal-associated protein, have been associated with this disease, most of the pathogenic variants that have been identified are frameshift or nonsense [142,

143]. ALMS incidence is less than one per million in the general population [143].

Joubert syndrome (JBTS) is characterised by the “molar tooth sign”, a specific and recognisable mid-hindbrain malformation, hypotonia, ataxia, intellectual disability, oculomotor apraxia, retinal dystrophy, renal disease, ocular colobomas, episodic tachypnoea, and other abnormalities. JBST prevalence is between 1:80,000 and 1:100,000 [144]. Thirty-four genes have been associated to JBTS, and a study on 375 families with JBTS identified *CCD2D2A, AHI1, C5orf42, CEP290* and *TMEM67* as the most commonly mutated [145].

Meckel-Gruber syndrome (MKS) phenotypically overlaps with JBTS, affected individuals show occipital encephalocele, cystic dysplastic kidneys, polydactyly, retinal dystrophy and other minor features. The worldwide incidence is 1:135,000 however, in consanguineous population is about 1:3500 [146]. Seventeen genes associated with this disease, with mutations in *MKS1* accounting for 7% of MKS cases and mutations in *TMEM67* account for 16% of cases [146].

Senior–Løken syndrome (SLS) is an oculo-renal syndrome with a prevalence of 1:1,000,000. Classical signs are nephronophthisis and LCA, mutations in *NPHP5* and *CEP290* are associated with greater propensity of RP. However, in most of the cases linked with mutations in other NPHP genes, mild RP is diagnosed in the first decade of life, [147]. Currently, 10 genes have been associated with this disease [148].

1.5.2.3 IRDs with other systemic features

Retinal dystrophies can occur as a consequence of many other disorders, in which retinal involvement may be secondary and highly variable in presentation.

In this landscape, mitochondrial disorders are one of the most common group of diseases, affecting 1:5000 adults [149]. Mitochondrial diseases, caused by mutations in the mitochondrial genome, affect energetic metabolism and manifest with a wide range of systemic features, neurological symptoms often being the principal manifestation. Retinal involvement is a variable feature and might manifest as ‘salt and pepper’ changes in the periphery to central vision loss. Mitochondrial disorder that include retinal dystrophy as a part of the associated clinical phenotype include: NARP (neuropathy, ataxia and RP) caused by mutations in *MT-ATP6;* MELAS (mitochondrial encephalomyopathy, lactic acidosis and stroke-like episodes) secondary to mutations in *MT-TL1* and Kearns-Sayre syndrome (KSS) caused by a large-scale deletion in the mitochondrial DNA [150].

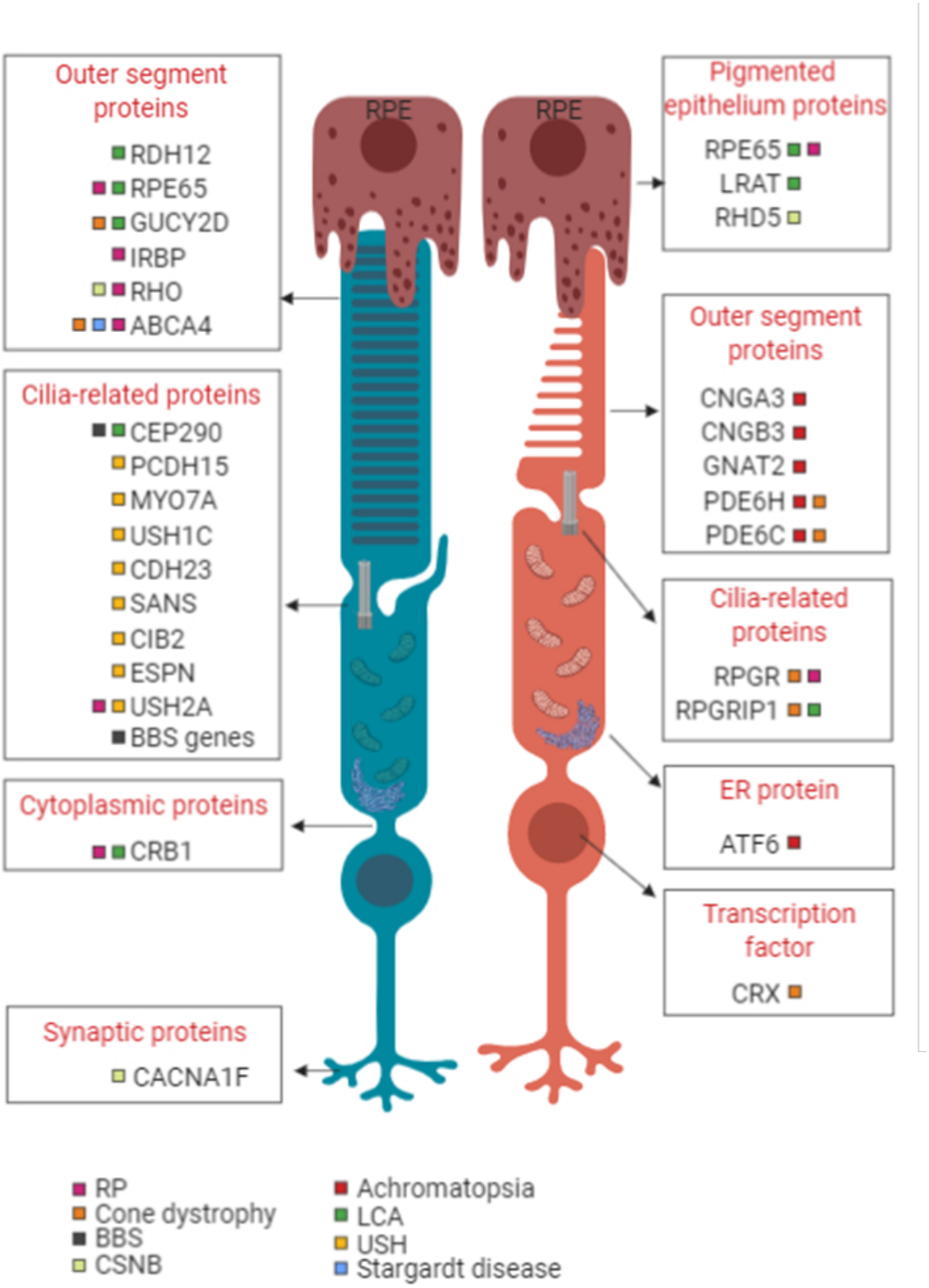

Figure 1.6 Schematic representation of some genes/proteins causing retinal dystrophies. *For the complete list of genes and their function see Appendix A. Image created with BioRender.*

1.6 IRD treatment

Recently, several therapies for IRDs have been developed, some of which are now in clinical trials, while other have been approved. The first gene therapy for RPE65 was described by Acland et al in 2001 [151], where the adeno-associated vector AAV2 injection was successfully performed on dogs affected by RPE65 retinopathy. The success of the canine and (later developed) murine models led to the advancement of clinical trials. In 2017, the FDA approved the first gene therapy, Luxturna, to treat RPE65-associated LCA; the therapy is based on an AAV for biallelic replacement of *RPE65* (AAV2-hRPE65v2) delivered by subretinal injection [152]. Results of the trial showed that Luxturna was able to improve light sensitivity, visual fields, and reduce night blindness in patients with RPE65 [152]. Moreover, gene therapies for LCA caused by mutations in *AIPL1, RPGRIP1, LRAT* and *RDH12* are currently at various stages of clinical trials [62].

RNA therapies such as antisense oligonucleotide and RNAi have proved successful when a gene mutation in an intron-exon splice site leads to the presence of transcripts with a cryptic exon. An example of this includes the *CEP290* c.2991+1655A>G alteration associated with LCA. Treatments with the antisense oligonucleotide QR-110 showed restoration of the correct mRNA transcript and function of human cilia in optic cups [153, 154]. Currently, QR-110 is in phase III clinical trial. Similarly, other antisense oligonucleotides are in development/clinical trial for *USH2A* c.7595-2144A>G causing Usher syndrome, *RHO* Pro23His causing adRP, and *ABCA4* c.5461-10T>C causing Stargardt disease (source: https://www.proqr.com/pipeline/).

Another therapeutic avenue currently being explored is the transplant of human embryonic stem cells (hESC) or human-induced pluripotent stem cells (hiPSC)-

derived RPE, some of these therapies are now in clinical trials for RP, Stargardt disease and age-related macular degeneration (AMD), and have shown to improve vision in some patients [155]. In particular, clinical trials using hESC-derived RPE cells for the treatment of Stargardt have to date proved safe, and improved vision and showed subretinal hyperpigmentation probably related to the release of pigment of transplanted cells [156, 157]. Unfortunately, use of hiPSC from the same patient means that the genetic defect needs to be corrected before the autologous transplant and might be achievable for RPE, however, transplantation of hiPSC-derived photoreceptors still faces many challenges due to low transplantation efficacy and inaccurate host-graft synapses [158].

Supplementations of vitamin A, E, DHA (docosahexaenoic acid), lutein, and beta-carotene have been tested in patients with RP and Best disease, and only supplementation with vitamin A, lutein and beta-carotene showed small beneficial effects on the progression of RP [159].

1.7 Next-generation technologies for gene discovery

The completion of the Human Genome Project [160] opened up new avenues for studying human disease at the molecular level. Moreover, the development of high throughput genomic techniques has paved the way for the discovery of new genes causing inherited diseases, with a significant reduction of costs.

Geographical and cultural isolation, and unions between individuals from the same community, has led to genetically distinct populations which may have an increased prevalence of certain inherited autosomal recessive disorders, typically due to the accumulation of regional founder genetic variants. This ‘founder effect’ happens when a pathogenic genetic alteration occurs in a

founder community member, and is transmitted to subsequent generations becoming stably maintained in the population, leading to an increased prevalence of associated diseases. Determination of regional distribution of founder mutations helps scientists and clinicians to establish specific clinical testing and management strategies to target to the specific genetic variants involved [161]. Affected individuals originating from such populations are typically homozygous for the same ancestral pathogenic genetic variant, but also for an extended adjacent genomic DNA segment (haplotype) on which the variant first arose in the ancestral founder individual. This provides a particularly powerful means to map candidate loci for autosomal recessive genes via whole genome single-nucleotide polymorphism (SNPs) genotyping and autozygosity mapping. Whereas other homozygous stretches of DNA (runs of homozygosity; ROH), present in the genome will be shared randomly among unaffected and affected siblings, autozygous genomic regions which house the causative homozygous founder mutation will be shared exclusively and consistently amongst affected individuals [161, 162]. Genome-wide SNP mapping is often accompanied with a next-generation sequencing (NGS) technology such as whole-exome sequencing (WES) [162] to identify the specific causative genetic variant. Whole-exome sequencing enables investigation of protein-coding DNA sequences, exons and splice sites (and nearby intronic material), which together account for 1-2% of the whole genome. Sequence variants in the exome and associated intron/exon splice junctions are the most common cause of Mendelian disease accounting for ~85% of disease, for which missense and nonsense mutations account for ~60% of cases [163, 164]. Polymorphisms in non-coding genomic regions, such as non-coding elements and non-coding

RNAs, can be detected with whole-genome sequencing (WGS) however, assessing the functional significance of such mutations remains challenging.

NGS panels specific for IRDs are also often used in the clinical setting, for example the Manchester Centre for Genomic Medicine offers an NGS mutation scan panel of 175 genes known to cause non-syndromic and syndromic IRDs. Interestingly, the panel does not cover *RPGR*-ORF15 as it is a highly repetitive region and the NGS is not able to sequence this region effectively, therefore dideoxy sequencing is necessary to uncover genetic alterations in that region.

1.8 Eye diseases in Pakistan

Pakistan (Fig. 1.7) is one of the largest developing countries in South Asia, with a population of 197 million people. Non-syndromic RP is considered one of the most common causes of inherited childhood blindness in the [58] South Asian population, encompassing 20% of cases in Pakistan [165]. A systematic review published in 2017 reported that the most common pattern of inheritance of retinal diseases in South Asian populations is autosomal recessive, with half of the genetic mutations reported to cause non-syndromic RP present in Pakistan [166] however, the lack of a proper collection of variants identified in Pakistan as associated with disease does not allow to have a detailed overview on the genetic causes of IRDs. The cultural and genetic make-up of Pakistan stems from the historical partition and then re-location of Indian Muslims, and later the immigration of populations from Afghanistan, Iran, and Bangladesh. This cultural diversity is reflected in the genetic diversity of each community, with distinct founder mutations being present in each region. This geographical and cultural isolation, and specific marriage practices typically within communities (first-cousin marriages reported to account for 50-70% of the total marriages in Pakistan), has led to numerous genetically distinct communities in which there

may be a high prevalence of certain inherited autosomal recessive disorders typically due to the accumulation of regional founder variants [167, 168]. While some papers report the exact regional location of affected individuals or families, many have failed on this, nevertheless the Punjabi population seems the more studied [169].

The isolation of these communities sometimes leads to atypical inheritance or intra-familiar locus heterogeneity which has been found associated with a cohort of Pakistani families with presumed autosomal recessive hearing loss [170]. It has also been found that in these communities where high rate of pathogenic variants are present due to the specific marriages pattern and geographical constraints, it is possible to find families in which the co-occurrence of variants in two different genes segregate with the disease [171]. Similarly, compound heterozygous variants have been known to cause IRDs in several populations [172, 173], including Pakistani [174] where the there is an elevated carrier frequency in the general population [175].

Isolation of certain communities in rural and remote areas with limited access to healthcare system and ophthalmic services, as well as limited possibilities to afford expensive diagnostic and genetic investigation, often makes the diagnosis of inherited ocular diseases challenging. This is often compounded by the highly heterogeneous nature (phenotypic and genetic) of inherited dystrophies. In this setting, knowledge of the community-relevant founder mutations is vital for providing improved care, counselling, and targeted genetic testing for families affected by rare disorders.

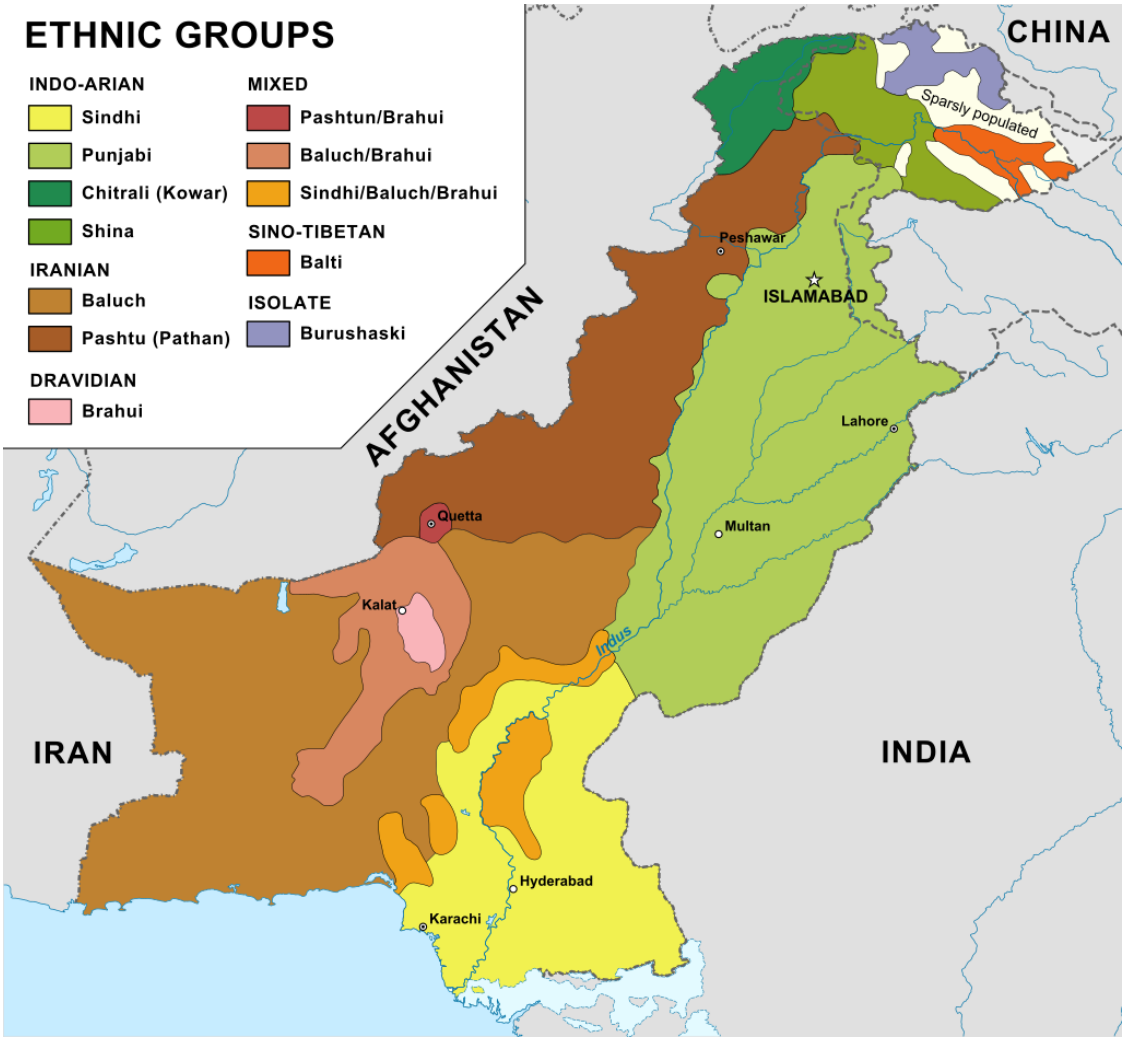

Figure 1.7 Map of Pakistan that highlight the major ethnic groups for each region https://en.wikipedia.org/wiki/Ethnic_groups_in_Pakistan

1.9 Aims of this thesis

While previous genetic and molecular studies have improved medical and scientific knowledge of the causes and biological basis of inherited retinal disease, a great deal remains to be learned in this area. However, recent progress in defining the molecular mechanisms underlying hereditary ocular disorders has proven to be instrumental for the development of personalised

therapies. Additionally, genomic knowledge of retinal disease is important to aid diagnosis and counselling due to overlapping phenotypes, and clinical heterogeneity, of rare retinal diseases. Therefore, a molecular genetic diagnosis is invaluable in aiding patient management, and in defining therapeutic options.

The overarching aim of this thesis is to improve understanding, and characterise the genetic and phenotypic spectrum, of genetic retinal diseases in Pakistan while further improving scientific understanding of the genetic and biological basis of these conditions. The key aims of this study were:

1. To define and confirm a new cause of autosomal recessive RP due to a founder mutation of the *CLCC1* gene identified in families from Pakistan.
2. To learn more about the molecular role of CLCC1, and pathomolecular basis of CLCC1-associated RP.
3. To more comprehensively characterise the molecular spectrum of inherited retinal diseases in Pakistan and relate specific pathogenic variants to particular regions and communities, to facilitate the future development of efficient and targeted genetic testing strategies to enable improved disease diagnosis and early intervention.

CHAPTER 2

MATERIALS AND METHODS

CHAPTER 2 MATERIALS AND METHODS

2.1 Buffers, reagents and stock materials

All general-purpose chemicals and alcohols were purchased from Fisher Scientific and Sigma-Aldrich. All solutions for cell culture were supplied by Lonza, except for sera, Neurobasal media, DMEM:F12 Glutamax, and B27 supplement which were obtained from Gibco.

Plasticware for tissue culture was acquired from Greiner Bio-one and other general laboratory consumables purchased from Fisher Scientific. Kits for DNA gel extraction, PCR purification, Miniprep and Midiprep were purchased from Qiagen; restriction enzymes were supplied by Promega and New England Biolabs (NEB).

Plasticware for PCR were purchased from 4titude and StarLab.

Buffers used were reported in Table 2.1

Table 2.1 Solutions used in this study

4% PFA	4% (w/v) paraformaldehyde, in PBS, pH adjusted to 7.4
4% PFA + 0.2% Glutaraldehyde	4% (w/v) paraformaldehyde, 0.2% (v/v) glutaraldehyde, in PBS, pH adjusted to 7.4
3T3 medium	10% (v/v) heat-inactivated calf serum (HI BCS), 100 U/ml penicillin, 100 µg/ml streptomycin, in DMEM
Ampicillin	100 mg/ml in dd.H_20
Destain	40% (v/v) MeOH, 10% (v/v) acetic acid, in dd.H_20
DNA loading buffer	30% (v/v) glycerol, 0.25% (w/v) bromophenol blue, 0.25% (w/v) xylene cyanol
HE lysis buffer	25 mM HEPES, 5 mM EDTA, 1 mM $MgCl_2$, 10% (v/v) Glycerol, 1% (v/v) Triton X-100, 100 µM PMSF
HEK293 medium	10% (v/v) heat-inactivated foetal bovine serum (HI FBS), 100 U/ml penicillin, 100 µg/ml streptomycin, in DMEM
IP lysis buffer	20 mM Tris-HCl pH 8.0, 150 mM KCl, 0.1% Triton X-100, 1X complete protease and phosphatase inhibitors
Kanamycin	50 µg/ml in dd.H_20
LAB Buffer	10 mM Lithium acetate, 10 mM Boric acid
Laemmli sample buffer	10% (v/v) glycerol, 2% (w/v) SDS, 5% (v/v) β-2 mercaptoethanol, 0.002% (w/v) bromophenol blue, 0.125M Tris-HCl (pH 6.8)
LB agar	15 g/L agar, 10 g/L tryptone, 10 g/L NaCl, 5 g/L yeast extract
LB broth	10 g/L tryptone, 10 g/L NaCl, 5 g/L yeast extract
Lysine block	5% (v/v) horse serum, 5% (v/v) goat serum, 50 mM lysine, 0.2%

	(v/v) Triton X-100
Primary neuronal culture medium	180 µM HEPES, 0.5 mM L-glutamine, 100 U/ml penicillin, 100 µg/ml streptomycin, 2% (v/v) B27 supplement, in Neurobasal media, Phenol Red-free, glutamine-free
Running buffer	25 mM Tris-base, 19 mM glycine, 0.1% (w/v) SDS
SHSY-5Y medium	10% (v/v) heat-inactivated foetal bovine serum, 100 U/ml penicillin, 100 µg/ml streptomycin, in DMEM:F-12 Glutamax
Slagboom buffer	5% (w/v) SDS, 1X TEN buffer
SOC	10 mM NaCl, 2.5 mM KCl, 10 mM $MgSO_4$, 20 mM Glucose, 10 mM $MgCl_2$, sterilised by push filtration
STE buffer	250 mM Sucrose, 5 mM Tris, 2 mM EGTA, pH 7.4
TAE	40 mM Tris-base (pH 7.6), 20 mM acetic acid, 1 mM EDTA
TBS	20 mM Tris base, 150 mM NaCl
TBS-T	20 mM Tris base, 150 mM NaCl, 0.1% (v/v) Tween-20
TEN buffer	10 mM Tris base, 1 mM EDTA, 100 mM NaCl
Transfer buffer	25 mM Tris-base, 192 mM glycine, 0.1% (w/v) SDS, 20% (v/v) Methanol

2.2 Family recruitment and sample acquisition

Research was carried out in compliance with the Code of Practice for Human Tissue and Research (code E) provided by the Human Tissue Authority (HTA), which defines human tissue as relevant material consisting of, or containing cells, therefore includes blood samples. All blood samples, and subsequent DNA extractions, used in this project were used and stored in HTA-licensed premises with research carried out in accordance with the Human Tissue Act 2004.

Recruitment to this project requires submission of the appropriately signed consent (projects approved by Ethical Committees of International Islamic University, Islamabad, Pakistan; FBAS-2018-3598, Khyber Medical College; 8936, the Institute of Biomedical and Genetic Engineering; Ethical board of University of Health Sciences, Lahore, National Centre of Excellence in Molecular Biology and National Institutes of Health, CNS USA, and the University of Exeter Medical School), clinical details and a blood or buccal

sample. Signed consent is given, in accordance with the HTA's code of practice, only when individuals, or parents of individuals, feel they are sufficiently informed, about the purpose of the research, how their samples are to be stored and used and satisfied with the purpose of the research in which they are to be involved. All the individuals participating to this study were phenotypically assessed by local clinicians. Medical history and documentation of symptoms was collected when possible. For affected individuals, visual acuity testing using Snellen charts, colour vision testing using Ishihara charts and funduscopic examination by direct ophthalmoscopy was performed by clinicians locally. Additional targeted clinical investigations were undertaken subsequent to molecular genetic studies to clarify the clinical significance of any candidate variants identified.

2.3 Data management

On receipt of blood or DNA samples from their respective collection locations, each sample was assigned a sample ID, and this as well as clinical and molecular information was recorded in a password protected database. The vessels containing the samples were anonymised and labelled with the relevant sample ID.

2.4 DNA extraction from whole blood

Human DNA was extracted from whole blood using ReliaPrep™ Blood gDNA Miniprep system (Promega). Upon arrival blood samples were stored at -20 °C and thawed at room temperature. Samples were mixed for 10 minutes (min) in a rotisserie shaker and 200 µl of blood were mixed with 20 µl of Proteinase K. 200 µl of cell lysis buffer (CLB) were added to the tube, the content vortexed for 10 seconds (sec), and incubated at 56 °C for 10 min. Two hundred fifty µl of binding buffer (BBA) were added to the tube and mixed by vortexing for 10 sec.

The tube content was added to the ReliaPrep™ Binding Column, spun for 1 min at maximum speed and the flow-through was discarded. The column was moved into a clean collection tube and 500 µl of column wash solution (CWS) were added to the column and centrifuged for 3 min at maximum speed, the flow-though was discarded. This step was carried out 3 times. The column was placed in a clean microfuge tube and the DNA was eluted by addition of 50 µl of nuclease-free water to the column that was incubated for 1 min and then centrifuged for 1 min at maximum speed.

The yield and quality of the DNA was assessed using the Nanodrop 200c UV-Vis Spectrophotometer (Thermo Scientific), by measuring the absorption at 260 nm (A260) of 1 µl of undiluted sample. The NanoDrop software automatically calculated the concentration (in ng/µl) using a modified Beer-Lambert equation. DNA purity was assessed simultaneously by measuring absorption at 280 nm (A280). A ratio of A260 to A280 of ~1.8 indicates “pure” DNA. A secondary measure of absorbance at 230 nm (A230) was also taken, values for a “pure” nucleic acid are often higher than the respective A260/A280 values being within the range of 1.8-2.2.

2.5 Primer design

DNA sequence was obtained from UCSC Genome browser (https://genome.ucsc.edu/), and PCR primer pairs were designed using Primer 3 (www.bioinformatics.nl) following these rules:

- Primer size were 18-25 bp.
- Melting temperature was kept as similar as possible for both primers.
- Where possible the guanine-cytosine (GC) content was kept below 60%.

- *In silico* PCR analysis was performed to assure the 100% matching with the desired sequence.
- Primer sequences were not chosen if DNA stand contained common SNPs.
- Primers sequences were not chosen if they bind repeated sequences.

2.6 Optimisation of PCR conditions

The optimal annealing temperature for oligonucleotide primers during PCR was determined using a temperature gradient of 52-64 °C across the PCR block of an Eppendorf Mastercycler thermocycler Ep Gradient. Twelve PCR reactions for each primer pair were set, using good quality control DNA. Each reaction had a different annealing temperature which increased incrementally across the PCR block from 52 °C to 64 °C, by approximately 1 °C. PCR conditions, as the primer concentration or the addition of 10% (v/v) dimethyl sulfoxide (DMSO) if the GC content was above 60%, were altered if the PCR product produced weak or no product across the range of temperatures.

2.7 Polymerase chain reaction (PCR), agarose gel electrophoresis and dideoxy sequencing

Primers were purchased from Integrated DNA Technologies (IDT) and resuspended at 100 μM with molecular biology grade water. The PCR reaction mixture contained 10-20 ng of template DNA, 1x DreamTaq buffer (Thermo Fisher), 10 mM dNTPs (Solis BioDyne), 5 pM/μl of each primer, and appropriate units of DreamTaq polymerase. The mixture was placed in the thermocycler (Eppendorf Mastercycle ep Gradient S), following a 'touchdown' PCR protocol. This method improves the binding specificity of primers and helps to avoid amplification of other genomic regions. The method is based on incrementally lowering the annealing temperature by 2 °C every two cycles from an initial

temperature that is 4 °C greater than that of the annealing temperature (Tm) until the desired Tm is reached (Table 2.2).

Table 2.2 Touchdown PCR thermocycler programme

Number of cycles	Temperature (°C)	Time (Sec)
1	95 (denaturation)	120
2	95 (denaturation)	30
	Tm plus 4	-
	72 (elongation)	-
2	95 (denaturation)	30
	Tm plus 2	-
	72 (elongation)	-
35	95 (denaturation)	30
	Tm (annealing)	-
	72 (elongation)	-
1	72 (elongation)	300

The Tm for each pair of primers is reported in Appendix F. The elongation step was performed for 30 sec for PCR product <500 bp or 45 sec for PCR products with a size between 500-1000 bp.

After the PCR was performed, the presence of a single amplicon was verified on a 1.0% (w/v) agarose gel in LAB buffer containing ethidium bromide (Fisher Scientific), using 1 kb DNA plus ladder (Thermo Fisher) as reference.

For Sanger sequencing 5 µl PCR product was purified from unwanted primers and nucleotides using 2 µl Exonuclease I - Shrimp Alkaline Phosphatase (ExoSap) (NEB). The mixture was heated at 37 °C for 30 min for digestion and then at 95 ˚C for 5 min to inactivate the enzyme. Sanger sequencing was performed by Source Bioscience.

2.8 Single nucleotide polymorphism (SNP) genotyping

SNP genotyping was carried out using Illumina CytoSNP-12v2.1 array following the Infinium® HD Assay Ultra manual protocol and assistance from Dr Barry Chioza, University of Exeter.

The protocol is undertaken over three days and the assay requires 200 ng of DNA per sample at a concentration of 50 ng/µl with each chip holding 12 samples.

Day 1: DNA samples were denatured using a buffer containing 0.1N NaOH and then neutralised in preparation for amplification. Samples were incubated overnight at 37 ^{o}C to amplify.

Day 2: Amplified DNA samples were enzymatically fragmented using the Illumina FMS buffer which utilises end-point fragmentation (to avoid over-fragmentation). The DNA was then precipitated using 2-propanol and the Illumina solution PM1, then collected via a 20 min centrifugation carried out at 4 ^{o}C. Following resuspension, using the Illumina solution RA1, the DNA was denatured at 95 ^{o}C for 20 min. The denatured samples were cooled then 12 µl of each sample was loaded onto the BeadChip. This was then incubated in the Illumina Hybridisation Oven at 48 ^{o}C for a minimum of 16 h (but no more than 24 h).

Day 3: The BeadChips were prepared for the staining process. This involved washing away any un-hybridised and non-specifically hybridised DNA using the PB1 Illumina buffer. Following the wash step, labelled nucleotides were dispensed onto the BeadChip through the Flow-Through Chambers to perform single-base extension of primers hybridised to the DNA. The BeadChips where

then stained using the Illumina XStain HD BeadChip process then imaged on an Illumina iScan Reader.

The iScan Reader uses a laser to excite the fluorophores of the single-base extension product on the beads of the BeadChip. Light emissions from the fluorophores were recorded by the reader, taking high-resolution images of the BeadChip. The data from these images were analysed using the Illumina GenomeStudio Integrated Informatics Platform allowing for the genotype to be determined. Further analysis was then undertaking by exporting the data into Microsoft Excel and using a macro to highlight notable regions of homozygosity (>1Mb) and to compare genotyping across samples.

2.9 TruSight One sequencing panel

The Illumina TruSight One capture kit (Illumina 5200 Illumina Way San Diego, California USA) targets 4811 clinically relevant genes. Next-generation sequencing was performed on the NextSeq 500 platform. Bioinformatic pipeline was performed as described in O'Gorman et al. 2019 [176]. FastQ data were aligned to the hg38 human reference genome with BWA-MEM (v0.7.12). GATK version 3.720 was used to call SNPs and short indels in a multisample VCF file. Annotation was performed using ANNOVAR v2015Dec to collate variant consequence, variant allele frequency (1000 Genomes Project, Exome Sequencing Project and Exome Aggregation Consortium) and pathogenicity scores with CADD and MaxEntScan for splice site variants. Further annotation was included from InterVar (2018) and Human Gene Mutation Database. Coverage was determined using SAMtools v1.3.1 and BEDtools v2.17.0. Variants were categorised on pathogenicity, and defined pathogenic in ClinVar. The sequencing was performed by Luke O'Gorman at the University of Southampton.

2.10 Whole-exome sequencing (WES) and Whole-Genome Sequencing (WGS)

WES and WGS were performed by BGI Tech Solutions (Hong Kong) on the BGISEQ-500 sequencing system. Typically, a total of 1,403,229,858 clean reads were aligned to the human reference genome (GRCh37) using the Burrows-Wheeler Aligner (BWA), with on average, 99.79% of the whole genome excluding gap regions had at least 99.40% had at least 4X coverage and 98.20% at least 10X coverage. Average sequencing depth was typically ~45X.

The FASTQ files obtained from BGI were mapped to the reference genome using the Burrows-Wheeler Aligner BWA-MEM algorithm (version 0.7.17) [177, 178]. This algorithm was used due to its improved performance, compared to other BWA algorithms, being faster and more accurate than previous versions as well as providing higher quality queries. The sequence alignment map (SAM), was converted to binary SAM format (BAM) to produce a smaller file and to increase the processing speed.

Duplicate reads were marked by Picard (version 2.15). The BAM file was then realigned, to account for indels, with variants called using GATK-HaplotypeCaller (version 3.70) and subsequently quality filtered based on; mapping quality, strand bias, the average position of a variant in a read and SNP quality. The variant call file (VCF) was annotated using the Alamut Software (version 1.8) Suite. Copy number variants were called using SavvyCNV (https://github.com/rdemolgen/SavvySuite) and ExomeDepth. Variants were quality control (QC) checked and filtered for rare, non-synonymous exonic or splice variants, with a population frequency of <0.005 in control databases (including the Genome Aggregation Database; gnomAD, the

Exome Aggregation Consortium; ExAC, and the 1000 Genomes Project) (Interactive Biosoftware).

2.11 Constructs

Plasmids for expression studies (Table 2.3) were subcloned by PCR into a backbone containing the chick β-actin promoter, pCAβ, which allows expression in chick neurons (gift of Dr. J. Chilton). An intermediate step using the shuttle vector pILES, based upon pBlueScript, was necessary for the addition of restriction sites for convenient cloning into pCAβ. Maps of expression vectors and cloning schemes can be found in Appendix C.

Table 2.3 Constructs. *All fluorescent proteins were fused to the N-terminus of the protein of interest except where an asterisk (*) indicates fusion to the C-terminus. CMV= cytomegalovirus, CAG = (C) Cytomegalovirus early enhancer, (A) promoter first exon and intron of chicken beta-actin gene, (G) splice acceptor of the rabbit beta-globin gene.*

Origin	Cat. #	Gene	Fusion protein	Promoter	Bacterial resistance
J.Chilton		CLCC1	FLAG*	CAG	Ampicillin
J.Chilton		CLCC1-Asp25Glu	FLAG*	CAG	Ampicillin
J.Chilton		CLCC1	eYFP	CAG	Ampicillin
J.Chilton		CLCC1-Asp25Glu	eYFP	CAG	Ampicillin
IHC		CLCC1	eYFP and FLAG	CAG	Ampicillin
IHC		CLCC1 isoform 2	eYFP	CAG	Ampicillin
IHC		CLCC1 isoform 3	eYFP	CAG	Ampicillin
IHC		CLCC1 isoform 4	eYFP	CAG	Ampicillin
IHC		KDEL	mCherry	CAG	Ampicillin
J.Chilton		R-Pre	RFP	CAG	Ampicillin
A.Ververis		SigmaR1	eGFP	CMV	Ampicillin
Addgene	48138	hSpCas9	eGFP	CBh	Ampicillin

Addgene	64324	Cas9	mCherry	CBh	Ampicillin

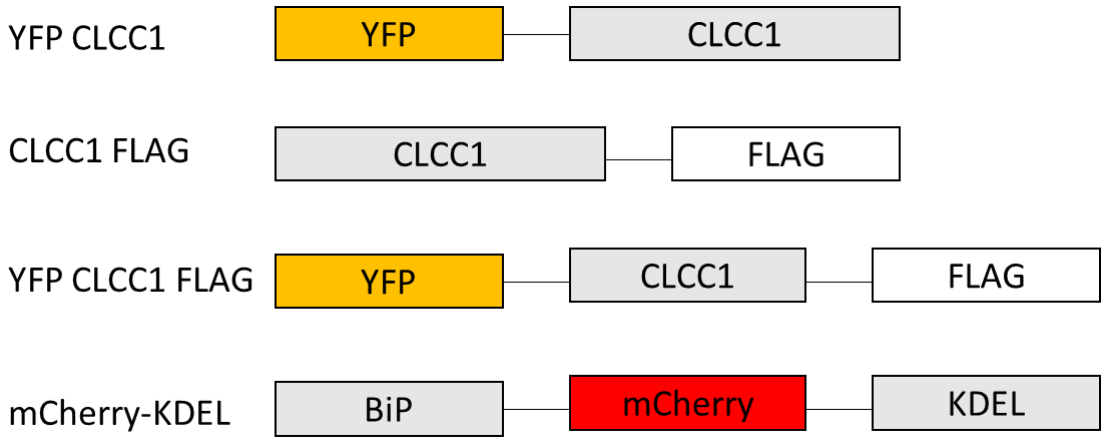

Figure 2.1 Schematics of fusion proteins reported in Table 2.3

2.12 Plasmid preparation

All work with live bacteria was carried out under sterile conditions, using a category 2 biological safety cabinet, sterile consumables and sterile media. Plasmids ordered from Addgene arrived as a live bacterial stab culture, they were streaked out onto Luria agar plates containing 1 µg/µl of ampicillin. Plates were incubated overnight at 37 °C for the formation of the colonies.

Colonies were selected from the agar plate and individually cultivated in 5 ml of LB broth supplemented with the appropriate antibiotic in a 20 ml sterile bacterial tube (VWR), shaken at 220 rpm overnight at 37 °C.

To assess the presence of the correct plasmid, 1.5 ml of bacterial culture was collected and centrifuged at 17,900 x *g* for 1 min, the supernatant was

discarded. The QIAprep Spin Miniprep protocol was followed (Qiagen): 250 µL of P1 solution (50 mM Tris-HCl, pH 8.0; 10 mM EDTA; 100 µg/ml RNAse A, without LyseBlue reagent) was added to the tube and the bacterial pellet was resuspended by vortexing. 250 µL of P2 solution (200 mM NaOH; 1% w/v SDS) was added and tubes inverted 6 times, bacterial lysis was neutralised with 350 µL of N3 buffer (a proprietary acetate-buffered solution containing chaotropic salt). The solution was then centrifuged at 17,900 x *g* for 10 min to eliminate the cellular debris, the supernatant was collected and placed in a QIAprep spin column and centrifuged at 17,900 x *g* for 1 min. The flow-throw was discarded and the column washed by addition of 750 µL of Buffer PE (proprietary solution with high ethanol and low salt concentrations). The column was again centrifuged at 17,900 x *g* for 1 min, the flow-through discarded, and the column was centrifuged as before to eliminate residual ethanol. The column was transferred to a clean microfuge tube and the DNA eluted with 50 µL of molecular biology grade water, the column was incubated 1 min before the final spin at 17,900 x *g* for 1 min.

Midipreps were used to obtain high yields of plasmid DNA (approximately 0.3-0.5 µg/µl), using HiSpeed Midi Prep Kit (Qiagen). Fifty µl of starter culture were diluted 1:1000 in 50 ml of LB broth with the appropriate antibiotic selection and grown overnight. Bacteria were spun at 4000 x *g* for 15 min and suspended in 6 ml of pre-chilled Buffer P1. The cells were lysed by adding 6 ml of buffer P2, mixing by inversion 6 times and incubating for 5 min at room temperature. Precipitation of cellular debris was carried out using 6 ml of buffer P3 (3 M potassium acetate, pH 5.5) and the tube was inverted 6 times, the mixture was then added to a QIAfilter Midi Cartridge and incubated at room temperature for 10 min. At the same time the Qiagen HiSpeed Midi Tip was equilibrated with

the addition of 4 ml of Buffer QBT (750 mM NaCl; 50 mM MOPS, pH 7.0; 15% v/v isopropanol; 0.15% v/v Triton X-100), emptied by gravity. Cell lysate was pushed into the column where the lysate flowed through under gravity. The column was washed with 20 ml Buffer QC (1 M NaCl; 50 mM MOPS, pH 7.0; 15% v/v isopropanol) and the DNA was eluted from the column adding 5 ml Buffer QF (1.25 M NaCl; 50 mM Tris-HCl, pH8.5; 15% v/v isopropanol). DNA was precipitated by the addition of 0.7 volumes of isopropanol, the tube was inverted 6 times to mix the components and incubated 5 min at room temperature. Precipitated DNA was pushed through a QIAprecipitator module and washed with 2 ml of 70% (v/v) ethanol. DNA was recovered by addition of 750 µL of Buffer TE (10 mM Tris-HCl, pH 8.0; 1 mM EDTA)

The appropriate amount of DNA was precipitated using 2 volumes of 100% ethanol and 10% 3 M sodium acetate pH 5.2 for 30 min at -25 °C. The DNA was then centrifuged at 17,900 x *g* for 30 min, supernatant discarded, and once the ethanol had evaporated the DNA was resuspended in the appropriate amount of Buffer TE to obtain a final concentration of 1 µg/µl.

Once the plasmid has been confirmed by restriction digestion the bacteria culture was stored in the form of a glycerol stock. Eight hundred µl of bacteria were added to 200 µl of sterile glycerol in a microfuge tube, mixed by vortexing, and stored at -80 °C.

2.13 Restriction digestion

Restriction digestion of plasmid DNA was carried out at 37 °C (or other optimal temperature for enzyme) for 1 h. One µg of plasmid DNA were mixed with 5.6 µl of water, 1 µl of the 10x buffer and 2-4 U of restriction enzyme.

2.14 Primers design for plasmid DNA

All primers (Table 2.4) for cloning the gene of interest into pILES and pClink were designed having flanking sequences containing convenient restriction sites for restriction digest whilst following the general rules as described in Paragraph 2.5.

Table 2.4 Primers used to clone the gene of interest into plasmids.

Sequence (5'-3')	Forward	Reverse complement	Restriction site	Gene
ATTAGTCGACCTAGCAGCTGCTGACCGG		X	Sal I	CLCC1
ATATAAGCTTGGACTTTTTCATGATTTTGAAACATGGAAGTGGC	X		Hind III	CLCC1 isoform 2
ATATAAGCTTGGACTTCTAGCTTTTGCACAGCATCAGGCTGAAG	X		Hind III	CLCC1 isoform 3
ATATAAGCTTGGACTTGCACTTGCAGTTACATTCACCACATTGG	X		Hind III	CLCC1 isoform 4
AATAGGATCCATGAAGCTCTCCCTGGTGGCCGCGATGCTGCTGCTGCTCAGCGCGGCGCGGGCCGTGAGCAAGGGCGAGGAGGATAAC	X		Bam HI	BiP
ATATCTCGAGTCATAGCTCGTCTTTCTTGTACAGCTCGTCCATGCC		X	Xho I	KDEL

2.15 Polymerase chain reaction for amplifying plasmid DNA

Plasmid DNA primers were designed to have flanking sequences containing restriction enzymes sites whilst following the rules described in paragraph 2.5. PCR was carried out in a total volume of 50 µl as follows: 100 ng of template DNA, 1X polymerase buffer, 200 µM dNTPs (NEB), 3 U Pfu polymerase (Promega), 25 pmol of each primer. The PCR was performed using the following programme: 95 °C for two minutes to denature the DNA, 30 sec of DNA strand melting, and 45 sec annealing step at 55 °C. The extension step lasted 1 min per Kb of final PCR product. Melting, annealing and extension steps were repeated 35 times, followed by a final heating to 72 °C for 10 min for the final extension. The PCR was performed using the SimpliAmp Thermal Cycler, Applied Biosystems by Life Technologies. A 5 µl aliquot was taken from the tube, combined with DNA loading buffer and subjected to electrophoresis on a 0.8 % (w/v) agarose gel in TAE buffer containing 1:20,000 SYBR Safe (Life Technologies) to verify that the amplicon was of the predicted size. The PCR product was purified from unwanted enzymes and nucleotides using QIAquick PCR purification kit before restriction digestion. One volume of PCR sample was mixed with 5 volumes of Buffer PB and 10 µl of 3 M sodium acetate pH 5.0. The mixture was placed in a QIAquick spin column and spun for 1 min at 17,900 x *g*, the flow-through discarded and the column washed with 750 µl of Buffer PE, containing ethanol. The flow-though was discarded and the column spun for 1 min at 17,900 x *g* to eliminate any residue of ethanol. The column was placed in a 1.5 ml microfuge tube and the DNA eluted in 30 µl of water upon centrifugation.

2.16 Plasmid DNA gel extraction

After restriction digestion, plasmid DNA was run on a 0.8% (w/v) agarose gel in TAE buffer containing 1:20,000 SYBR Safe (Life Technologies) until DNA bands could be resolved and the appropriate fragment excised and placed into a microfuge tube. The DNA was purified using a QIAquick Gel Extraction Kit (Qiagen). Following the manufacturer's instructions the volume of gel was estimated by weight 100 mg ≈ 100 µl. Three volumes of buffer QG were added, and the tube was incubated at 50 °C for 10 min to allow the agarose to melt. To ensure the correct pH of the mixture 10 µl of 3 M sodium acetate were added. The solution was placed into a QIAquick column and spun at 17,900 x *g* for 1 min. The column was washed with 750 µL of Buffer PE (proprietary solution containing high ethanol and low salt concentrations) and spun at 17,900 x *g* for 1 min. The flow-through was discarded and the column spun again at 17,900 x *g* for 1 min to remove the residual buffer. The column was then transferred to a clean microfuge tube and DNA eluted in 30 µl of molecular biology grade water, by centrifugation at 17,900 x *g* for 1 min.

2.17 Ligation

To ligate DNA in the plasmid backbone the following mixture was used: 1 µl 10X T4 Ligase Buffer (500 mM Tris-HCl; 100 mM $MgCl_2$; 10 mM ATP; 100 mM DTT; NEB); 2 U T4 DNA Ligase (NEB), 80 ng of restriction digest backbone and 240 ng restriction digest insert. The mixture was incubated at 14 °C overnight.

2.18 Bacterial transformation

Forty µl of competent *E.Coli* DH5α (NEB) were thawed on ice and 1 µl of ligated DNA was added, and incubated for further 15 min on ice. Bacteria were heat shocked at 42 °C for 45 sec and immediately placed on ice for 2 min. Bacteria were added to LB broth supplemented with SOC (10 mM NaCl, 2.5 mM KCl, 10

mM $MgSO_4$, 20 mM Glucose, 10 mM $MgCl_2$) and placed in a shaker at 37 °C for 1 hour at 225 rpm to allow the expression of bacterial proteins. The bacteria were centrifuged at 4000 rpm for 2 min, resuspended in 100 µl of media and plated in an agar plate containing the appropriate antibiotic.

2.19 Embryonic chick retinal ganglion cell isolation and nucleofection

Fertilized hens' eggs (*Gallus gallus*) (Henry Stewart & Co. Ltd., Lincs.) were incubated in a humidified, forced-draft incubator (Lyon, USA) at 38 °C. Embryos were staged according to Hamburger and Hamilton, 1992 [179]. At embryonic day 7 (E7) the egg shell was punctured using sterile scissors and an aperture in the shell was made to allow the extraction of the embryo. The chicken embryo was placed in a sterile dish containing HBSS (Hank's Balanced Salt Solution) Ca^{2+} and Mg^{2+}-free media and the head was separated from the body using a sterile forceps. Normal development of head and limbs was assessed before proceeding with the dissection. Eyes were separated from the head using a forceps and the soft tissue surrounding the eye was removed. The retinal pigmented epithelium was gently separated from the retinal ganglion cell layer, the lens and the vitreous humor were carefully removed as well. The resulting white layer of tissue was the retinal ganglion cell (RGC) layer.

Explants were centrifuged at 800 rpm for 3 min at room temperature (RT), HBSS aspirated and replaced with 1 ml of trypsin, the tube was placed at 37°C for 10 min to allow dissociation of the cells. Trypsin was inhibited by adding an equal volume of DMEM supplemented with 10% chicken serum, and cells were centrifuged at 1000 rpm for 5 min. Cells were resuspended in DMEM and 10% chicken serum and manually dissociated by trituration with a flame-polished glass Pasteur pipette. Cells were counted with a haemocytometer, and 5.0 x 10^5 cells were resuspended in 20 µL of P3 Primary Cell Nucleofector solution

(Lonza) with 0.4 µg of DNA, transferred to the nucleocuvette strips and nucleofected using the 4D-Nucleofector system X-unit (Lonza), DR-114 programme (parameters not disclosed by Lonza). Cells were removed from the strip and seeded in a 30 mm diameter plastic dish containing 2 ml of pre-warmed Neurobasal medium (Phenol-red free, Glutamine free (Gibco)), supplemented with 180 µM Hepes (Sigma-Aldrich), 0.5 mM L-Glutamine, 10 U/mL penicillin/streptomycin, and 2% B27 supplement, for 1h, to allow fibroblasts and other non-neuronal cells to adhere to the dish. The desired number of cells was then seeded on acid etched (1 M HCl, 1 hour at 65 °C), ethanol sterilised, 13 mm diameter glass coverslips (Karl Hecht, Thermo Fisher) treated with poly-D-Lysine (20 µg/ml, 30 min, room temperature) and Laminin (20 µg/ml, 1 hour at 37 °C). RGC were cultivated overnight in fully supplemented Neurobasal media. After 24 h cells were fixed with a mixture of 4% Paraformaldehyde and 0.2% Glutaraldehyde for 15 min at 37 °C. Fixative was removed and coverslips rinsed 3 times for 5 min each with 1XPBS.

2.20 Cell line culture

Each cell line was cultivated in its own medium as stated in the Table 2.1 and incubated at 37 °C, 5% CO_2, and routinely passaged at 80-90% confluency. Cells were grown on 13 mm diameter glass cover slips and transfected with Lipotectamine LTX (Invitrogen) when 60-70% confluency was reached. Following the manufactures instructions plasmid DNA was combined with serum-free DMEM and incubated for 5 min at room temperature. The specified amount of Lipofectamine LTX was combined with the mixture and incubated 30 min at room temperature. The mixture was then added to the culture media present in the dish and the cells were incubated for a further 18-20 h to allow expression of the transfected plasmid.

2.21 Cell treatments

2.21.1 MitoTracker

MitoTracker™ Red CMXRos (M7512, Thermo Fisher) was dissolved in DMSO and used at a final concentration of 150 nM, cells were treated for 15 min at 37 °C. Cells were washed 3 times with 1X PBS and then fixed with 4% (w/v) of PFA.

2.21.2 ER stressors

Thapsigargin (T-650; Alomone Labs) was dissolved in DMSO, cells were treated with a final concentration of 5 µM for 30 min at 37 °C. Tunicamycin (T7765; Sigma Aldritch) was dissolved in DMSO and cells were treated with a final concentration of 2 µg/ml for 30 min at 37 °C.

2.21.3 Metabolic stressors

2-Deoxy-D-glucose (2-DG) (D8375; Sigma Aldritch) was dissolved in NIH/3T3 culturing media (Table 2.1) at a final concentration of 100 mM. Oligomycin A (75351; Sigma-Aldritch) was dissolved in DMSO and used at a concentration of 50 µM. Lonidamine (1-(2,4-Dichlorobenzyl)-1H-indazole-3-carboxylic acid) (L4900; Sigma Aldritch) was dissolved in DMSO and used at a final concentration of 400 µM. 17-AAG (17-(Allylamino)-17-demethoxygeldanamycin) (A8476; Sigma Aldritch) was dissolved in DMSO and used at a final concentration of 100 nM. All these treatments were carried for 20 min at 37 °C.

2.21.4 SigmaR1 agonist and antagonist

PRE-084 hydrochloride (2-(4-Morpholinethyl) 1-phenylcyclohexanecarboxylate hydrochloride) (#0598; Tocris) was used as SigmaR1 agonist, while BD1047 dihydrobromide (N-[2-(3,4-Dichlorophenyl)ethyl]-N-methyl-2-(dimethylamino)ethylamine dihydrobromide) was used as antagonist of

SigmaR1. Both of them were dissolved in DMSO and used at final concentration of 10 μM for 30 min at 37 °C.

2.22 Freezing cell lines

Cells were harvested using trypsin when plates were 70% confluent, and spun at 1000 rpm. Media was aspirated and cells were resuspended in freezing media containing 10% DMSO (Invitrogen), 20% FBS and 80% serum free DMEM and placed in cryovials (Starstead). Cryovials were inserted in Mr. Frosty (ThermoFisher) and kept at -80 °C for 24 h prior to long-term storage in liquid nitrogen.

2.23 CRISPR/Cas9 gene editing

sgRNA oligonucleotides were designed using Benchling (https://benchling.com/) to disrupt Exon 2 and Exon 3 of the human CLCC1 gene. sgRNA sequences (Table 2.5) were chosen based on the optimal prediction scores of on target and off target effects, and for the presence of the sequences in all known CLCC1 isoforms. Unique binding to the CLCC1 sequence was assessed with BLASTN (NCBI) (https://blast.ncbi.nlm.nih.gov) and BLAT (UCSC) (https://genome.ucsc.edu/). Oligonucleotides were purchased from Integrated DNA Technologies (IDT).

Table 2.5 gRNA sequences

sgRNA	Sequence	On target prediction	Off target prediction
Exon 2 top	caccGCCAGCAACAGACATTCACAA,	77.1	63.5
Exon 2 bottom	aaacTTGTGAATGTCTGTTGCTGGC	77.1	63.5
Exon 3 top	caccGTCATCAGCACATGACAAGTC	56.9	69.6
Exon 3 bottom	aaacGACTTGTCATGTGCTGATGAC	56.9	69.6

2.23.1 Annealing

Oligos were reconstituted at 100 µM in ddH_20 and annealed following the recipe: 1 µl sgRNA top, 1 µl sgRNA bottom, 1 µl of 10X T4 PKN Ligation buffer (700 mM Tris-HCl; 100 mM $MgCl_2$; 50 mM DTT; pH 7.6; NEB), and appropriate units of T4 PKN ligase (NEB) (the PKN was used to phosphorylate the sgRNA, otherwise they are not able to be ligate with the plasmid). The thermocycler program followed the steps: 37 °C for 30 min, 90 °C for 5 min, ramp down to 25 °C at 5 °C min^{-1}, and then held at 25 °C infinite.

2.23.2 Ligation

Exon 2 gRNA was ligated into pSp-Cas9(BB)-2A-EGFP (PX458) (was a gift from Feng Zhang (Addgene plasmid # 48138 ; http://n2t.net/addgene:48138 ; RRID:Addgene_48138)) and Exon 3 gRNA was ligated into pU6-(BbsI)_CBh-Cas9-T2A-mCherry (was a gift from Ralf Kuehn (Addgene plasmid # 64324 ; http://n2t.net/addgene:64324 ; RRID:Addgene_64324)) following the recipe: 100 ng plasmid DNA, 2 µl gRNA diluted 1:200, 2 µl of 10X FastDigest Buffer (proprietary solution; Thermo Fisher), 1 µl of FastDigest BpiI (Thermo Fisher), 1 µl 10mM DTT, 1 µm ATP, appropriated units of T4 ligase (NEB), 2 µl of 10X T4 Ligation Buffer. Tubes were placed into the thermocycler and followed 6 steps of heat at 37 °C for 5 min, and 21 °C for 5 min.

2.23.3 Digestion

Bacterial transformation and minipreps were executed as described in sections 2.12 and 2.16.

The presence of gRNA inside the plasmid backbones was assessed with restriction digestion, using appropriate units of EcoRI (Promega) and FastDigest BpiI (Thermo Fisher) restriction enzymes and 1 µl of 10X Buffer H (900 mM

Tris-HCl; 100 mM $MgCl_2$; 500 mM NaCl; pH 7.5; Promega), at 37 °C for 1 hour. The correct size of the DNA bands was assessed on a 0.8% agarose gel in TAE buffer.

2.23.4 Nucleofection of SH-SY5Y cells

At 80% confluency SH-SY5Y cells were washed with HBSS and harvested using trypsin for 5 min at 37 °C, collected in a centrifuge tube and centrifuged at 1000 rpm for 5 min. Cells were resuspended in 5 ml of media and counted using a haemocytometer. One million cells per nucleofection were centrifuged and resuspended in 100 µL of SF Cell Line 4D-Nucleofector solution (Lonza) containing 2 µg total of a mixture of plasmid DNAs and transferred to the nucleocuvette vessel. Nucleofection was performed in the 4D-nucleofector X unit using the programme CA-137 (parameters are not disclosed by Lonza). Five-hundred µL of warmed media was used to resuspend the cells in the nucleocuvette and transferred to a 100mm diameter petri dish. Cells were incubated overnight at 37 °C to allow the expression of plasmid DNAs.

2.23.5 Fluorescence-activated cell sorting

Twenty-four hours after the nucleofection cells were harvested with trypsin and resuspended in 1 mL DMEM/F-12 phenol-red free supplemented with 10 U/mL penicillin/streptomycin and 10% foetal bovine serum. Using the FACS ARIA III (BD Biosciences), cells expressing GFP and mCherry were selected. EGFP was detected with an excitation wavelength of 488 nm and 530/30 nm bandpass filter, mCherry plasmid was detected with an excitation wavelength of 561 nm and 610/20 nm bandpass filter. Single, sorted cells were placed in a 96 well plate containing 100 µL of pre-warmed media and incubated at 37 °C.

2.23.6 DNA extraction

Confluent cells in the 96 well plate were dissociated by pipetting, 20% of the cell suspension volume was seeded in a 24 well plate, the remaining 80% of cells was used for the extraction of genomic DNA. Cells were centrifuged at 1000 rpm for 5min and resuspended in 250 µl of 1X Slagboom buffer (Table 2.1), and incubated at 37 °C for 45 min. Five µl of 10 mg/ml Proteinase K was added to the mixture and incubated at 60 °C for 1 hour. Genomic DNA was extracted using the phenol-chloroform method: 400 µl of 25:24:1 v/v UltraPure phenol:chloroform:isoamyl alcohol (Invitrogen) was added to the sample, mixed thoroughly and centrifuged at 14000 rpm for 2 min, this procedure was carried out twice. As residues of phenol could affect subsequent analysis, a supplementary wash with 400 µl chloroform was performed. The mixture was spun at 17,900 x *g* for 2 min and the upper layer collected. The DNA was precipitated by addition of 400 µl of isopropanol and centrifugation at 17,900 x *g* for 2 min. The DNA pellet was washed with 400 µl of 70% (v/v) ethanol and spun at 17,900 x *g* for 2 min. The ethanol was removed and once the pellet air-dried at 37 °C for a few minutes. The DNA was resuspended in 20 µl of Buffer TE, the concentration and quality of DNA were assessed as previously described.

2.23.7 Genotyping of CRISPR colonies

Primers for genotyping of CRISPR colonies were designed as described in Paragraph 2.5. Two pairs of primers were designed: one pair within the site to be deleted, and one pair of primers outside the deletion sites (Figure 2.2).

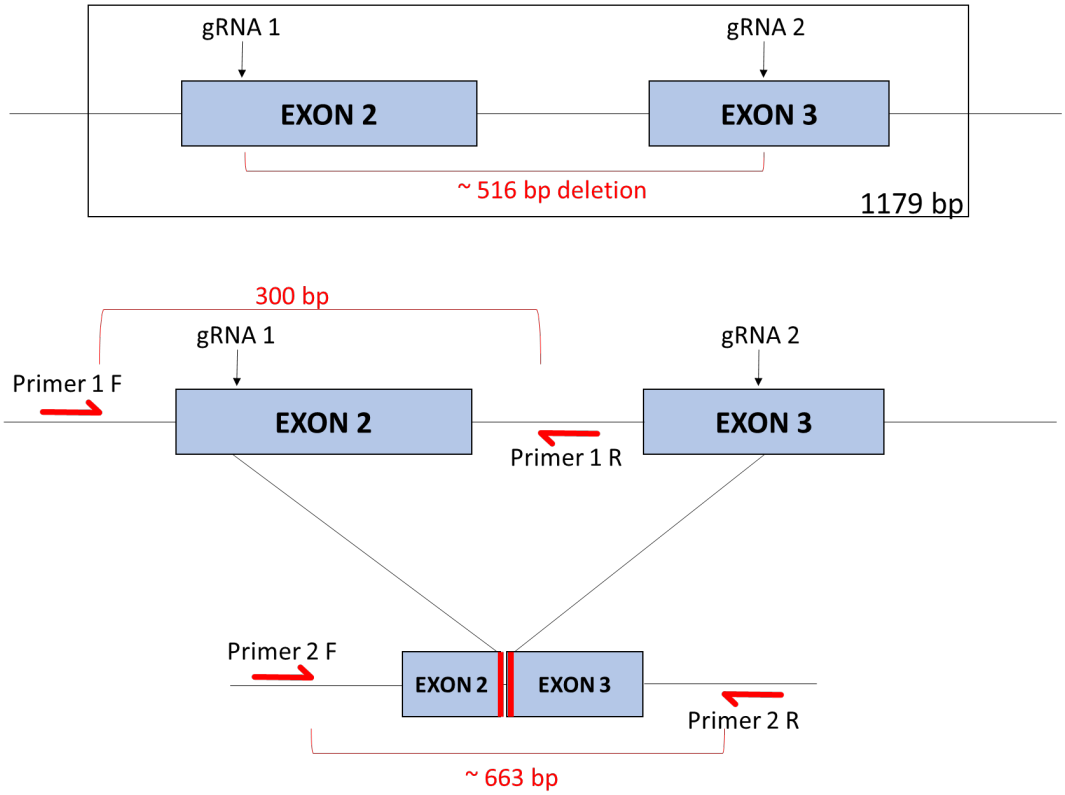

Figure 2.2 Schematics of genotyping strategy. *A segment of about 516 bp was targeted for deletion between exon 2 and axon 3 of CLCC1. Primers set 1 (Primer 1 F and Primer 1 R) were designed to amplify 300 bp of exon 2, inside the deleted region. An amplicon corresponding to the 300 bp would be present only if the deletion does not happen. If the deletion occurred, the primers set 2 (Primer 2 F and Primer 2 R) would be able to amplify a stand of about 663 bp of DNA corresponding to the initial segment of exon 2 and the final segment of exon 3. If the deletion doesn't occur, primers set 2 will amplify 1179 bp of DNA, corresponding to exon 2 and exon 3 and their surrounding introns.*

2.24 Western blotting

2.24.1 Cell lysate preparation for co-immunoprecipitation

To analyse the levels of endogenous proteins or fusion protein expression, cells were seeded in a 100 mm diameter dish and lysed when the 80% confluence was reached. Media was aspirated from the dish, and cells washed with 1X

PBS. Cells were trypsinised for 5 min at 37 °C, collected and centrifuged at 1000 rpm for 5 min. Media was aspirated and the cell pellet resuspended in 10 ml of ice-cold PBS, spun at 1000 rpm for 5 min. PBS was removed and cells resuspended in 700 µl of lysis buffer (20 mM Tris-HCl, 150 mM KCl, 0.1% Triton X-100, 1 mM PMSF, complete protease and phosphatase inhibitors (Sigma-Aldritch)), placed in a microfuge tube and rotated at 4 °C for 30 min. Afterwards, the lysate was centrifuged at 17,900 x *g* for 20 min at 4 °C, and the supernatant carefully transferred to a clean microfuge tube. For positive control whole lysate was used, while for negative control whole lysate minus the immunoprecipitated complexes was used.

2.24.2 Co-immunoprecipitation with Dynabeads

Co-immunoprecipitation (Co-IP) is used to study protein-protein interactions. Antibodies against the protein of interest are used to pull-down the protein complexes which are then visualised by Western blotting.

The co-immunoprecipitation was carried out using Dynabeads Protein A (Invitrogen). 25µl of beads were transferred to a clean microfuge tube, the supernatant was removed and the required concentration of antibody (see Appendix B) diluted in 200 µl of PBS + 0.02% (v/v) Tween-20 was added to the beads, incubated at room temperature for 1 hour, on a rotating wheel. The supernatant was removed and beads washed gently with 200 µl of PBS + 0.02% (v/v) Tween-20. Once the PBS was removed and the cell lysate was added to the beads and resuspended, the tubes were incubated for 2 hours at 4 °C, on a rotating wheel. The supernatant was collected and placed at -20 °C for further analysis. The beads were washed three times with washing buffer (20 mM Tris-HCl pH 8.0, 150 mM KCl, 10% (v/v) Triton X-100, and protease inhibitors) and transferred to a clean microfuge tube. Supernatant was removed

and the elution of protein was carried out using 50 µl of elution buffer (4X Nu Page LDS Sample buffer (Invitrogen), 10% beta-mercaptoethanol (v/v)), heating the sample for 10 min at 70 °C. The supernatant containing the precipitated proteins was collected in a clean tube and used immediately for Western Blotting or frozen at -80 °C for future use.

2.24.3 Co-immunoprecipitation with GFP-Trap

GFP-Trap was carried out to immunoprecipitate proteins tagged with GFP/YFP. HEK293 cells in a 100 mm plate were transfected with YFP CLCC1 WT/Asp25Glu, as previously described in Paragraph 2.20. After 24h from the transfection, cells were harvested using trypsin and spun at 1000 rpm for 5 min. Supernatant was aspirated and the cell pellet was resuspended in ice-cold PBS, spun again and cells were resuspended in GFP-Trap lysis buffer (1% NP-40, 130 mM NaCl, 20 mM Tris, ph 8.0). Tubes were placed on a rotating wheel at 4 °C for 30 min, and the lysate was clarified through a centrifugation at max speed (14800 rpm) for 15 min at 4 °C (Thermo Scientific Heraeus Fresco 21 Centrifuge).

Ten µl of GFP-Trap beads (Chromotek) (per 100 mm plate) were transferred to a centrifuge tube and spun at 700 x *g* for 1 min. The tube was rotated at 180 º and centrifuged again at 700 x *g* for 10 sec. Beads were left 1 min to incubate on ice and then the supernatant was discarded. Beads were washed with 500 µl of lysis buffer and centrifuged for 1 min at 700 x *g.* The supernatant was discarded, the beads were resuspended in protein lysate and incubated overnight on a rotating wheel at 4 °C. Beads were centrifuged for 1 min at 700 x *g* and the supernatant was removed and stored at -80 °C (subsequently used as the Co-IP negative control). Beads were washed twice with 400 µl of lysis buffer and spun for 1 min at 700 x *g,* 4 °C. Immunocomplexes were eluted

using Laemli buffer at 95 °C for 5 min, in a total volume of 30 µl. Tubes were spun at 700 x *g* for 1 min and stored at -80 °C.

2.24.4 Subcellular fractionation

SH-SY5Y cells (wild type and CLCC1$^{-/-}$ KO) were seeded on 150 mm dish, and harvested once 90% confluent. Cells were resuspended in 1.5 ml of 1X STE (Sucrose – Tris – EGTA buffer, Table 2.1) + 0.5% BSA and homogenate in a manual homogeniser with 20 strokes. Homogenate was clarified with a spun at 1000 x *g* for 10 min at 4 °C. Ultracentrifuge tubes were filled with 25% Percoll solution (1/4 Percoll, 1/4 2X STE buffer, 2/4 1X STE + 0.5% BSA) and the clarified homogenate was put on top. Tubes were spun at 80.000 x *g* average for 40 min at 4 °C (Beckmann Coulter). The supposedly upper layer containing the ER and lower mitochondria layer were collected separately and washed 3 times with STE buffer without BSA, the layers were spun at 10.400 x *g* for 10 min at 4 °C. The pellet obtained was resuspended in STE buffer without BSA, and spun at max velocity for 2 min. The pellet was resuspended with STE buffer without BSA and spun, this process was repeated again and the pellet resuspended in PBS, spun again and finally resuspended in 200 µl of PBS.

2.24.5 Protein quantification

Quantification of protein concentration in clarified cell lysate was carried out using the Pierce bicinchoninic acid (BCA) Protein Assay Kit (Thermo) according to the manufacturer's protocol. In a 96-well plate, bovine serum albumin (BSA) protein standard at 2 mg/ml was diluted to 0.2-1.2 µg/ml in 1:10 lysis buffer:PBS. Samples were also diluted 1:10 with PBS. Both samples and standards were loaded into wells in triplicate. BCA solution was prepared mixing 50 parts of reagent A and 1 part of reagent B, 200 µl were added to each well containing samples and standards.

Plate was shaken for 8 min at RT on an orbital shaker (LSE Low Speed Orbital Shaker, Corning), and absorption at 562 nm was measured using PHERAstar FS microplate reader (BMG Labtech) and the concentrations of each sample were calculated against the standard curve.

2.24.6 SDS polyacrylamide gel electrophoresis.

To separate the proteins based on their size, electrophoresis on polyacrylamide gel was carried out. The procedure is also called SDS-Page (Sodium Dodecyl Sulphate Poly Acrylamide Gel Electrophoresis). The percentage of acrylamide inside the gel determines the separation of proteins (Table 2.6).

Table 2.6 Determination of gel percentage

Protein size (kDa)	Gel percentage (%)
4-40	20
12-45	15
10-70	12.5
15-100	10
25-200	8

SDS-PAGE gels were prepared using the Mini-PROTEAN TM Tetra Handcast System (BioRad), according to the recipe in the Table 2.7. Ammonium persulphate (APS) and N,N,N',N'-tetramethylethane-1,2-diamine (TEMED) were added last to initiate polymerisation of the acrylamide. For Co-IP 10 µl of each sample were loaded in each well of the gel and run at 150V on ice for 90 min.

***Table 2.7 Gel recipes**. The volumes (in ml) are for 40% Acrylamide/Bis solution (Fisher Scientific) 37.5:1 ratio and makes 2 gels.*

	Stack	***Resolve***				
%	**4**	**7.5**	**10**	**12**	**15**	**20**
dd.H2O	5.28	13.7	12.1	10.9	9.0	2.5
40% Acrylamide/Bis	0.7	4.7	6.3	7.5	9.4	12.6
1.5M Tris HCL pH 8.8	-	6.25	6.25	6.25	6.25	6.25
1.0M Tris HCL pH 6.8	0.88	-	-	-	-	-
10% SDS	0.07	0.25	0.25	0.25	0.25	0.25
10% ammonium perisulfate (APS)	0.07	0.125	0.125	0.125	0.125	0.125
TEMED	0.0025	0.0025	0.0025	0.0025	0.0025	0.0025
Volume (ml)	*7*	*25*	*25*	*25*	*25*	*25*

2.24.7 Transfer to membrane

After separation of proteins, the gel was allowed to equilibrate in transfer buffer for 10 min and re-hydrate. The gel was sandwiched between chromatography-grade filter paper (GE Healthcare) and proteins were transferred onto Immobilon-P polyvinylidene difluoride (PDVF) transfer membrane (Merck), applying current at 250 mA.

2.24.8 Probing and immunodetection

To prevent non-specific binding of the antibody to the membrane, after the transfer of the proteins, the membrane was blocked in 5% (w/v) skimmed milk (Oxoid) or 5% BSA (Sigma) in Tris-Buffered Saline + 0.01% (v/v) Tween-20

(TBS-T) for 1 h at RT. The membrane was removed from the blocking solution and incubated overnight with the appropriate primary antibody (Appendix B, Table 1). Afterwards the membrane was washed three times for 5 min with TBS-T to remove excess antibody and incubated for 1 h with the appropriate horseradish peroxidase (HRP) conjugated secondary antibody (Appendix B, Table 2). Proteins were detected using electrochemiluminescence and the LI-COR C-DiGit (LI-COR).

2.25 Immunocytochemistry

Cells were seeded at $1x10^4$ cells per 13 mm diameter coverslip and cultured for two days. Cells were fixed for 15 min at room temperature with 4% (w/v) paraformaldehyde, pre-warmed to 37 °C, added directly to the culture medium as matching volumes and then replaced with fresh pre-warmed paraformaldehyde. Coverslips were rinsed 3 times for 5 min each with 1X PBS to eliminate residual paraformaldehyde. Cells were permeabilized and the non – specific binding sites were blocked using lysine block (5% goat serum, 5% horse serum, 5 mM L-lysine, 0.2% Triton-X) for 15 min at room temperature. Primary antibodies (Appendix B, table 1) were diluted in lysine block and incubated with the cells for 1 hour at room temperature. Following 3 washes with 1X PBS, 5 min each, to eliminate unbound primary antibody, cells were incubated with the secondary antibody (Appendix B, table 2) for 1 hour at room temperature. DAPI (4,6- diamidino-2-phenylindole, dihydrochloride, Invitrogen) was used to stain the nuclei diluted 1:5000 in PBS for 5 min. Coverslips were washed 3 times for 5 min each to eliminate any residual antibody and DAPI, and were mounted on glass slides (VWR) using FluorSave (Calbiochem) mounting media, left to dry in the dark, at room temperature, overnight.

2.26 3-(4,5-Dimethylthiazol-2-Yl)-2,5-Diphenyltetrazolium Bromide (MTT) assay

To assess cell viability the MTT assay (Abcam) was used. The assay is based on the assumption that the metabolic activity of SH-SY5Y cells reflects the number of viable cells present in the dish. Water-soluble MTT (3-(4,5-dimethylthiazol-2-yl)-2,5-diphenyltetrazolium bromide) can be converted to insoluble formazan crystals through the mitochondrial succinate dehydrogenase. The measure of the resulting absorbance at OD 590nm is taken as proportional to the number of viable cells present in the plate.

Following manufacturer's instructions 10000 cells/well were seeded in a 96-well plate and cultivated for 24, 48, 72, and 96 h in 100 µl of SH-SY5Y media. Prior to the addition of MTT reagent, cells were treated for 30 min at 37 °C with 5 µM of Thapsigargin (Alomone Labs) or 2 µg/ml of Tunicamycin (Sigma-Aldritch). Control cells were treated with the same amount of DMSO. After the treatments, media was aspirated and 50 µl of serum-free media and 50 µl of MTT reagent were added to each well. For the background control wells 50 µl of fully supplemented media and 50 µl of MTT reagent were used. The plate was incubated at 37 °C for 3 h. Afterwards, 150 µl of MTT solution were added into each well and the plate was wrapped in foil and shaken for 15 min. Absorbance at OD 590 nm was read using the PHERAstar FS microplate reader (BMG LABTECH).

2.27 Microscopy and image analysis

Fluorescence microscopy was performed with a Leica TSC SP8 inverted confocal laser scanning system with a piezoelectrict stage, HC Plan-Apochromat x63 (1.4 NA) oil objective, and temperature-controlled environmental chamber. Leica Application suite X was used to control the

microscope on the PC. Image analysis was performed using Fiji [180].

2.28 Statistical analysis

Statistical analysis was performed using Graphpad Prism 5. Differences between groups were assessed using two-way ANOVA with a post-hoc Bonferroni test.

For not normally distributed data, a Kruskal-Wallis test with Dunn's multiple comparisons post hoc test was used to assess differences. Not normally distributed data were also analysed with Mann Whitney U test.

2.29 Web resources

www.benchling.com/

www.bioinformatics.nl/cgi-bin/primer3plus/primer3plus.cgi

https://genome.ucsc.edu/

https://blast.ncbi.nlm.nih.gov

https://prosite.expasy.org/cgi-bin/prosite/mydomains/

https://www.uniprot.org/

https://string-db.org/

http://www.hgmd.cf.ac.uk/ac/index.php

https://biorender.com/

https://www.ncbi.nlm.nih.gov/clinvar/

CHAPTER 3

MUTATION IN THE INTRACELLULAR CHLORIDE CHANNEL CLCC1 ASSOCIATED WITH AUTOSOMAL RECESSIVE RETINITIS PIGMENTOSA

CHAPTER 3: MUTATION IN THE INTRACELLULAR CHLORIDE CHANNEL CLCC1 ASSOCIATED WITH AUTOSOMAL RECESSIVE RETINITIS PIGMENTOSA.

3.1 Introduction

RP is a heterogeneous retinal disease caused by alteration of genes involved in a broad range of molecular roles in the maintenance and function of photoreceptors. The molecular pathways affected by the pathological events leading to the disease are multiple, they involve both photoreceptor-specific functions, and more generic pathways related to proteins associated with RNA or development [181].

One of the most common and best studied genes associated with RP is *RHO,* which encodes for rhodopsin. Most of its alterations are associated with adRP however, it could also cause arRP and CSNB. Pathways affected were classified depending on where the variant resides within the protein; C-terminus variants affect the post-Golgi trafficking and OS targeting, transmembrane domains alterations cause misfolding, ER retention and instability, a single variant in the position Asp135 has been associated with disruption of vesicular traffic and endocytosis [52]. Post-translational modifications and reduced stability have been associated with variants in the N-terminus of RHO [52]. Recently, *REEP6* gene variants have also been associated with RP [182] lack of REEP6 results in the increased amount of endoplasmic reticulum (ER) membrane present near the OS, the number of mitochondria and the trafficking of cGMP to the OS [183].

RNA splicing can be also affected in genetic alterations associated with RP, for example an Asp170Gly variant in *RP9* may cause RP by altering splicing of

retinal genes through a decrease in RP9 phosphorylation [184, 185]. Similarly, the pre-mRNA splicing factor *DHX38* has been associated with RP and it was first discovered in a Pakistani family [186].

Proteins associated with developmental pathways have been also linked to RP, an example of this is *SEMA4A* [187, 188], semaphorins act as repulsive or attractive cue for growth cones during axon guidance. Loss of function of *SEMA4A* in mice showed reduced length of the OS and defect in the RPE layer, therefore it has been suggested that Sema4a functions as transmembrane ligand for a receptor present on photoreceptors [189]. Another report suggested that variants in SEMA4A cause oxidative stress, ER stress, and defective endosomal sorting [190, 191]. Variants in this gene have been firstly reported in Pakistani families [187].

As introduced above, genes identified in Pakistan have helped to understand the molecular bases of RP. Alongside *SEMA4A* and *DHX38*, *ZNF513* and *CC2D2A* have also been described for the first time in Pakistani population. *ZNF513*, a zinc finger DNA-binding protein, regulates gene expression of photoreceptor-specific genes; sequence alterations in this gene cause the loss of binding of ZNF513 with its targets [192]. *CC2D2A,* which has been associated with RP and mental retardation [193]*,* is involved in Rab8-dependent vesicular trafficking [194]. Loci on chromosomes 1, 2, and 11 have also been associated with RP exclusively in the Pakistani population [169, 195, 196] however, the genes alteration within the loci which cause RP have not been defined yet.

Every year new genes and new molecular pathways associated with RP in Pakistani communities have been highlighted, expanding the knowledge in

terms of clinical presentation, genetic, and molecular aspects, as well as the potential new treatments and management strategies that can be developed,

In this chapter, eight Pakistani families affected by arRP were investigated using cutting-edge genetic technologies, and a new genetic cause of their disease has been defined.

3.2 Results

3.2.1 Clinical findings of eight families affected by arRP

As part of an international study we investigated eight families with multiple affected individuals with arRP. Three families (families 1-3) were investigated at the University of Exeter (IBCS), and five (families 4-8) were investigated at the NEI, USA. Families 1 and 2 originated in Pakistan, Family 2 was from Bhakkar district, Punjab. Family 3 was a British-Bangladeshi family, investigated at Moorfields Eye Hospital. Families 4 to 8 originated from Punjab region in Pakistan.

Due to regional constraints, a variable amount of clinical information was available on each family. Affected individuals demonstrated broadly consistent findings typical of arRP. These included retinal findings of pale optic discs, retinal vessel attenuation, and intra-retinal pigment migration on fundoscopy, typical clinical presentations for arRP with night blindness being the initial symptom in the first or second decade of life in all affected individuals. Clinical findings of Family 5 and 8; the presenting symptom in both families were reported to be night blindness by approximately 10 years of age. All affected family members displayed moderate loss of visual acuity. The clinical characteristics of Family 4 were previously published [195].

Table 3.1 Clinical finding of affected individuals of Families 3, 5, and 8.

Family ID (individual)	Gender	Age	First symptoms	Age of onset	Visual acuity	Pale optic disc	Artery attenuation	Pigmentation
Family 3 (II:2)	Male	18	Night blindness	1-2	6/60			
Family 5 (V:1)	Male	24	Night blindness	11	6/60	Yes	Yes	Full fundus
Family 5 (IV:7)	Male	35	Night blindness	12	PL	Yes	Yes	Full fundus
Family 8 (V:3)	Male	30	Night blindness	10	6/60	Yes	Yes	Full fundus
Family 8 (V:4)	Male	26	Night blindness	9	6/60	Yes	Yes	Full fundus
Family 8 (V:6)	Female	28	Night blindness	9	6/60	Yes	Yes	Full fundus

Fundus photographs of individual V:1 of Family 5 (Fig. 3.1 (i-ii)), individual V:3 of Family 8 (Fig. 3.1 (iii-iv)) and individual IV:3 of Family 1 (Fig. 3.1 (vii-viii)) revealed findings similar to those seen in Family 4, including obvious bone spicule-shaped pigment deposits in the mid-periphery, waxy-pale optic discs, attenuation of the retinal arteries, and a generalised grayish carpet-like retinal degeneration as compared to a normal fundus (Fig. 3.1 (v-vi)). Affected members of Families 4 and 1 also showed maculopathy, which was not observed in Families 5 and 8. ERGs of affected individuals when performed as adults were non recordable (Fig. 3.2).

Family 3, individual II:1 presented with a history of night blindness from 1-2 years of age and an intermittent divergent squint with long-standing photophobia. Presenting visual acuity was 6/9 in each eye and at last review at age 18 years had deteriorated to 6/60 each eye with severely restricted visual fields to less than 15 degrees to confrontation (Table 3.1). There was a myopic astigmatic refractive error of right 0.25/-1.25 x 21° and left 0.25/-2.25 x 160°. Electrophysiology performed at age 7 was unrecordable. Colour fundus

photographs for the affected individual in family 8 revealed attenuated retinal vessels, mid-peripheral coarse pigment clumping and white dots at the level of the retinal pigment epithelium. Fifty-five degree fundus autofluorescence imaging show widespread loss of autofluorescence more marked over the pigment clumps in the mid-periphery. Optical coherence tomography (OCT) demonstrated loss of outer nuclear and photoreceptor layers throughout the macula with occasional small foci of retained photoreceptors (Fig. 3.3).

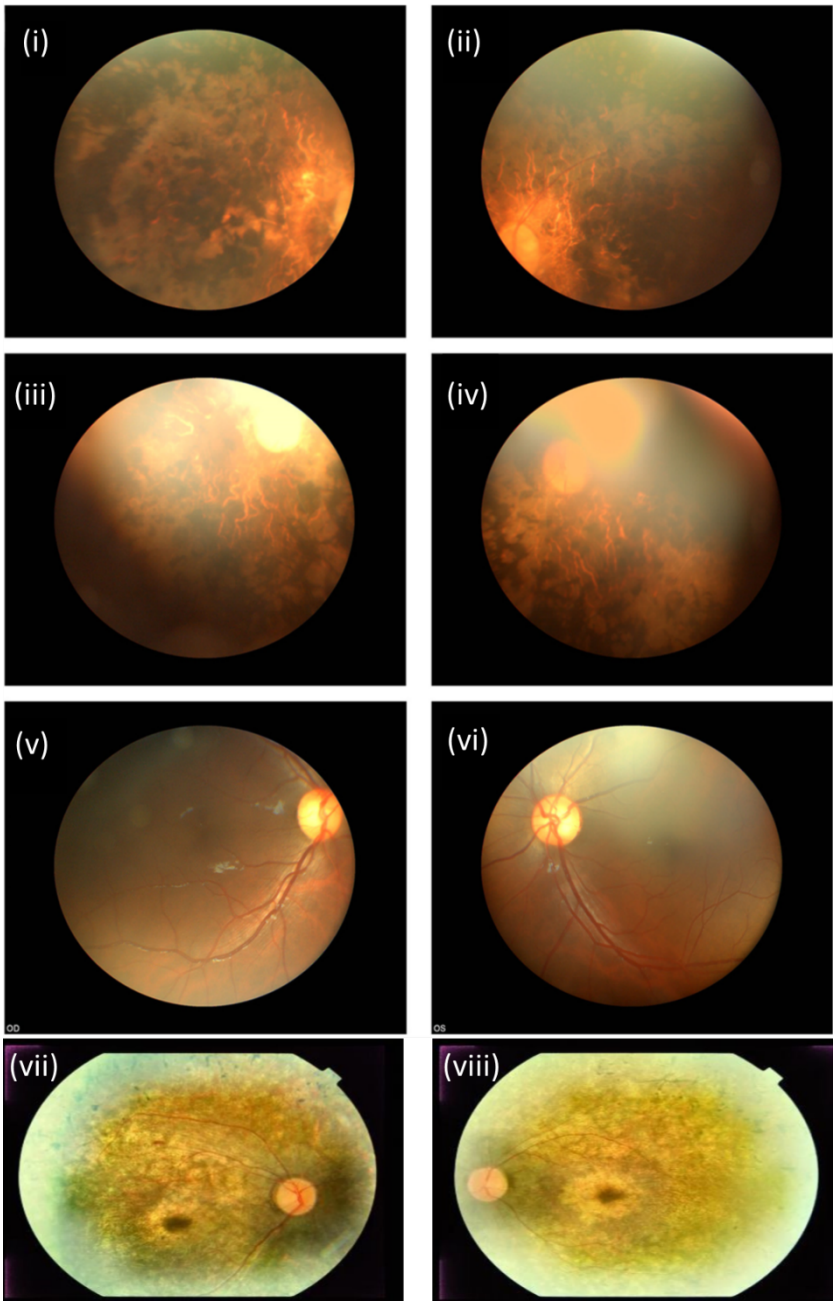

Figure 3.1 Fundus photographs. (i-ii) *Individual V:1 of Family 5 (right eye and left eye, respectively),* ***(iii-iv)*** *individual V:3 of Family 8 (right eye and left eye, respectively) and;* ***(vii-viii)*** *individual IV:3 of Family 1 showed bone spicule-shaped pigment deposits in the mid-periphery, pale optic discs, attenuation of the retinal arteries;* ***(v-vi)*** *healthy individual (right eye and left eye, respectively) showed normal fundus. Figure made at the NEI.*

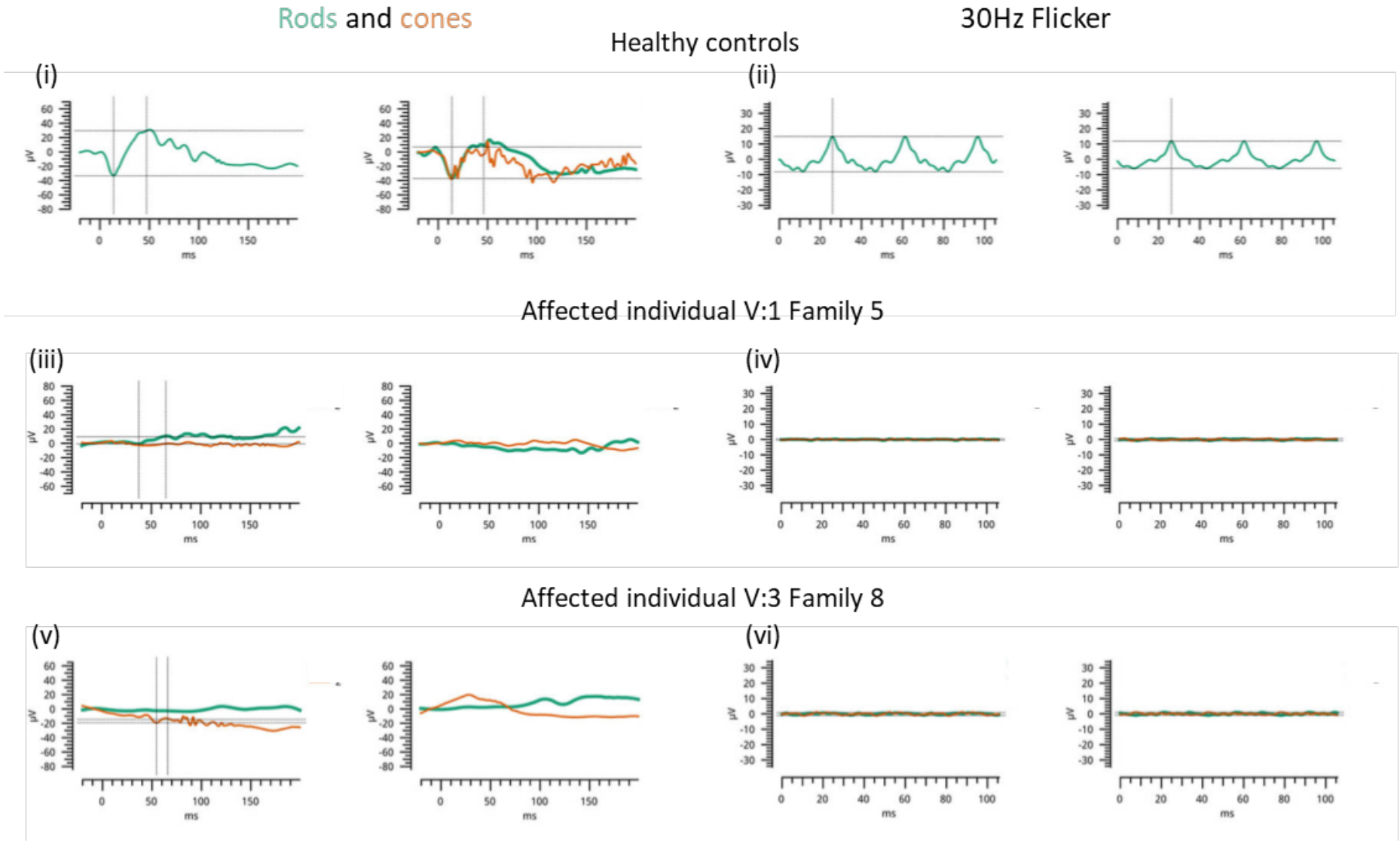
Rods and cones
30Hz Flicker
Healthy controls
(i)
(ii)
Affected individual V:1 Family 5
(iii)
(iv)
Affected individual V:3 Family 8
(v)
(vi)
µV
ms

Figure 3.2 ERG recordings of affected individuals. (i) *rod (green) and cone (orange) response: right eye and left eye, respectively; and* ***(ii)*** *30Hz flicker response: right eye and left eye, respectively of an healthy individual.* ***(iii)*** *rod (green) and cone (red) response: right eye and left eye, respectively; and* ***(iv)*** *30Hz flicker response of individual V:1 of Family 5.* ***(v)*** *rod (green) and cone (orange) response: right eye and left eye, respectively; and* ***(vi)*** *30Hz flicker of individual V:3 of Family 8. The affected individuals demonstrate loss of ERG responses in keeping with advanced RP. Y axis μV; X axis ms. Figure made at NEI.*

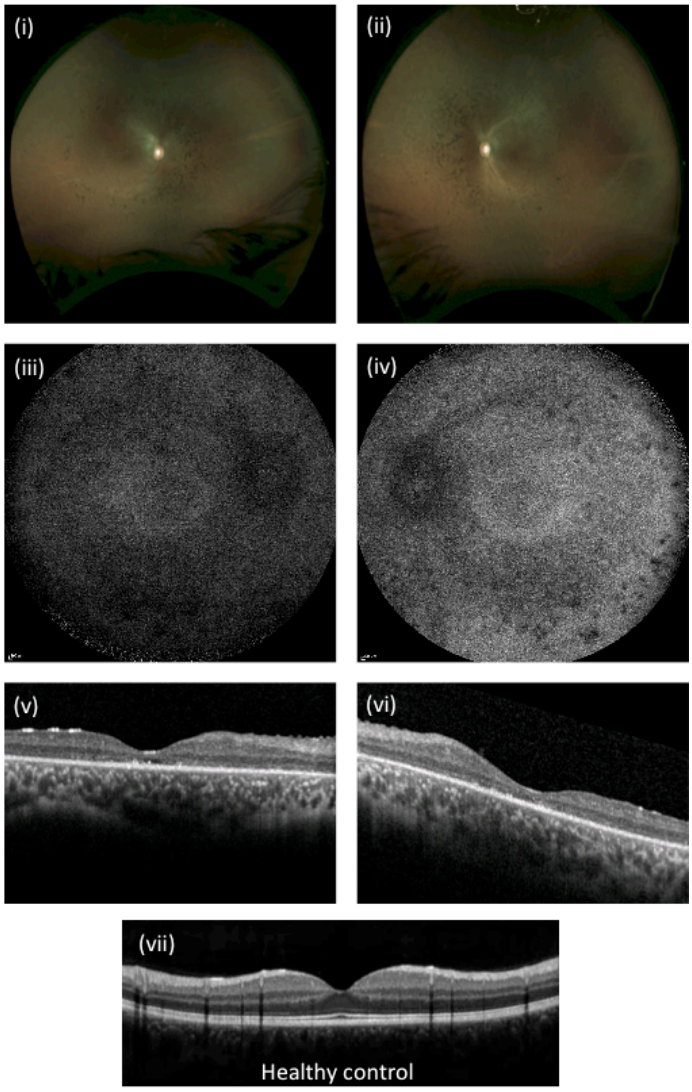

Figure 3.3 Fundus photographs of individual II:1, Family 3. (i-ii) *Fundus photographs (right eye and left eye, respectively) showed attenuated retinal vessels and mid-peripheral pigment clumping.* ***(iii-iv)*** *55 degree fundus autofluorescence imaging (right eye and left eye, respectively) showed loss of autofluorescence more marked over the pigment clumps.* ***(v-vi)*** *OCT (right eye and left eye, respectively) demonstrated loss of outer nuclear and photoreceptor layers throughout the macula with occasional small foci of retained photoreceptors. Photographs of individual II:1, Family 3 was taken at the Moorfield Eye Hospital.* ***(vii)*** *Healthy control. Section vii was adapted from Meunier et al [197].*

3.2.2 Genetic findings

For Family 1, 2 and 3, studies at IBCS involved whole-genome SNP mapping which identified a single notable homozygous region particular to affected individuals of a small 1.2Mb interval on chromosome 1p13.3 (flanked by markers rs17020437 and rs587727) [hg38]), demarcating the likely disease locus and indicative of the presence of a founder mutation causing the disease. In order to identify the causative mutation, WES was performed on a single affected individual for each family (III:1, Family 1; III:2, Family 2; II:1, Family 3). After filtering for call quality, potential pathogenicity, and population frequency, a single candidate genetic alteration was identified genome-wide which was located within the 1.2Mb critical interval; a missense alteration within the chloride channel CLCC-like 1 (*CLCC1*) gene (rs750180668; chr1:g.108950363G>T, NM_001048210.2:c.75C>A), predicated to result in a p.(Asp25Glu) amino acid substitution. The p.Asp25Glu substitution in CLCC1 is predicted to be damaging by bioinformatic analysis using Polyphen2 (HumDIV, 1, HumVar, 0.998), not tolerated by SIFT (0), and deleterious by Condel (0.546). It is absent from >200 ethnically matched control chromosomes, and the dbSNP and 1000 Genomes databases, although it is listed in heterozygous form in 12 individuals in the Genome Aggregation Database [198] (gnomAD: 12 heterozygotes and no homozygotes in the South Asian population, allele frequency = 0.0003924 in South Asians, 0.00004778 overall, (https://gnomad.broadinstitute.org/variant/1-109492985-G-T)).

In parallel with this, studies of families 4 to 8 were undertaken at NEI. Family 4 [61030] was screened using microsatellite genome-wide mapping, which identified a 3.4cM (3.05Mb) homozygous interval of chromosome 1p13.3 shared by all affected family members. To identify the causative gene, whole exome

sequencing was undertaken in a single affected family member (Individual 12, Family 4). The data was filtered (allele frequency in genome databases, and prioritising deleterious variants in the genetic interval, as well as genome-wide). As with studies of families 1-3 (above), this identified only a single candidate gene variant, again within the linked region (Fig. 3.4), involving the same homozygous c.75C>A, p.(Asp25Glu) missense variant in exon 1 of the *CLCC1* gene. Dideoxy sequencing confirmed co-segregation of *CLCC1* variant in families 1-8, and in 123 additional Pakistani arRP families identified 4 further additional apparently unrelated families in which the same c.75C>A, p.(Asp25Glu) alteration co-segregated with the condition (Families 5 [61031], 6 [61328], 7 [61244], and 8 [61224]). All four families were found to be linked to markers in the chromosome 1p13,3 region containing the CLCC1 c.75C>A variant, producing maximum LOD scores of 8.9, 5.0, 3.86, 2.44, and 2.45 at $\theta=0$ (with the CLCC1 variant), respectively.

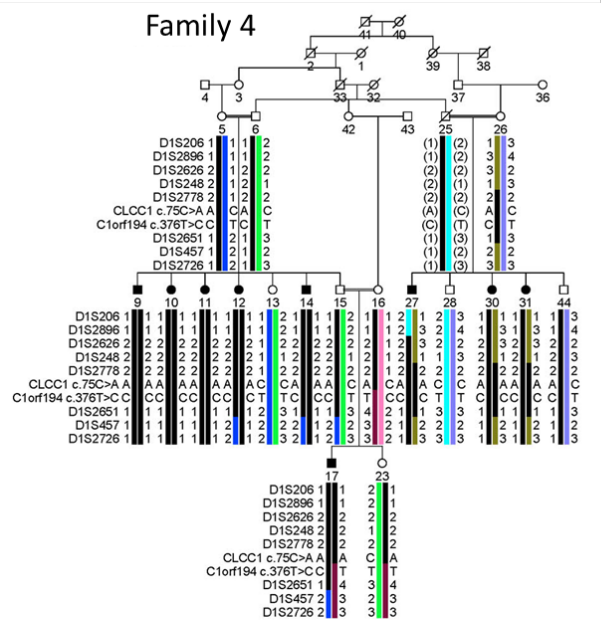
Family 4

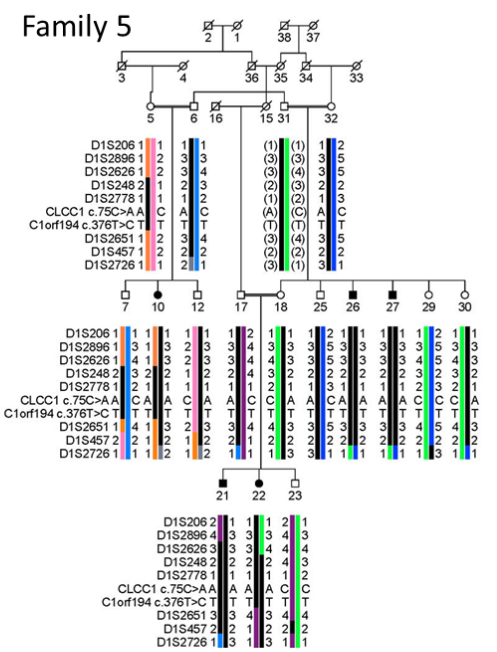
Family 5

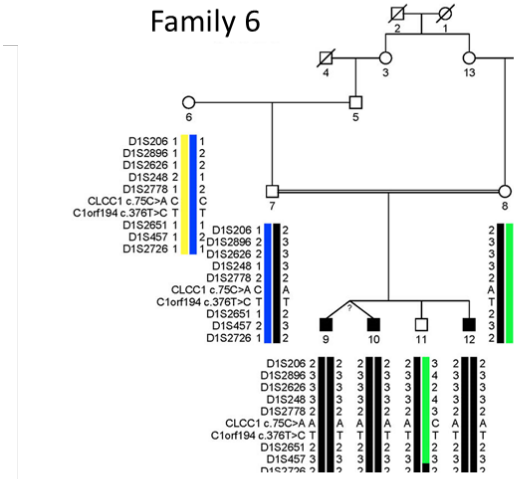
Family 6

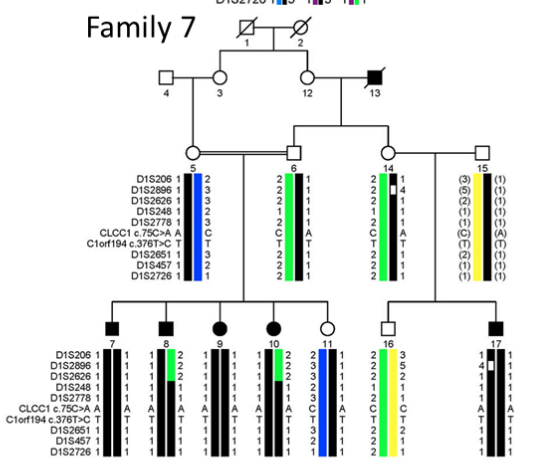
Family 7

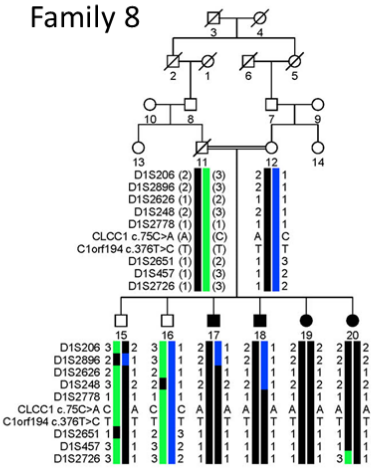
Family 8

Figure 3.4 Family pedigrees and CLCC1 locus haplotypes of Families 4-8. *Haplotypes of the CLCC1 region of families 4-8 showing the CLCC1 c.75C>A mutation, and surrounding microsatellite markers included. Figure made at the NEI.*

Importantly, whole genome SNP mapping in all eight families confirmed that all affected individuals were likely homozygous for the same single ancestral founder mutation event ($p = 2x10^{-11}$), and enabled a further refinement in the extent of the extended genomic haplotype on which the original founder mutation occurred to a very small ~322kb interval flanked by rs1333130-rs587727 (chr1: 108,820,610-109,142,651 [hg38]), containing 10 RefSeq genes (Fig 3.5, Fig 3.6). This includes the British-Bangladeshi family (Family 3), which is also likely to be of the same Pakistani (Punjab) origin. The identical SNP haplotype (Fig. 3.5), has an estimated frequency of 0.03 by the EM algorithm as incorporated into the Golden Helix SVS program (Bozeman MT).

			Affected individuals							
Chr	Position	SNP_ID	F.1	F.2	F.3	F.4	F.5	F.6	F.7	F.8
1	109073893	rs11101974	TT	TT	TT	TT	TT	TT	TT	TT
1	109108766	rs1353721	AA	AA	AA	AA	AA	AA	AA	AA
1	109126399	rs17024373	GG	GG	GG	GG	GG	GG	GG	GG
1	109131023	rs970860	CC	CC	CC	CC	CC	CC	CC	CC
1	109258918	rs11102288	CC	CC	CC	CC	CC	CC	CC	CC
1	109260357	rs4970804	AA	AA	AA	AA	AA	AA	AA	AA
1	109265563	rs4970808	TT	TT	TT	TT	TT	TT	TT	TT
1	109303307	rs4970811	GG	GG	GG	GG	GG	AA	GG	AA
1	109358958	rs6696787	CC	CC	CC	CC	CC	TT	CC	TT
1	109359502	rs1277213	CC	CC	CC	CC	CC	CC	CC	CC
1	109363232	rs1333130	TT	TT	TT	TT	TT	CC	TT	CC
1	109384436	rs10857972	CC	CC	CC	CC	CC	CC	CC	CC
1	109397229	rs12405585	CC	CC	CC	CC	CC	CC	CC	CC
1	109408765	rs2131905	GG	GG	GG	GG	GG	GG	GG	GG
1	109486196	rs338466	AA	AA	AA	AA	AA	AA	AA	AA
1	109505689	rs550743	GG	GG	GG	GG	GG	GG	GG	GG
1	109513274	rs11803800	AA	AA	AA	AA	AA	AA	AA	AA
1	109515028	rs12032662	CC	CC	CC	CC	CC	CC	CC	CC
1	109515735	rs570812	AA	AA	AA	AA	AA	AA	AA	AA
1	109685273	rs587727	AA	GG	GG	GG	GG	GG	GG	GG
1	109696968	rs595635	TT	TT	TT	TT	TT	TT	TT	TT
1	109714403	rs17014495	AA	AA	AA	CC	CC	CC	CC	CC
1	109739071	rs2478762	CC	CC	CC	CC	CC	CC	CC	CC
1	109740548	rs2296696	TT	TT	TT	TT	TT	TT	TT	TT
1	109749071	rs3197233	CC	CC	CC	CC	CC	CC	CC	CC
1	109752204	rs604500	TT	CC	CC	CC	CC	CC	CC	CC
1	109771701	rs669697	TT	GG	GG	GG	GG	GG	GG	GG
1	109783555	rs4246519	AA	AA	AA	AA	AA	AA	AA	AA
1	109788713	rs17035443	AA	GG	GG	GG	GG	GG	GG	GG

Figure 3.5 Conserved founder SNP haplotype encompassing the CLCC1 c.75C>A (p.Asp25Glu) genomic region*. SNP Haplotypes of the 8 families extending across the region show conservation in a 322kb region of chromosome 1 are shown in yellow. In red were highlighted the SNP flanking CLCC1. F.1, family 1; F.2, family 2; F.3, family 3; F.4, family 4; F.5, family 5; F.6, family 6; F.7, family 7; F.8, family 8. Figure made by Dr. Barry Chioza.*

The p.(Asp25Glu) variant co-segregated in all the affected individuals of the eight families (Fig. 3.6 (i)), and is located in a well conserved region of CLCC1

across all 22 species examined ranging from human to zebrafish, and is particularly highly conserved amongst mammals (Fig. 3.6 (iii)).

To robustly identify any other putative mutations in in non-coding regions of the common 322kb critical interval including in non-exonic regions, DNA from a single affected individual (III:1, Family 1) was subjected to whole genome sequencing (WGS). This failed to identify any intronic, splice site, promotor or other variants of likely functional consequence.

(i)

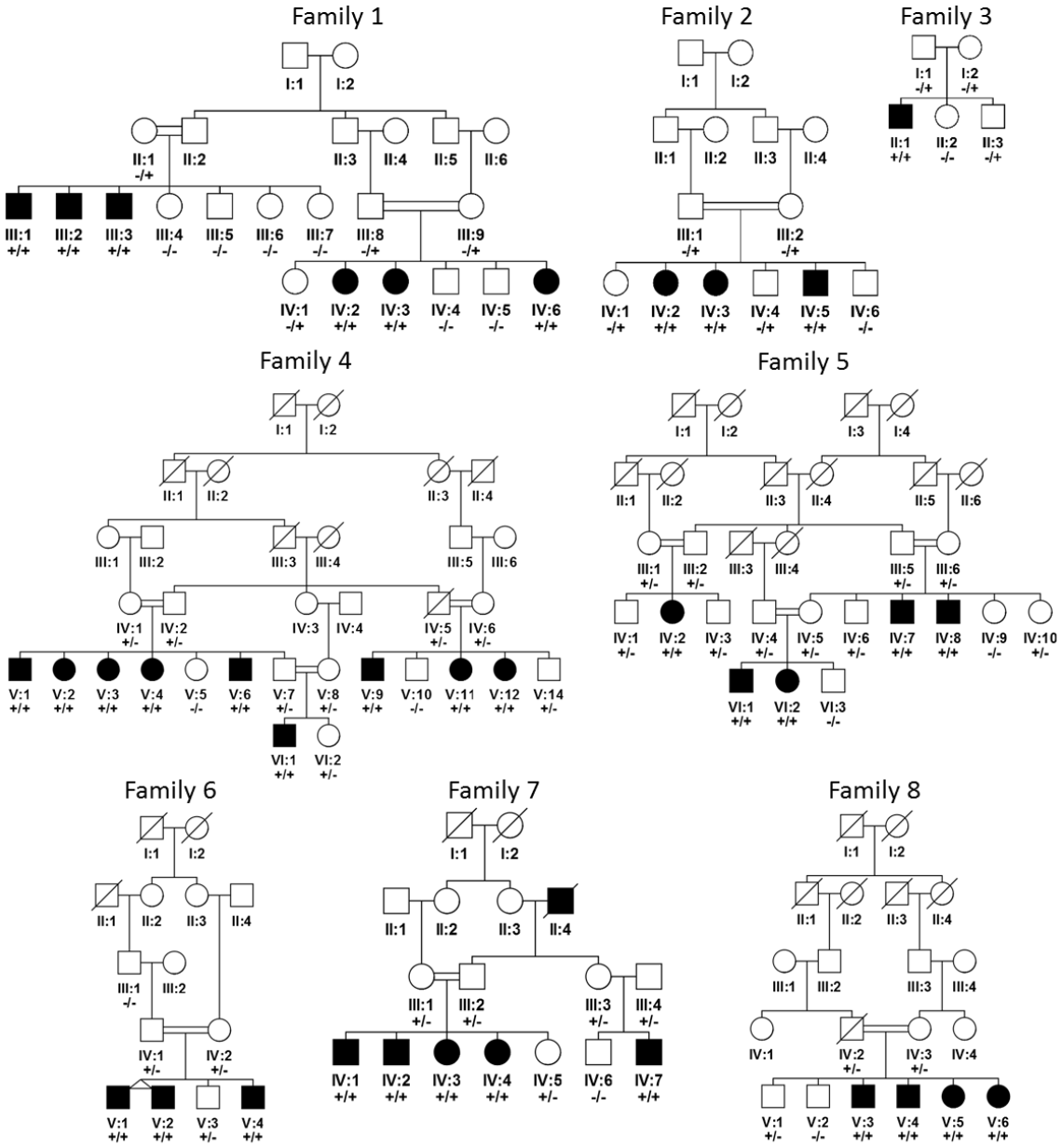

(ii)

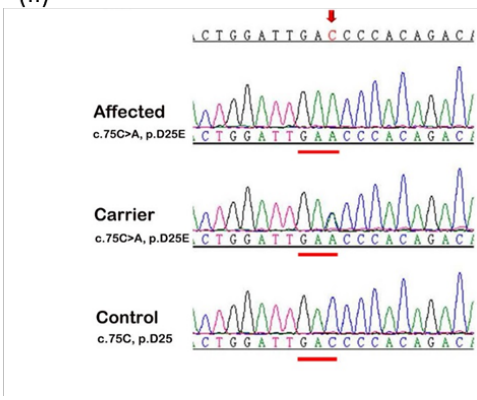

(iii)

	A_{18}	H_{19}	D_{20}	D_{21}	D_{22}	W_{23}	I_{24}	D_{25}	P_{26}	T_{27}	D_{28}	M_{29}	L_{30}	N_{31}	Y_{32}
Human	A	H	D	D	D	W	I	D	P	T	D	M	L	N	Y
Chimp	A	H	D	D	D	W	I	D	P	T	D	M	L	N	Y
Gorilla	A	H	D	D	D	W	I	D	P	T	D	M	L	N	Y
Rhesus	A	H	D	D	D	W	I	D	P	T	D	M	L	N	Y
Squirrel	A	H	D	D	D	W	I	D	P	T	D	M	L	N	Y
Mouse	A	H	D	D	D	W	I	D	P	T	D	M	L	N	Y
Rat	A	H	D	D	D	W	I	D	P	T	D	M	L	N	Y
Guinea_Pig	A	H	D	D	E	W	I	D	P	T	D	M	L	N	Y
Rabbit	A	H	D	D	E	W	I	D	P	T	D	M	L	N	Y
Pika	A	H	D	D	E	W	I	D	P	T	D	M	L	N	Y
Pig	A	H	D	D	D	W	I	D	P	T	D	M	L	N	Y
Dolphin	A	H	D	D	D	W	I	D	P	T	D	M	L	N	Y
Cow	A	H	D	D	E	W	I	D	P	T	D	M	L	N	Y
Sheep	A	H	D	D	E	W	I	D	P	T	D	M	L	N	Y
Horse	A	H	D	D	D	W	I	D	P	T	D	M	L	N	Y
Cat	A	S	D	D	D	W	I	D	P	T	D	M	L	N	Y
Dog	A	H	D	D	D	W	I	D	P	T	D	M	L	N	Y
Elephant	A	H	D	D	D	W	I	D	P	T	D	M	L	N	Y
Platypus	A	Q	D	D	E	W	I	D	P	T	D	M	L	N	Y
Chicken	A	Q	D	D	D	W	I	D	P	T	D	M	L	N	Y
Lizard	A	Q	D	D	D	W	I	D	P	T	D	M	L	N	Y
Zebrafish	-	Y	D	E	A	W	I	D	P	Y	D	M	L	N	Y

Figure 3.6 Co-segregation and conservation of CLCC1 c.75C>A alteration. ***(i)*** *Pedigrees of families involved in this study. Presence of the variant is indicated with '+', while absence with '-'.* ***(ii)*** *Electropherograms the sequence of an affected individual (top, V:8, Family 5), the sequence of a heterozygous carrier (middle, V:9, Family 5) and unaffected control sequence (bottom) surrounding the CLCC1 c.75C>A alteration.* ***(iii)*** *Amino acid sequence alignment around the Asp25 amino acid of CLCC1 (red) in 22 species ranging from human to zebrafish. Asp25 conserved in all species and the entire region is well conserved, especially amongst mammals.*

3.3 Discussion

Studies undertaken at IBCS as part of a collaborative study with workers at a number of other Institutions internationally provide extensive genetic, clinical and functional datasets defining CLCC1 alteration as a new cause of arRP. Our genetic findings of seven extended Pakistani Punjab families, as well as an eighth British-Bangladeshi family, determine that all families likely stem from the same ancestral origin, defining CLCC1 alteration as a new cause of arRP. Whole genome-SNP mapping identified a homozygous interval of 322 kb shared between affected individuals, an interval containing ten genes: *AKNAD1, GPSM2, CLCC1, WDR47, TMEM167B, C1orf194, KIAA1324, SPATA42, TAF13* and *SCARNA2.* None of these genes have been associated with retinal disease. *AKNAD1* has been associated with type 2 diabetes [199], *WDR47* has been linked to brain development [200], *C1orf194* variants cause Charcot-Marie-Tooth [201], and *TAF13* has been related to intellectual disability [202]. Interestingly, *GPSM2*, which codes for the putative whirlin protein complex-interacting molecule, previously implicated in Usher syndrome, been associated with Chudley-McCullough Syndrome (CMCS [MIM 604213]), a rare autosomal recessive disorder characterised by sensorineural deafness, agenesis of the corpus callosum, frontal polymicrogyria, interhemispheric cyst, and ventricular enlargement. Gpsm2 is important for stereocilia elongation, interacts with whirlin, and regulates actin dynamics in the growth cones of developing neurons [203]. Importantly none of the non-ocular features characteristic of CMCS are present in the affected individuals presented here. WES, WGS, and dideoxy sequencing of this interval identified only a single deleterious sequence alteration in the putative chloride channel *CLCC1* c.75C>A as the likely cause of the condition. Exon twelve of *CLCC1* overlaps with exon sixteen of *GPSM2*,

indicating that the c.75C>A variant at the genomic level may theoretically affect binding of transcription factors during *CLCC1* transcription, some of which are known to be active in the retina. However, the distance from promoter regions of *GPSM2* (or *CLCC1*), may not be consistent with an effect on transcription factor binding being the pathogenic mechanism, as opposed to functional effects on the CLCC1 protein itself. Consistent with this, genome sequencing of the c.75C>A *CLCC1* haplotype identified no additional intronic, promotor of other sequence alterations in the vicinity of *GPSM2* (or in other genes in the 322kb region) that might influence functionality. While these findings do not support involvement of *GPSM2* in the condition reported here, it remains unclear whether there may be any functional relationship between the two proteins that may be impacted by the p.Asp25Glu CLCC1 variant.

CHAPTER 4

CHARACTERISATION OF CLCC1

CHAPTER 4: CHARACTERISATION OF CLCC1

4.1 Introduction

The previous chapter described the discovery of *CLCC1* as a RP-associated gene.

CLCC1 (also called *MCLC*) cDNA was first isolated in 1996 [204], as a gene differentially expressed in *X. laevis* melanotropes in response to different coloured background (X92871, EMBL-EBI database, www.ebi.ac.uk) [204]. Subsequently, in 2001, Nagasawa et al. [205], looking for stretch- activated channels in rat genome with a sequence similar to the *MID1* gene in *S. cerevisiae*, found an expressed sequence tag homologous to X92871. From the partial sequence of the rat *MID-1*, the full-length of Mid-1- related chloride channel (*MCLC*) cDNA sequence was obtained. However, there were no close sequence similarities between *MID-1* and *MCLC,* or between *MCLC* and known channel families. *MCLC* was predicted to have four transmembrane domains, a consensus sequence for nuclear localisation, and an amino acid sequence in the third transmembrane domain resembling the CLIC family of chloride channels. *MCLC* has been shown to be expressed in rat spleen, liver, testis, brain, kidney and heart [205]. In Chinese hamster ovary (CHO) cells, MCLC localised to the perinuclear region, endoplasmic reticulum (ER) and in the Golgi apparatus, but not in the nucleus. Activity of the presumptive channel was assessed by microsomal insertion into a lipid bilayer: the channel was preferentially permeable to anions however blockers of anion channels, such as 4,49-diisothiocyanatostilbene-2,29-disulfonate (DIDS), did not block the channel activity [205].

A retrotransposon insertion in *CLCC1,* resulting in loss of function was reported in 2015 associated with cerebellar neurodegeneration in mice [206]. Moreover, ER localisation of CLCC1 was confirmed in HEK293 cells, and the loss of CLCC1 was linked with UPR (unfolded protein response) response and ER stress [206]. *CLCC1* loss of function has also been reported as increasing the levels of the ER chaperone BiP (GRP78), consistent with the induction of ER stress [206].

Although the presence of anion channels in the ER including a member of the CLIC family, CLC4, have been reported [207-209], the functions of CLCC1 either as a chloride channel or a mediator of ER stress remains to be confirmed. The ER is involved in calcium storage, lipid and protein metabolism, protein folding, secretion and degradation. Protein synthesis occurs on the cytosolic side of the ER, to which ribosomes localise and where the complex ribosome:mRNA:nascent polypeptide bind the signal recognition particle (SRP) receptor, and the nascent polypeptide is co-translationally translocated into the ER lumen though Sec61/SecY channel [210]. Proteins must fold correctly before leaving the ER through secretory pathways, if they cannot reach a native structure due to mutations or misfolding, proteins are degraded though the ER-associated degradation (ERAD). Misfolded or unfolded proteins are recognised by chaperones and lectines, and diverted to the dislocon through which proteins are translocated. Polyubiquitination of those proteins ensure the degradation though the cytosolic 26S proteasome [211].

Stress signalling, collectively called the unfolded protein response (UPR), occurs when there is an imbalance between unfolded protein load and chaperone reserve [212]. Triggering of the UPR may result in restoration of cellular homeostasis or apoptosis. Misfolded proteins are translocated into the

cytosol where they are ubiquitinated and degraded via the 26S proteasome; a process called ER-associated degradation (ERAD). Several studies report the ER as a major organelle implicated in retinal dystrophies, glaucoma, diabetic retinopathy [213, 214]. For example, the P23H mutation in rhodopsin, a gene associated with RP, induces misfolding of the protein and ER stress [52, 215].

The UPR (Fig. 4.1) is controlled by three sensors: inositol requiring enzyme 1 (IRE1) [216, 217], protein kinase RNA-activated (PKR)-like ER kinase (PERK) [218], and activating factor 6 (ATF6) [219]. All of them consist of three domains: a cytosolic domain, a single pass transmembrane domain, and an ER luminal domain. In homeostatic conditions, the ER luminal domains of the three sensors are bound to the heat shock protein A5 (also known as GRP78 or BiP), which keeps the sensors in an inactive state [213]. Accumulation of misfolded protein in the ER lumen induces the disengagement of BiP from the sensors, IRE1 and PERK oligomerise, and auto-phosphorylate, activating the downstream pathway.

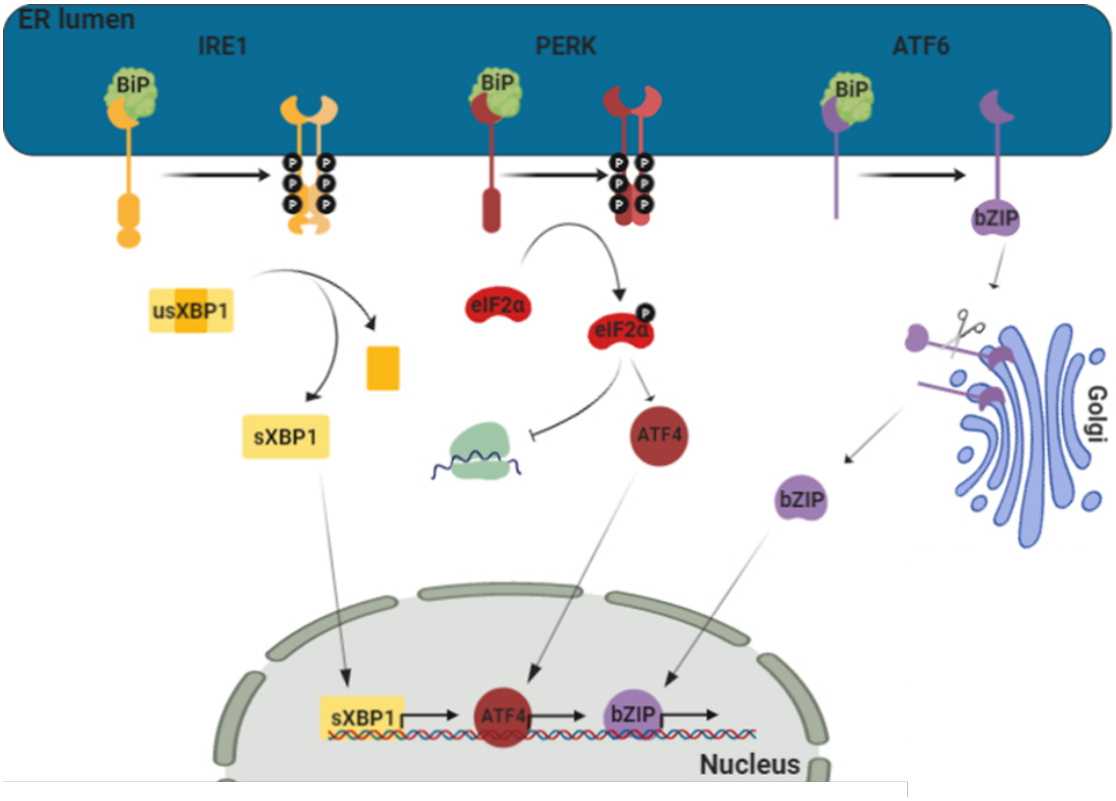

Figure 4.1 Unfolded protein response (UPR) signalling. *The UPR signalling starts in the ER when there is an imbalance of misfolded proteins. The chaperone BiP is released from the three UPR sensors; IRE1, PERK and ATF6. IRE1 auto-phosphorylation induces the splicing of the transcription factor usXBP1 into sXBP1, which migrates into the nucleus. Active PERK, phosphorylates eIF2α, blocking protein synthesis, and induces the translocation into the nucleus of the transcription factor ATF4. The release of BiP from ATF6 induces the translocation of ATF6 to the Golgi apparatus, where the bZIP domain is cleaved and acts as a transcription factor in the nucleus. sXBP1, ATF4 and ATF6 induce the expression of genes that will help to increase the protein folding capacity of the ER. Figure created with BioRender.*

IRE1 activation induces a selective cleavage of dual stem loops within the X-box binding protein 1 (usXBP1; unspliced XBP1), which is a basic leucine

zipper (bZIP) transcription factor. The sXBP1 (spliced XBP1) activation induces the transcription of chaperones and metabolic pathways which help to reduce the protein load in the ER [220].

Active PERK phosphorylates eukaryotic translation initiation factor-2α (eIF2α) inhibits eIF2B activity, blocking protein synthesis and translation. Activation of PERK induces synthesis of ATF4 that can bind to the C/EBP-ATF site of CAAT/enhancer-binding protein (C/EBP) homologous protein (CHOP)/GADD153. ATF4 and CHOP induce genes involved in the UPR to enhance folding capacity (Fig. 3.1). The activation of ATF6 results in its export to the Golgi apparatus where it is cleaved by the two Golgi-resident proteases, releasing a fragment of ~400 amino acids corresponding to ATF6 cytosolic N-terminal portion (ATF6f). ATF6f comprises a transcriptional activation domain (TAD), a bZIP domain, a DNA-binding domain, and nuclear localisation signals. In the nucleus, bZIP induces UPR gene expression of CREB, XBP1, CHOP [213, 221] (Fig. 4.1).

The ER is the major storage site of intracellular calcium (Ca^{2+}), rapid release of Ca^{2+} in the cytoplasm is necessary for diverse cell functions; cytoplasmic Ca^{2+} acts as second messenger and regulates cytosolic Ca^{2+}- dependent proteins. Cytosolic Ca^{2+} deregulation induces cell damage and may lead to cell death [222]. Preservation of correct Ca^{2+} gradients in the ER is important as the ER relies on the correct Ca^{2+} concentration, or folding, apoptosis, stress and transcriptional activities. Total Ca^{2+} concentration within the ER is ~1 mM, of which 200 μM is free Ca^{2+}, while the rest is buffered via ER resident proteins [223]. Ca^{2+} release from the ER lumen happens via the inositol-1,4,5-triphosphate receptor (IP_3R) and/or the ryanodine receptor (RyR) [224]. ER Ca^{2+} uptake from the cytosol ensures the maintenance of cytoplasmic calcium

concentration ($[Ca^{2+}]_{cyt}$) at about 100 nM [223] through the activity of sarcoplasmic–endoplasmic reticulum Ca^{2+} -ATPase (SERCA) [225].

In the ER, calcium homeostasis is maintained by calcium-binding proteins such as calreticulin, a 46-kDa soluble protein found in the ER lumen and consisting of three domains. The N and P domains are essential for the chaperone activity, while calreticulin's high binding capacity for Ca^{2+} (25 mole of Ca^{2+} per mole of protein) originates from the C-domain, containing clusters of acidic amino acid residues consisting of aspartic and glutamic acid interrupted with basic residues of lysine and arginine. Calreticulin alone binds approximately 50% of the Ca^{2+} stored in the ER lumen [226, 227]. Calreticulin is also implicated in many other cellular processes, such as folding of glycoproteins together with calnexin, a 90 kDa membrane protein [227]. Calnexin and calreticulin share ~39% of sequence identity and have identical lectin-binding specificity. Calnexin possess the same high affinity for calcium of calreticulin [228]. Other important calcium-binding proteins are GRP94 and BiP. BiP is a 78 kDa protein that binds calcium at relatively low capacity (1-2 mole of Ca^{2+} per mole of protein) and low affinity however, it is expressed at higher levels than calreticulin and therefore responsible for as much as 25% of the Ca^{2+} binding capacity of the ER [227, 229, 230]. GRP94 (94 kDa protein) binds Ca^{2+} at high capacity (15 to 28 mol of Ca^{2+} per mol of protein) through its four sites of high affinity with Ca^{2+} [231].

Store-operated Ca^{2+} entry (SOCE) is a mechanism activated when the concentration of Ca^{2+} in the ER is decreased. The major regulatory components of SOCE are stromal interaction molecule (STIM) proteins, STIM1 and STIM2. Upon store depletion, STIM1 translocates to the ER-plasma membrane junction and couples with ORA1, a Ca^{2+}-selective ion pore present on the plasma membrane, creating the Ca^{2+} release-activated Ca^{2+} (CRAC) channels, thus

inducing the entrance of Ca^{2+} directly into the ER from the extracellular space [224, 232].

Secretory pathways from the ER to the Golgi (and vice versa), though vesicular movements, ensure the transport of newly synthesised proteins and lipids between compartments [233]. Lipids are a major component for energy production in cells, they are stored and transported under the form of lipid droplets, emerging from the ER. Lipid droplets contain neutral lipids (triacylglycerols and sterol esters), as well as proteins, mainly enzymes, involved in lipid metabolism. During periods of starvation or growth, lipids enclosed in lipid droplets sustain membrane biogenesis and metabolic processes [234].

This chapter describes the studies undertaken to identify the subcellular localisation and functional role of *CLCC1*, a new gene causing arRP in the Pakistani population, including defining likely molecular binding partners and pathways in which *CLCC1* might be involved, using proteomics and genetic modification in cell lines.

4.2 Results

4.2.1 Expression of CLCC1 in the retina during development

Studies of mouse and zebrafish were coordinated through our collaborators at the NEI.

Levels of *Clcc1* expression in mouse eye (FVB/N mouse strain), at different stage of life, from four weeks to nine months, were assessed using qPCR. In the retina, *Clcc1* was highly expressed at four weeks, with a peak at six weeks, decreasing from eight weeks to nine months. Iris, optic nerve, sclera, and cornea showed moderate expression (Fig. 4.2 (i)). *Clcc1* was not expressed in the lens at any developmental stage.

In developing zebrafish larvae *clcc1* mRNA expression was assessed with in situ hybridization, using digoxigenin-labelled cRNA probe. At 24 hours post fertilisation (hpf), high expression of *clcc1* was present in hindbrain (HB), swim bladder (SB), and the eye (Fig. 4.2 (ii-iii), arrows). At 72 hpf (Fig. 4.2 (iv), arrows), the expression was most prominent in the retina, especially the GCL, ONL, and RPE, (Fig. 4.2 (v-vi), arrows).

Expression of CLCC1 in adult human eye (NEI core histology lab) was assessed using formalin fixed and paraffin embedded retinas. Immunohistochemistry detected the presence of CLCC1 in the lamina cribrosa (LC), optic nerve (ON), GCL, INL, ONL and RPE (Fig. 4.2 (vii-x), arrows).

These results indicate that *CLCC1* is important during retinal development in divergent species including mammals and inferior vertebrates.

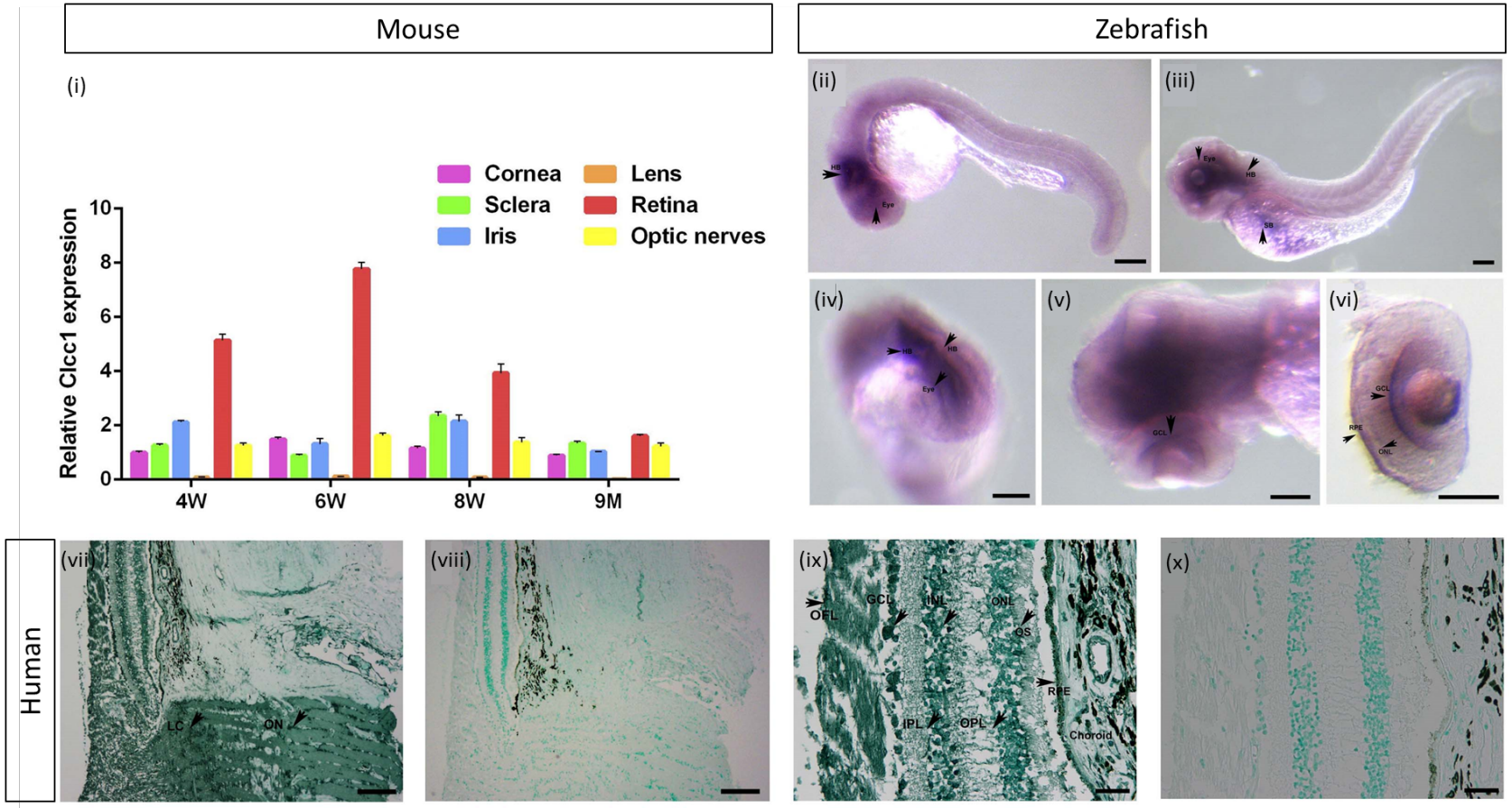
Mouse
Zebrafish
Human
(i)
Relative Clcc1 expression
Cornea
Sclera
Iris
Lens
Retina
Optic nerves
4W
6W
8W
9M
(ii)
(iii)
(iv)
(v)
(vi)
(vii)
(viii)
(ix)
(x)
HB
Eye
SB
GCL
RPE
ONL
LC
ON
OFL
INL
OS
IPL
OPL
Choroid

Figure 4.2 Relative expression of Clcc1 in mouse, zebrafish and human retina. (i) *Levels of Clcc1 mRNA expression in mouse cornea, lens, iris, optic nerve, and retina by qRT-PCR at different ages. Values represent the mean (± SD) on an arbitrary scale (y axis) and were calculated from at least three independent experiments.* ***(ii-vi)*** *In situ hybridization of clcc1 probes in zebrafish showed positive staining in the HB, SB, and eye at 24 hpf, and in the GCL, ONL, and RPE at 72 hpf ; scale bar: 100 µm.* ***(vii-x)*** *Immunohistochemistry on a human retina demonstrated CLCC1 is expressed extensively in the retina and optical nerves. More intense CLCC1 staining (arrow) was present in the LC, ON, GCL, INL, ONL and RPE in the retina (counter stain is methyl green). Scale bar: (vii-viii), 50 µm; (ix-x) 20µm.*

4.2.2 Knockdown and knockout of *clcc1* expression in zebrafish

To evaluate the functional role of *clcc1* in developing retina *in vivo,* morpholino oligonucleotide (*clcc1*-MO) knockdown of *clcc1* was performed in zebrafish embryos. The specificity of the clcc1-MO was validated by demonstrating inhibition of translation of EGFP mRNA fused to a morpholino sensitive sequence at its 5'-end (5'-modified EGFP) by injection of a *clcc1*-MO, but not a mismatch morpholino (MM-MO). In contrast, translation of unmodified EGFP mRNA was not affected by injection of either *clcc1* or MM-MO (Fig. 4.3 (i-vi)).

At 24 hpf, embryos treated with the *clcc1*-MO showed normal development however, at 36 hpf *clcc1*-MO embryos showed reduced eye size (N=30, 0.13 vs. control 0.178 mm^2, p= $7.942x10^{-9}$), compared to the MM-MO (N=30) or buffer control embryos (N=30) (Fig. 4.3 (vii-xii)). Interestingly, lens size was decreased proportionately (0.019 vs. control 0.026mm^2, p= $2.8x10^{-8}$), so that

the lens/eye ratio was unchanged (0.146 vs. control 0.149, p=0.48) (Fig 4.3 (xiii)). These results indicate that reduced expression of *clcc1* influences eye growth during early zebrafish development.

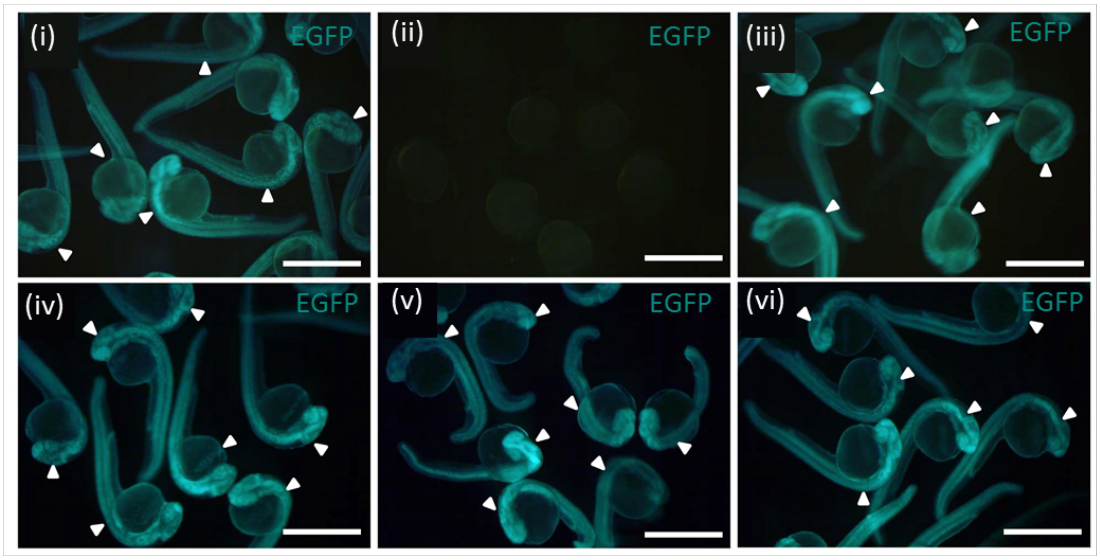

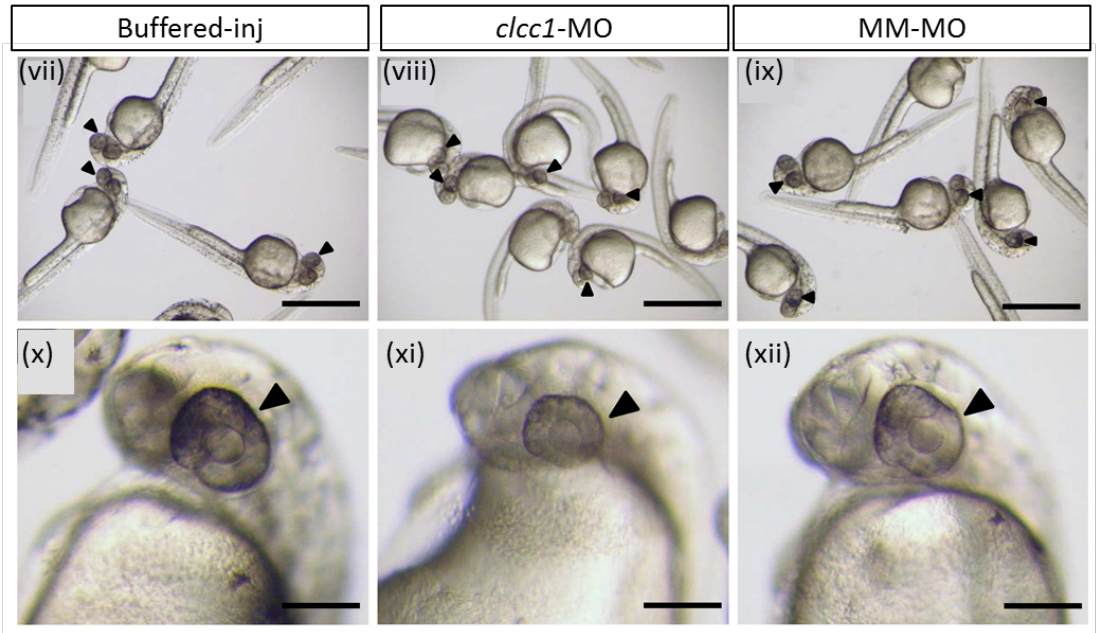

	Area (mm^2)		Ratio	Average of thickness (µm)				
	Lens	Eye	Lens/Eye	GCL	IPL	INL	ONL	Rod cell (N/10µm)
MMMO	0.026 ± 0.006	0.178 ± 0.034	0.149 ± 0.018	25.48 ± 1.74	12.30 ± 1.89	36.12 ± 1.73	12.90 ± 0.70	63.30 ± 8.42
MO	0.019 ± 0.005	0.13 ± 0.032	0.146 ± 0.019	40.08 ± 3.28	7.82 ± 1.43	36.78 ± 2.39	9.09 ± 1.13	22.50 ± 11.20
t	6.17	6.46	0.71	3.93	5.51	0.83	8.71	8.84
P	2.777E-08	7.942E-09	0.482	0.0011	0.0000475	0.21	1.809E-07	1.483E-07

Figure 4.3 clcc1 morpholino validation. *Embryos at 24 hpf* ***(i)*** *injected with the 5'-modified EGFP or* ***(iv)*** *the unmodified EGFP showed a fluorescent signal (arrowheads).* ***(ii)*** *Co-injection of the clcc1-MO eliminated the fluorescent signal from morpholino-sensitive 5'-modified EGFP mRNA but* ***(v)*** *not unmodified EGFP.* ***(iii, vi)*** *Co-injection of the MM-MO had no effect. Eye size at 36 hpf:*

(viii, xi) *injection of the clcc1-MO significantly reduced eye size (black arrows) compared to* ***(ix, xii)*** *MM-MO, and buffer-injected. Scale bar (i-ix) 1 mm; (x-xii) 100 μm*.

Retinal frozen sections of 4 dpf MM-MO- (Fig. 4.4 (i-ii)) and *clcc1*-MO-injected (Fig. 4.4 (iii-iv)) embryos were stained for PKCß1 to evidence bipolar cell, Zpr-1 for cone photoreceptors, 1D1 for rod photoreceptors, and DAPI. Retinal layers as IPL, and ONL of clcc1-MO-treated larvae were significantly thinner in the *clcc1*-MO-treated than MM-MO-treated larvae (7.82 vs. control 12.30µm p= 4.75 x 10^{-5} and 9.1 vs. control 12.9µm, p=1.8x10^{-7}) (Fig. 4.3). In contrast, the INL showed little change (36.78 vs. control 36.12µm, p=0.21) and the GCL increased in thickness (40 vs. control 25.48µm, p<0.0011). The *clcc1*-MO-treated larvae showed a reduced number of rod cells (22.5 vs. control 63.3, p=1.5x10^{-7}) (Fig. 4.3). Those rod cells present were visible for the most part only at the retinal margin, a region of persistent neurogenesis in fish, and even at the margin, rod cells often showed abnormal morphology or were pyknotic (Fig. 4.4 (i,iii)). Cone opsin positive staining was also decreased, and disrupted photoreceptor cell bodies were apparent for *clcc1*-MO-injected embryos compared to the MM-MO injected (Fig. 4.4 (ii, iv)). Retinal sections were also stained for the different cone opsins: anti-blue opsin (v-vi), anti-green opsin (vii-viii), anti-red opsin (ix, x), or anti-UV opsin (xi, xii), and 4D2 to mark rhodopsin. All photoreceptors in *clcc1*-MO-injected embryos show reduced staining and damaged photoreceptor cell structure however, the greatest decreases was seen in blue and green opsin cones.

Specificity of the morpholino effect was confirmed by co-injection of *clcc1* RNA in 1-cell embryos with the *clcc1*-MOs, to rescue the phenotype. Rescue of the normal eye size phenotype was almost complete (87%) with co-injected WT mRNA suggesting that the observed phenotype was specifically caused by knockdown of endogenous *clcc1* protein levels (Fig. 4.4 (xiii)).

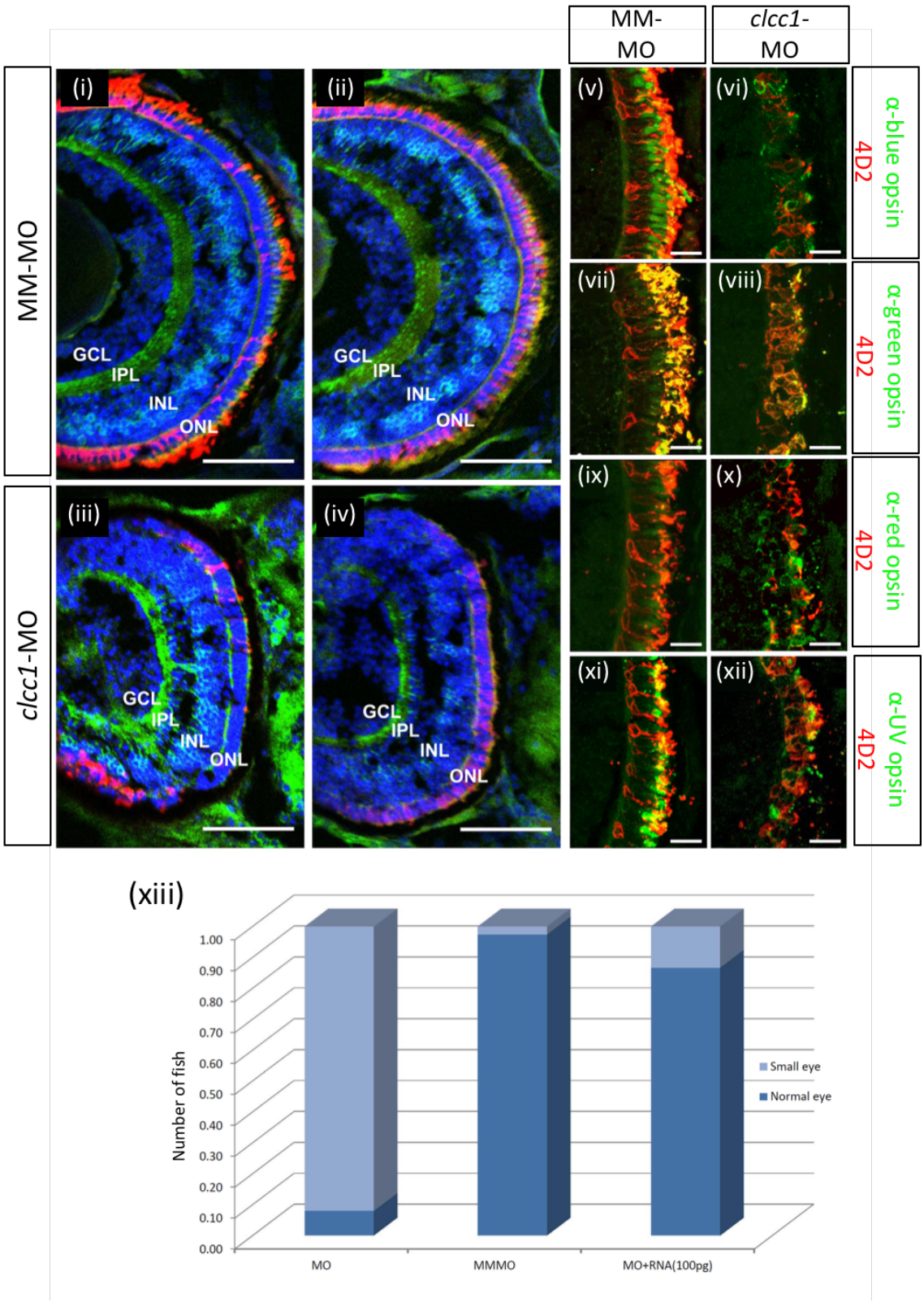

Figure 4.4 Retinal sections of embryos at 4 dpf. (i-ii) *MM-MO- and* ***(iii-iv)*** *clcc1-MO-injected embryos stained for PKCß1 (bipolar cells, green), Zpr-1 (cone receptors, red, (ii, iv)), 1D1 (rod receptors, red, (i, iii), and DAPI (nuclei, blue).clcc1-MO injected embryos show decreased thickness of ONL and IPL*

layers. ***(v-xii)*** *MM-MO-injected and clcc1-MO-injected embryos were stained with anti-blue opsin, anti-green opsin, anti-red opsin, or anti-UV opsin, and 4D2 (Rhodopsin). All photoreceptors in clcc1-MO-injected embryos showed reduced staining and damaged photoreceptor cell structure, with the greatest decreases in blue and green opsin cones.* ***(xiii)*** *clcc1-MO injection and rescue by co-injected clcc1 WT mRNA. Forty clcc1-MO-treated embryos and forty-one MM-MO-treated embryos were analysed. Scale Bar: (i-iv) 50 µm; (v-xii) 10 µm.*

In order to further confirm the specificity and nature of the phenotypic effects of the clcc1 mutant in zebrafish larvae a transcription activator–like (TAL) effector nuclease (TALENs) was used to produce a 7 bp deletion in exon1, (c.100_106het_delAATGATG, p.Asn34Argfs*9) of clcc1 at one allele (clcc1+/TALEN). The homozygous *clcc1*$^{-/-}$ genotype alteration was lethal at around 11 dpf with no *clcc1*$^{-/-}$ larvae detected at 15 dpf, suggesting that *clcc1* plays an essential role in vertebrate development. Similar to morpholino knockdown fish, 5 dpf *clcc1*$^{-/-}$ KO larvae showed abnormalities in the various retinal layers including the IPL, the ONL, the rod photoreceptor layer (Fig. 4.5 (i-iv)), and less severe effect on cones. When *clcc1*$^{-/-}$ KO zebrafish embryos were injected with WT and p.Asp25Glu mutant *clcc1* mRNA, the WT but not mutant mRNA was able to reverse changes in both the ONL thickness and rod cell numbers (Fig. 4.5 (ix)). While the ONL thickness did not return to the values in the WT injected with buffer control (11.26 ± 0.4 vs. 12.54 ± 0.21, p = 0.22), it is well above the KO value of 9.9 ± 0.28, p = 0.00819, and that of the KO injected with p.Asp25Glu mutant *clcc1* mRNA (9.04 ± 0.50, p = 0.0082). It should be noted that morpholino and TALENS KO eyes were separate approaches examined on different equipment and by different investigators, so while

changes relative to controls are consistent, the absolute values for some of the measurements vary. The TALENS induced *clcc1* mutant also allowed confirmation of the functional effects of absence of *clcc1* expression on the retina. The cone responses (PIII) for 6dpf WT and TALEN *clcc1* mutants were isolated with Na Aspartate, which blocks post-synaptic ERG signals arising from inner retinal neurons. Stimuli were saturating at 490 nm. Cone PIII ERGs showed a 50-60% depression of both cone amplitudes and sensitivity in *clcc1*$^{+/-}$ *KO* zebrafish relative to WT fish at 6 dpf (Fig. 4.5 (v, vii)). ON bipolar responses (b2) were isolated by the AMPA/KA antagonist CNQX, which blocks excitation for OFF bipolar, horizontal, amacrine, and ganglion cells (Fig. 4.5 (vi, viii)). ON bipolar cell spectral sensitivity was reduced by 50% in 5 dpf mutants (Fig. 4.5 (vi, viii)). Thus, the structural disarray and degeneration seen in *clcc1*$^{+/-}$ KO fish was accompanied by correspondingly decreased function of the cone system.

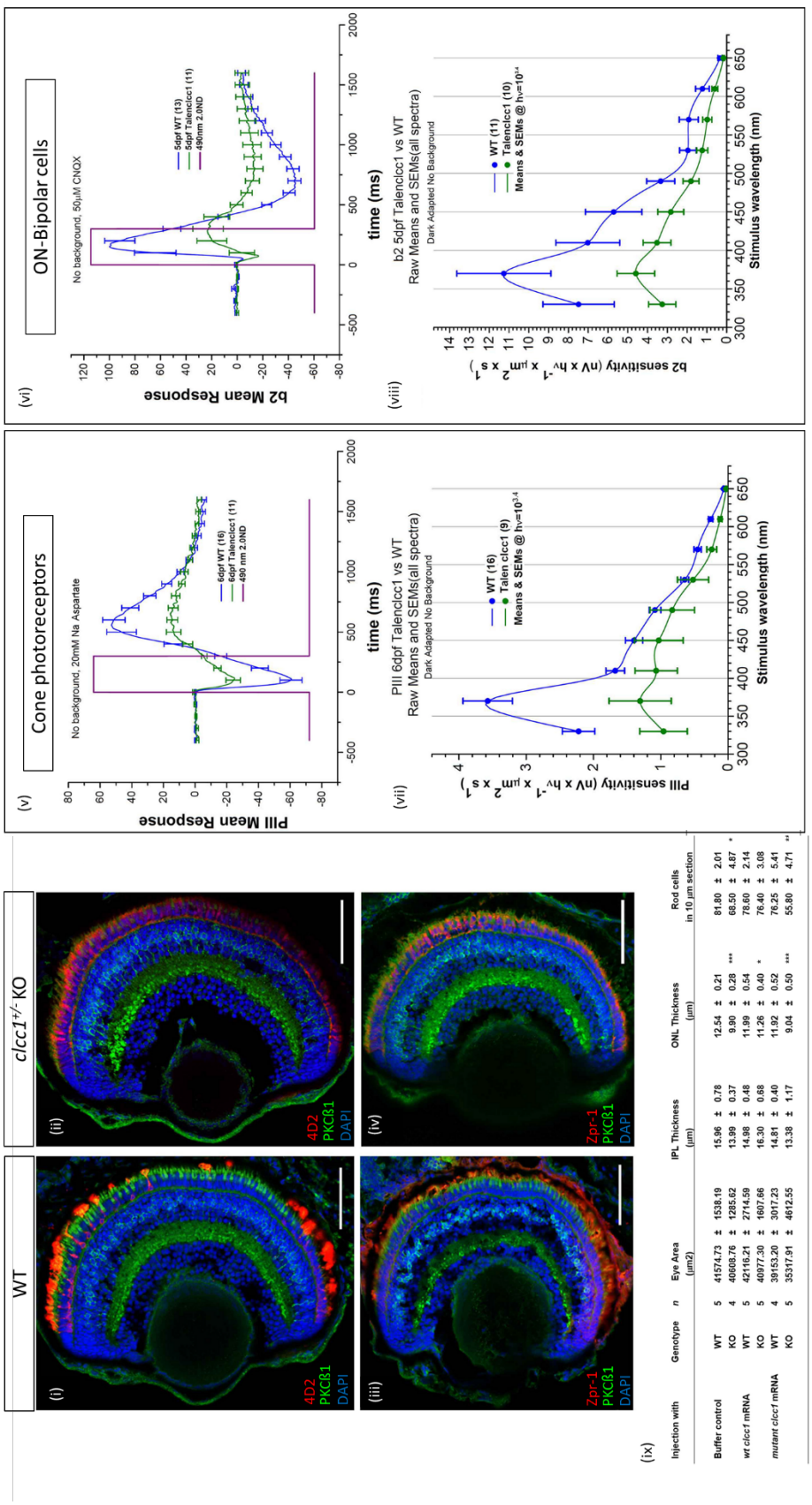

Figure 4.5 Retinal morphology and function is altered in TALEN clcc1$^{+/-}$ KO zebrafish. (i-iv) *Merged photographs of frozen retinal sections prepared*

from the heads of 5 dpf larvae. Merged photos of frozen sections from WT (i-iii) and KO (ii-iv) embryos stained for PKCß1 (bipolar cells, green), 4D2 (rod receptors, red, (i) and (iii)), Zpr-1 (cone receptors, red, (ii) and (iv)), and DAPI (nuclei, blue). clcc1$^{+/-}$ KO embryos show destruction of the rod photoreceptor layer compared with WT. While somewhat better preserved than in the morpholino Clcc1 knockdown embryos, cone photoreceptors and the other retinal layers also appear decreased. Scale bar 100 μm. ***(v)*** *Mutant cone responses are 50% depressed relative to WT.* ***(vi)*** *Cone spectral sensitivity is depressed about 60% in mutants.* ***(vi)*** *For signals from ON bipolar cells, which are 2X more sensitive than cone signals, TALEN clcc1 mutant responses decrease by over 50%. Stimuli are saturating at 490nm.* ***(viii)*** *ON bipolar cell spectral sensitivity is depressed over 50% in mutants. Sensitivity axis is in units of nV per quantum as calculated from the amplitude of responses to constant quanta stimulation across the spectrum (Eq.1). The quanta level of 2500 hv·μm^{-2}·s^{-1} at the cornea is below semi-saturation for all cone types.* ***(ix)*** *co-injection of zebrafish embryos with WT but not p.D25E mutant clcc1 mRNA can rescue the KO phenotype. *p 0.022 vs. WT injected with buffer control, p = 0.0082 vs KO injected with Asp25Glu mutant clcc1 mRNA, ** p = 0.00095 vs. WT injected with buffer control *** p > 0.00012 vs. WT injected with buffer control. Buffer control injected in WT zebrafish (N=5), and in KO zebrafish (N=4); injection of WT CLCC1 mRNA in WT zebrafish (N=5) and in KO zebrafish (N= 4); injection of Asp25Glu CLCC1 mRNA in WT zebrafish (N=4) and in KO zebrafish (N=5). Figure made at the NEI.*

4.2.3 Ocular characteristics of *CLCC1*$^{+/-}$ knockout mice

To gain further insight into the effects of loss of CLCC1 function on retina, vision and retinal morphology in mammals, *Clcc1* KO mice (Jackson Laboratories, stock number: 027239, B6N(Cg)-Clcc1$^{tm1b(KOMP)Mbp}$/2J) were investigated. A lack of *Clcc1*$^{-/-}$ KO mice in intercrosses of *Clcc1*$^{+/-}$ KO mice suggested that total lack of *Clcc1* activity was embryonic lethal, so the effect of heterozygosity for the *Clcc1* KO on the retina was studied (Fig. 4.6). Mice showed no abnormalities in their extraocular phenotypes. Haematoxylin & eosin staining of 7-months old *Clcc1*$^{+/-}$ KO mice retinas showed that the overall structure of the retina was preserved however, the photoreceptor layer showed disarray and reduced thickness, with reduction of cells in the outer and inner nuclear as well as OPL and IPL (Fig. 4.6 (i)) in *Clcc1*$^{+/-}$ KO mice compared to the WT.

Reduction of the number of cone cells was confirmed with immunohistochemistry when retinal sections were stained for the antibody against cone arrestin. *Clcc1*$^{+/-}$ KO mice displayed were about the half the cone density in compared to the WT (Fig. 4.6 (ii)). The ability to respond to light stimuli of retinal neurons was assessed using ERGs. *Clcc1*$^{+/-}$ KO mice showed depression of amplitude responses of scotopic a-wave, derived from the rods, and b-wave, derived from the inner retina, predominantly Muller and ON-bipolar cells, compared with WT mice (Fig. 4.6 (iii)), suggesting degeneration of rods and secondary order neurons. Moreover, *Clcc1*$^{+/-}$ KO mice exhibited a significant decreased amplitude of the photopic b-wave, derived from cones, compared with WT mice (Fig. 4.6 (iv)), indicating possible dysfunction of the cone photoreceptors response. These results were also consistent with the decreased density of cones seen with immunohistochemistry (Fig. 4.6 (iii-iv)).

(i)

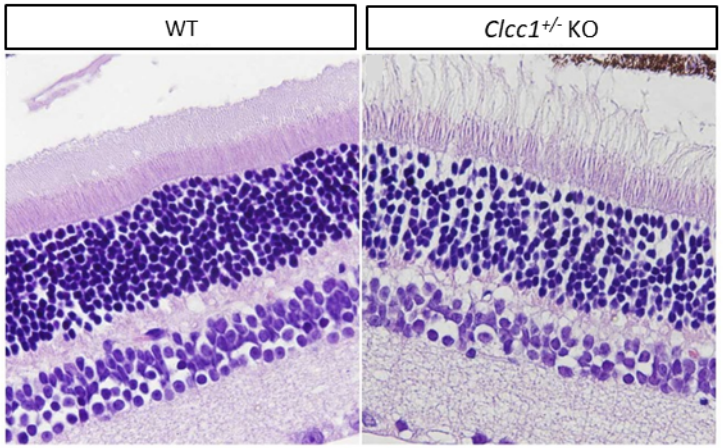
WT
Clcc1+/- KO

(ii)

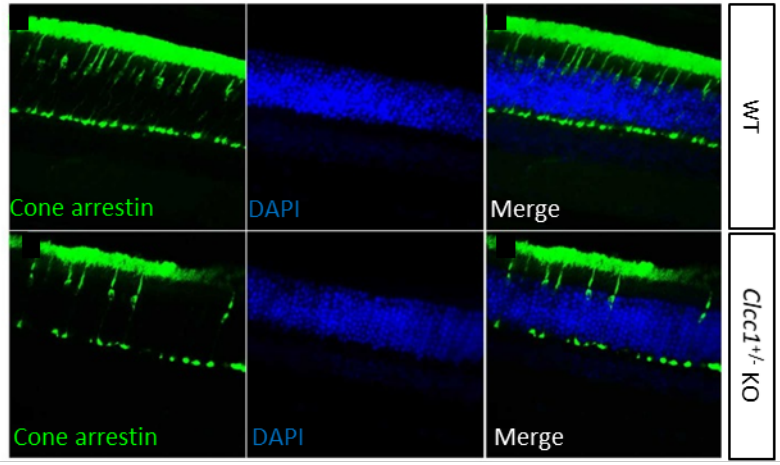
Cone arrestin
DAPI
Merge
WT
Cone arrestin
DAPI
Merge
Clcc1+/- KO

(iii)

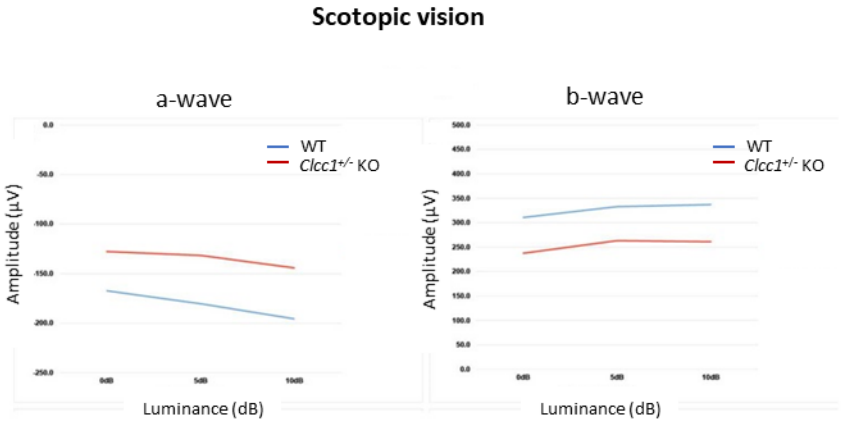
Scotopic vision
a-wave
b-wave
WT
Clcc1+/- KO
Amplitude (µV)
Luminance (dB)

(iv)

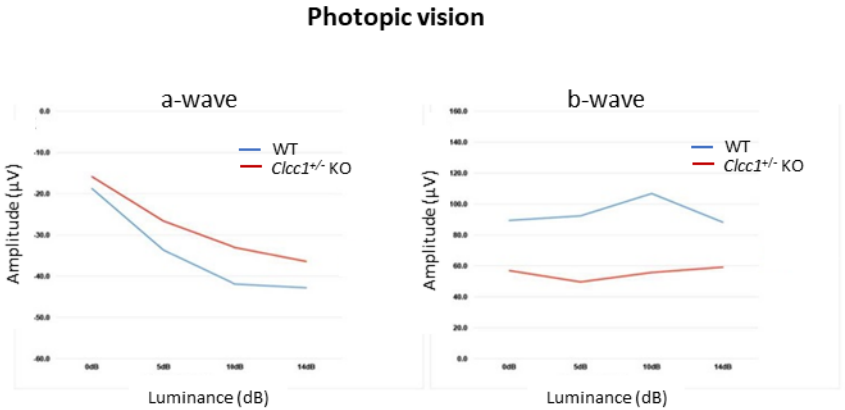
Photopic vision
a-wave
b-wave
WT
Clcc1+/- KO
Amplitude (µV)
Luminance (dB)

Figure 4.6 Effects of heterozygosity for Clcc1 KO on mouse retinas. (i) *Haematoxylin & eosin staining of WT and Clcc1$^{+/-}$ knockout 7-month-old mouse retinas. While the overall structure of the retina was preserved, staining revealed decreased cell density in the outer and inner nuclear layers, as well as the outer and inner plexiform layers as well as structural disarray of the photoreceptor layer in Clcc1$^{+/-}$ KO mice compared with the WT mice.* ***(ii)*** *Immunostaining of cone arrestin in WT and Clcc1$^{+/-}$ KO mice. The WT mice exhibit normal cone photoreceptors staining pattern while Clcc1$^{+/-}$ KO mice revealed reduced number of cone photoreceptors.* ***(iii-iv)*** *Electroretinography of wild-type and Clcc1$^{+/-}$ KO mice showed approximately 20-50% decreases in the amplitude of both the scotopic and photopic a- and b- wave amplitude responses in Clcc1$^{+/-}$ KO mice compared to WT at all levels of luminance. Figure made at NEI.*

4.2.4 CLCC1 localises in the ER

To confirm the ER localisation of CLCC1 reported by Jia et al. [206], HEK293 cells were cultivated, fixed, and immunolabelled with CLCC1 antibody and ER markers including calreticulin, KDEL, and calnexin. The tetrapeptide KDEL is located at the C-terminus of several ER luminal proteins, and it is a retrieval motif essential for the precise sorting of proteins along secretory pathways [235]. These markers have been chosen based on what was already available in the lab, and based on the compatibility with CLCC1 antibody. CLCC1 staining showed a punctate distribution in the cytoplasm, in particular in the perinuclear region and nuclear envelope. CLCC1 showed partial co-localisation with KDEL (Fig. 4.7 (i), arrows), but not with calnexin the expression of which appeared more defined (or clustered) than CLCC1 (Fig. 4.7(i)). NIH/3T3 cells were also

used to verify the distribution of endogenous CLCC1 in mouse fibroblasts (Fig. 4.7(ii)). The localisation pattern of CLCC1 in murine cells was punctate and comparable to that seen in human cells, indicating conservation of function. It was not possible to double stain the cells with CLCC1 and calreticulin as both antibodies were raised in rabbit. This result indicates that CLCC1 may co-localise with proteins carrying the KDEL sequence at their C-terminus.

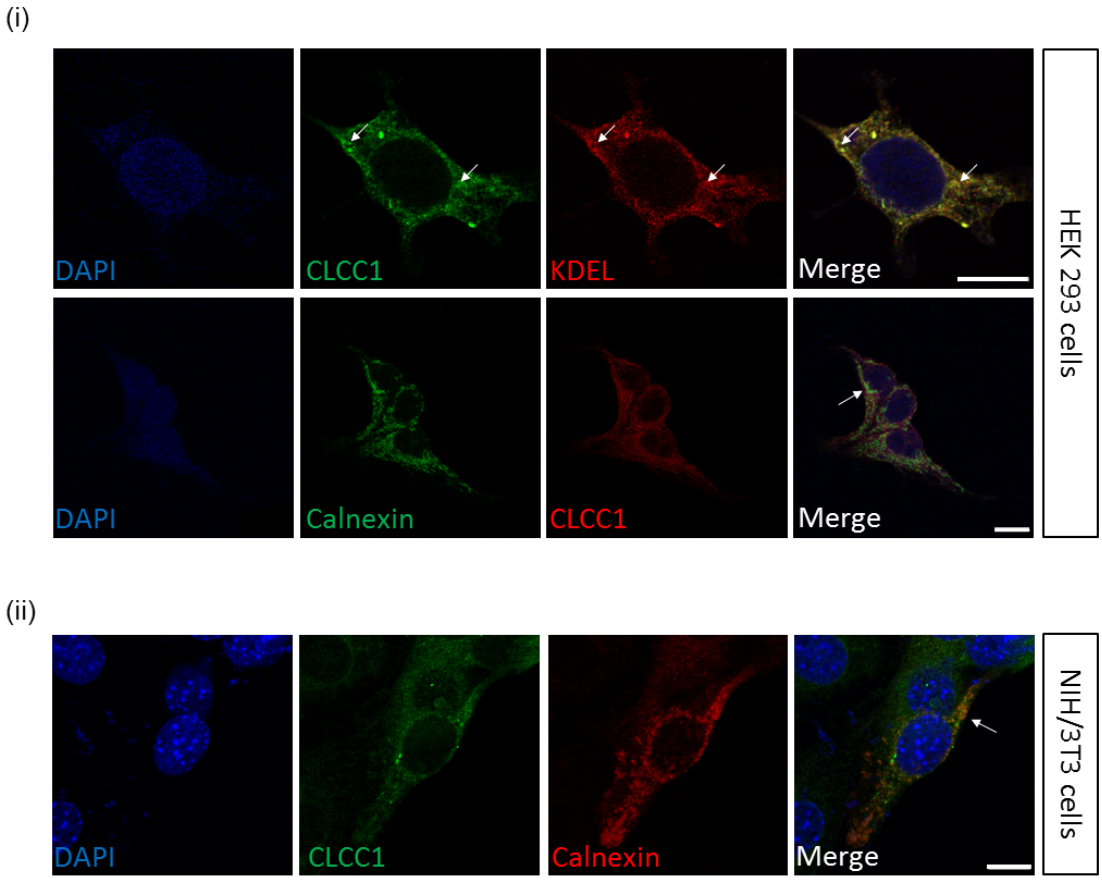

Figure 4.7 CLCC1 localisation with ER markers. ***(i)*** *In HEK293 cells, endogenous CLCC1 co-localises with KDEL but not with calnexin.* ***(ii)*** *In NIH/3T3 cells, the endogenous distribution of CLCC1 was similar to HEK293 cells, also the localisation of CLCC1 relative to calnexin was similar as well. Scale bar 10 μm.*

To overcome problems in compatibility between antibodies and to verify the localisation of mutated CLCC1, expression studies were performed using N-terminal YFP-tagged CLCC1 and C-terminal FLAG tagged CLCC1 (gifts of Dr. John Chilton). Both YFP and FLAG tags were used because of the tendency of fluorescent proteins to impair the folding or binding sites of the tagged protein; the FLAG tag is smaller in size, therefore less likely to affect the activity of a target protein. Overexpression of both YFP tag or FLAG-tag plasmids did not influence the localisation of CLCC1 within the ER, as demonstrated by co-staining with calreticulin. (Fig. 4.8), giving confidence that the tagged forms of CLCC1 may faithfully represent the localisation of the endogenous molecule. Moreover, there were no observable differences in localisation between endogenous CLCC1 and tagged constructs, or between the wild type protein and the Asp25Glu mutant.

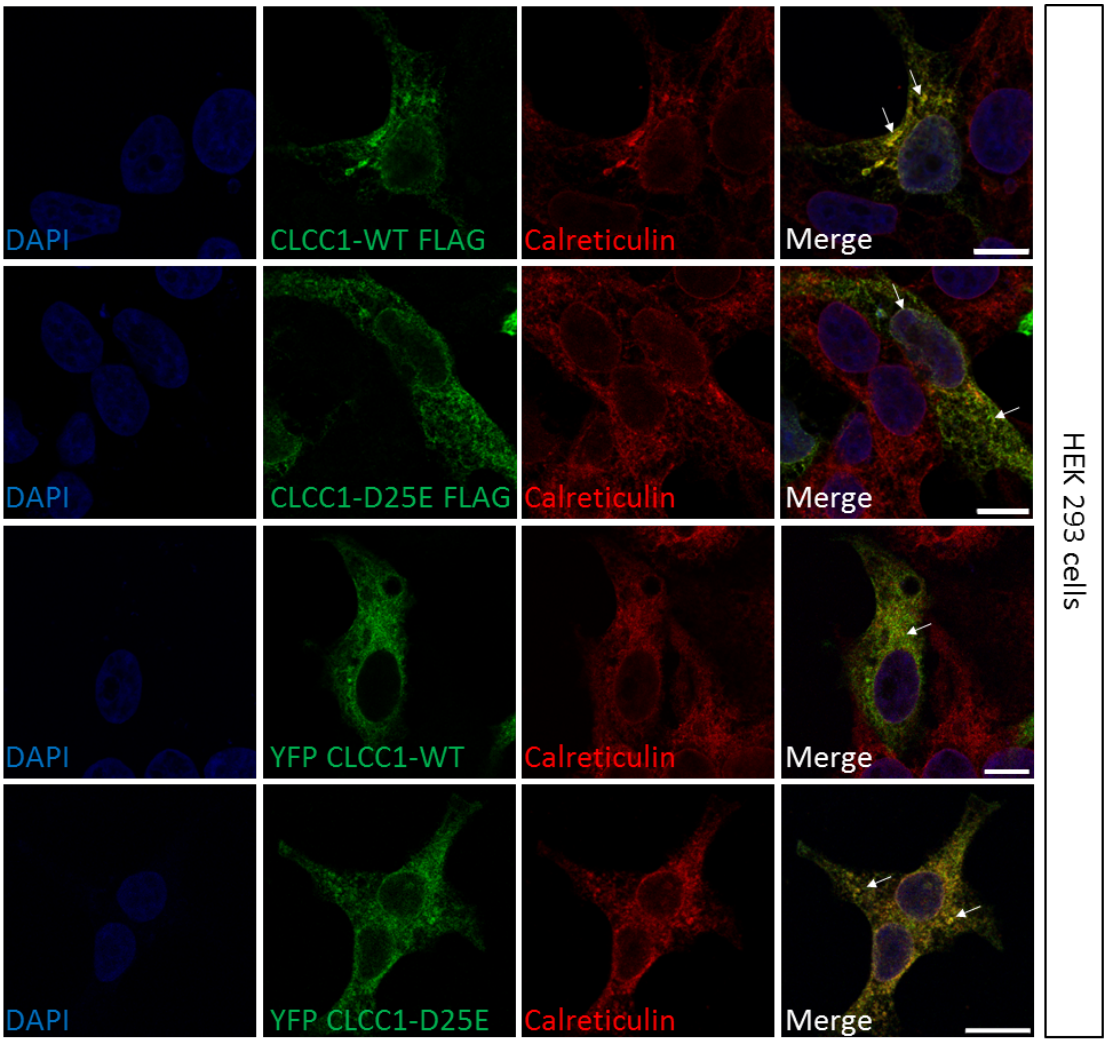

Figure 4.8 CLCC1 localisation with Calreticulin in HEK293 cells. *HEK293 cells were transiently transfected with different constructs containing CLCC1-WT and CLCC1-Asp25Glu. Both CLCC1-WT and CLCC1-Asp25Glu show co-localisation with calreticulin. Scale bar 10 µm.*

To assess the localisation of CLCC1 in a more physiologically relevant cell type, E7 chick retinal ganglion cells (RGC) were investigated. E7 RGC cells were chosen for two main reasons: (i) RGC differentiate at early stages of development, therefore at E7 a relatively pure population of primary neurons can be readily obtained and (ii) they are routinely available in the laboratory and

they are straightforward to culture. Unfortunately, the expression of endogenous CLCC1 could not be assessed as the antibody did not recognise the chick epitope. However, based on our earlier data showing that epitope-tagging did not appear to interfere with the localisation of CLCC1 (Fig. 4.8) it was decided to nucleofect RGC with CLCC1-WT FLAG/CLCC-Asp25Glu FLAG, and mCherry-KDEL, as tubular ER marker [236]. CLCC1 was found to co-localise with KDEL in the cell body and in the axonal ER (Fig. 4.9 (i-ii)).

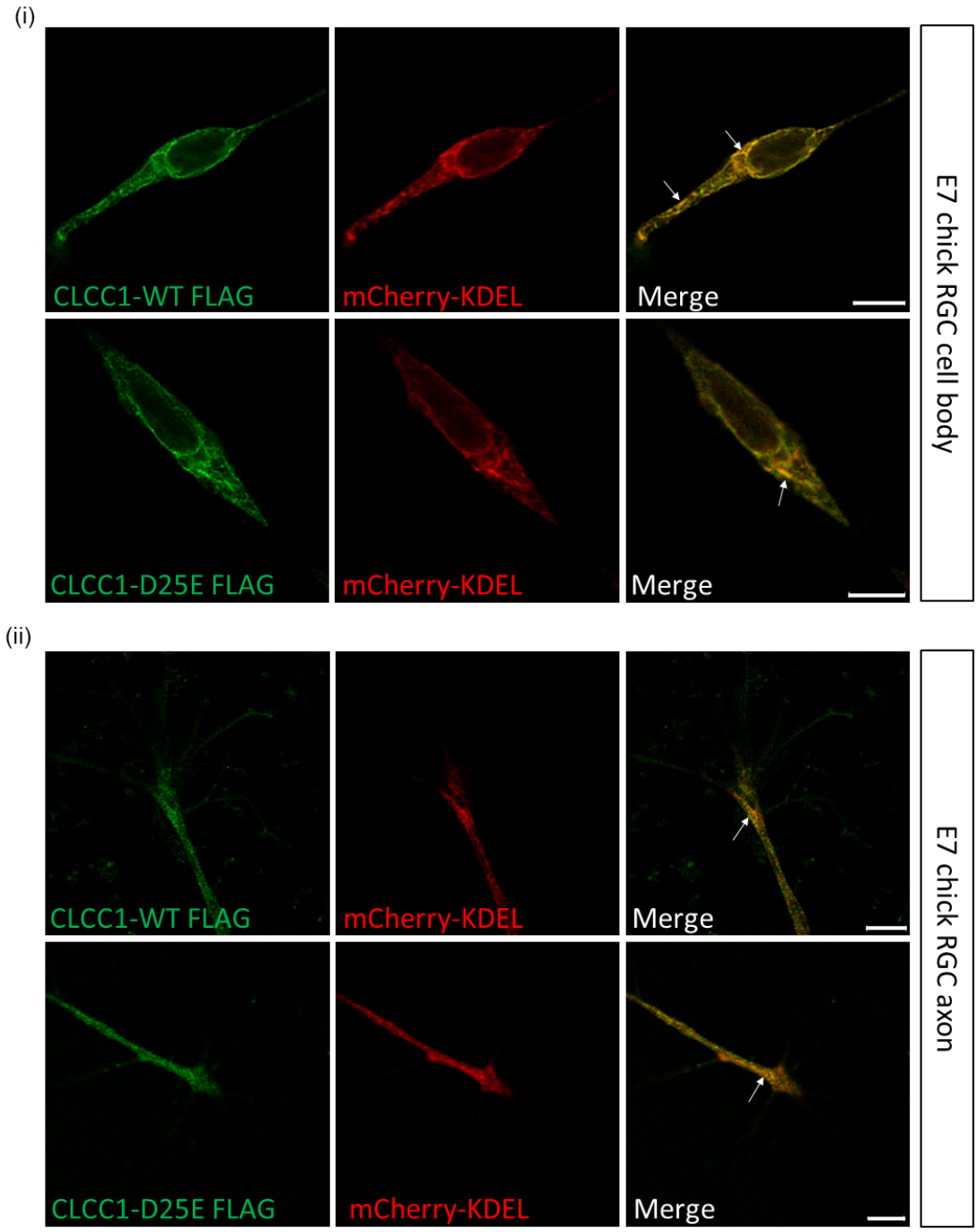

Figure 4.9 CLCC1 wild type and Asp25Glu variant in E7 chick retinal ganglion cells. *E7 RGC were dissociated and co- nucleofected with CLCC1 WT or Asp25Glu and mCherry-KDEL. CLCC1 WT and mutant co-localise with KDEL in the RGC cell bodies* ***(i)*** *and growth cones* ***(ii)****. Scale bar 5 µm.*

4.2.5 CLCC1 isoforms

CLCC1 is predicted to have four different isoforms produced by alternative splicing (www.uniprot.org) (Fig. 4.10). The canonical isoform (isoform 1) is stems from twelve *CLCC1* exons encoding 551 amino acids (aa) with a predicted molecular weight of ~62 kilodalton (kDa) (Fig. 4.10 (i)); isoform 2 is shorter than the canonical isoform, using an alternate splice site in the 5' UTR, lacking exon 1, but maintaining the reading frame (Fig. 4.10 (i)). It has a length of 501 aa and a predicted molecular weight of ~56 kDa. Both isoforms 1 and 2 contain three transmembrane domains, with a cytoplasmic N-terminus (N-term) and a luminal C-terminus (C-term) (Fig. 4.10 (ii)). The third isoform differs in the 5' UTR, lacking two consecutive exons in the coding region (exon 5 and 6) (Fig. 4.10 (i)); it comprises 430 aa with a predicted molecular weight of ~47 kDa with a single transmembrane helix (Fig. 4.10 (ii)). Isoform 4 is the shortest isoform, lacking four consecutives exons (from exon 5 to exon 8) (Fig. 4.10 (i)), with a length of 366 aa and a predicted molecular weight of ~39 kDa. It differs from the other isoforms by the presence of two transmembrane domains and cytoplasmic C- and N-termini (Fig. 4.10 (ii)). Transmembrane domains (TM) of isoform 1 were encoded by amino acids Val185 to Thr205 (exon 5 and 6), Leu217-Phe237 (exon 6), and Ile330-Cys350 (exon 9 and 10). Isoform 2 TMs were encoded by amino acids Tyr133-Trp154 (exon 5 and 6), Val166-Trp183 (exon 6), Ala282-Ala302 (exon 9 and 10). Isoform 3 TM was encoded by exon 10 Ala211-Ala232, while for isoform 4 they were encoded by amino acids Ile103-Thr124 in exons 4 and 9, and Ile145-Gly169 in exons 9 and 10.

While the TM domain encoded by exons 9 and 10 were common to all isoforms, isoforms 1 and 2 showed two TM domains encoded by exon 5 and 6, and 6 respectively. Isoform 4 instead presented a TM domain encoded by exon 4 and

exon 9. Absence of a publicly available 3D structure does not allow the prediction of which exon encodes for a precise TM, and the location of each TM region remains hypothetical. Additionally, tagged gene constructs indicated that all isoforms were restricted to the ER (Fig. 4.11). However it has been possible to verify the existence of isoforms 1 and 2 by western blotting (see Fig. 4.13 (i)).

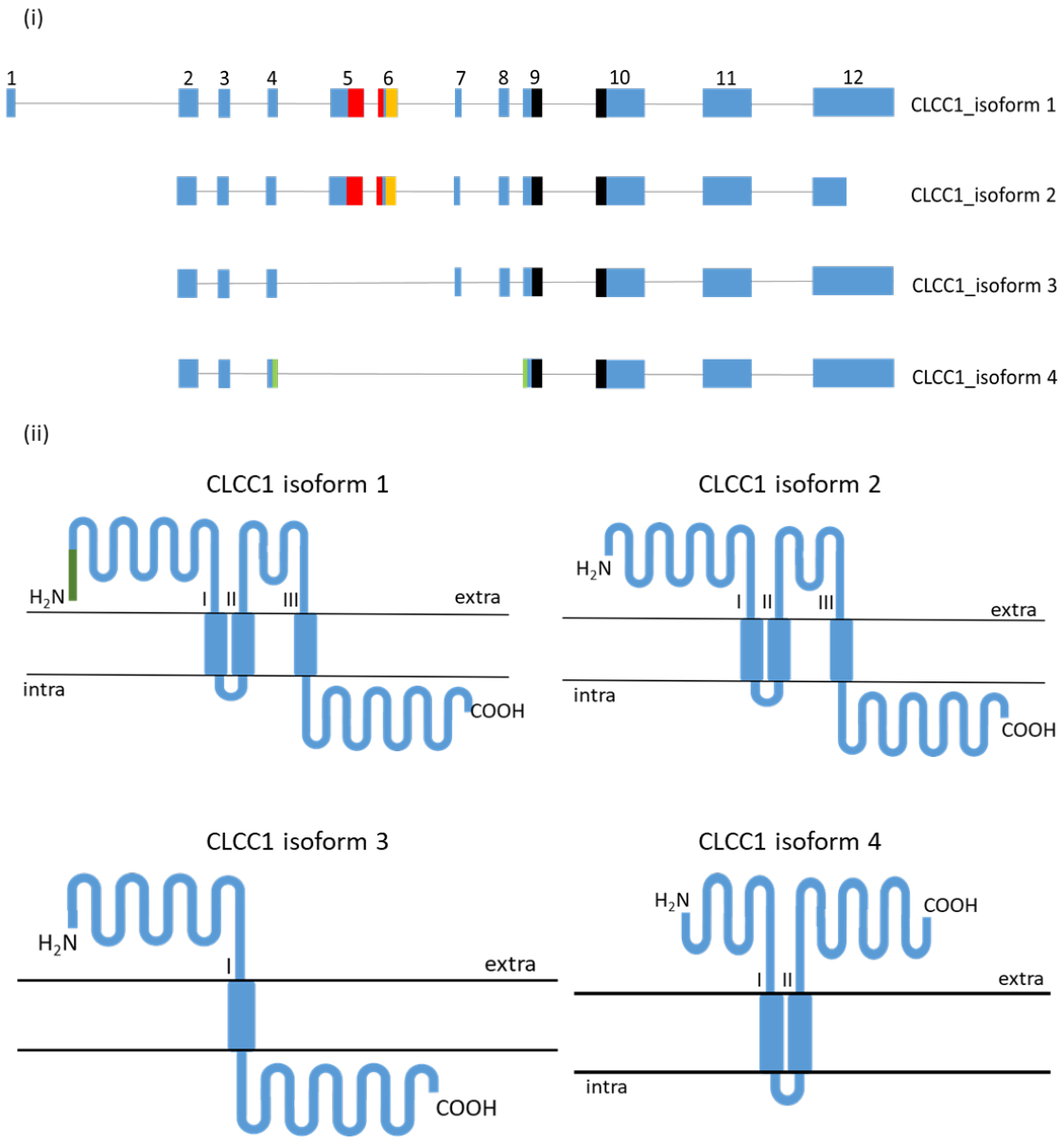

Figure 4.10 Topology of CLCC1 predicted isoforms. ***(i)*** *Schematic representation of CLCC1 isoforms. The numbers indicate the exons, while the colours indicate which part of exons code for a TM domain.* ***(ii)*** *CLCC1 isoform 1 has 3 transmembrane domains and 18 aa signal peptide indicated by the green bar. Isoform 2 is similar to isoform 1 but lacks the signal peptide at 5'UTR. The third isoform has only one transmembrane domain. Isoform 4 has two transmembrane helices and both C- and N-termini are cytoplasmic. The number of TM domains was indicated with I, II, III.*

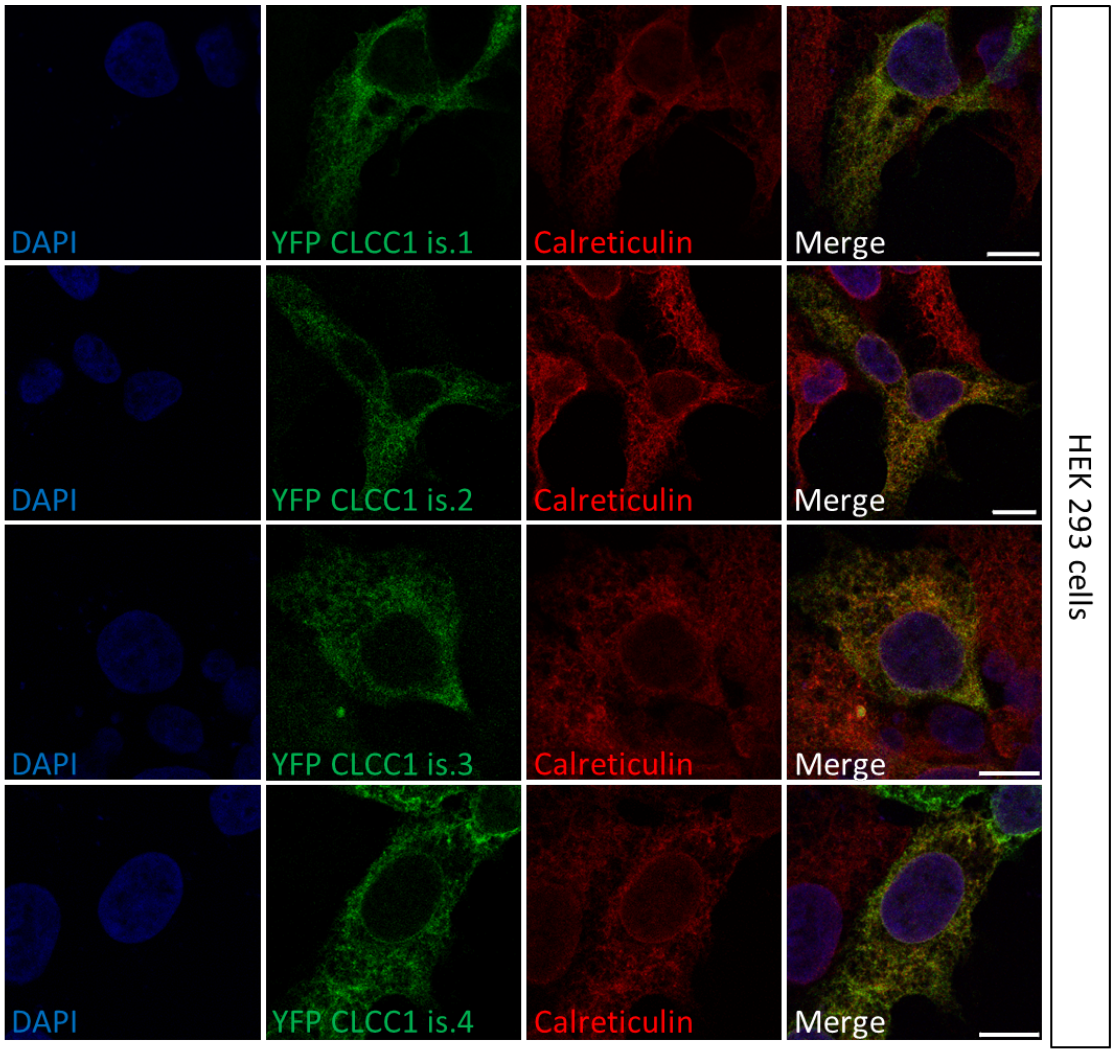

Figure 4.11 Co-localisation of CLCC1 isoforms with calreticulin. *HEK293 cells were transiently transfected with the different YFP CLCC1 isoforms and immunolabelled for calreticulin. All CLCC1 isoforms localise in the ER, co-localising with calreticulin. Scale bar 10 µm.*

The orientation of full-length CLCC1 within the membrane was assessed using a vector incorporating YFP at the N-terminus of CLCC1, and the FLAG tag at the C-terminus. HEK293 cells were transfected with YFP-CLCC1-FLAG, fixed and stained with anti-FLAG and calreticulin antibodies (Fig. 4.12 (i)). To assess the relative co-localisation the Pearson's coefficient was calculated using

ImageJ plug-in JACOP, for YFP vs calreticulin and FLAG vs calreticulin. There was no significant difference between the two sets of data (Fig 4.12 (ii)). To further investigate and obtain a more definitive result, a semi-permeabilisation with 0.1% saponin was performed on NIH/3T3 cells transfected with CLCC1-WT FLAG and stained calreticulin (Fig.4.12 (iii)). With the assumption that if the C-termini of CLCC1 was in the ER lumen, no fluorescence of FLAG and calreticulin should have been detected, as the antibody should not be able to enter inside the ER, while if the C-termini of CLCC1 was cytoplasmic, only the FLAG fluorescence should have been detected. However, inconsistent results amongst replicates did not gave a conclusive answer, an example of these results is in Figure 4.12 (iii).

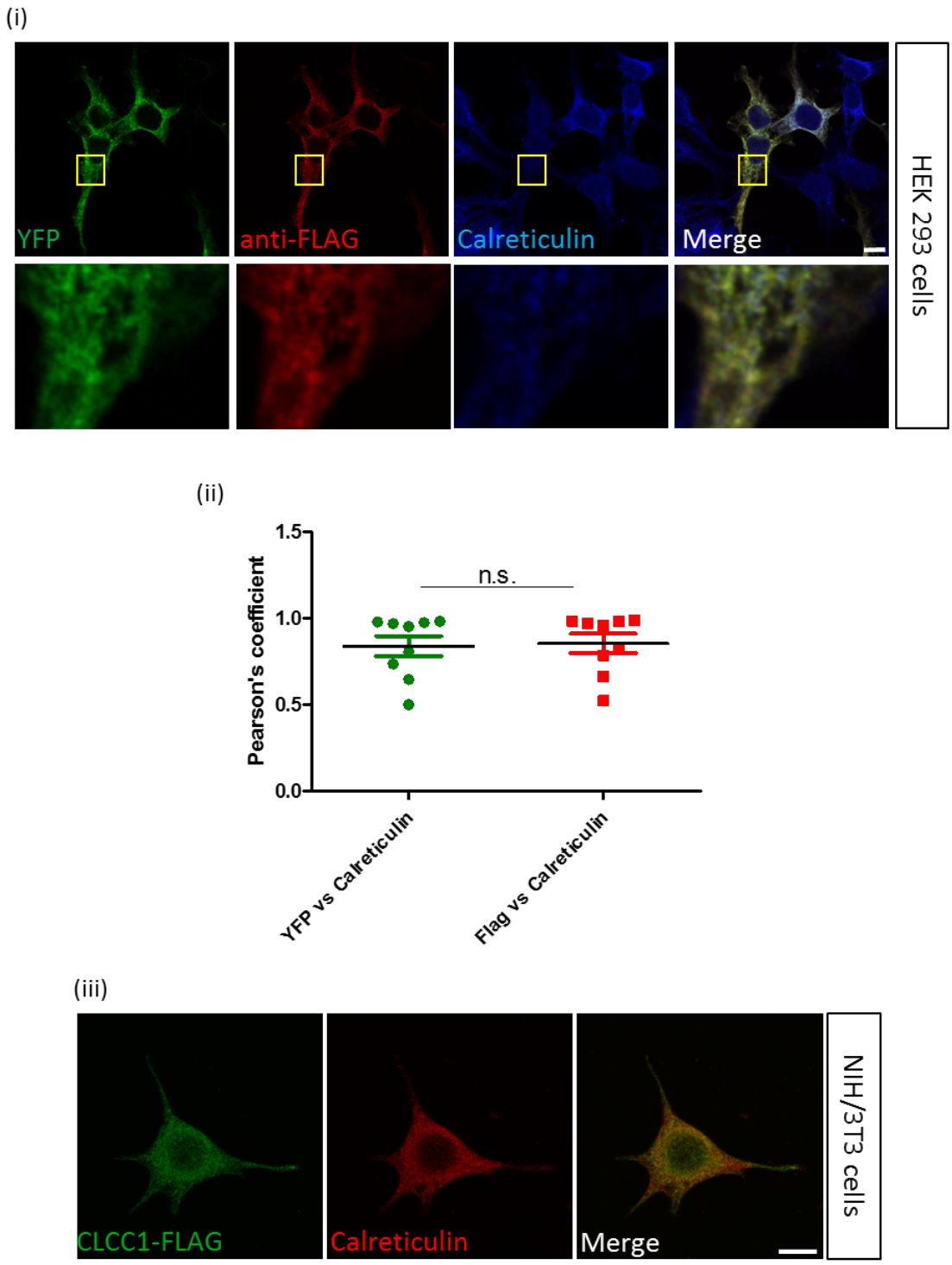

Figure 4.12 Assessment of C- and N-termini localisation (i) *HEK293 cells were transfected with YFP-CLCC1-FLAG vector, and stained with calreticulin.* ***(ii)*** *Co-localisation of YFP vs calreticulin and FLAG vs calreticulin was calculated using Pearson's coefficient. Mann-Whitney U-test was used to determine that there was no significant difference between the groups (n=9;*

p=0.6048). ***(iii)*** *Semi-permeabilisation of NIH/3T3 cells gave inconsistent results. Scale bar 10 µm.*

4.2.6 Co-immunoprecipitation of CLCC1 and calreticulin

To determine if CLCC1 directly interacts with calreticulin, immunoprecipitation was performed using the CLCC1 antibody as bait, and proteins were visualised by Western blot. In the immunoprecipitated sample (IP) two bands were detected when the blot was probed with the CLCC1 antibody, one band of ~65 kDa and a second band of ~50-55 kDa (Fig 4.13 (i)), indicating the successful pull-down. No CLCC1 was present in the '-' lane, corresponding to the negative control of the IP (it contains proteins that are not interacting with the immunoprecipitated protein), and in the input sample. A band corresponding to calreticulin (~50-55 kDa) was detected when endogenous CLCC1 was precipitated (Fig 4.13 (ii)). Conversely, when endogenous calreticulin was pulled down, a single band corresponding to a single CLCC1 isoform was present on the blot (Fig 4.13 (iii-iv)).

To define if the interaction of CLCC1 with calreticulin happened also when CLCC1 was overexpressed, HEK293 cells were transiently transfected with CLCC1-WT/Asp25Glu FLAG and YFP CLCC1-WT/Asp25Glu, and pulled down using the tags as bait. Western blot (Fig. 4.14 (i)) revealed that calreticulin was not present in the CLCC1-WT FLAG sample (lane 1), as well as in the CLCC1-Asp25Glu sample (lane 3). However, some calreticulin was detected in lanes 2 and 4, respectively the negative controls of CLCC1-WT FLAG and CLCC1-Asp25Glu FLAG, indicating that the FLAG tag at the C-terminus of CLCC1 likely impairs the binding between CLCC1 and calreticulin.

To evaluate if the C-terminal FLAG tag may obstruct the binding site of CLCC1 with calreticulin, HEK293 were transiently transfected with N-terminal YFP tagged CLCC1. The immunoprecipitation was performed using the GFP-trap as widely used for co-immunoprecipitation of GFP/YFP plasmids. Western blot (Fig. 4.14 (ii)) showed that calreticulin was exclusively present in negative controls (lanes 2 and 4) and absent in the IP samples (YFP CLCC1-WT in lane 1, and YFP CLCC1-Asp25Glu in lane 3). These results indicate that the function of CLCC1 may be related to calreticulin however, the multitude of pathways in which calreticulin is involved makes it difficult to predict which CLCC1 may participate in. Also, the pulldown of plasmids expressing CLCC1 showed no co-immunoprecipitation of calreticulin, suggesting that tags on either the C-terminus or N-terminus may prevent the association of CLCC1 with other proteins.

In future studies it would be interesting to perform a pull-down using an anti-KDEL antibody however the validity of this approach needs to be carefully considered as the KDEL antibody binds every protein containing the KDEL sequence.

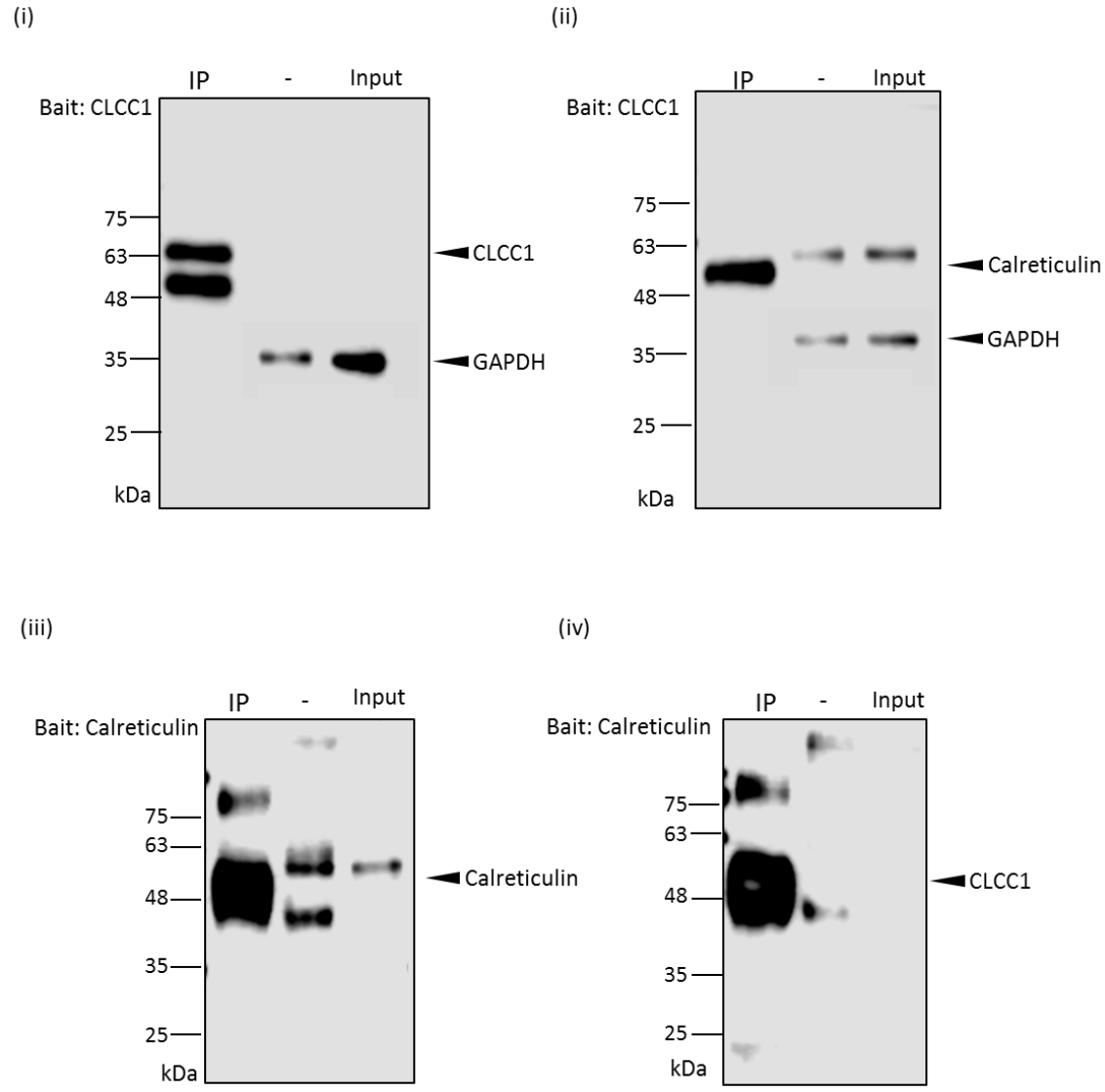

Figure 4.13 Endogenous CLCC1 co-immunoprecipitates with calreticulin. ***(i)*** *immunoprecipitation of endogenous CLCC1 using CLCC1 antibody. The membrane was stained with CLCC1 and GAPDH to evaluate the efficacy of the pulldown. In the 'IP' lane the two bands of weight ~65 kDa and ~50-55 kDa indicate the presence of two CLCC1 isoforms. It was not possible to detect CLCC1 in the input sample and in the '-' lane, which contains all the proteins except those present in the 'IP' sample. GAPDH was only present in the '-', and input samples.* ***(ii)*** *A band corresponding to calreticulin was identified in the 'IP' samples, indicating that calreticulin co-immunoprecipitates with CLCC1.* ***(iii)***

Endogenous calreticulin was pulled down using calreticulin antibody. Western blot showed a band corresponding to calreticulin (~50-55 kDa) in all the lanes. Presence of calreticulin in the '-' lane indicates that not all calreticulin attached to the beads during the pulldown. ***(iv)*** *When endogenous calreticulin was pulled down, a band corresponding to the size of CLCC1 (about 50 kDa) was present in the 'IP' lane.*

(i)

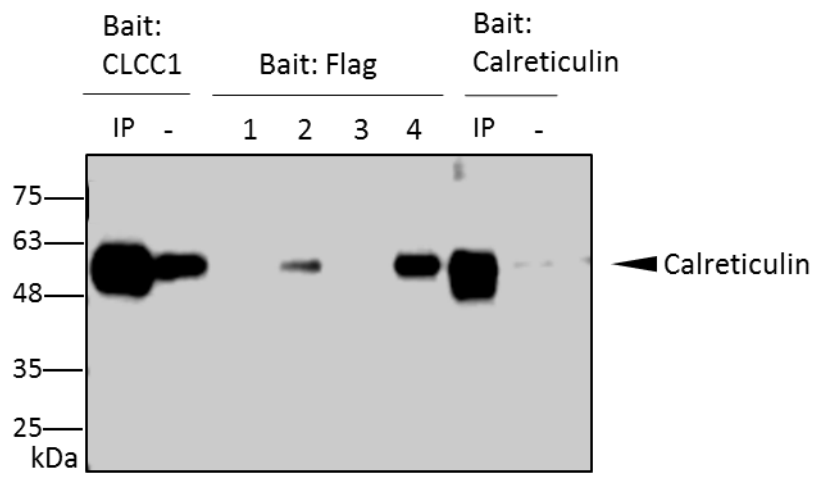

(ii)

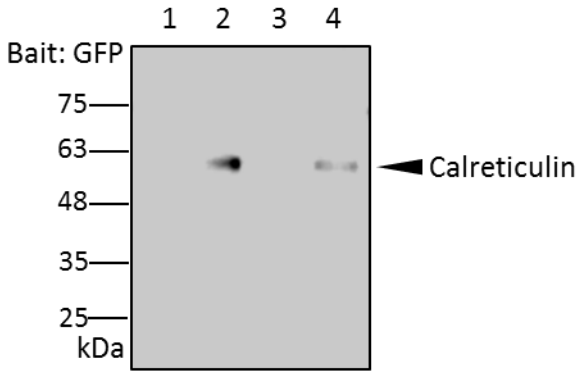

Figure 4.14 Calreticulin does not co-immunoprecipitate with CLCC1-WT/Asp25Glu FLAG or YFP CLCC1-WT/Asp25Glu. (i) *HEK293 cells were transiently transfected with CLCC1-WT FLAG or CLCC1-Asp25Glu FLAG, the co-immunoprecipitation was performed using the FLAG epitope as bait. Western blot showed that calreticulin was only present in lanes 2 and 4, corresponding to the negative controls of CLCC1-WT FLAG and CLCC1-Asp25Glu FLAG. Absence of calreticulin proteins was detected in the IP of CLCC1-WT FLAG and CLCC1-Asp25Glu FLAG. Pulldown of endogenous CLCC1 and endogenous calreticulin were used as positive controls.* ***(ii)*** *pulldown of YFP CLCC1-WT and YFP CLCC1-Asp25Glu using GFP trap*

showed that calreticulin was not present in the IP samples (lanes 1 and 3) however, it was possible to detect a small amount of calreticulin in the negative controls.

4.2.7 Mass spectrometry analysis of CLCC1 binding partners

To identify other putative CLCC1 binding partners and learn more about CLCC1 function, Liquid Chromatography with tandem Mass Spectrometry (LC-MS/MS) analysis was performed at the University of Bristol, Proteomics Facility.

Endogenous CLCC1, CLCC1-WT FLAG, and CLCC1-Asp25Glu FLAG from HEK293 cells were immunoprecipitated using the Co-IP protocol as described before. For each experimental condition, the analysis was performed in two replicates. Results of the mass spectrometry were filtered following the pipeline described in Fig 4.15. Proteins identified in the controls were labelled as 'Negative' and each CLCC1-#-FLAG replicate was compared to the 'Negative'. Proteins not present in the 'Negative' or present with a 2.5-fold, or greater, increase in the protein score were added to the 'True Positives' lists. All the proteins present in both 'True Positives' lists were then included in the 'Double Positives' list. To classify the proteins based on score, the average of the scores of each replicate was performed. STRING (https://string-db.org/) was used to visualise connections and networks between proteins. Connections were visualised based on experimental data and information derived from curated databases, disconnected nodes were not shown. Clustering was performed using k-mean.

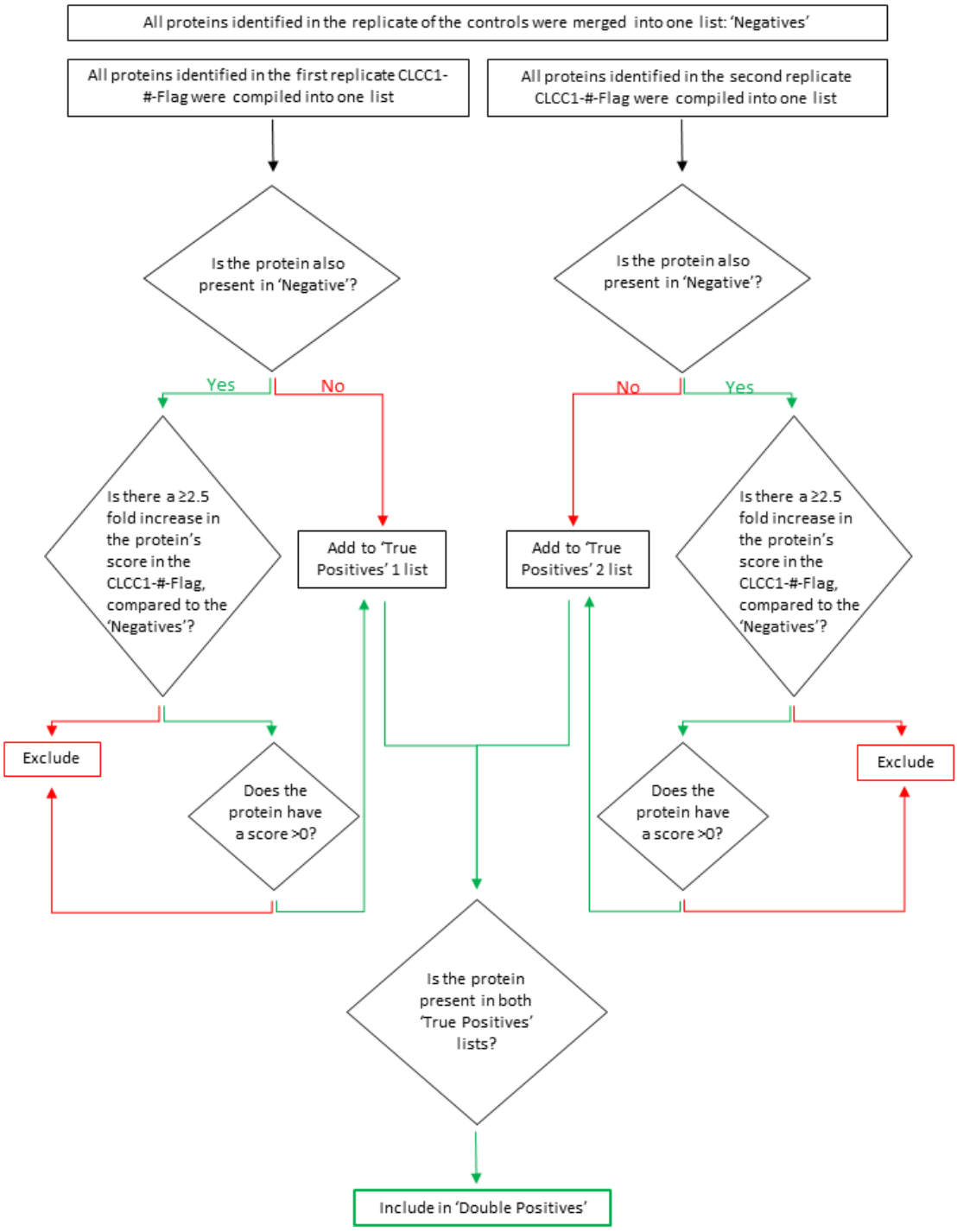

Figure 4.15 The process used to filter the LC-MS/MS data.

For endogenous CLCC1, hits were filtered against the control data sets used for FLAG tagged proteins pulldown. This identified 116 proteins as possible interactors with endogenous CLCC1, for which cluster analysis with STRING identified three main clusters. The biggest cluster contained 17 ribosomal proteins, RLPs proteins (Figure 4.16 (i), light green cluster), related to mRNA processing, which constitute one out of five major biological processes (Figure 4.16 (ii)) and molecular function gene ontology (GO) terms (Figure 4.16 (iv)). 13 proteins (Figure 4.16 (i), dark green cluster) were related to protein processing, in particular the cluster contained chaperones as HSPA8, and members of the TRiC chaperone complex, CCT3, CCT4, CCT5, which regulates telomere maintenance [237] and BBSome assembly [238]. The third cluster identified with STRING contained proteins related to intracellular transport (Figure 4.16 (i), blue cluster) as tubulins, TUBB2B and TUBB4A, cytoplasmic dynein DYNC1H1, coatomer complex COPB1, and KDELR1, a receptor involved in retention of proteins in the ER.

These results indicate that CLCC1 may be involved in folding, protein transport, or translation of proteins. The enrichment of mRNA-related hits could also be explained by the ability of the antibody used to pulldown CLCC1 to recognise the nascent CLCC1 protein still attached to the ribosome during protein translation.

Interestingly, calreticulin was not present in either duplicate of unfiltered hits.

(i)

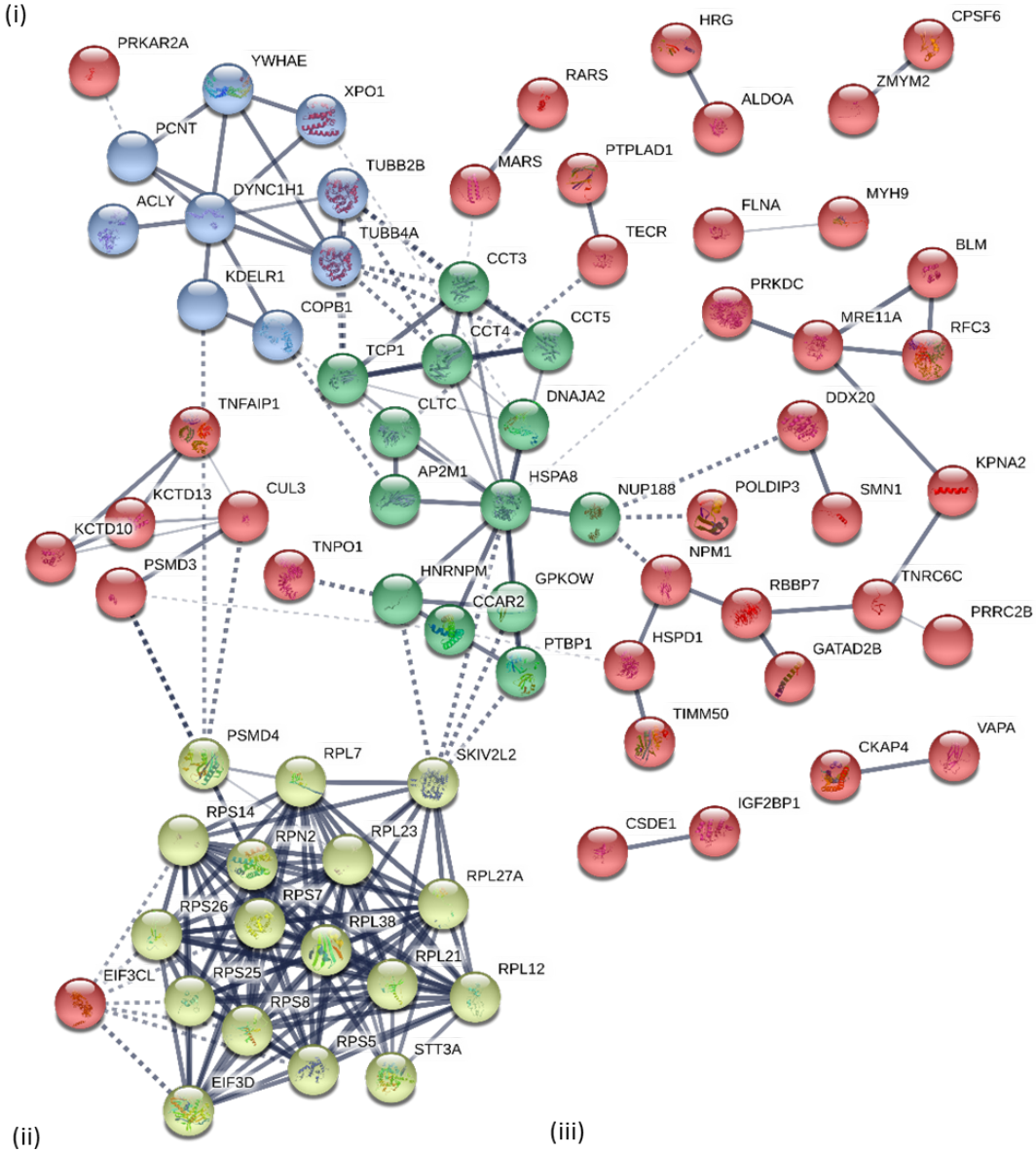

(ii)

Biological Process GO term description	Count in network	FDR
establishment of localization in cell	37	3.15e-12
protein localization to endoplasmic reticulum	14	5.14e-12
intracellular transport	34	5.14e-12
mRNA metabolic process	25	5.14e-12
intracellular protein transport	27	5.14e-12

(iii)

Cellular Component GO term description	Count in network	FDR
protein-containing complex	65	3.48e-15
cytosol	64	5.90e-14
intracellular part	98	2.55e-11
intracellular organelle part	79	2.37e-10
cytoplasmic part	81	2.71e-10

(iv)

Molecular Function GO term description	Count in network	FDR
RNA binding	31	9.90e-16
heterocyclic compound binding	60	7.68e-10
organic cyclic compound binding	60	9.86e-10
nucleic acid binding	43	8.99e-08
structural molecule activity	19	1.43e-07

Figure 4.16 STRING analysis of endogenous CLCC1 interactions. (i) *Clusters of proteins were highlighted with different colours. Light green cluster*

contained proteins related to the ribosome and mRNA processing, dark green cluster was composed by proteins with chaperone activity, while the blue cluster indicates proteins involved in intracellular trafficking. Proteins that do not belong to either cluster are shown in red. Line thickness represents the strength of the data support. ***(ii)*** *GO terms for biological processes.* ***(iii)*** *GO terms for cellular components.* ***(iv)*** *GO terms for molecular function.*

When CLCC1-WT FLAG was pulled down, 236 proteins were identified as possible interactors; STRING network analysis identified three main clusters of proteins. A cluster contained hits related to the proteasome (Fig. 4.17 (i), light green), as PSMB1, PSMD4, PSMC1, other proteasome subunits, and ubiquitin. The second main cluster (Fig. 4.17 (i), dark green) contained proteins related to the ER, in particular proteins associated to the translocon such as SEC61A, SPCS3, SSR1; proteins related to ribosomes such as RPS12, RPLP0; recycling carriers as SCAMP3; and proteins associated to N-glycosilation like ALG10, MAGT1, KRTCAP2 and DDOST. The third cluster (Fig. 4.17 (i), blue) was made of proteins necessary for transport like tubulins, TUBB2B, TUBB4B; dyneins, DYNC1H1 and DYNC1LI1; non-clathrin coated vesicles such as COPA, COPB2, COBP1; and KDELR1 and KDELR2 which retain soluble proteins into the ER. All the other proteins (Fig. 4.17 (i), red) showed no clustering with either of the three main clusters. Some of them had ATPase activity such as ATP1A1, ATP1B3; others had chaperone activity like HSPA8, HSPA5 and CALX. GO terms for cellular components identified all the proteins as related to the ER and nuclear outer membrane-ER interface (Fig. 4.17 (iv)). This is consistent with the observed pattern of CLCC1 expression seen in HEK293 and RGC on the boundary between the nuclear envelope and the ER (Fig. 4.8 and Fig. 4.9).

Interestingly, the proteasome cluster was not present in the endogenous CLCC1 dataset which instead presented the ribosomal cluster, much less represented in the CLCC1-WT FLAG dataset. The presence of high represented proteasome pathway might be caused by the overexpression of plasmids itself, as the cells might increase protein degradation levels to reduce the protein overload which was caused by overexpression. Overexpression of proteins could also explain the presence of the high number of hits related to protein translocation into the ER, induced by higher levels of translation than in homeostatic conditions.

(i)

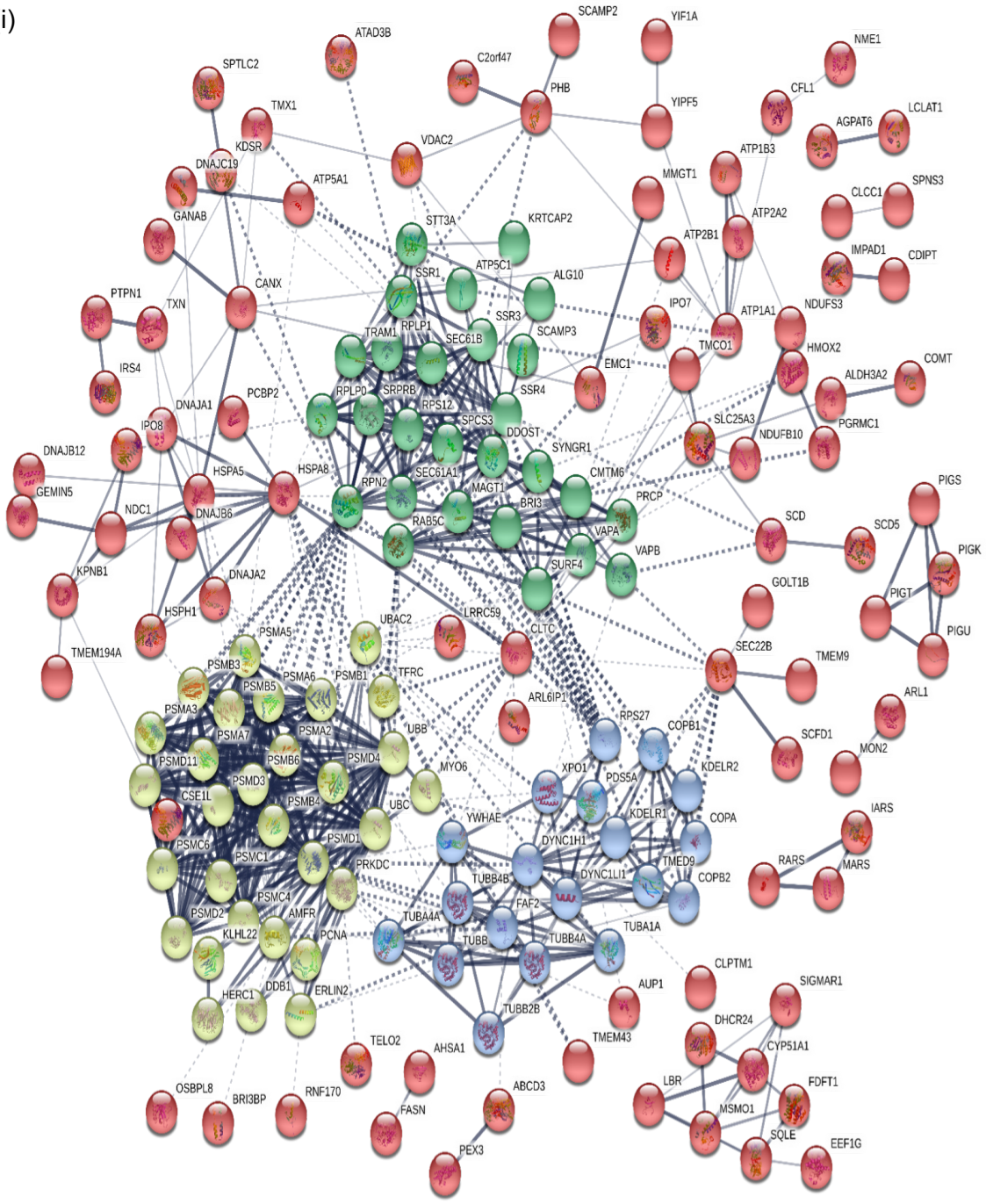
SCAMP2
YIF1A
ATAD3B
NME1
C2orf47
SPTLC2
PHB
CFL1
YIPF5
TMX1
LCLAT1
AGPAT6
KDSR
VDAC2
ATP1B3
DNAJC19
MMGT1
SPNS3
ATP5A1
CLCC1
GANAB
STT3A
KRTCAP2
ATP2A2
ATP2B1
IMPAD1
CDIPT
ATP5C1
SSR1
ALG10
CANX
PTPN1
TXN
SSR3
IPO7
ATP1A1
NDUFS3
TRAM1
RPLP1
SEC61B
SCAMP3
TMCO1
HMOX2
COMT
IRS4
EMC1
ALDH3A2
RPLP0
SRPRB
SSR4
PCBP2
DNAJA1
RPS12
SPCS3
SLC25A3
PGRMC1
IPO8
DDOST
NDUFB10
DNAJB12
SYNGR1
HSPA5
HSPA8
SEC61A1
CMTM6
PIGS
GEMIN5
RPN2
MAGT1
PRCP
NDC1
DNAJB6
BRI3
SCD
SCD5
RAB5C
VAPA
PIGK
KPNB1
VAPB
SURF4
DNAJA2
GOLT1B
PIGT
HSPH1
UBAC2
LRRC59
CLTC
PSMA5
PIGU
TMEM194A
SEC22B
TMEM9
PSMB3
PSMA6
PSMB1
TFRC
ARL1
PSMB5
ARL6IP1
RPS27
COPB1
PSMA3
UBB
SCFD1
PSMA7
PSMA2
MON2
PSMD11
PSMB6
PSMD4
XPO1
KDELR2
PSMD3
MYO6
PDS5A
CSE1L
PSMB4
UBC
IARS
YWHAE
KDELR1
COPA
PSMC6
PSMD1
DYNC1H1
PSMC1
TMED9
RARS
PRKDC
DYNC1LI1
MARS
TUBB4B
COPB2
PSMC4
FAF2
PSMD2
AMFR
TUBA4A
TUBA1A
KLHL22
PCNA
TUBB
TUBB4A
CLPTM1
DDB1
ERLIN2
AUP1
SIGMAR1
HERC1
TUBB2B
DHCR24
TELO2
AHSA1
TMEM43
CYP51A1
OSBPL8
ABCD3
LBR
FDFT1
BRI3BP
RNF170
MSMO1
FASN
SQLE
EEF1G
PEX3

(ii)

Biological Process GO term description	Count in network	FDR
transport	118	6.12E-20
localization	126	7.15E-16
intracellular transport	55	1.91E-12
organic substance transport	65	5.39E-11
cellular localization	67	8.59E-11

(iii)

Molecular Function GO term description	Count in network	FDR
threonine-type endopeptidase activity	10	8.52E-10
transporter activity	36	0.00011
ATPase regulator activity	6	0.0018
ATPase activator activity	5	0.002
nucleoside-triphosphatase activity	24	0.0025

(iv)

Cellular Component GO term description	Count in network	FDR
endoplasmic reticulum subcompartment	89	2.15E-48
nuclear outer membrane-endoplasmic reticulum membrane network	89	4.15E-48
endoplasmic reticulum membrane	88	5.99E-48
endoplasmic reticulum part	92	5.17E-44
organelle subcompartment	98	8.84E-42

Figure 4.17 STRING analysis of CLCC-WT FLAG interactions. (i) *Clusters of protein were highlighted with different colours. Three main clusters were highlighted by different colours. Light green cluster contained proteins related to the proteasome, dark green cluster was composed by proteins related to the ER, while the blue cluster indicates proteins involved in intracellular transport. In red were highlighted proteins that do not belong to either cluster. Line thickness represents the strength of the data support.* ***(ii)*** *GO terms associated with biological process.* ***(iii)*** *GO terms for cellular components.* ***(iv)*** *GO terms for molecular function.*

To investigate whether the Asp25Glu alteration may have a substantial effect on CLCC1 molecular interactions, two datasets (CLCC1-WT and CLCC1-Asp25Glu) were investigated to define interactions lost and/or gained with the alteration. From the list of proteins interacting with CLCC1-WT FLAG, 95 out of the 236 were present exclusively in the WT list when compared with the Asp25Glu mutant list (Fig. 4.18 (i)). These potentially represent the interactions lost in presence of the Asp25Glu alteration. As expected, most of the interactors

belonged to clusters already present into the WT list, the proteasome (Fig. 4.18 (i) light green), protein translocation into the ER (Fig. 4.18 (i) dark green), and protein trafficking (Fig. 4.18 (i) blue).

Mass spectrometry for CLCC1-Asp25Glu FLAG identified 249 binding partners, 109 were present exclusively in the Asp25Glu mutant, representing the interactions that were potentially gained following the alteration (Fig. 4.19). STRING clustering analysis highlighted a set of proteins related to intracellular transport such as ACTR1A, TMED10, GOSR2 (Fig. 4.19 (i) blue). The second cluster (Fig. 4.19 (i) dark green) contained proteins related to translocation into the ER, such as SEC61B and RPS5; and N-Glycosylation such as DAD1 and STT3B. The third cluster (Fig. 4.19 (i) light green) contained proteins involved in the translocation of RNA though the nuclear pore like RAN, NUP210, XPO4.

(i)

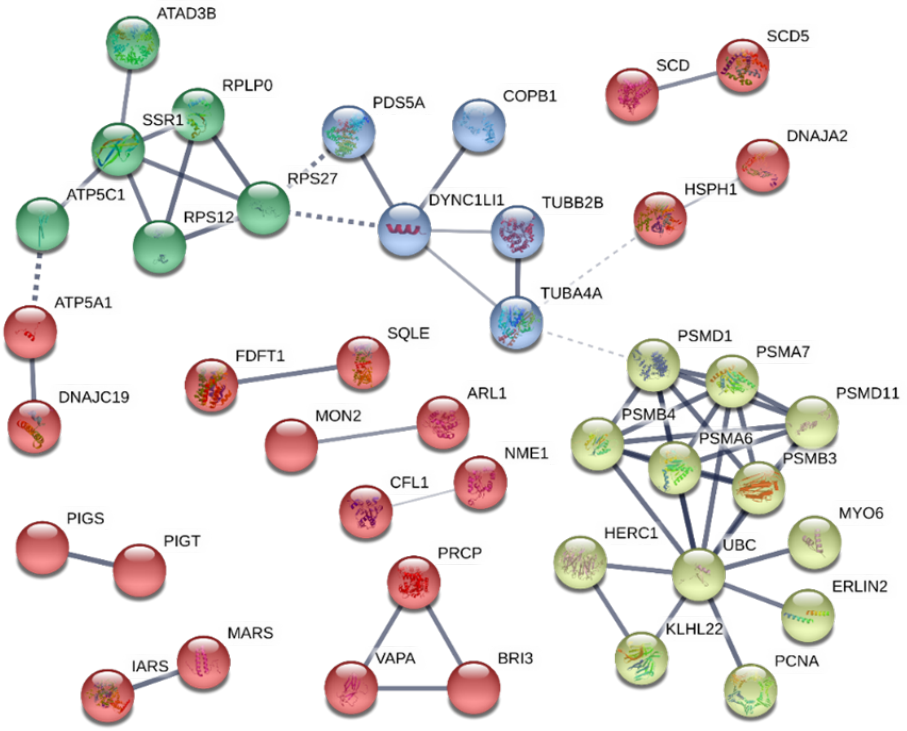

(ii)

Biological Process GO term description	Count in network	FDR
organonitrogen compound biosynthetic process	21	0.002
regulation of cholesterol biosynthetic process	5	0.0022
lipid biosynthetic process	13	0.0022
regulation of cholesterol metabolic process	5	0.0028
intracellular transport	19	0.0054

(iii)

Molecular Function GO term description	Count in network	FDR
threonine-type endopeptidase activity	4	0.0019
oxidoreductase activity, acting on CH-OH group of donors	6	0.0061
stearoyl-CoA 9-desaturase activity	2	0.0194
GPI-anchor transamidase activity	2	0.0194
ATPase regulator activity	3	0.0415

(iv)

Cellular Component GO term description	Count in network	FDR
cytoplasmic part	77	1.27E-10
organelle membrane	45	2.45E-10
endoplasmic reticulum subcompartment	25	6.45E-10
endoplasmic reticulum membrane	25	6.45E-10
endomembrane system	50	7.71E-10

Figure 4.18 STRING analysis of CLCC-WT FLAG interactions not present in CLCC1-Asp25Glu FLAG. *These interactions represent lost binding partners caused by the Asp25Glu alteration.* ***(i)*** *Clusters of protein were highlighted with different colours. Light green cluster contained proteins related to the proteasome, dark green cluster was composed by proteins related protein*

translocation into the ER, while the blue cluster indicates proteins involved in intracellular transport. In red were indicated proteins that do not belong to either cluster. Line thickness represents the strength of the data support. ***(ii)*** *GO terms associated with biological process.* ***(iii)*** *GO terms for cellular components.* ***(iv)*** *GO terms for molecular function.*

(i)

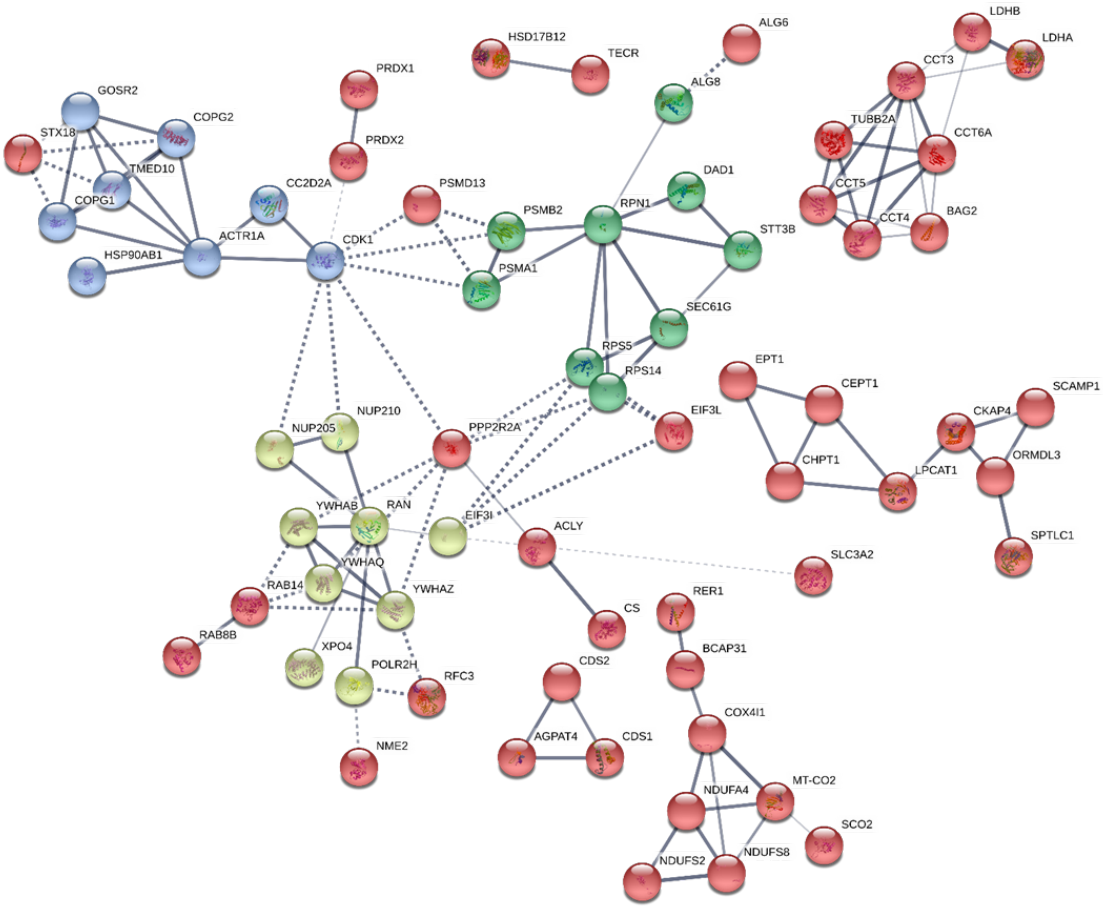

(ii)

Biological Process GO term description	Count in network	FDR
organonitrogen compound biosynthetic process	29	2.59E-07
organophosphate metabolic process	25	2.59E-07
organophosphate biosynthetic process	18	1.56E-06
lipid biosynthetic process	18	1.56E-06
nucleobase-containing small molecule metabolic process	18	6.40E-06

(iii)

Molecular Function GO term description	Count in network	FDR
CDP-alcohol phosphatidyltransferase activity	4	6.19E-05
phosphotransferase activity, for other substituted phosphate groups	5	6.19E-05
catalytic activity	55	6.19E-05
oxidoreductase activity	16	0.00016
diacylglycerol cholinephosphotransferase activity	3	0.00023

(iv)

Cellular Component GO term description	Count in network	FDR
cytoplasmic part	91	1.61E-14
nuclear outer membrane-endoplasmic reticulum membrane network	33	1.61E-14
organelle subcompartment	40	1.61E-14
endoplasmic reticulum subcompartment	32	2.49E-14
endoplasmic reticulum membrane	32	2.49E-14

Figure 4.19 STRING analysis of proteins gained with the CLCC1-Asp25Glu FLAG. *These interactions were present exclusively in the CLCC1-Asp25Glu FLAG, indicating new protein interactions gained with the Asp25Glu alteration.*

(i)*Clusters of protein were evidenced with different colours. Lines thickness represents the strength of the data support.* ***(ii)*** *GO terms associated with biological processes.* ***(iii)*** *GO terms for cellular components.* ***(iv)*** *GO terms for molecular function.*

Comparison between cellular component GO terms of different data sets (Fig. 4.20) identified that for CLCC1-WT FLAG the interactions mainly represented ER proteins (59%) or nuclear outer membrane-ER proteins (20%). Binding partners lost with the Asp25Glu alteration were mostly ER related (37%), although a substantial number were cytoplasmic (28%) relating to the endomembrane system (18%), and the organelle membrane (17%). The analysis of cellular component terms of binding partners gained with the Asp25Glu mutant identified a majority of them as cytoplasmic proteins (40%), 28% of which were related to the ER, 14% related to the nuclear outer membrane-ER boundary, and 18% of proteins related to organelle membrane. KEGG (Kyoto Encyclopaedia of Genes and Genomes) analysis of pathways indicated that most of the proteins CLCC1 interacted with were related to metabolic pathways, the proportion of them slightly increasing in both lost and gained interactions caused by the Asp25Glu alteration. Proteasome-related proteins are not represented in the dataset interactions gained by the alteration, which might indicate that the alteration *per se* does not increase protein degradation.

These results indicate that the function of CLCC1 may mainly relate to the cytoplasm and the ER, with limited involvement of other organelles. Interestingly, the nuclear outer membrane-ER compartment is not represented

in the set of proteins lost with the alteration. Amongst all datasets false discovery rate (FDR) confidence for cellular components GO terms was several orders of magnitude higher than biological process or molecular function.

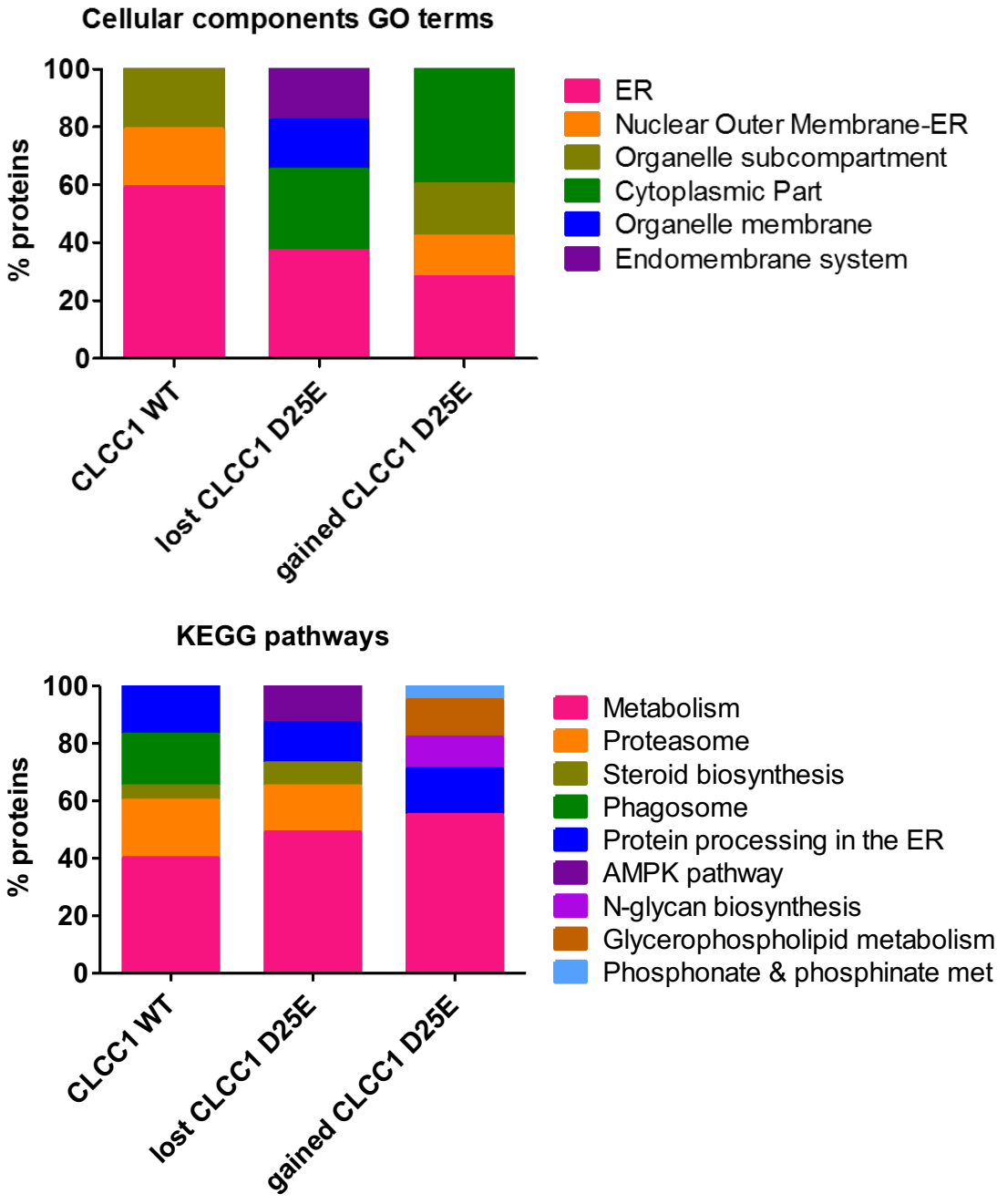

Figure 4.20 Cellular components and KEGG pathways analysis of mass spectrometry hits for the three data sets.

Mass spectrometry hits were also manually searched on PubMed to define which proteins have been reported as expressed in the retina (Fig. 4.21). Proteins were considered only if the protein score was over 10. Thirty-nine proteins were found reported as expressed in the retina, four of them present exclusively in the CLCC1-WT dataset, and twelve of them present exclusively in the CLCC1-Asp25Glu dataset. Twenty-three proteins were present in both datasets.

Subdivision of the thirty-nine proteins based on subcellular localisation found in UniProtKB/Swiss-Prot (www.uniprot.org/) and Human Protein Atlas (www.proteinatlas.org) showed that the compartments most represented were the cytosol, nucleus, and ER (Fig. 4.22).

Taken together, these results confirm that CLCC1 interacts primarily with ER proteins, consistent with ours and others immunocytochemical localisation studies (Fig. 4.8-4.9) [206]. The Asp25Glu alteration causes loss of ER interactions in favour of cytoplasmic ones. Identifying what is lost from the ER and what is gained in cytoplasm might provide evidence for CLCC1 function. The cellular components analysis suggests that, even though no change in subcellular localisation was detected, the alteration may alter interactions that occur at/in the ER. Interestingly, the mass spectrometry analysis did not report as binding partner calreticulin, supporting the evidence that the tag on proteins might interfere with the binding of functional partners.

From the analysis and clustering of mass spectrometry results we choose four interactions to analyse further: HSPA5 (BiP), SGMR1, CALX and EMC1. These proteins were present exclusively in the datasets where CLCC1 was overexpressed and absent in the endogenous CLCC1 dataset. All four proteins were expressed in the retina (Fig. 4.21) and located in the ER (Fig. 4.22), having different functions.

(i)

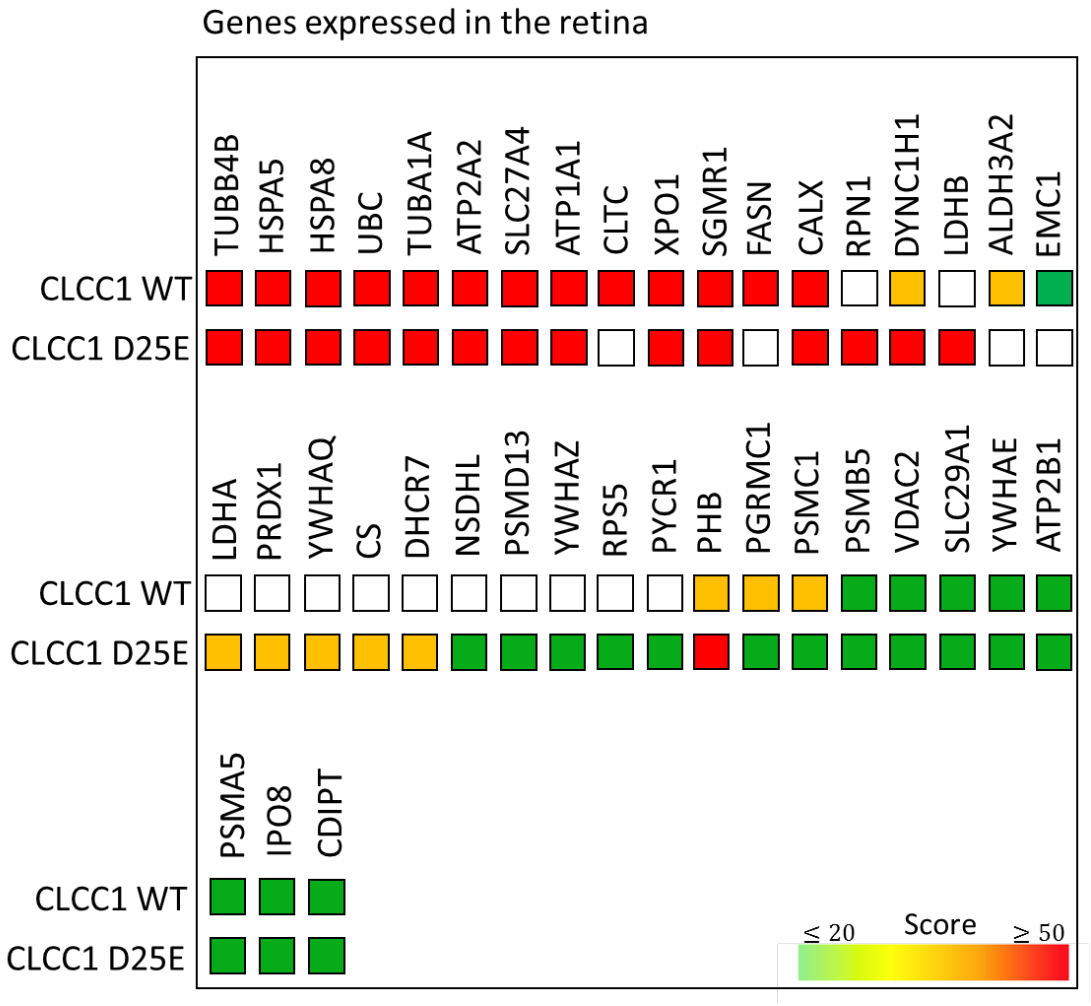

Figure 4.21 Genes reported as expressed in the retina. *Pubmed search of proteins/genes resulting from the mass spectrometry as expressed in the retina. Mass spectrometry protein scores over 50 are indicated with red squares, scores between 50 and 20 indicated by orange squares and scores lower than 20 indicated by green squares. White squares indicate protein/gene not reported in the data set.*

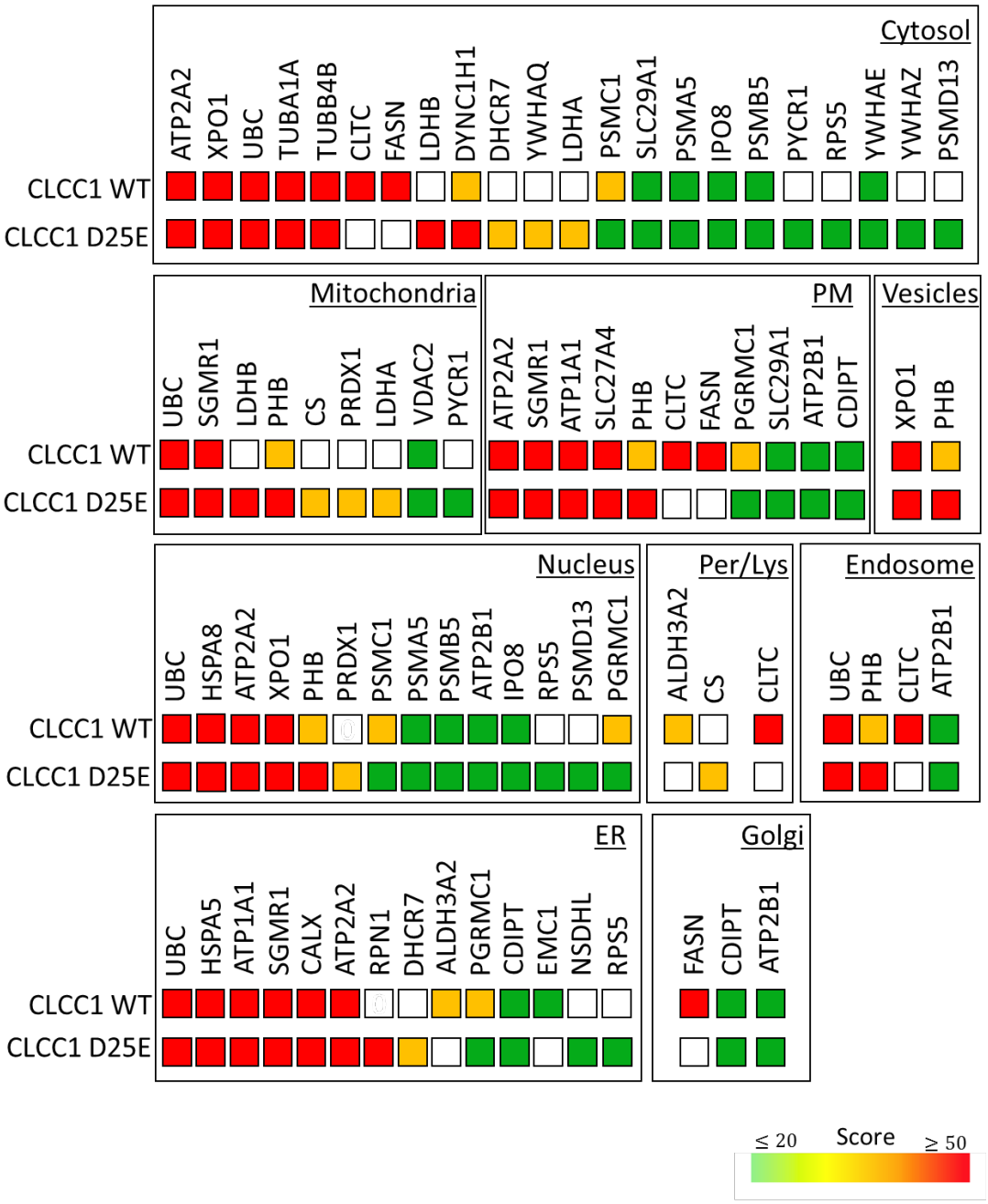

Figure 4.22 Subdivision of proteins based on intracellular compartmentalisation. *Subcellular localisation was searched on UniProtKB/Swiss-Prot and Human Protein Atlas. Mass spectrometry protein scores over 50 are indicated with red squares, scores between 50 and 20 indicated by orange squares and scores lower than 20 indicated by green squares. White squares indicate protein/gene not reported in the data set.*

4.2.8 Analysis of CLCC1 binding partners

From mass spectrometry analysis four proteins were chosen to further investigate their relationship with CLCC1. EMC1 is part of the ER membrane protein complex (EMC), a multi protein complex present in eukaryotes, which has 10 members. EMC1 disruption has been reported as associated with neurological degeneration [239] and retinal dystrophy [240]. EMC serves as insertase for weakly hydrophobic transmembrane domains of tail-anchored proteins [241], modulates the co-translational expression of multi-pass membrane proteins with challenging TMDs [242], promotes accuracy of G-protein-coupled receptor (GPCR) biogenesis through insertion of their first trans membrane domain [243], and maintains cholesterol homeostasis by promoting biogenesis of sterol-related enzymes [244]. Moreover, in Drosophila photoreceptors, EMC has been reported as an essential component for the stabilisation of immature rhodopsin and other multi-pass membrane proteins [245].

SGMR1 (also called SigmaR1) has been associated with hereditary motor neuropathy and amyotrophic lateral sclerosis [246, 247], and reported as expressed in the retina [248]. The SigmaR1 is a receptor, localising in mitochondria-associated membrane (MAM), which are the contact sites between ER and mitochondria, where calcium handling proteins such as IP3Rs, are high compartmentalised. Normally, SigmaR1 binds BiP, but upon stimulation SigmaR1 dissociates leading to a prolonged Ca^{2+} signalling into the mitochondria via IP3R. Upon ER stress or loss of calcium from the ER, SigmaR1 moves in the ER and is able to interact with PM proteins. Increased expression of SigmaR1 leads to the reduction of ER stress, probably this is related to the chaperone activity the SigmaR1 possess [249]. The association of

SigmaR1 with STIM1 induces a slow recruitment of STIM1 to ER-PM junction and reduces the binding to Orai1 [250].

BiP belongs to Hsp70 family of chaperons and has a major role in the ER. BiP is involved in chaperoning newly synthesised proteins, export of misfolded proteins to the proteasome, UPR signal transduction, calcium homeostasis, and protein translocation into the Sec61 complex [251-253].

Calnexin (CALX) is a transmembrane calcium-binding protein, a soluble paralogue of calreticulin. Calnexin binds partially folded glycoproteins to determine if they can be released from the ER or sent to the proteasome [254], and controls intracellular Ca^{2+} oscillation via interaction with SERCA [255].

To confirm that the selected proteins pulled-down with CLCC1 we co-immunoprecipitated endogenous CLCC1, and CLCC1-WT FLAG and CLCC1-Asp25Glu FLAG molecule after overexpression in HEK293 cells. Membranes were stained for EMC1, BiP, calnexin and SigmaR1. While the probing with BiP and EMC1 did not work, probing with anti-mouse SigmaR1 and calnexin showed a band in exclusively present in the lanes 1 and 3 corresponding to CLCC1-WT FLAG pull-down and CLCC1-Asp25Glu FLAG pull-down (Fig. 4.23), although absent in the endogenous CLCC1 pulldown. This indicates that these proteins co-immunoprecipitated with CLCC1 when overexpressed, confirming the mass spectrometry results.

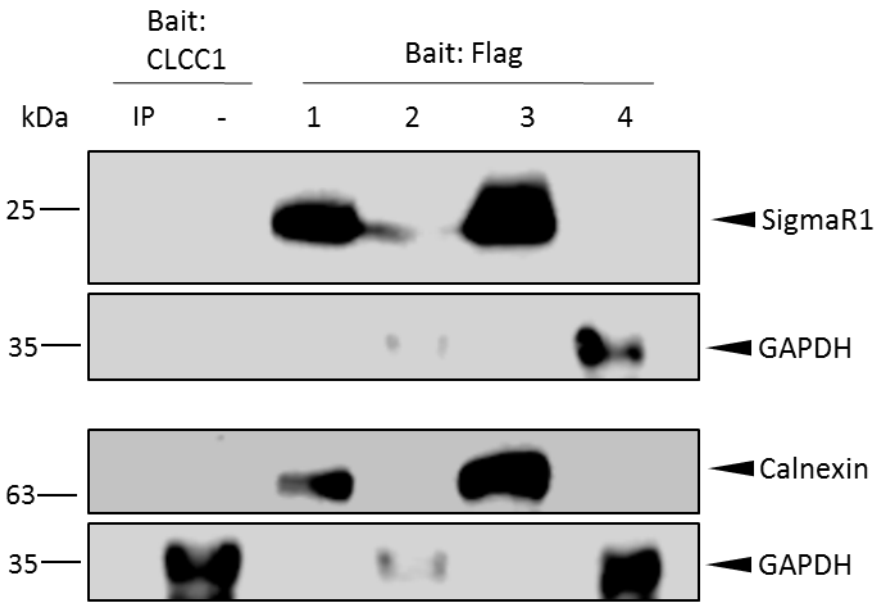

Figure 4.23 Calnexin and SigmaR1 co-immunoprecipitated with CLCC1-WT and Asp25Glu FLAG *HEK293 cells were transiently transfected with CLCC1-WT FLAG or CLCC1-Asp25Glu FLAG, the co-immunoprecipitation was performed using the FLAG epitope as bait, and CLCC1 antibody was used to co-immunoprecipitate the endogenous CLCC1. Western blot showed that calnexin and SigmaR1 were only present in lanes 1 and 3, corresponding to the CLCC1-WT FLAG and CLCC1-Asp25Glu FLAG. Both proteins were absent in the endogenous CLCC1 pull-down, confirming the mass spectrometry data.*

To confirm co-localisation between CLCC1 and the chosen proteins, NIH/3T3 cells were seeded and transfected with CLCC1-WT/Asp25Glu FLAG or YFP CLCC1-WT/Asp25Glu and stained with the various antibodies. Staining of CLCC1-WT/Asp25Glu FLAG transfected cells with EMC1 antibody showed punctate pattern; EMC1 primarily localised in the perinuclear area likely corresponding to ER sheets, and unexpectedly on the plasma membrane (Fig. 4.24 (i)). Co-localisation of EMC1 with CLCC1 was partial for both WT and Asp25Glu mutant. To confirm whether EMC1 was present in the ER, cells were co-transfected with YFP CLCC1-WT/ Asp25Glu and mCherry-KDEL. Again, EMC1 appeared to localise with the ER with and positive staining was again present on what were likely the ER sheets, and on the plasma membrane (Fig. 4.24 (ii), arrows). Presence of EMC1 at the plasma membrane may be the result of inappropriate binding of the antibody to other (i.e. non-EMC) targets, as presence of EMC on the plasma membrane has not been reported in literature.

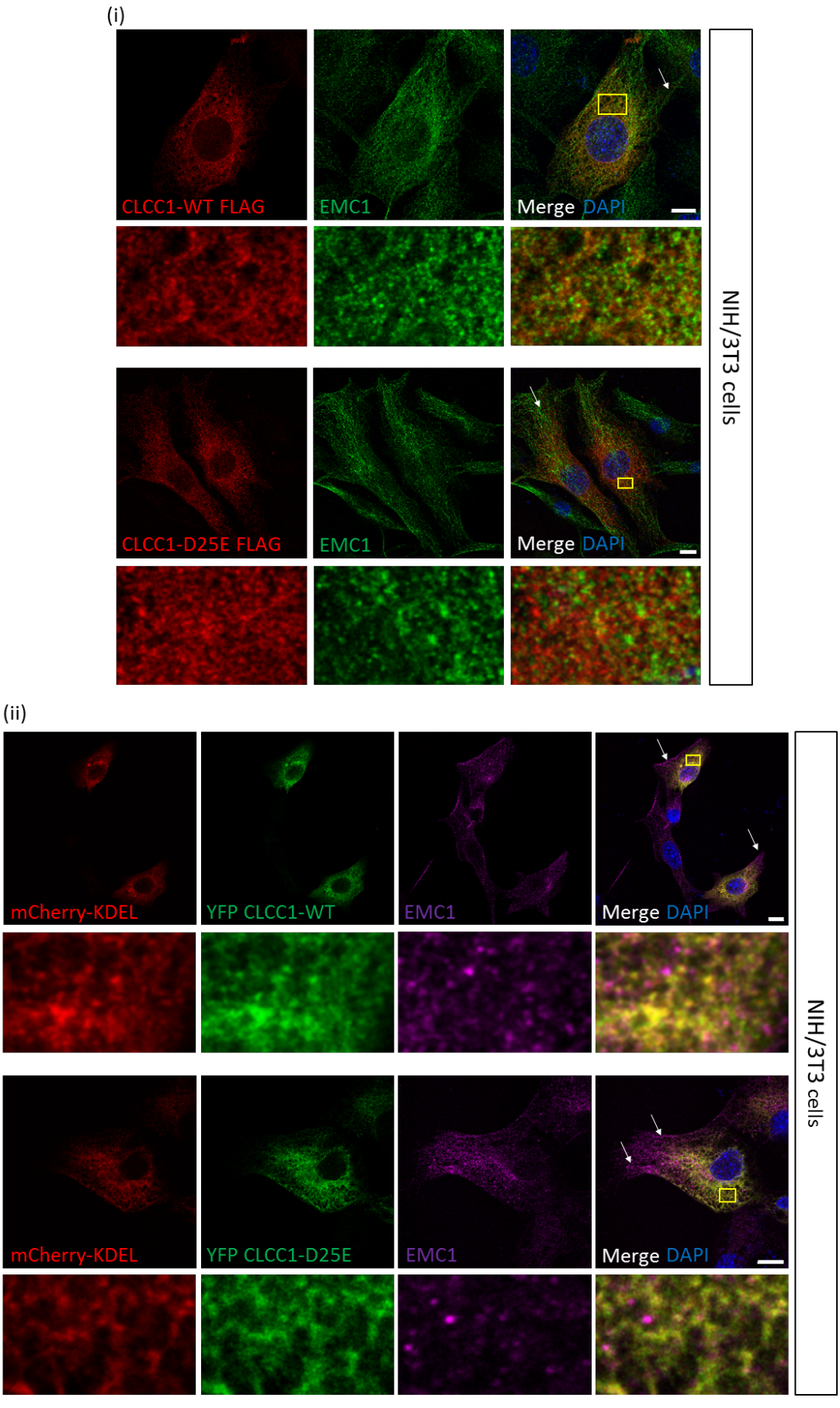
(i)
CLCC1-WT FLAG
EMC1
Merge DAPI
CLCC1-D25E FLAG
EMC1
Merge DAPI
NIH/3T3 cells
(ii)
mCherry-KDEL
YFP CLCC1-WT
EMC1
Merge DAPI
mCherry-KDEL
YFP CLCC1-D25E
EMC1
Merge DAPI
NIH/3T3 cells

Figure 4.24 Partial co-localisation between CLCC1 and EMC1. *NIH/3T3 cells were transfected with* ***(i)*** *CLCC1-WT/Asp25Glu FLAG and stained for EMC1 or* ***(ii)*** *mCherry-KDEL and YFP CLCC1-WT/Asp25Glu and stained with EMC1 antibody. In both cases EMC1 localises on the plasma membrane (arrows) and structures that resemble ER sheets (asterisks). Scale bar 10 μm.*

Staining of CLCC1-WT/ Asp25Glu FLAG transfected cells with SigmaR1 antibody showed a punctate pattern. SigmaR1 displayed a similar localisation to CLCC1 (to both WT and Asp25Glu FLAG tagged molecules), where SigmaR1 and CLCC1 were in close proximity (Fig 4.25 (i), arrows). SigmaR1 also partially co-localised with mCherry-KDEL, indicating its presence in the ER. However, its expression was also delocalised from the ER (Fig 4.25 (ii), arrows), indicating that SigmaR1 was probably present at the contact sites between ER and probably mitochondria. To confirm that SigmaR1 was near mitochondria, cells were treated with 150 nM of MitoTracker Red for 15 min at 37 °C (Fig. 4.26). The labelling indicated the presence of SigmaR1 and CLCC1 in a region between the ER and mitochondria, consistent with it being located at the contact sites (or MAM). Unfortunately, co-labelling of MitoTracker Red and mCherry-KDEL was not possible as both were associated with a red fluorescent protein, therefore the relative position of SigmaR1 with respect to the ER and mitochondria was not verifiable with the tools available in laboratory, in a time-appropriate manner. These results indicate that CLCC1 and SigmaR1 occupy similar spaces inside the cell, and they may have a related function.

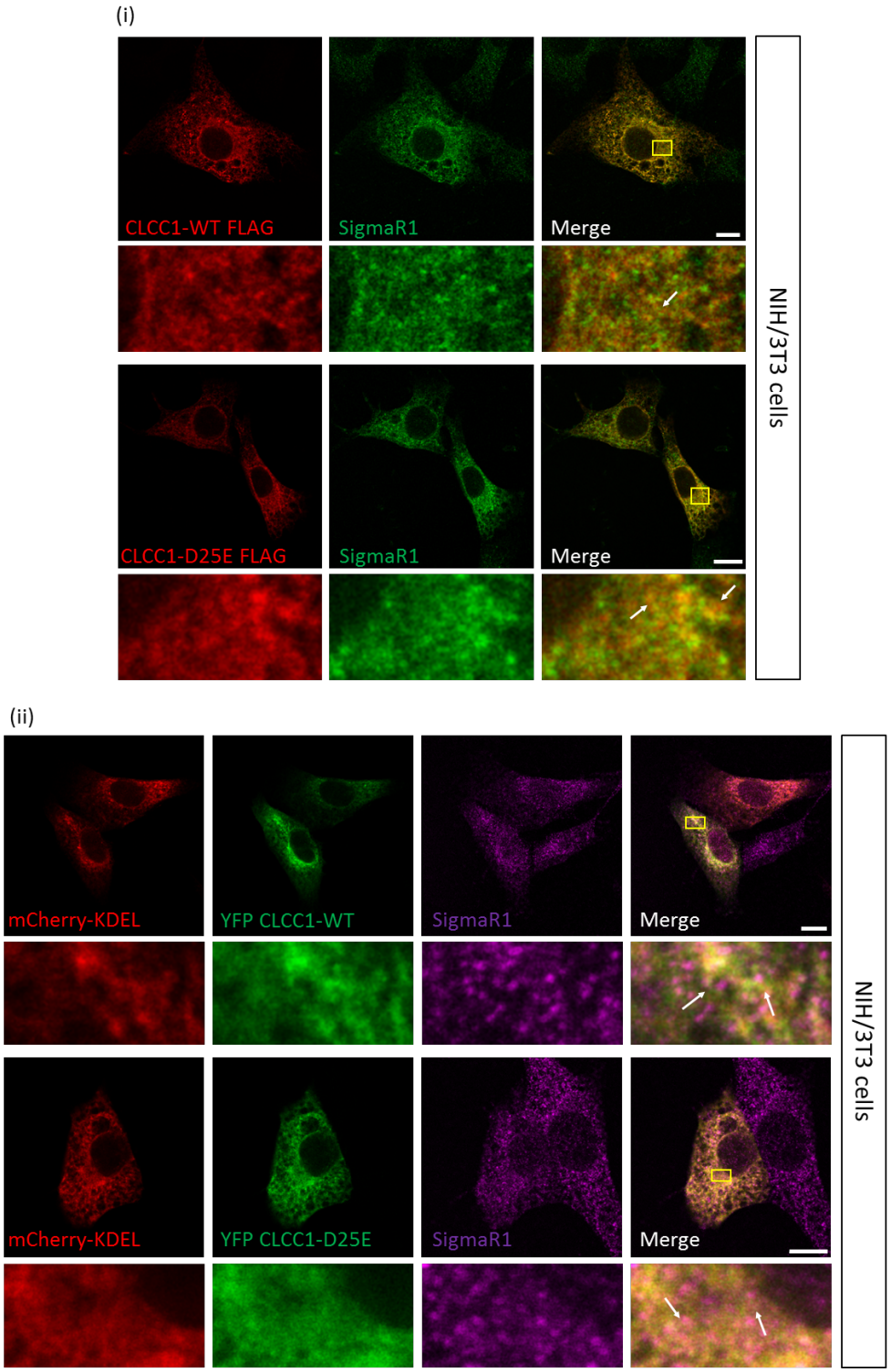

Figure 4.25 Co-localisation between CLCC1 and SigmaR1. *NIH/3T3 cells were transfected with* ***(i)*** *CLCC1-WT/Asp25Glu FLAG and stained for SigmaR1 or* ***(ii)*** *mCherry-KDEL and YFP CLCC1-WT/Asp25Glu and stained with SigmaR1 antibody. SigmaR1 partially co-localised with CLCC1 and ER marker, indicating its presence in proximity of the ER. Scale bar 10 μm.*

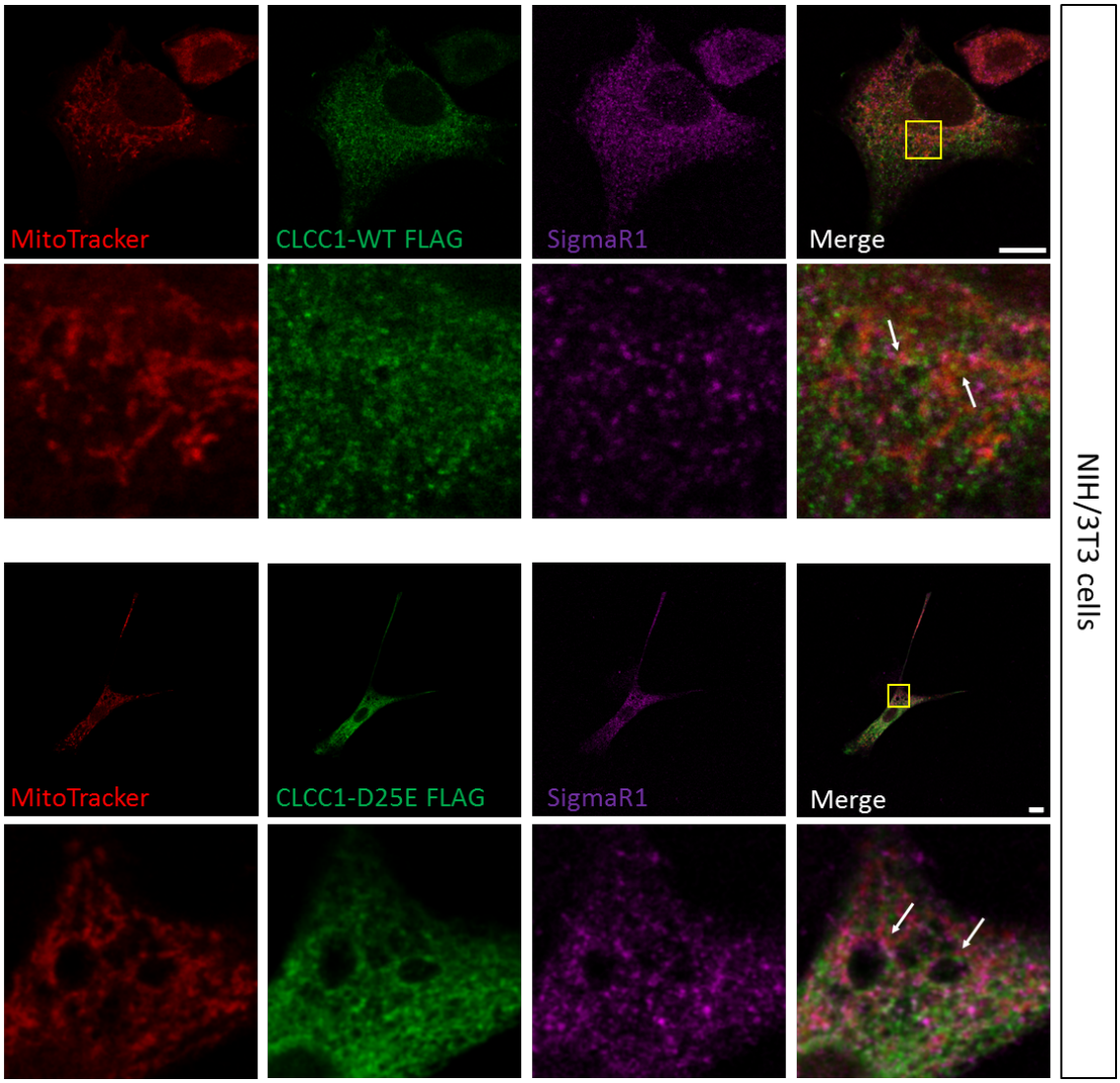

Figure 4.26 CLCC1 transfected cells stained with MitoTracker Red *showed the presence of SigmaR1and CLCC1 in the region of ER-mitochondria contact sites. Scale bar 10 μM.*

Cells transfected with CLCC1 FLAG or YFP CLCC1 (both WT and Asp25Glu; not shown) displayed an increase of SigmaR1 (anti-rabbit SigmaR1, SigmaR1(R)) fluorescence (Fig. 4.27 (i) arrows), compared to untransfected cells. This effect was independent from the species in which the antibody was raised, anti-mouse SigmaR1 (SigmaR1(M)) showed a similar pattern. This effect was not likely specifically caused by the overexpression of CLCC1 because cells transfected with R-pre-mRFP (gift of Dr. John Chilton), a probe based on the C-terminus of K-Ras [256] to evidence the plasma membrane, showed the same increase of SigmaR1 fluorescence. This experiment may indicate that plasmid overexpression can't be used effectively in combination with SigmaR1 antibody. Increased lipid burden due to transfection with liposome fusion to the cell membrane might increase the amount of SigmaR1 associated with lipid rafts on both plasma membrane and other compartments [257].

To verify if overexpression of SigmaR1 caused increased CLCC1 fluorescence, NIH/3T3 cells were transfected with EGFP-SigmaR1 (gift of Dr. Antonis Ververis) and stained with CLCC1 antibody or co-transfected with CLCC1-WT FLAG. Cells transfected with EGFP-SigmaR1 and stained with the CLCC1 antibody (Fig. 4.27 (ii) upper panel) showed a high degree of co-localisation, similar to the one seen when cells were transfected only with CLCC1 plasmid or the combination CLCC1 and mCherry-KDEL (see Fig. 4.26 (i-ii)). In comparison, cells overexpressing both CLCC1 and SigmaR1 (Fig. 4.27 (ii) lower panel, asterisks) displayed a slightly different expression. This might be caused by the overexpression itself, therefore co-transfection of CLCC1 and SigmaR1 were not used for further experiments.

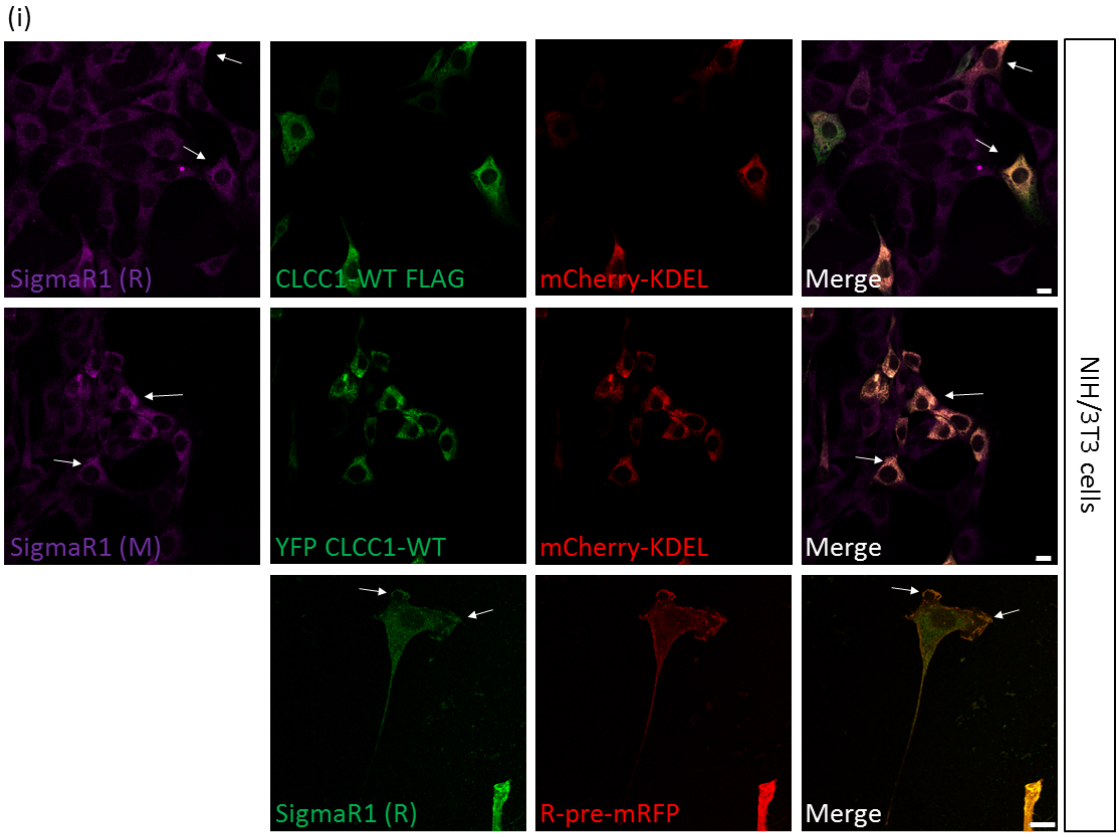
(i)
SigmaR1 (R)
CLCC1-WT FLAG
mCherry-KDEL
Merge
SigmaR1 (M)
YFP CLCC1-WT
mCherry-KDEL
Merge
SigmaR1 (R)
R-pre-mRFP
Merge
NIH/3T3 cells

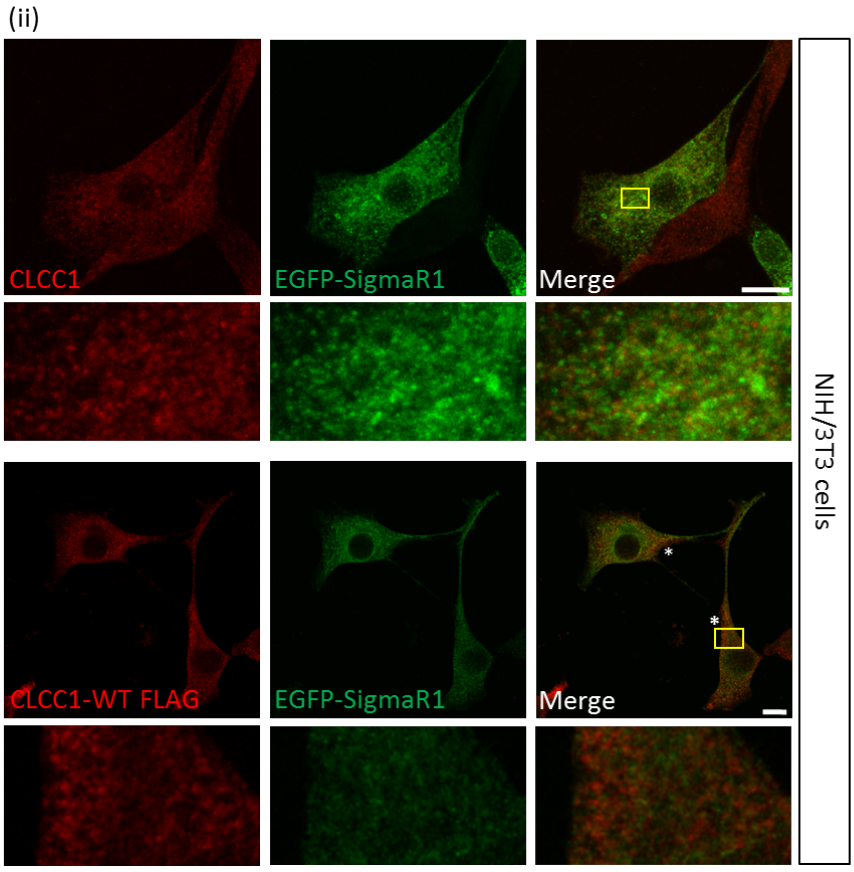
(ii)
CLCC1
EGFP-SigmaR1
Merge
CLCC1-WT FLAG
EGFP-SigmaR1
Merge
NIH/3T3 cells

Figure 4.27 Co-localisation between EGFP-SigmaR1 and CLCC1. (i) *NIH/3T3 cells transfected with CLCC1 plasmids and mCherry-KDEL showed higher fluorescence of SigmaR1, of both mouse (M) and rabbit (R) antibodies, in comparison with untransfected cells. Similarly, higher fluorescence of SigmaR1 was present when cells were transfected with R-pre-RFP, indicating that transfection of cells with plasmid is not compatible with SigmaR1 antibody staining.* ***(ii)*** *Cells transfected with EGFP-SigmaR1 plasmid and stained for endogenous CLCC1 showed co-localisation, while cells co-transfected with CLCC1 and SigmaR1 plasmid showed less co-localisation compared to cells transfected only with SigmaR1. Scale bar 10 μm.*

4.2.9 Effects of ER calcium stores depletion on CLCC1

One of the major functions of the ER is maintaining calcium homeostasis, therefore we looked at the potential involvement of CLCC1 in calcium signalling in the ER. The involvement of CLCC1 in those pathways was also supported by the results of the mass spectrometry, as one of the possible CLCC1 binding partners was *ATP2A2*, which encodes SERCA2. Moreover, SigmaR1 has been shown to inhibit store-operated Ca^{2+} entry by attenuating coupling of STIM1 with Ora1. A potential co-localisation with STIM1 was investigated instead of SERCA2 due to its' link with SigmaR1. To verify if CLCC1 co-localises with STIM1, NIH/3T3 cells were stained with antibodies against CLCC1 and STIM1; CLCC1 was often in proximity of STIM1, however there was no apparent colocalisation (Fig. 4.28 (i)) consistent with its absence from the mass spectrometry results. To understand if CLCC1 might interact with STIM1 following depletion of ER calcium stores, NIH/3T3 cells were transfected with mCherry-KDEL and CLCC1-WT FLAG and 24h later treated with 5 μM of

thapsigargin, a non-competitive inhibitor of the SERCA, or DMSO for 30 min at 37 °C. Thapsigargin induces the activation of the translocation of STIM1 at the PM-ER junction where it couples with ORAI1 to allow the influx of Ca^{2+} in the ER. Fixed cells were stained with the STIM1 antibody and cells were analysed by confocal microscopy. Cells treated with thapsigargin showed the translocation of STIM1 at the membrane (Fig. 4.28 (ii), arrow) however CLCC1 seemed to be unaffected. Co-localisation between the endogenous CLCC1 and endogenous STIM1 was not significantly affected by treatments with thapsigargin (Fig. 4.28 (ii)). Cells were double transfected with mCherry-KDEL and CLCC1-WT FLAG and treated with thapsigargin. In both DMSO-treated and thapsigargin-treated cells the overexpression of CLCC1 appeared to increase the fluorescence however, cells treated with DMSO showed less co-localisation between STIM1 and CLCC1 (Fig. 4.28 (iii), arrow), compared to the thapsigargin-treated cells where the pattern of distribution of STIM1 and CLCC1-WT FLAG was similar. The increase of localisation between STIM1 and CLCC1 could be the results of the overexpression itself, as showed for SigmaR1, therefore the link between calcium and CLCC1 needs to be evaluated in term of calcium currents though calcium imaging and recording, for example loading the cells with FURA2 and analysing the calcium dynamics.

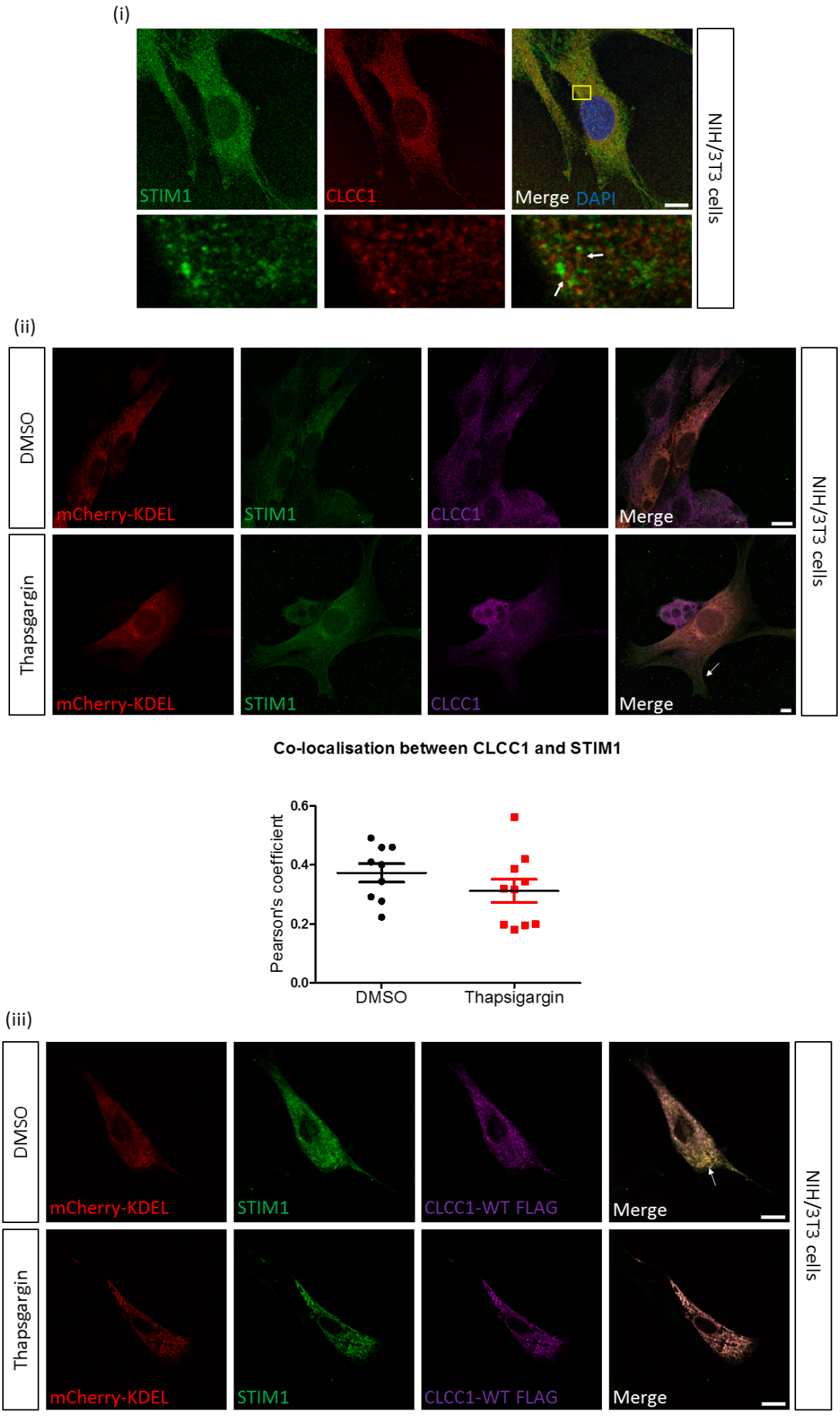
(i)
STIM1
CLCC1
Merge DAPI
NIH/3T3 cells
(ii)
DMSO
Thapsgargin
mCherry-KDEL
STIM1
CLCC1
Merge
NIH/3T3 cells
Co-localisation between CLCC1 and STIM1
Pearson's coefficient
0.6
0.4
0.2
0.0
DMSO
Thapsigargin
(iii)
DMSO
Thapsgargin
mCherry-KDEL
STIM1
CLCC1-WT FLAG
Merge
NIH/3T3 cells

Figure 4.28 Localisation of CLCC1 with STIM1. (i) *Cells stained for the endogenous CLCC1 and STIM1 showed very little co-localisation.* ***(ii)*** *Cells were nucleofected with mCherry-KDEL and treated with DMSO or 5 μM thapsigargin for 30 min and stained with anti-STIM1 and anti-CLCC1. Cells treated with thapsigargin showed a localisation of STIM1 at the membrane however no change in CLCC1 localisation was noted. Quantification of the co-localisation coefficient between CLCC1 and STIM1 in DMSO (N=9; 40 cells) or thapsigargin-treated cells (N=10; 20 cells) was not significant (Mann Whitney U test; p=0.18)* ***(iii)*** *Cells co-nucleofected with mCherry-KDEL and CLCC1-WT FLAG and stained with STIM1 showed a higher degree of localisation between the CLCC1 and STIM1 when cells were treated with thapsigargin compared to cells treated with DMSO where STIM1 was still having a distinct pattern.*

4.2.10 Pharmacological manipulation of SigmaR1

To determine whether CLCC1 is associated with the function of SigmaR1 we took advantage of the fact that SigmaR1 can be pharmacologically manipulated with a variety of commercially available drugs; Pre-084 as agonist and BD1047 as antagonist of the receptor were selected. NIH/3T3 cells were transfected with CLCC1-WT FLAG and mCherry-KDEL or with EGFP-SigmaR1 and mCherry-KDEL and 24h later treated with 10 μM of Pre-084 or 10 μM of BD1047, for 30 min at 37 °C, control cells were treated with the same amount of DMSO.

Cells transfected with CLCC1-WT FLAG and mCherry-KDEL were not stained with SigmaR1 antibody because the overexpression of proteins cause the increased fluorescence of SigmaR1, as previously assessed. Therefore, focus was placed on the effects of activation or de-activation of SigmaR1 on CLCC1

localisation. While cells treated with DMSO showed the classical pattern of localisation of CLCC1 within the ER, both cells treated with Pre-084 and BD1047 showed less co-localisation between CLCC1 and the ER marker mCherry-KDEL (Fig. 4.29 (i), arrows), in particular CLCC1 seemed to localise more on the plasma membrane.

To determine if CLCC1 changed position as a result of SigmaR1, avoiding artefacts due to CLCC1 overexpression, cells were co-transfected with EGFP-SigmaR1 and mCherry-KDEL and stained with CLCC1 antibody. In this case, overexpression of Sigma did not impact the levels of fluorescence of CLCC1. Moreover, the localisation of the endogenous CLCC1 did not seems to change when compared across the three treatments (DMSO, PRE-084 and BD1047) (Fig. 4.29 (ii), arrows).

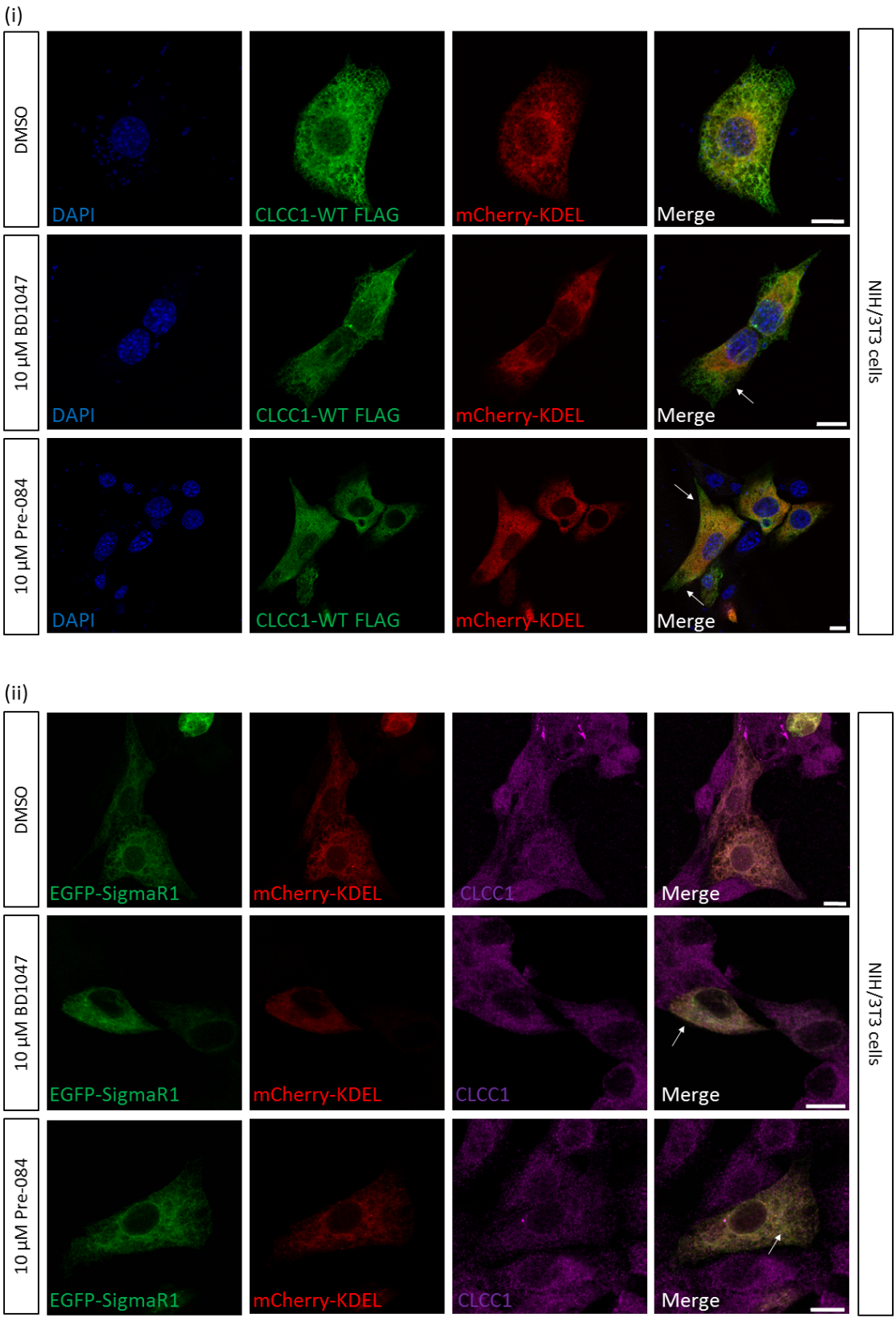
(i)
DMSO
10 µM BD1047
10 µM Pre-084
DAPI
CLCC1-WT FLAG
mCherry-KDEL
Merge
NIH/3T3 cells
(ii)
DMSO
10 µM BD1047
10 µM Pre-084
EGFP-SigmaR1
mCherry-KDEL
CLCC1
Merge
NIH/3T3 cells

Figure 4.29 Effects of SigmaR1 manipulation on CLCC1. (i) *Cells transfected with YFP CLCC1-WT and mCherry-KDEL and treated with 10 μM of agonist (PRE-084) or 10 μM of antagonist (BD1047) for 30 min at 37 ºC showed reduced localisation in the ER with increased of expression on the plasma membrane.* ***(ii)*** *Cells transfected with EGFP-SigmaR1 and mCherry-KDEL showed no change in localisation of CLCC1 when treated with SigmaR1 agonist and antagonist.*

4.2.11 Analysis of metabolic stress on CLCC1

KEGG pathway analysis of mass spectrometry data suggested that proteins related to metabolic pathways were highly represented in all datasets examined however, no indication was given about the specific subtype of metabolic pathway in which those proteins were involved. Moreover, when proteins expressed in the retina were divided by organelle in which they localise, the mitochondria section presented proteins related to glycolysis and tricarboxylic acid (TCA) pathway. Therefore, to examine the potential involvement of CLCC1 in energetic pathways cells were NIH/3T3 cells were transfected with mCherry-KDEL, and 24h later treated with a variety of drugs already available in lab. The effects on the localisation of endogenous CLCC1 was examined with confocal fluorescent imaging.

2-Deoxy-D-Glucose is a glucose analogue that inhibits glycolysis as it is phosphorylated by hexokinase to 2-Deoxy-D-glucose-6-phosphate which cannot be metabolised, resulting in cellular ATP depletion [258]. Cells were treated with 100 mM, for 20 mins at 37 °C. Treatments with 2-DG (Fig. 4.30 (i))

showed that the localisation of CLCC1 within the ER in treated cells was similar to the control cells.

Oligomycin A acts as an inhibitor of mitochondrial H^+-ATPase function, thus blocking oxidative phosphorylation. Treatments with 50 μM of Oligomycin for 20 min at 37°C did not have any effect on CLCC1 localisation and expression patterns (Fig. 4.30 (ii)).

Lonidamine has several targets, it principally inhibits aerobic glycolytic activity through the blocking of hexokinase, it blocks voltage-dependent anion channel (VDAC) which regulates mitochondria-initiated apoptosis, and acts on Complex II of electron transport chain, also known as succinate dehydrogenase [259]. Cells were treated with 400 μM of Lonidamine or the same volume of DMSO for 20 min at 37°C (Fig. 4.30 (iii)). The pattern of both CLCC1 and mCherry-KDEL looked substantially different from the other treatments (e.g. Oligomycin), the staining was much more punctate, and the ER tubules were less defined. However, this pattern was consistent between DMSO-treated cells and Lonidamine-treated cells and may likely be caused by the high concentration of DMSO with which the cells had been treated. Apart from the mentioned difference, no other distinction in terms of CLCC1 localisation was noted.

Having defined that changes in energetic state do not affect the localisation of the endogenous CLCC1, in future it would be interesting to analyse the metabolic rates of aerobic and anaerobic glycolysis in cells lacking CLCC1 or carrying the Asp25Glu alteration to define whether the lack or the alteration of CLCC1 indirectly induce changes in energetic metabolism. It would also be interesting to assess if these drugs have any effect on CLCC1 protein levels.

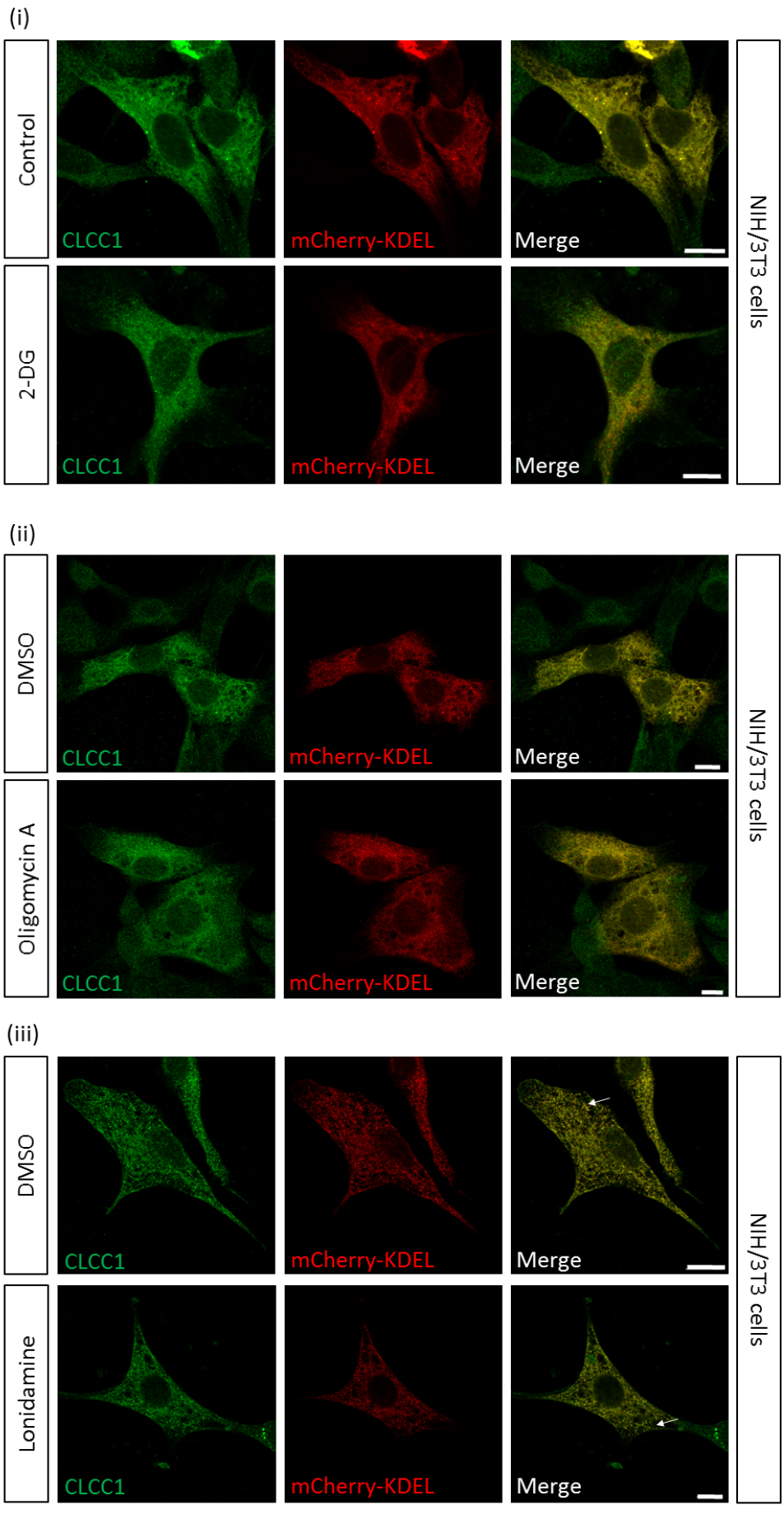
(i)
Control
2-DG
CLCC1
mCherry-KDEL
Merge
NIH/3T3 cells
(ii)
DMSO
Oligomycin A
CLCC1
mCherry-KDEL
Merge
NIH/3T3 cells
(iii)
DMSO
Lonidamine
CLCC1
mCherry-KDEL
Merge
NIH/3T3 cells

Figure 4.30 Treatments of NIH/3T3 with energetic metabolism inhibitors. (i) *Treatments with 100 mM of 2-DG did not change localisation of CLCC1 within the ER.* ***(ii)*** *Cells treated with 50 μM of Oligomycin A did not show any difference of CLCC1 localisation compared to the DMSO-treated cells.* ***(iii)*** *Cells treated with 400 μM of Lonidamine or the same volume of DMSO showed a more distinctive punctate pattern of both CLCC1 and mCherry-KDEL which was probably caused by high DMSO concentration. Scale bar 10 μM.*

The potential involvement of CLCC1 was also investigated in pathways related to protein processing and folding. To this purpose, NIH/3T3 cells transfected with mCherry-KDEL were then treated with 17-N-Allylamino-17-demethoxygeldanamycin (17-AAG), or tanespimycin, and tunicamycin. 17-AAG binds Hsp90 which mediates protein folding and maturation, and is considered a potential cancer treatment [260]. Interestingly, Hsp90 inhibition protects against degeneration of photoreceptors in a model of RP [261]. Treatment of mCherry-KDEL transfected cells with 100 nM of 17-AAG for 20 min did not induce any change in localisation of endogenous CLCC1 within the cell (Fig. 4.31 (i))

Tunicamycin inhibits N-linked glycosylation by preventing core oligosaccharide addition to nascent polypeptides and thereby blocking protein folding and transit through the ER thus inducing ER stress [262]. Cells transfected with mCherry-KDEL and treated with 2 μg/ml with tunicamycin for 30 min did not show any change of localisation of CLCC1 (Fig. 4.31 (ii)).

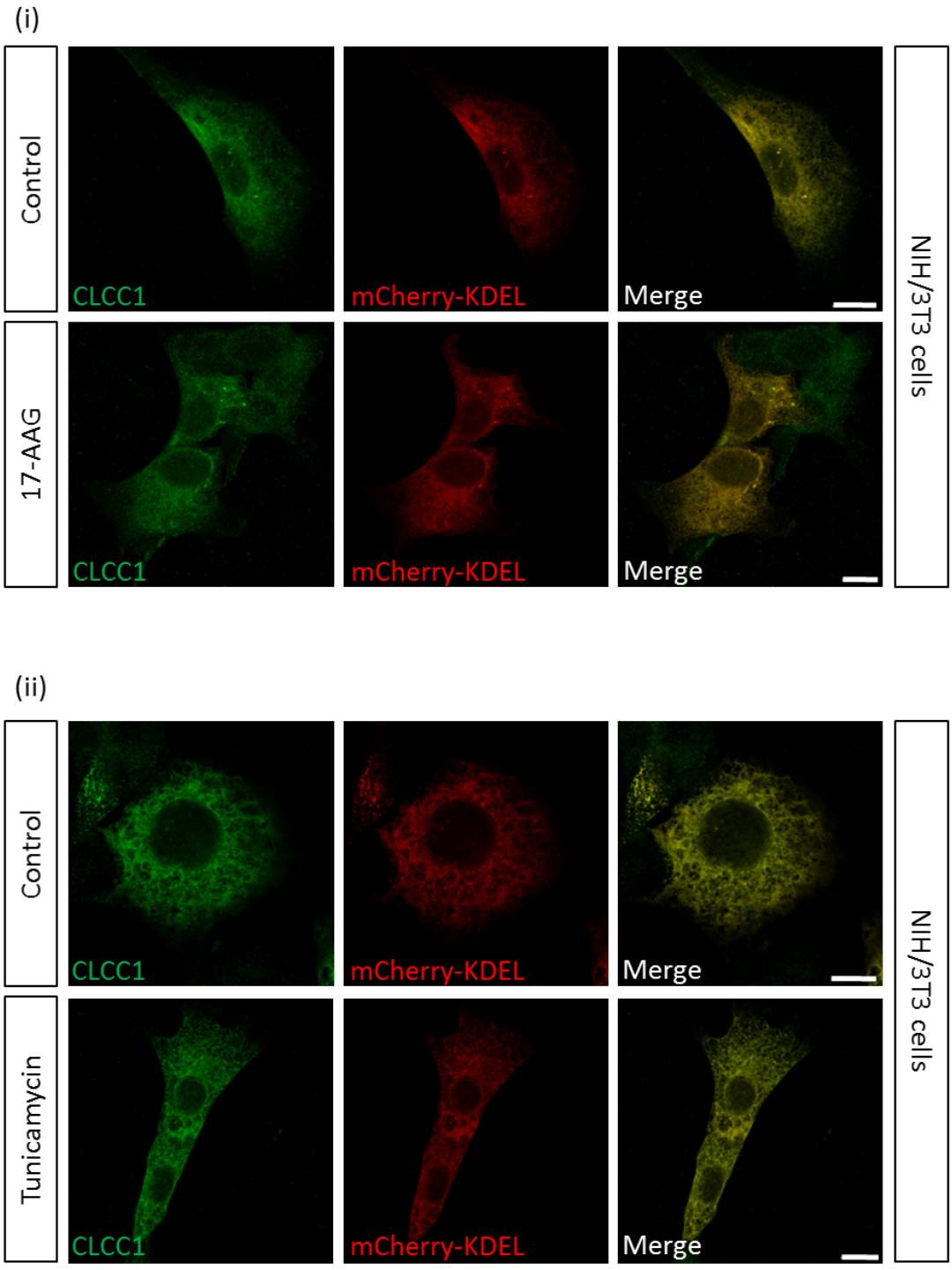

Figure 4.31 NIH/3T3 cells treated with 17-AAG and Tunicamycin. (i) *cells treated with 500 nM of 17-AAG for 20 min did not showed any change in localisation of CLCC1. (ii) cells treated with 2 µg/ml of tunicamycin for 30 min did not show changes in localisation of CLCC1.*

Taken together, these results indicate that metabolic stress does not influence the localisation of CLCC1, however, these results do not exclude the involvement of CLCC1 in metabolic pathways though the action of CLCC1 on other proteins.

4.2.12 CLCC1 knockout in SH-SY5Y cells.

To provide an important resource for more wide-ranging studies to define the physiological role of CLCC1 in cells, gene knockout was performed in SH-SY5Y cells using CRISPR-Cas9 by deletion spanning CLCC1 exons 2-4, which were common between the predicted isoforms, and are predicted to create a frameshift alteration. SH-SY5Y were considered a suitable cell line for carrying the knockout as they are diploid, able to survive in single-cell colonies, express *CLCC1*, are already available in the laboratory, and even though they are not retinal cells they are considered a pseudo-neuronal cell line. In brief, SH-SY5Y cells were co-nucleofected with the plasmid containing the gRNA for CLCC1_exon 2 and CLCC1_exon 3; both plasmids were labelled with different fluorescent proteins, mCherry and GFP. Double positive cells were selected with FACS sorting and grown as a single cell colony in a 96-well plate. Once confluent, cells were collected, and DNA extracted. PCR spanning exons 2 to 4 was performed; colonies showing a single amplicon of about 600 bp corresponded to homozygous KO cells, while heterozygous KO cells showed a band of about 600 bp and one of about 1200 bp (Fig. 4.32 (i)) Homozygous KO cells were Sanger sequenced to verify that the deletion between exon 2 and 4 was present and that it resulted in a frameshift alteration (Fig. 4.32 (ii)). Morphology was assessed with the brightfield microscope, *CLCC1*$^{-/-}$ colonies did not show changes in morphology compared to WT cells (Fig. 4.32 (iii)). Unfortunately, as explained in paragraph 5.2.3 western blot for CLCC1 on

whole lysate did not work, therefore, to assess the protein levels of CLCC1 in KO vs WT, cells were stained with the CLCC1 antibody and analysed at the confocal microscope (Fig. 4.32 (iv)). WT cells showed high levels of CLCC1 staining while *CLCC1*$^{-/-}$ KO cells showed only background stain, probably due to the secondary antibody. The immunofluorescence experiment supported the genotyping results indicating the successful knockout of *CLCC1* in SH-SY5Y cells.

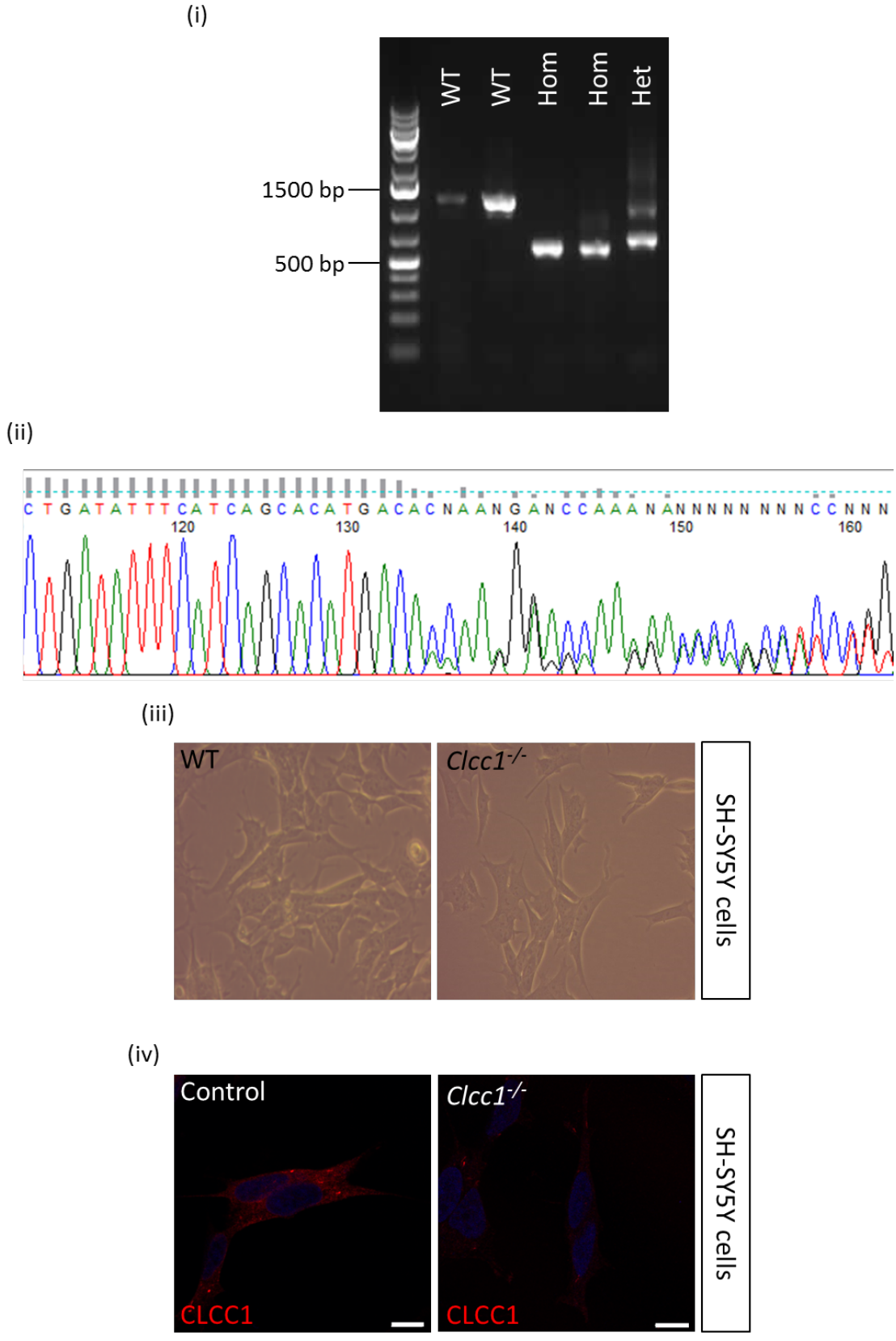

Figure 4.32 Assessing CRISPR colonies genotype for CLCC1. (i) *PCR of DNA extracted from cultures derived from single cell colonies, spanning CLCC1*

exon 2-4. WT cells showed a single amplicon of about 1500 bp, homozygous KO cells showed a single amplicon of about 600 bp, while heterozygous KO cells showed two amplicons, one corresponding to the WT band and to the KO band. ***(ii)*** *Dideoxy sequencing for homozygous KO cells showed the presence of a frameshift alteration and the absence of the intended deleted region.* ***(iii)*** *Inverted microscopy photographs of WT and CLCC1$^{-/-}$ cells showing their morphology.* ***(iv)*** *Immunofluorescence of CLCC1-stained WT and KO cells showed absence of CLCC1 in CLCC1$^{-/-}$ cells, indicating the successful knockout. Scale bar 10 µm.*

To verify that the knockout of *CLCC1* did not induce major defects on organelles, WT and *CLCC1*$^{-/-}$ KO cells were stained with antibodies already available in the laboratory. Cytoskeleton was labelled with Tubb4 for microtubules, and Phalloidin for F-actin (Fig. 4.33 (i)), while endosomal trafficking was identified with Rab11 (Fig. 4.33 (ii)), mitochondria with ATP5A (Fig. 4.33 (ii)), and the ER with calreticulin and calnexin (Fig. 4.33 (iii)). None of the above markers showed substantial change, indicating that the knockout of CLCC1 does not cause gross morphological alterations of organelles. In particular, ER proteins calreticulin and calnexin seem to have the same distribution within the ER in *CLCC1*$^{-/-}$ KO compared to the WT, indicating that the knockout does not have a delocalisation effect on those proteins.

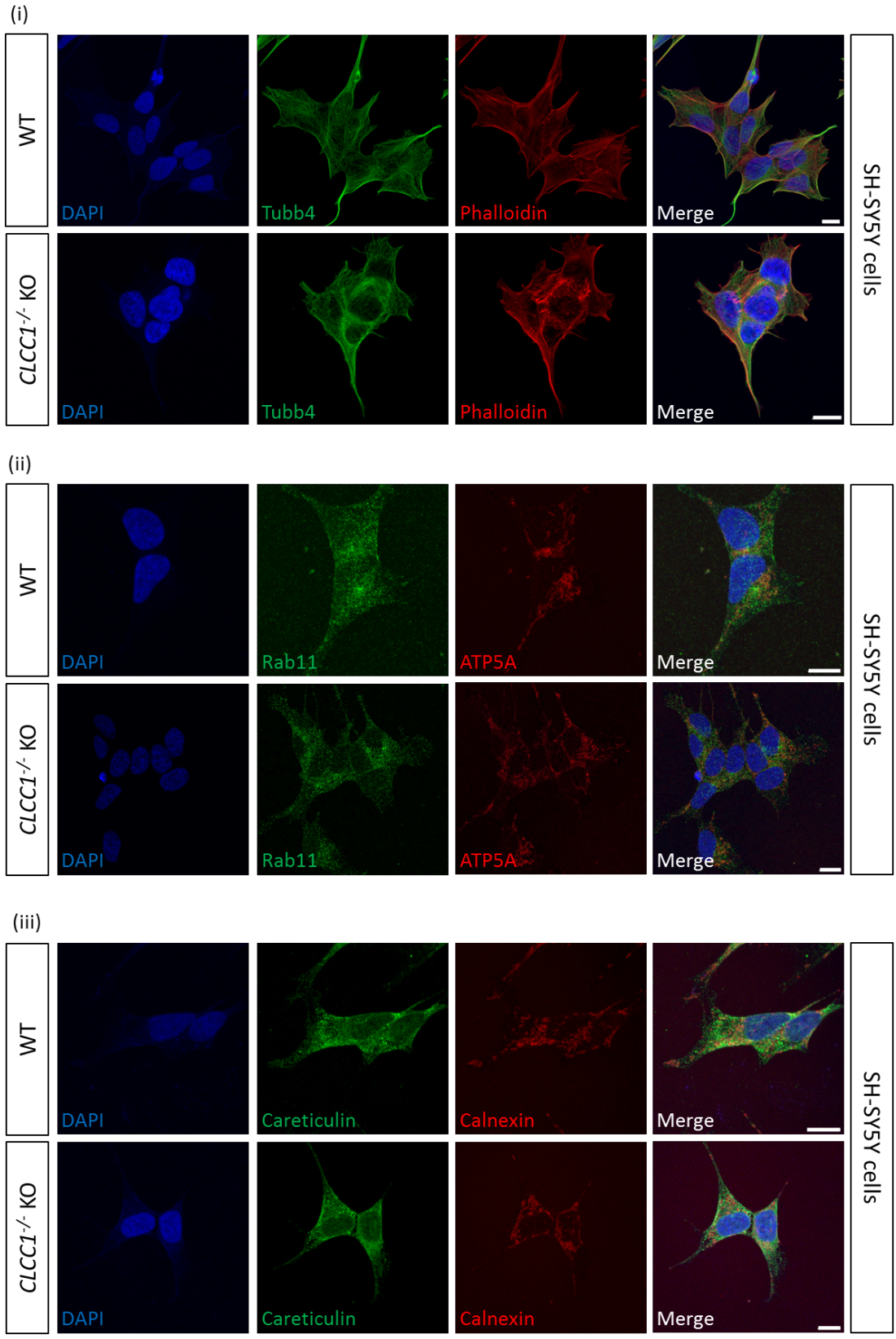

Figure 4.33 Staining of CLCC1$^{-/-}$ KO cells. (i) *Tubb4 and phalloidin showed that the CLCC1$^{-/-}$ KO cells did not induce any changes in the cytoskeleton.* ***(ii)***

Both Rab11 (endosomes) and ATP5A (mitochondria) showed the same pattern of localisation in CLCC1$^{-/-}$ cells compared to the WT. ***(iii)*** *ER proteins calreticulin and calnexin showed the same distribution in CLCC1$^{-/-}$ cells, indicating that the knockout does not affect their localisation.*

To assess the effect of the knockout on targets identified with the mass spectrometry, WT and of *CLCC1*$^{-/-}$ KO cells were stained with several antibodies. In SH-SY5Y cells, EMC1 showed a similar localisation to that seen in NIH/3T3 cells, staining was present near the nucleus and on the plasma membrane (Fig. 4.34 (i)). These results indicate that the localisation of EMC1 in the cells is not directly linked to CLCC1, however the disruption of the binding might have effects not visible using this assay. Similarly, staining with STIM1 did not showed any mis-localisation of the protein due to the knockout of *CLCC1* (Figure 4.34 (ii)).

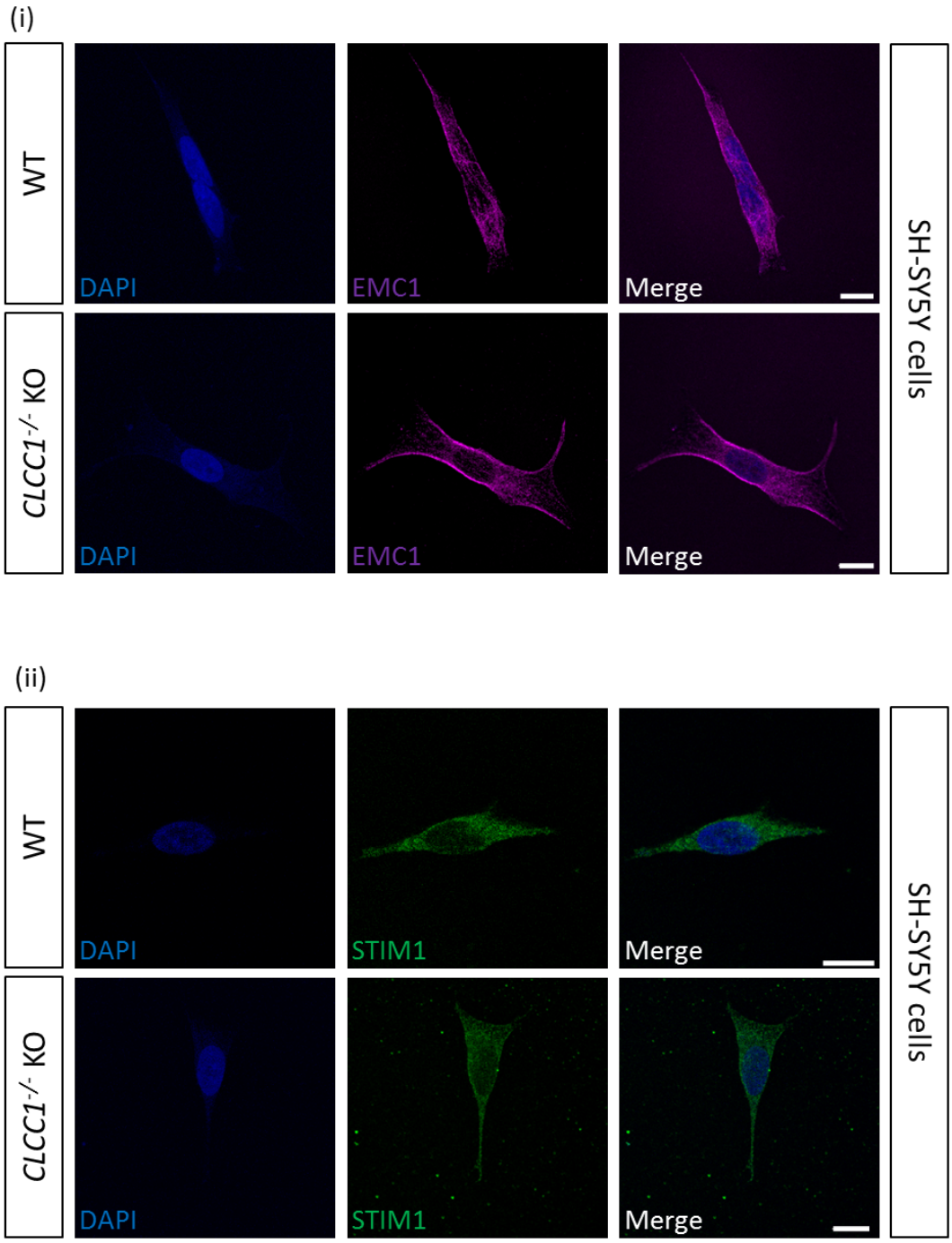

Figure 4.34 Localisation of EMC1 and STIM1 in CLCC1$^{-/-}$ KO cells. (i) *EMC1 showed similar localisation between WT and CLCC1$^{-/-}$ KO cells.* ***(ii)*** *STIM1 showed similar localisation between WT and CLCC1$^{-/-}$ KO cells. Scale bar 10 µM.*

Expression pattern of SigmaR1 in *CLCC1*$^{-/-}$ KO cells (Fig 4.35 (i)) was also no different to wild type cells. The dynamics of ER and SigmaR1 movements in cells were also assayed, using live cell imaging. Wild type and *CLCC1*$^{-/-}$ KO cells were co-nucleofected with mCherry-KDEL and EGFP-SigmaR1 and 24h later were imaged. Cells showed the presence of SigmaR1 in the ER, and while wild type cells showed a very dynamic remodelling and movement of ER tubules containing SigmaR1, in *CLCC1*$^{-/-}$ KO cells these this dynamic remodelling seemed slower (Appendix E, media 1 and 2). Similarly, cells treated with PRE-084 and BD1047 (Appendix E, media 3, 4, 5, 6) were imaged to verify if the overactivation of SigmaR1 might overcome the presumptive reduced dynamic remodelling of the ER in of *CLCC1*$^{-/-}$ KO. Unfortunately, a method to quantify those movements was not found therefore these remain simple observations.

Staining with BiP antibody showed a punctate pattern consisting of the presence of very bright and well-defined spots. This pattern seemed consistent between wild type and the *CLCC1*$^{-/-}$ KO cells (Fig 4.35 (ii)).

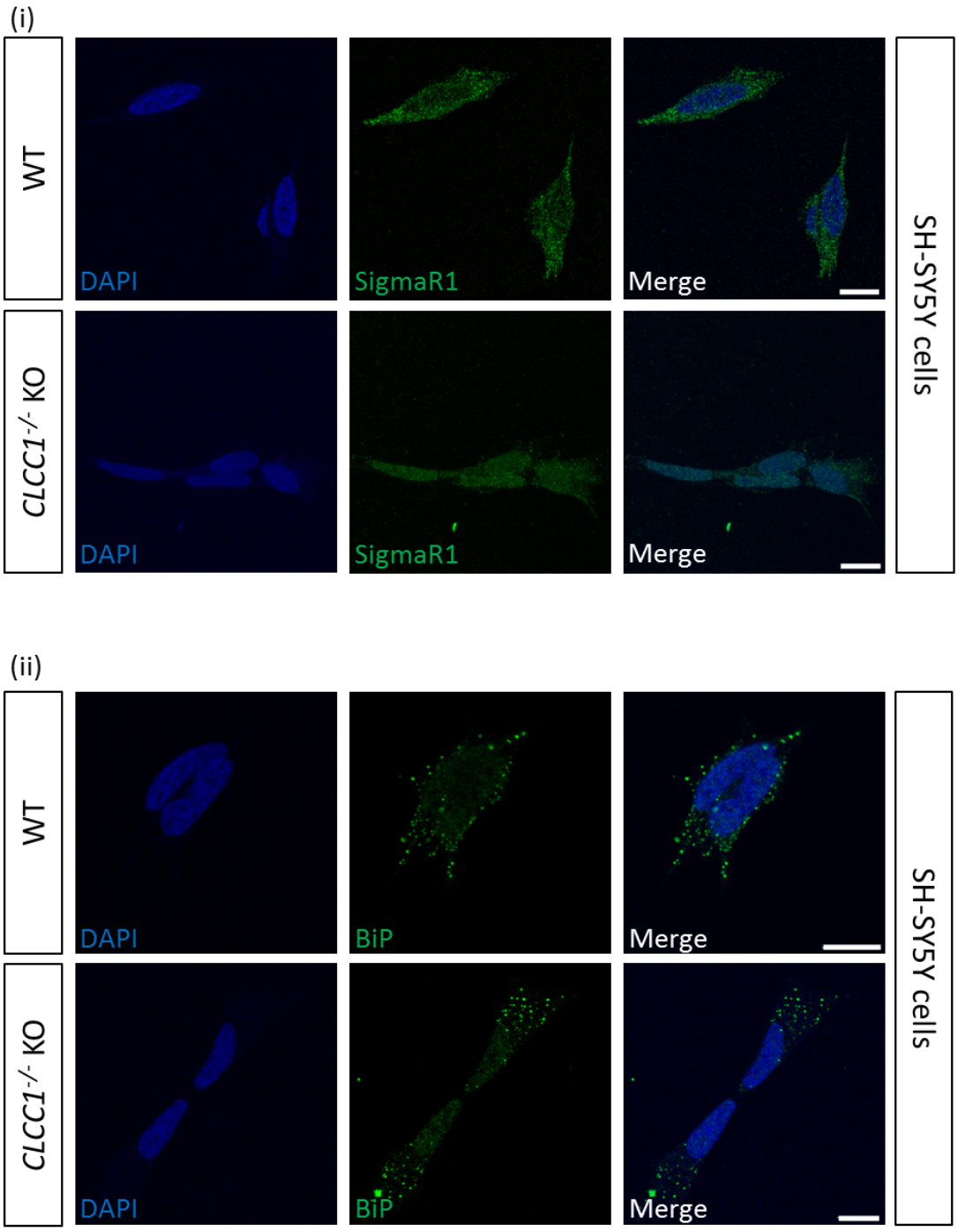

Figure 4.35 CLCC1 KO cells stained with BiP and SigmaR1. (i-ii) *BiP showed similar localisation between WT and CLCC1$^{-/-}$ KO cells. Scale bar 10 µM.*

As Jia et al [206] showed that loss of *CLCC1* increases the expression of BiP, we took advantage of the fact that BiP showed such defined expression pattern, and quantified its expression by counting puncta. (Fig. 4.36). For each image, 3 z-stacks were taken in 1 µm depth; with consistent zoom and laser gain. Particles (n. of BiP dots) were counted using Fiji, all the images were processed in the same way. *CLCC1*$^{-/-}$ KO cells (N=18; 268 cells) did not show a significant increase of BiP expression when compared to the wild type (N=18; 427 cells) (Mann Whitney U test; p=0.93), indicating that the lack of *CLCC1* does not induce ER stress (Fig 4.36 (i)). To understand if the *CLCC1*$^{-/-}$ KO cells were more sensitive to ER stress inducers, wild type and *CLCC1*$^{-/-}$ KO cells were treated with 5 µM of thapsigargin or 2 µg/ml of tunicamycin for 30 min at 37 °C, and the same volume of DMSO as control. Both wild type and *CLCC1*$^{-/-}$ KO cells treated with tunicamycin (Fig. 4.36 (ii)) did not show an increase of BiP expression when compared to the DMSO-treated cells (Kruskal-Wallis test with Dunn's multiple comparison test; ns). The treatment with thapsigargin (Fig. 4.36 (iii)) instead caused a significant increase of BiP expression in *CLCC1*$^{-/-}$ KO cells (N=12; 307 cells) when compared with CLCC1$^{-/-}$ KO cells treated with DMSO (N=18; 334 cells) (Kruskal-Wallis test with Dunn's multiple comparison test; p<0.05; *). *CLCC1*$^{-/-}$ KO cells treated with thapsigargin also showed a significant increase in BiP expression when compared with wild type cells treated with thapsigargin (N=18; 368 cells) (Kruskal-Wallis test with Dunn's multiple comparison test; p<0.05; *), and wild type cells treated with DMSO (N=18; 312 cells) (Kruskal-Wallis test with Dunn's multiple comparison test; p<0.05; ***).

These results demonstrate that basal levels of BiP do not change in cells lacking the *CLCC1* gene, and that treatment with tunicamycin does not increase

BiP expression. As an increase of BiP was expected in wild type cells and these results also were not consistent with what demonstrated by Jia et al [206] and, western blot analysis is needed to further evaluate the impact of tunicamyin on wild type and *CLCC1*$^{-/-}$ KO cells. Thapsigargin instead increases expression of BiP in *CLCC1*$^{-/-}$ KO cells when compared to the same cells treated with DMSO, and wild type cells treated with thapsigargin. However, thapsigargin-treated wild type cells did not show a significant change of BiP expression when compared to the wild type cells treated with DMSO. Again, these results need to be confirmed by western blot.

These results showed that the homozygous loss of *CLCC1* in SH-SY5Y did not have major effects on the organelle shape, and in particular did not affect the localisation of BiP, SigmaR1, EMC1, STIM1 and calnexin. These results also indicated that the Asp25Glu alteration did not affect the localisation of those proteins as well. This also showed that while basal levels of BiP were present in both wild type and knockout cells, those displayed a significant higher expression of BiP when they were treated with thapsigargin but not with tunicamycin.

(i)

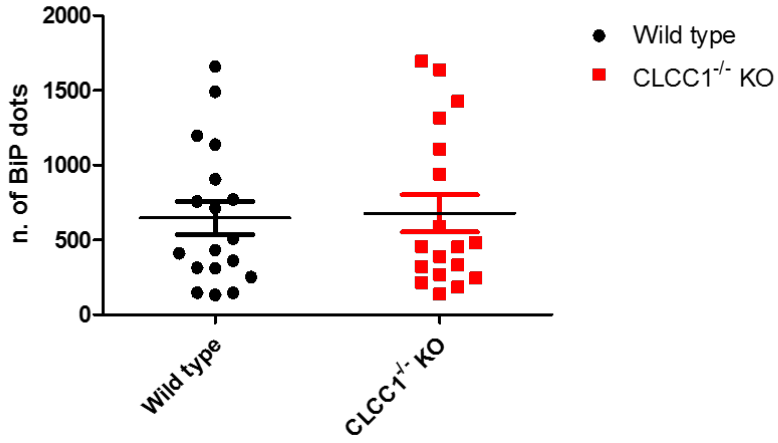
2000
1500
1000
500
0
n. of BiP dots
Wild type
CLCC1-/- KO
Wild type
CLCC1-/- KO

(ii)

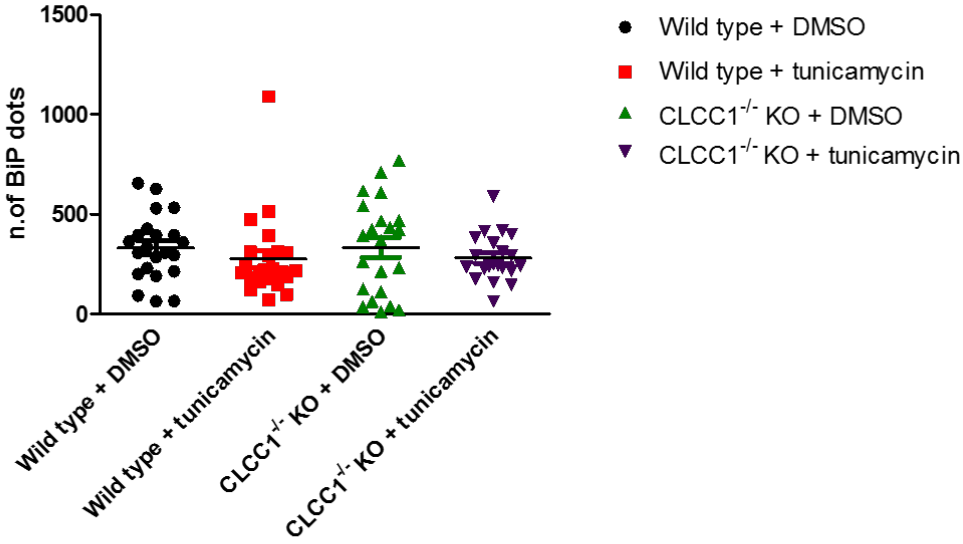
1500
1000
500
0
n.of BiP dots
Wild type + DMSO
Wild type + tunicamycin
CLCC1-/- KO + DMSO
CLCC1-/- KO + tunicamycin
Wild type + DMSO
Wild type + tunicamycin
CLCC1-/- KO + DMSO
CLCC1-/- KO + tunicamycin

(iii)

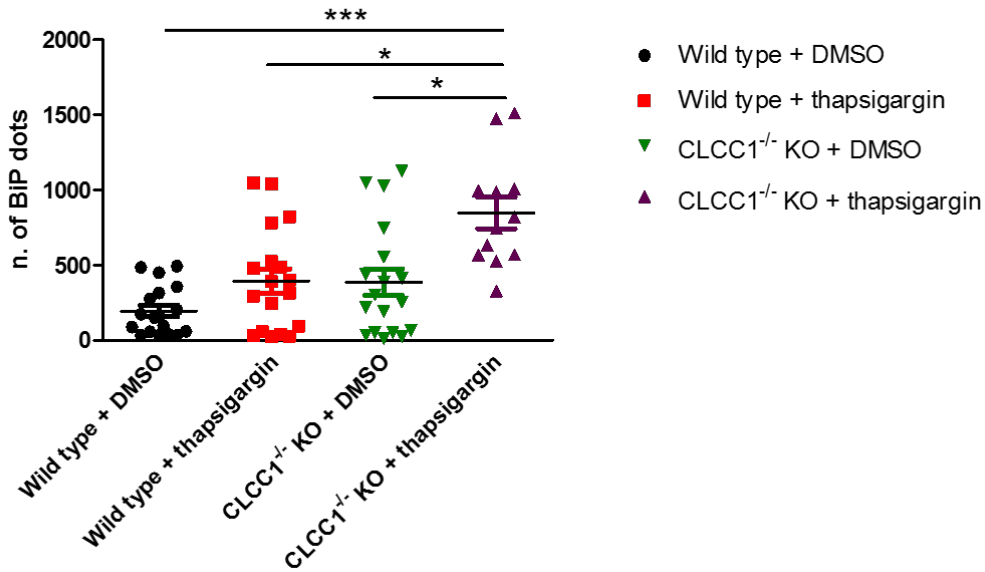
***
*
*
2000
1500
1000
500
0
n. of BiP dots
Wild type + DMSO
Wild type + thapsigargin
CLCC1-/- KO + DMSO
CLCC1-/- KO + thapsigargin
Wild type + DMSO
Wild type + thapsigargin
CLCC1-/- KO + DMSO
CLCC1-/- KO + thapsigargin

Figure 4.36 Quantification of BiP expression. (i) *Wild type (N=18; 427 cells) and CLCC1$^{-/-}$ KO cells (N=18; 268 cells) showed no difference in BiP (Mann Whitney U test; p=0.93).* ***(ii)*** *Tunicamycin treatment did not influenced expression of BiP in both wild type (N=23, 388 cells) and CLCC1$^{-/-}$ KO cells (N=21; 419 cells) (Kruskal-Wallis test with Dunn's multiple comparison test; ns). Wild type + DMSO treated cells (N=22; 432 cells); CLCC1$^{-/-}$ KO DMSO treated cells (N=22; 344 cells). CLCC1$^{-/-}$ KO cells treated with DMSO (N=22; 466 cells).* ***(iii)*** *Wild type cells treated with thapsigargin (N=22; 456 cells) showed an increase of cleaved caspase-3 expression when compared to the wild type cells treated with DMSO (N=22; 420 cells) (Kruskal-Wallis test with Dunn's multiple comparison test; p<0.05; **). Similarly, an increase of BiP protein expression was found in CLCC1$^{-/-}$ KO cells treated with thapsigargin (N=21; 381 cells) when compared with CLCC1$^{-/-}$ KO cells treated with DMSO (N=22; 573 cells) (Kruskal-Wallis test with Dunn's multiple comparison test; p<0.05; *). These results showed an increase of BiP expression in CLCC1$^{-/-}$ KO cells only when they were treated with thapsigargin, consistent with the induction of ER stress response.*

Moreover, to verify the effect of the Asp25Glu alteration in a condition in which cells did not have any endogenous CLCC1, the CLCC1-Asp25Glu FLAG construct was nucleofected into *CLCC1$^{-/-}$* KO cells. When CLCC1 Asp25Glu was introduced inside the cell, its localisation was similar to the one shown before. Staining with EMC1 (Fig. 4.37 (i)) STIM1 (Figure 4.37 (ii)), SigmaR1 (Fig. 4.38 (i)), and BiP (Figure 4.38 (ii)) did not seem to change in comparison to cells carrying the wild type CLCC1 or the introduction of the Asp25Glu mutant CLCC1.

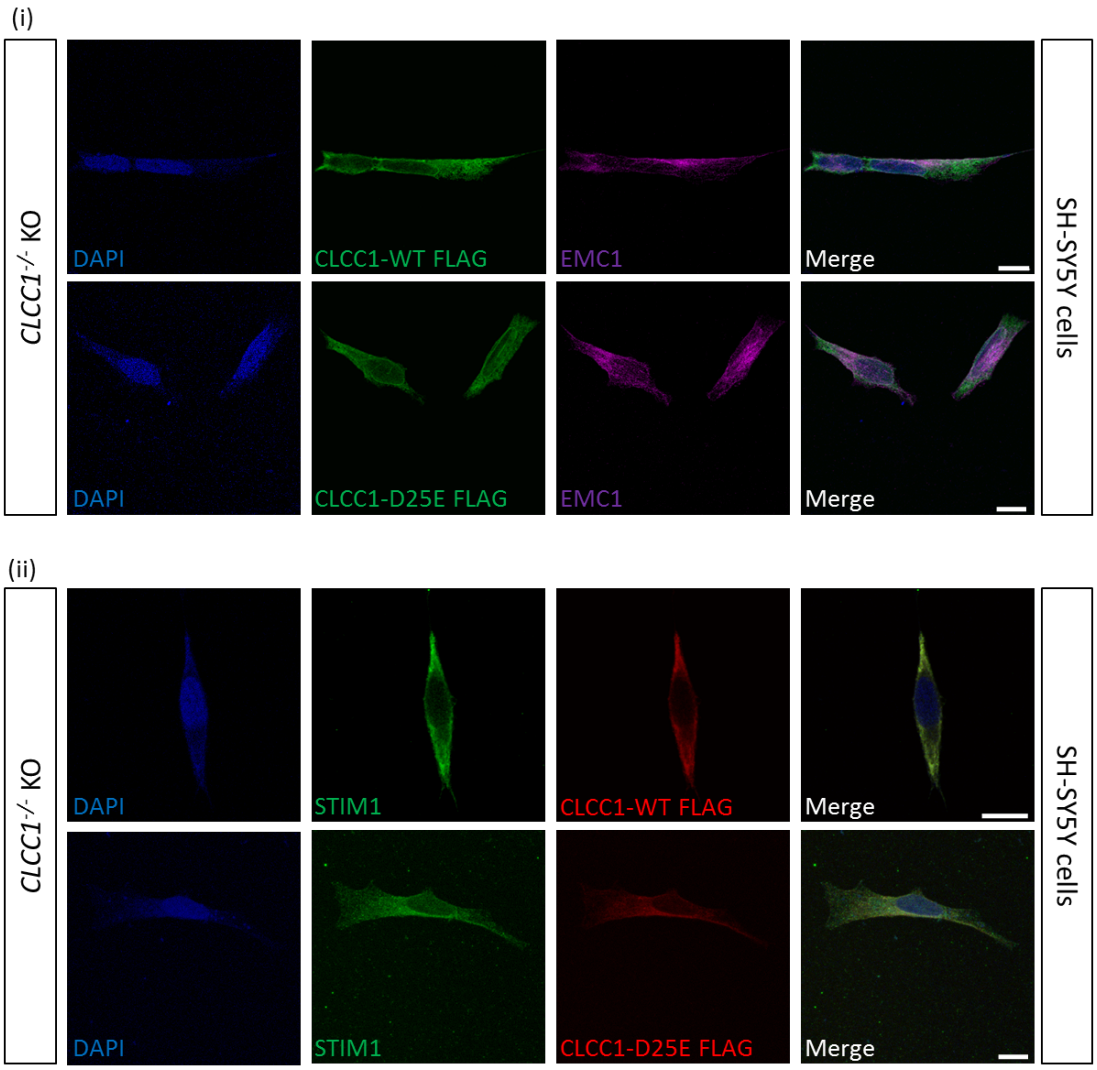

Figure 4.37 Re-introduction of CLCC1-Asp25Glu FLAG into CLCC1$^{-/-}$ KO cells, stained with EMC1 and STIM1. *When CLCC1$^{-/-}$ KO cells were nucleofected with the CLCC1-Asp25Glu FLAG and stained with* ***(i)*** *EMC1 and* ***(ii)*** *STIM1 did not show any change in localisation. Scale bar 10 μM.*

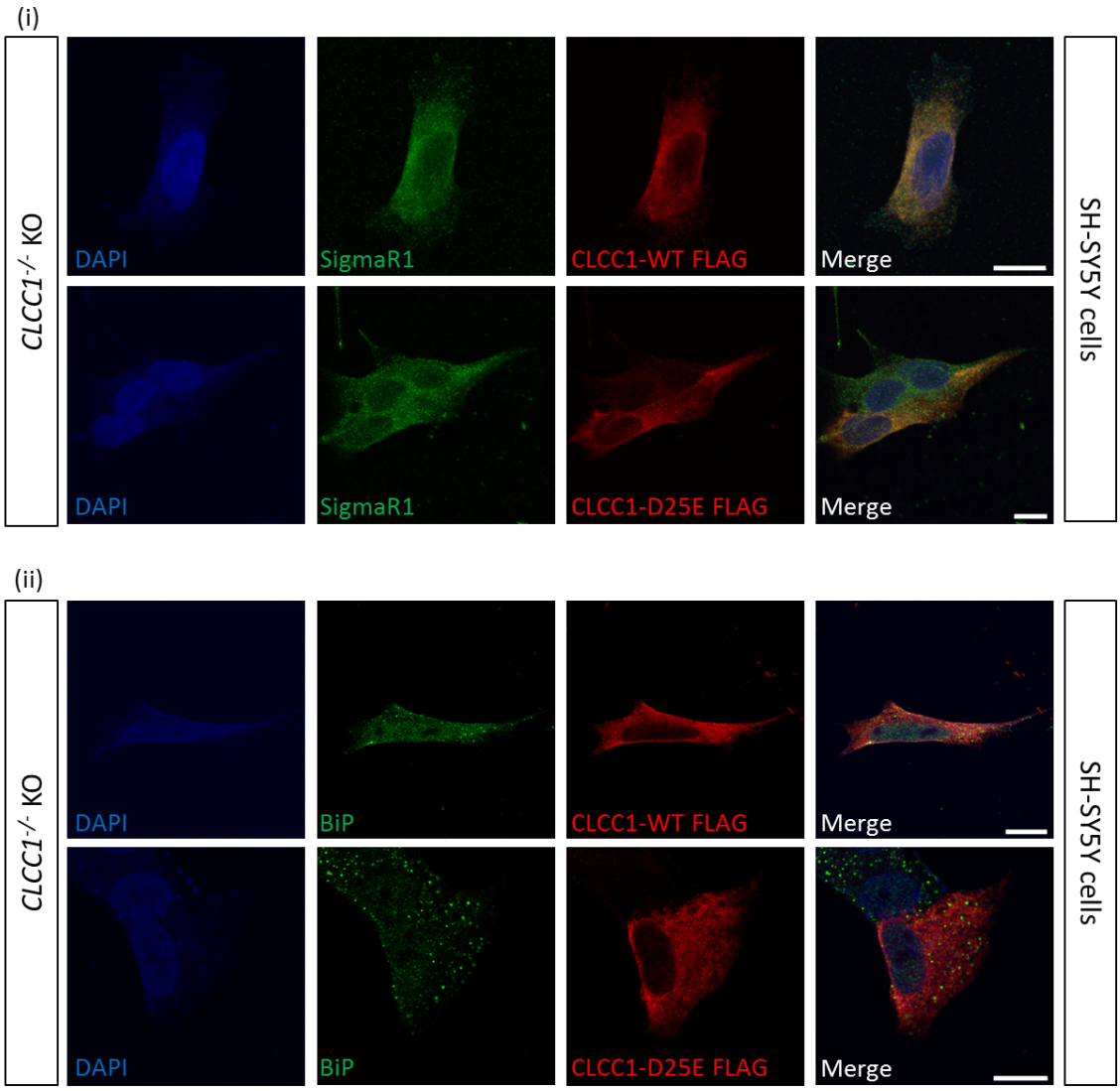

Figure 4.38 Re-introduction of CLCC1-Asp25Glu FLAG into CLCC1$^{-/-}$ KO cells, stained with SigmaR1 and BiP. *When CLCC1$^{-/-}$ KO cells were nucleofected with the CLCC1-Asp25Glu FLAG and stained with* ***(i)*** *SigmaR1 and* ***(ii)*** *BiP did not show any change in localisation. Scale bar 10 μM.*

4.2.13 Fractionation of CLCC1$^{-/-}$ KO cells

Subcellular fractionation was attempted to separate ER and mitochondria and analyse protein levels in these organelles in wild type versus *CLCC1*$^{-/-}$ KO cells. Unfortunately, this experiment did not work however, western blot with the whole homogenate for wild type and *CLCC1*$^{-/-}$ KO cells gave some very preliminary results. In particular, ATP5A used as mitochondrial marker, and calnexin, calreticulin, BiP and EMC1 were detected (Fig. 4.39). For BiP and EMC1 the loading control was not detectable. Due to time constraints this experiment was performed only once and ought to be repeated with densitometric measurements (whole membrane blots in Appendix G).

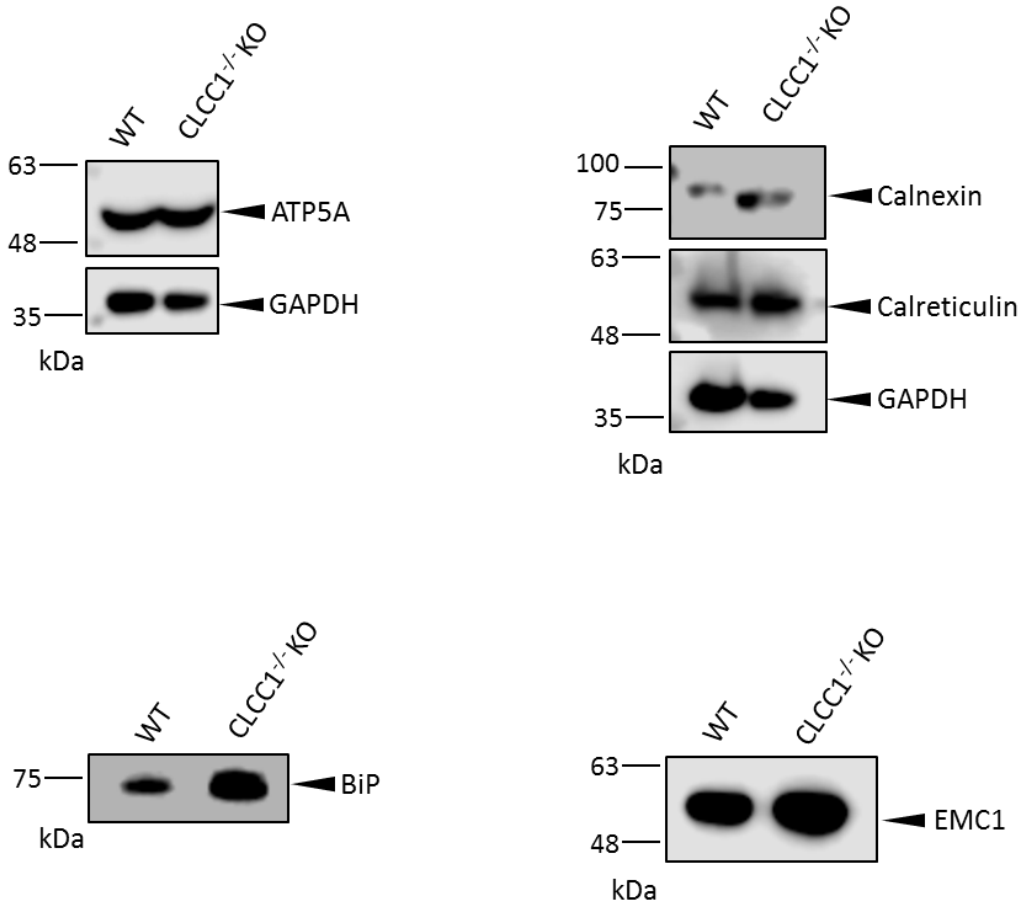

Figure 4.39 Western blot of wild type and CLCC1$^{-/-}$ KO cells. *Western blot for the whole homogenate in wild type and CLCC1$^{-/-}$ KO cells. Protein levels were detectable for ATP5A, calnexin, calreticulin, BiP and EMC1.*

4.2.14 Proliferation and apoptotic rates of CLCC1$^{-/-}$ KO cells

To understand if the loss of *CLCC1* reduces the viability of cells, the MTT assay, which measures the metabolic rate of cells which is an indirect measure of their proliferative rate, was carried out over five days.

Proliferative rate was calculated by subtracting the background readings (cell media) to the readings obtained for the wild type and *CLCC1$^{-/-}$* KO cell. Two way-ANOVA with Bonferroni post test showed no significant differences between wild type and knockout at any time point (Fig. 4.40 (i)). Similarly, proliferative rate was also assessed when cells were treated for 30 min with 2 µg/ml of tunicamycin (Fig. 4.40 (ii)) or 5 µM of thapsigargin (Fig. 4.40 (iii)) to see if an increase of ER stress could also decrease proliferative rate of *CLCC1$^{-/-}$* KO cells, compared to the wild type. None of the treatments decreased the viability at any time point. A factor that might have influenced this experiment was the short time of treatment with ER stressors as once the drug was removed, 4 hours were needed before the plate was read and therefore treatments for a longer period of time might influence cell viability.

(i)

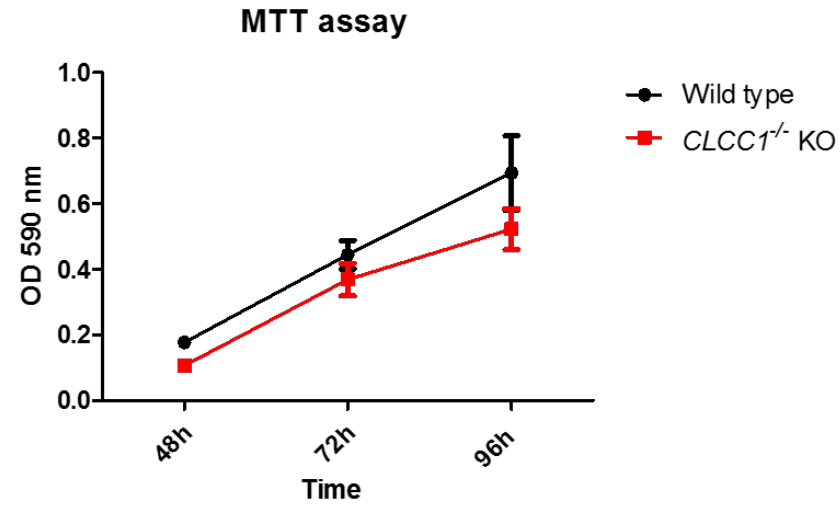
MTT assay
OD 590 nm
1.0
0.8
0.6
0.4
0.2
0.0
48h
72h
96h
Time
Wild type
CLCC1-/- KO

(ii)

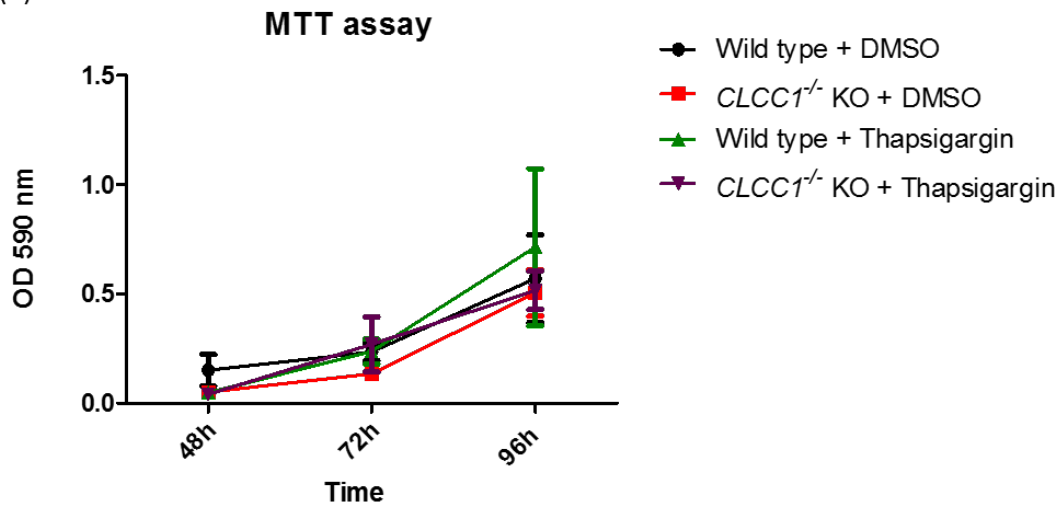
MTT assay
OD 590 nm
1.5
1.0
0.5
0.0
48h
72h
96h
Time
Wild type + DMSO
CLCC1-/- KO + DMSO
Wild type + Thapsigargin
CLCC1-/- KO + Thapsigargin

(iii)

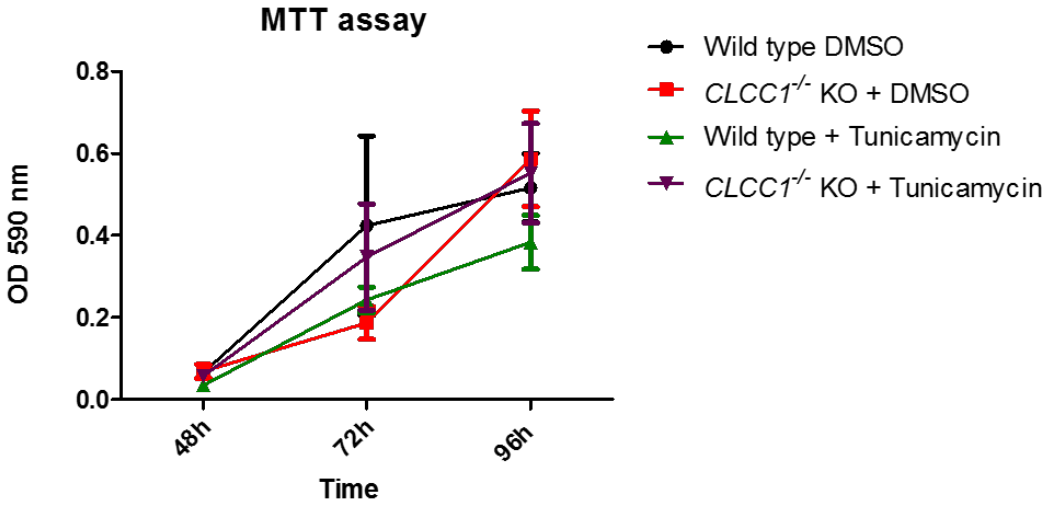
MTT assay
OD 590 nm
0.8
0.6
0.4
0.2
0.0
48h
72h
96h
Time
Wild type DMSO
CLCC1-/- KO + DMSO
Wild type + Tunicamycin
CLCC1-/- KO + Tunicamycin

Figure 4.40 MTT assay for WT vs CLCC1$^{-/-}$ KO cells. (i) *Two ways ANOVA with Boneferroni post hoc on MTT assays in wild type versus CLCC1$^{-/-}$ KO cells (N=36) showed no significant difference between the groups. Thapsigarin* ***(ii)*** *and tunicamycin* ***(iii)*** *treatments did not decrease viability of wild type or knockout cells compared to the DMSO treated cells (N=9). Each experiment was carried in triplicate.*

To determine if the loss of *CLCC1* cause unbalanced homeostatic conditions leading to cell death, wild type and knockout cells were stained with anti-cleaved caspase-3 as indicator of apoptosis. Caspase-3 is the major executioner caspase that is cleaved and activated by the initiator caspases, caspase-8 and caspase-9 [263]. Activation of executioner caspases leads to cell death [263]. Expression of cleaved caspase-3 was analysed by confocal microscopy. For each image, 3 z-stacks were taken in 1 µm depth; with consistent zoom and laser gain. After thresholding, particles (number of cleaved caspase dots) were counted using Fiji, all the images were processed in the same way (Fig 4.41).

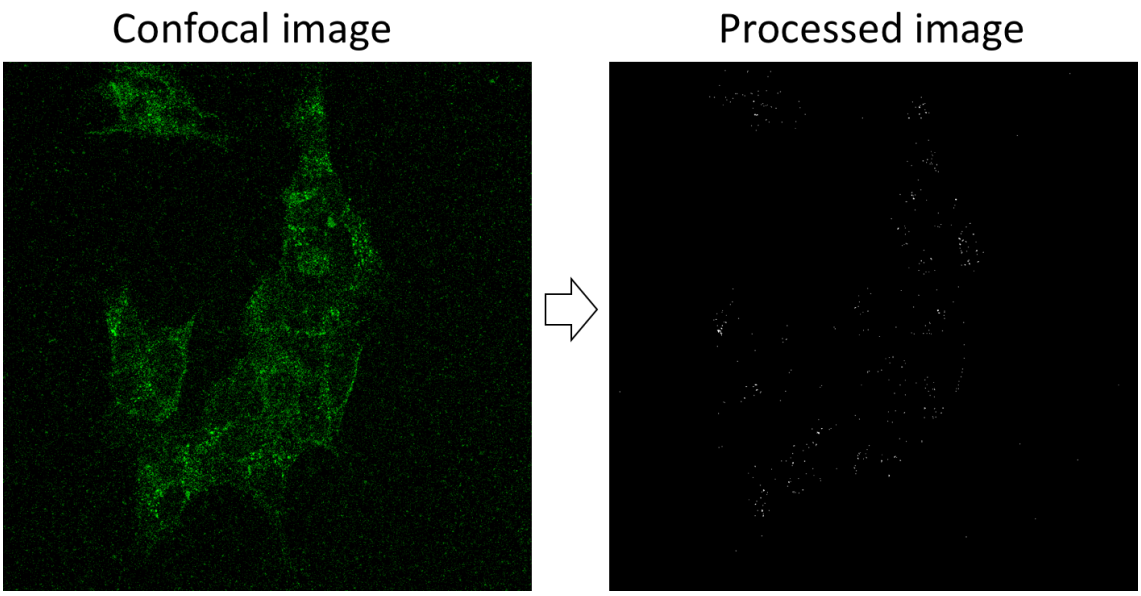

Figure 4.41 Example of caspase-3 fluorescent pictures processed for analysis. *Confocal images (left) were transformed in 8-bit, inverted, threshold (right) and the number of particles were counted.*

CLCC1$^{-/-}$ KO cells (N=22; 451 cells) compared to the wild type (N=22; 476 cells) did not show any significant change in cleaved caspase-3 expression (Mann Whitney U test; p=0.55), indicating that the lack of CLCC1 does not induce increasing of cell death (Fig 4.42 (i)). To understand if the *CLCC1*$^{-/-}$ KO cells were more sensitive to ER stress inducers, wild type and *CLCC1*$^{-/-}$ KO cells were treated with 5 µM of thapsigargin or 2 µg/ml of tunicamycin for 30 min at 37 °C, and the same volume of DMSO as control. Cells treated with tunicamycin (Fig. 4.42 (ii)) showed a significant increase of the expression of cleaved caspase-3 in wild type cells (N=22; 640 cells) compared to the *CLCC1*$^{-/-}$ KO cells (N=25; 498 cells) (Kruskal-Wallis test with Dunn's multiple comparison test; p<0.05; **). Similarly, wild type cells treated with thapsigargin (Fig. 4.42 (iii)) showed increased expression of cleaved caspase-3 (N=22; 456 cells)

compared to the same cells treated with DMSO (N=22; 420 cells) (Kruskal-Wallis test with Dunn's multiple comparison test; $p<0.05$; **) and *CLCC1*$^{-/-}$ KO cells treated with DMSO (N=22; 573 cells) (Kruskal-Wallis test with Dunn's multiple comparison test; $p<0.05$; *). Surprisingly, *CLCC1*$^{-/-}$ KO cells did not show an increase of cell death following treatments with drugs causing ER stress, while wild type cells were responsive to the ER stress stimuli. These results might indicate that the lack of CLCC1 has a protective effect from apoptosis.

Future experiments using propidium iodine to evaluate the ratio between apoptotic, necrotic, and healthy cells are necessary to confirm these results. Also, to evaluate if ER stress signalling branches activates preferentially following the drug stimulus, qPCR and western blot could be performed for CHOP, ATF6, and ATF4 as their expression increases following ER stress, as well as marker for cell death such as caspase-3, BCL-2 and Bax.

Taken together these results indicate that the lack of CLCC1 does not induce a decrease in cell viability or an increase of apoptosis in neuroblastoma cells.

(i)

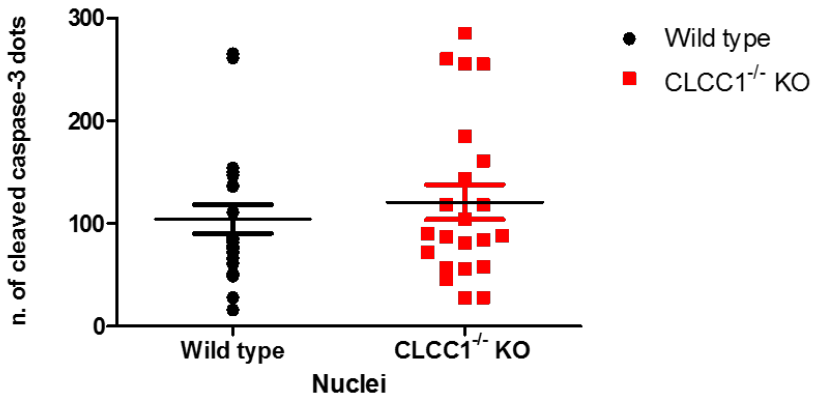
n. of cleaved caspase-3 dots
300
200
100
0
Wild type
CLCC1-/- KO
Nuclei
Wild type
CLCC1-/- KO

(ii)

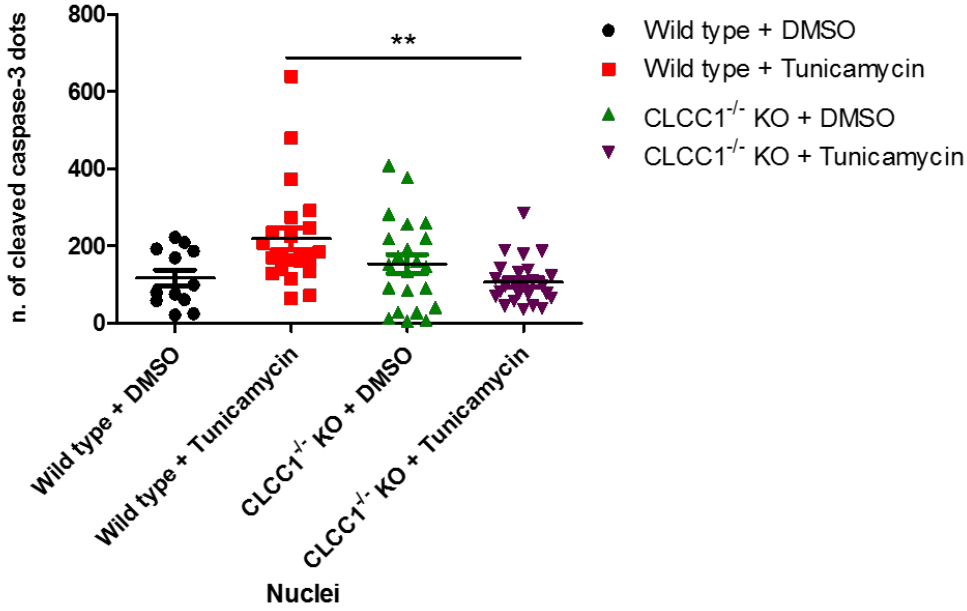
n. of cleaved caspase-3 dots
800
600
400
200
0
**
Wild type + DMSO
Wild type + Tunicamycin
CLCC1-/- KO + DMSO
CLCC1-/- KO + Tunicamycin
Nuclei

(iii)

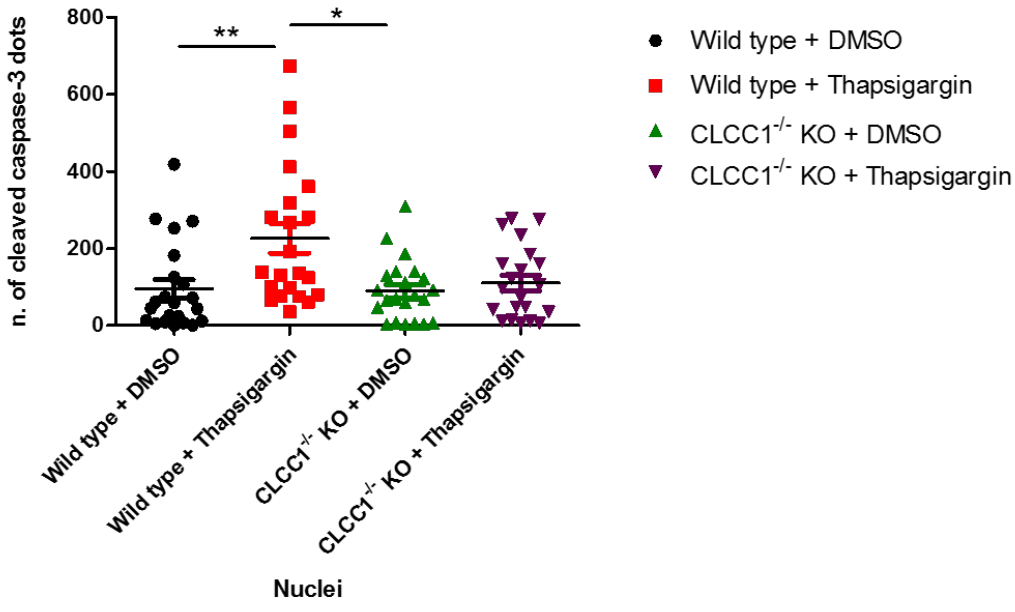
n. of cleaved caspase-3 dots
800
600
400
200
0
**
*
Wild type + DMSO
Wild type + Thapsigargin
CLCC1-/- KO + DMSO
CLCC1-/- KO + Thapsigargin
Nuclei

Figure 4.42 Cleaved caspase-3 expression. (i) *Wild type (N=22; 476 cells) and CLCC1$^{-/-}$ KO cells (N=22; 451 cells) showed no difference in cleaved caspase-3 expression (Mann Whitney U test; p=0.55).* ***(ii)*** *Wild type cells treated with tunicamycin (N=22; 640 cells) showed an increase of cleaved caspase-3 expression when compared to CLCC1$^{-/-}$ KO cells treated with tunicamycin (N=25; 498 cells) (Kruskal-Wallis test with Dunn's multiple comparison test; p<0.05; **). However, the increase was non-significant when compared to wild type + DMSO treated cells (N=12; 333 cells). CLCC1$^{-/-}$ KO cells treated with DMSO (N=22; 466 cells).* ***(iii)*** *Wild type cells treated with thapsigargin (N=22; 456 cells) showed an increase of cleaved caspase-3 expression when compared to the wild type cells treated with DMSO (N=22; 420 cells) (Kruskal-Wallis test with Dunn's multiple comparison test; p<0.05; **), and when compared to CLCC1$^{-/-}$ KO cells treated with DMSO (N=22; 573 cells) (Kruskal-Wallis test with Dunn's multiple comparison test; p<0.05; *). CLCC1$^{-/-}$ KO cells treated with thapsigargin (N=21; 381 cells) did not showed any significant change compared with the other groups.*

Graphical summary

1. *CLCC1* is expressed in the eye in different species, when is knockout the retinal layers appear disorganized with loss of photoreceptors

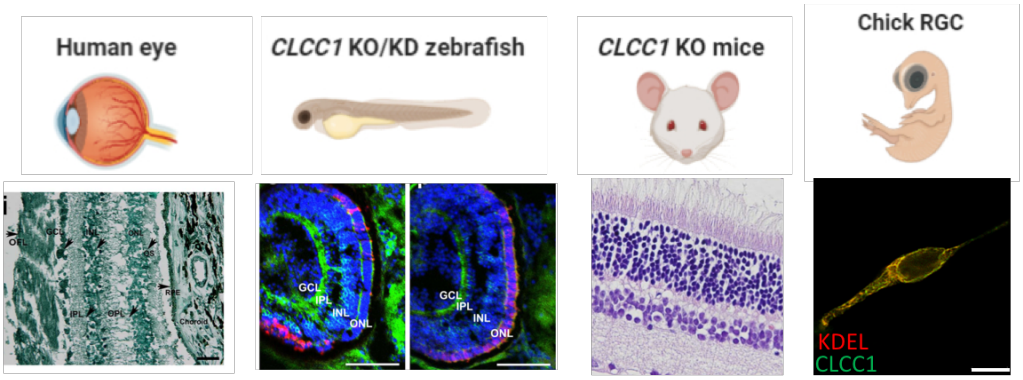

2. CLCC1 is an ER-resident protein

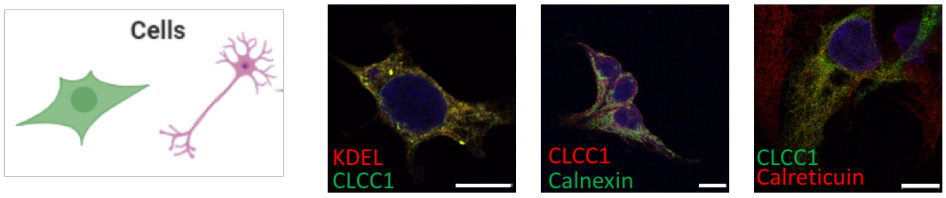

3. Mass spectrometry revealed that CLCC1 could interact with EMC1, SigmaR1, and Calcium-related proteins

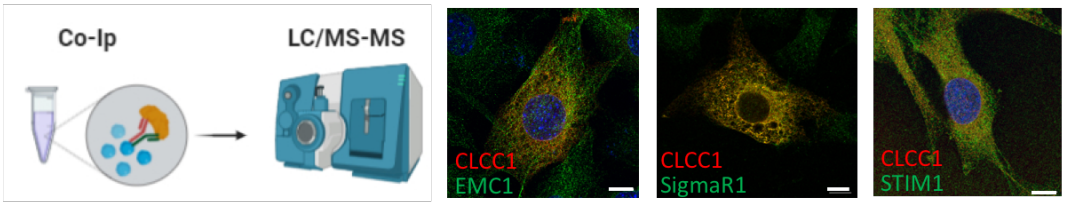

4. CLCC1 knockout in a neuronal cell line showed no change in Proliferation, apoptosis, and ER stress

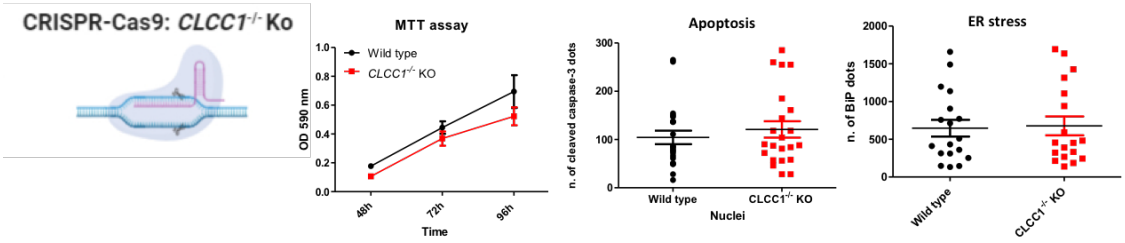

Figure 4.43 Graphical summary of the findings. *Analysis of human, mice, zebrafish and chick retinal tissues revealed that CLCC1 in expressed in the retinal layers. The knockout or knockdown in zebrafish and mice of CLCC1*

resulted in the loss of photoreceptors and disorganisation of retinal layers. In cells, CLCC1 colocalised with ER markers such as Calreticulin, KDEL, and Calnexin. Other potential binding partners of CLCC1 were identified using mass spectrometry which showed that CLCC1 could be involved in ER stress, Calcium signalling or protein insertion in membrane. EMC1, SigmaR1 and STIM1 were thought to be interesting proteins to investigate however, only SigmaR1 showed colocalisation with CLCC1 at the MAM. The functional role of this interaction still needs to be defined. CLCC1 was knockout in a neuronal-like cell line using CRISPR-Cas9: no changes in proliferation, apoptosis or ER stress were found, indicating that the loss of CLCC1 might only impact the normal physiology of retinal cells. Cartoons in the figure were created with BioRender.

4.3 Discussion

4.3.1 CLCC1 is necessary for retinal development

This study provides multiple lines of evidence to define an important role of CLCC1 for maintaining normal retinal structure and function. In addition to the human genetic data, retinal morphology, and ERGs in zebrafish and *Clcc1*$^{-/+}$ KO mice. In zebrafish, both knockdown and knockout influenced eye growth during early development, reduced the thickness of IPL and ONL layers, as well as impaired the morphology of photoreceptors. The pathogenicity of p.Asp25Glu CLCC1 in retinal development and homeostasis is illustrated by the inability of p.Asp25Glu mutant mRNA to rescue the phenotype in *clcc1*$^{-/-}$ KO zebrafish, which were similar in phenotype to the *clcc1* knockdown zebrafish. These data highlighted the importance of *clcc1* during early retina development.

The time course of *Clcc1* expression in mouse retina suggests a greater requirement for CLCC1 activity in the early postnatal period, at which time retinal cytogenesis has ended while changes in cell volume and especially the thickness of various retinal layers continue to occur, with the plexiform layers increasing and the nuclear layers decreasing in thickness and rearranging internally. In addition, retinal morphological abnormalities and decreased photopic and scotopic ERG amplitudes in *Clcc1*$^{-/+}$ KO mice support the critical requirement for full activity of CLCC1 for retinal function and perhaps development and structural integrity.

Broad expression of CLCC1 throughout the body, as well as embryonic lethality of *Clcc1*$^{-/-}$ KO mouse and zebrafish models, begs the question of why affected individuals in these families have isolated RP without any discernible systemic signs or symptoms. While the reason for the retinal specificity of the phenotype is currently unclear, there is ample precedent for isolated retinal degeneration

occurring as a result of higher retinal requirements for widely expressed proteins, including components of the spliceosome (PRPF31 [264], PRPF8 [265], PRPF3 [266], SNRNP200 [267], PRPF6 [268], and PRPF4 [269]) and transcription factors (ZNF513) [270]. High levels of CLCC1 retinal expression and especially in the photoreceptors and RPE, are consistent with CLCC1 alteration causing a retinal degeneration as is the finding that knocking out CLC3, another endosomal chloride channel, results in degeneration of the retina [271] and hippocampus [272].

Recently Jia et al. [206] identified a retrotransposon insertion in the *Clcc1* gene as a cause of autosomal recessive progressive cerebellar granule cell death and peripheral motor axon degeneration in mice, although they did not comment on retinal morphology or function. Patients with the p.Arg25Glu *CLCC1* alteration showed no signs of cerebellar or peripheral nerve dysfunction on examination or compatible symptoms by history, although it is possible that subtle subclinical findings were not recorded. Besides the different phenotypes, there were additional differences in the two systems.

4.3.2 CLCC1 is an ER-associated protein

Molecular and functional characterisation of CLCC1 has been minimal since its initial description, and its role in cellular metabolism, and in particular its role the retina, remains unclear. Nagasawa et al. [205] showed that CLCC1 is not susceptible to inhibitors of known chloride channels, suggesting that it is functionally distinct to previously described anion channel protein families, to which it bears little sequence homology. Although several proteins contain portions of the MCLC domain present in CLCC1, a Blast search of Homo sapiens transcripts using the *CLCC1* variant 1 mRNA displays significant similarity only to G-protein signalling modulator 2 (GPSM2), and a long

intergenic non-protein coding RNA (LINC00504). However, sequence alignments between GPSM2 and CLCC1 polypeptides identify no obvious regions of homology, and a BlastP search with the CLCC1 variant 1 polypeptide identifies only CLCC1 precursors and orthologues, and two hypothetical *Macaca* proteins.

As CLCC1 is a poorly characterised protein, we firstly looked at its localisation within the ER, repeating the localisation experiment published by Jia et al. [206] on human cells and murine cells, confirming that CLCC1 is present in the ER and in the ER-nuclear envelope region in human and mouse cell lines, where CLCC1 partially co-localised with KDEL. The partial co-localisation might be due to the fact that the anti-KDEL antibody binds a variety of soluble proteins carrying the ER retention signal KDEL, which cannot be discriminated using a generic KDEL antibody. The staining of cells for calnexin, a calcium-binding chaperone, which does not have a KDEL sequence, showed absence of co-localisation with CLCC1, while staining cells with calreticulin, which does have a KDEL sequence, showed both co-localisation and co-immunoprecipitation with CLCC1. However, these results do not necessarily suggest that CLCC1 localises only with proteins carrying the KDEL sequence at their C-terminus. In chick RGC cells, a more physiologically relevant type of cells, CLCC1 was present in both soma and axonal ER; the localisation of CLCC1 in the axon might suggest its involvement in neuronal development.

Plasmids for CLCC1 were used with a YFP tag at N-terminus or FLAG tagged to the C-terminus to overexpress the wild type and the mutant protein. While the tags did not affect the localisation of CLCC1, they affected the binding with calreticulin which was not pulled-down with the tagged CLCC1, neither wild type nor mutated. It is known that GFP can interfere with the folding, ubiquitination

[273] and normal cell physiology, for example impairing actin-myosin interactions [274], however the YFP, a derivative of GFP, seems to have an improved folding and sensitivity [275]. Nevertheless, CLCC1 seems to be sensitive when linked to fluorescent proteins as plasmids CLCC1-YFP, mCherry-CLCC1 and mCardinal-CLCC1 did not function when they were expressed in cells. The use of FLAG tag (DYKDDDDK) was considered a better choice as its hydrophilicity should not denature or inactivate proteins to which they are attached. Consequently, the use of tags should be carefully evaluated when used for mass spectrometry experiments, as we demonstrated that they might interfere with binding of partners to the protein of interest.

CLCC1 localisation analyses defined that the alteration Asp25Glu does not induce any change in localisation of CLCC1 in HEK293 cells, the lack of mis-localised mutant protein might be due to the presence of endogenous CLCC1 in the cells, however, experiments in *CLCC1*$^{-/-}$ KO cells suggest that this was not the case. Regardless of the effect the alteration promotes on the protein itself or on the binding with other proteins, the Asp25Glu variant does not promote mis-localisation from the ER of CLCC1.

CLCC1 is predicted to have four isoforms deriving from alternative splicing. Isoform 1 and 2 have three TM domains, isoform 3 one TM domain while isoform 4 has two TM domains. While isoform 1, 2 and 3 have the TM domains encoded by the same exons, one TM domain of isoform 4 derives from the corresponding exons 4 and 9 of isoform 1. We were able to identify by western blot isoform 1 and 2 however, the existence of isoform 3 and 4 still need to be verified. When cells were transfected with plasmids carrying the various isoforms, they all localised in the ER and nuclear membrane, confirming the results obtained with the staining of cells with the CLCC1 antibody which also

recognise all the isoforms. Unfortunately, the efforts to confirm the orientation of CLCC1 on the membrane, obtained with sequence analysis software, were fruitless, leaving the question still open.

The ER is composed by continuous membrane structures including the nuclear envelope, ER sheets and the peripheral ER tubules. In each of these domains, structural proteins help to maintain its shape [276], changes in the amount of these proteins induce morphological alteration of the ER and changes in ratio of sheets/tubules. For example, overexpression of some reticulon isoforms induce the expansion of tubules [277], while overexpression of Climp63, an transmembrane ER protein, leads to proliferation of ER sheets [276, 278]. Whether changes in CLCC1 expressions lead to variation in ER domains ratio or ER shape was not thoroughly assessed, although substantial changes following overexpression or knockout have not being seen, future experiments using electron microscopy to exclude its involvement in these processes would be necessary.

Liquid chromatography tandem-mass spectrometry (LC-MS/MS) is a widely used technique in proteomics and has become an established platform for proteins quantification [279] and for the identification of proteins interactome [280-283]. Therefore, mass spectrometry was used to identify binding partners of CLCC1. For endogenous CLCC1, binding partner analysis indicated that CLCC1 is likely to be involved in ER function, mRNA processing and intracellular transport. While this last category, containing tubulin and dynein, is probably enriched because the ER is tightly related to the cytoskeleton [284]. The high number of hits related to the ribosome and mRNA processing could be explained by the fact that the CLCC1 antibody might recognise newly translated

proteins still attached to the ribosome, the cluster related to protein processing in the ER seems to be the most relevant.

The dataset for CLCC1-WT FLAG showed the presence of high represented proteasome pathway, which might be caused by the overexpression of plasmids itself, as the cells might increase protein degradation levels to reduce protein overload which due to overexpression. Indeed, this pathway was not represented in the endogenous CLCC1 dataset, where the presence of CLCC1 is at physiological levels. Unless CLCC1 is related to the insertion of proteins in the ER membrane, the overexpression of CLCC1 could potentially explain the presence of the high number of hits related to protein translocation into the ER, which is induced by higher levels of translation than in homeostatic conditions. Although the overexpression of CLCC1 increases the rate of protein degradation, it does not induce the activation of the UPR as the number of chaperones present in several datasets seems quite consistent. CLCC1-WT FLAG also showed high representation in cluster analyses related to nuclear outer membrane-ER boundary which is consistent with the staining of cells where CLCC1 was found localising near the nuclear membrane. This might also indicate that CLCC1 is involved in the transport of mRNA outside the nucleus or translocation of proteins in the ER.

To better look at the differences between CLCC1-WT and Asp25Glu FLAG datasets, the GO classification for cellular components was investigated. Molecular function and biological process GO terms had a lower FDR confidence which might be due by the fact that proteins present in the datasets have a variety of functions and implicated in different processes and their number in the dataset is not higher enough to reach a higher FRD confidence. The high number of hits deriving from mass spectrometry could also be

considered a limitation of the technique, as it does not uniquely point to a specific pathway. The cellular components classification provided evidence that the Asp25Glu alteration causes an increase of interactions with cytoplasmic proteins, which is consistent with the prediction of the topology of CLCC1, where the N-terminus tail containing the alteration is cytoplasmic. Therefore, a difference in cytoplasmic binding partners could explain the how the Asp25Glu alteration causes RP.

Interestingly, calreticulin was not present in both filtered dataset and raw files. This might indicate two things; (i) although the mass spectrometry is a good technique, it may not be totally reliable, and (ii) despite sample processing between the pull down experiments being consistent, the binding of CLCC1 to calreticulin might be time dependent or related to a specific state of the cells.

Trinkle-Mulcahy et al. [285] reported the specific proteome associated to the type of beads used to pull-down proteins in immunoprecipitation assays. Many of the proteins contaminating dynabeads, which we also used to pull-down our samples, were present in our dataset. For example, many chaperonin, coatomer-associated proteins, ribosomal proteins, and tubulins present in our datasets might be the result of inappropriate binding of proteins to the dynabeads. Some of these proteins (CLTC, DYNC1H1, XPO1, FASN and PSMA5) that result from the unspecific binding to the beads were not filtered out by our system, and they have also been associated with retinal function; none of these proteins was chosen for further analysis. These data validate our negative controls and demonstrate the strength of our two-layer filtering system based on the presence of the proteins in the mass spectrometry data and PubMed search.

Retinal degeneration is often a symptom of congenital disorders of glycosylation [286, 287]. N-glycosylation consists in modification of asparagine residues on a nascent protein in the ER, and the activity of calreticulin and calnexin amongst other chaperones ensure the secretion of glycoproteins from the ER [288, 289]. Although the mass spectrometry identified proteins participating in this pathway as possibly associated to CLCC1-WT and Asp25Glu FLAG (such as ALG10, MAGT1, KRTCAP2, DAD1, STT3 and DDOST), N-glycosylation has not been investigated in this work for the lack of definitive evidence supporting the involvement of those pathways. In particular we could not exclude that high representation of these proteins in our datasets was not induced by overexpression of our protein of interest, and the technical difficulties that analysis of protein spectra carries.

From the mass spectrometry results, four putative binding partners were selected. EMC1 is a member of the EMC complex; recently two papers in which mass spectrometry for EMC was performed identified CLCC1 as a candidate interacting partner. In particular, in Tian et al 2019 [290] performed mass spectrometry on extracts from HeLa cells, in which EMC4 and EMC6 were found binding CLCC1, while in Shurtleff et al 2018 [242] CLCC1 was found binding EMC2 in yeast. In our dataset EMC1 binds only CLCC1-WT FLAG however when looking at the raw, unfiltered data, EMC2, EMC6, and EMC8 were present in a single replicate and therefore filtered out. Similarly, EMC6 was present in both replicates in CLCC1-Asp25Glu FLAG, but filtered out as having a score of 5 as indicating low confidence matches. Thus the binding partner assays here are consistent with recently published other studies, strengthening a link between EMC and CLCC1. However, staining of cells both NIH/3T3 and SH-SY5Y cells with the anti-EMC1 antibody and CLCC1 did not

showed further a co-localisation, as EMC1 unexpectedly localised on the plasma membrane. Moreover, the knockout of *CLCC1* did not change expression of EMC1 when visualised by staining. EMC inserts tailed-anchored proteins in the ER membrane, which are defined as single transmembrane protein whose transmembrane domain is located within 50-70 amino acids from the C-terminus, however has been observed that EMC loss impairs rhodopsin, which is a GPCR, insertion in Drosophila [291]. Whether CLCC1 is inserted in membrane by EMC or CLCC1 participates in EMC activity needs to be established.

We also choose to look at calnexin although the staining previously performed did not show a great amount of co-localisation with CLCC1, its co-immunoprecipitation of CLCC1-WT and Asp25Glu FLAG confirmed the mass spectrometry data. Interestingly, calnexin has been reported as residing in the MAM other than the rough ER, and interacts with SERCA2b [292].

SigmaR1 was also considered a good candidate interacting partner to investigate. SigmaR1 is a MAM protein which regulates ER-mitochondrion Ca^{2+} signalling [293]. SigmaR1 also displays a chaperone activity and binds BiP in homeostatic conditions but upon chronic ER stress, it dissociates and translocate into the ER [249]. Moreover, upon Ca^{2+} depletion or via ligand stimulation, SigmaR1 dissociates from BiP and binds IP3Rs, prolonging Ca^{2+} signalling from the ER into mitochondria [249]. We demonstrated that SigmaR1 co-immunoprecipitate with CLCC1-WT and Asp25Glu FLAG confirming the mass spectrometry analysis. Staining of cells, showed that SigmaR1 and CLCC1 co-localise in the MAM, however pharmacological manipulation of SigmaR1 seems to not induce change in localisation of CLCC1.

The effect of calcium store-depletion on CLCC1 was also investigated because the ER is the major store of calcium inside the cells. Even though one of the mass spectrometry hits was SERCA2 common to CLCC1-WT and CLCC1-Asp25Glu, STIM1 was selected for investigation as it has been demonstrated that SigmaR1 is involved in controlling the dynamics of binding between STIM1 and ORAI1 [250]. Staining of endogenous CLCC1 and STIM1 showed little co-localisation, and treatments with thapsigargin activate STIM1 which appeared to localise on the plasma membrane, and have no effect on the localisation of CLCC1. This experiment does not evidence or discredit the involvement of CLCC1 in calcium signalling because we did not verify the total ER calcium content or at the calcium currents in wild type and knockout cells. It would also be interesting to verify if the knockout of CLCC1 might interfere with the action of SigmaR1 on STIM1-ORAI1 binding.

Jia et al. [206] reported that the knockdown of CLCC1 in HEK293 cells caused an increase of ER stress, measured with ATF6. Additionally, mice with a retrotransposone insertion in *CLCC1* (believed to cause the loss of function of CLCC1) showed increase of BiP and ubiquitin expression in cerebellar granule neurons. Recently, Chu et al. [294] demonstrated that CLCC1 interacts with the microprotein PIGBOS at the ER-mitochondria contact sites but their interaction did not affect the number of ER- mitochondria contacts, supporting our finding that CLCC1 is present at ER-mitochondria contact sites where it interacts with SigmaR1. They also demonstrated that treatments with tunicamycin of CLCC1 knockdown cells induced an increase of ER stress measured the ratio of XPB1 spliced and unspliced form. Here, we measured the expression of BiP in wild type and *CLCC1*$^{-/-}$ KO cells, while the same levels of BiP were present in both cell types. Following thapsigargin treatments an increased expression of BiP

was present in *CLCC1*$^{-/-}$ KO and was significantly higher than wild type cells subject to the same treatment. It is interesting to notice that evidences reported in literature suggested that thapsigargin treatment increases or decreases BiP expression depending on the cell type, for example INS-1E cells treated with thapsigargin showed decreased BiP expression [295] while in SH-N-SH cells the treatment induced increased expression of BiP [296]. These might indicate that neuronal-like cells may be more sensitive to changes of intracellular calcium levels. Discordantly from the two papers aforementioned, we did not find any difference in ER stress response when cells were treated with tunicamycin, which could be related to the timespan in which the experiments have been performed, therefore a 12h treatments could give the same results as reported in literature. Hence, repeating the tunicamycin treatments for a longer period of time and verify with qPCR and western blot which branch or the UPR response activates would be necessary.

Pathway analysis of mass spectrometry data evidenced that CLCC1 might be involved in metabolic pathways, and that the Asp25Glu alteration induces the increase of binding partners related to metabolism. Unfortunately, KEGG pathway did not give more information about which metabolic pathways our datasets were more enriched, and the KEGG term ‘metabolism’ comprises a variety of different metabolic pathways as energy metabolism, lipid metabolism, amino acid metabolism, glycan biosynthesis, etc. We decided to look at energy metabolism because glycolysis, oxidative phosphorylation, and Hsp90 inhibitors were already available in the lab. Moreover, photoreceptors metabolise glucose though aerobic glycolysis as cancer cells do, and the glucose uptake is necessary for the renewal of photoreceptors outer segment [297]. It has also been reported that in the later phases of RP, the stimulation of aerobic

glycolysis could induce the re-growth of the cone photoreceptors [297]. None of these inhibitors influenced the position of CLCC1 within the ER in NIH/3T3 cells. It would have been interesting looking at the protein levels of CLCC1 following the treatments but the anti-CLCC1 antibody does not detect protein levels of whole lysate on western blot. Energetic rate in wild type and knockout cells could also be measured with the Seahorse analyser which measure the oxygen consumption rate and extracellular acidification rate which are indicators of mitochondrial respiration and glycolysis.

SH-SY5Y cells with CLCC1 knocked out did not show decrease of viability or increase of apoptosis, indicating that the lack of CLCC1 does not influence the viability of neuronal-like cells, however animal model showed increased death and mis-shaped photoreceptors when CLCC1 was knockout, indicating that would be better to study the function of CLCC1 in retinal cells. Furthermore, to study the effect of the Asp25Glu variant, CRISP-Cas9 could be used to perform a single nucleotide change in either retinal cell lines or animal models.

In conclusion, the lack of identification of a clear functional outcome to explain the degeneration of retinal cells due to p.(Asp25Glu) CLCC1 substitution might relate to the fact that studies to date have primarily involved non-retinal cells. It is therefore possible that in these cell lines the CLCC1 pathway may be redundant, while in retinal cells its pathway has a more fundamental role. It is also important to consider that photoreceptors are post-mitotic cells, while cell lines are immortalised; therefore the lack of an apparent functional outcome of CLCC1 mutation/loss of function might be related to the constant division rate of SH-SY5Y cells and NIH/3T3, so the repercussions of the knockout of CLCC1 are not visible in the short period in which these cells are in culture.

4.4 Future directions

To fully uncover the role of CLCC1 into the cell, further investigation would be necessary.

CLCC1 was found to be important for the development of mouse and fish and in particular for the retina development, photoreceptors morphology, and function. As the function of CLCC1 was not known additional studies were necessary. These identify CLCC1 as an ER protein, although the functional significance of the Asp25Glu variant has not been defined yet. Through mass spectrometry CLCC1 was found to interact with a multitude of ER, mitochondrial, and cytosolic proteins however, a definite pathway in which CLCC1 is involved was not evidenced. Amongst the potential binding partners calretilculin, BiP, SigmaR1, calnexin, and EMC1 were further analysed. In particular, it is notable that CLCC1 and SigmaR1 interact in the MAM, however the functional significance of this remains unclear. The localisation of CLCC1 at the MAM was also recently reported [294], consistent with these findings work. It has been demonstrated that CLCC1 is involved in ER stress, in particular cells with *Clcc1* knockout or knockdown showed an increase of ER stress when treated with tunicamycin [206]. The studies here did not define any change in expression of BiP following tunicamycin treatments, however and increase of ER stress was found in CLCC1 knockout cells following treatments with thapsigargin. The degree of involvement of CLCC1 in ER stress was not conclusively demonstrated, so additional experiments in this area would be valuable.

In recent years the adoption of iPSC-derived retinal organoids from patients carrying the genetic alteration has become increasingly common and has allowed the discovery of pathogenic mechanisms as well testing of potential therapies [154, 298-300]. Thus, the use of patient-derived iPSC could help in

understanding the pathogenic effect of Asp25Glu CLCC1 on photoreceptors. Additionally, CRISPR-Cas9 gene editing could be employed to produce the Asp25Glu in CLCC1 in a retinal cell line.

As the key roles of CLCC1 have not yet been uncovered, it may be helpful to perform cellular fractionation on wild type and CLCC1 KO cells to determine if the knockout impact the concentration of binding partners in different districts of the cells (e.g. MAM, ER, mitochondria), as well as to determine if calcium concentration and dynamics may change following the knockout of CLCC1, and whether this may be related to SigmaR1 and STIM1. As CLCC1 has been shown to be related to the ER stress, longer treatments of cells with thapsigargin and tunicamycin may define if there is a preferential branch of the UPR response activated in CLCC1 knockout cells. To assess if CLCC1 and binding partners such as SigmaR1 interact, FRET or split GFP fluorescence complementation assays could be used. Alternatively SPLICS [301], a split-GFP-based methods to study narrow and wide ER-mitochondria contact sites, would be suitable to measure the range of interaction between SigmaR1 and CLCC1. SigmaR1 also binds sphingolipids, in which the MAM is enriched, and participates in cholesterol trafficking and steroidogenesis at the MAM [302]; therefore the potential role of CLCC1 in SigmaR1-related cholesterol trafficking could be investigated.

The interaction between CLCC1 and EMC should be carefully studied. A split GFP fluorescence complementation approach could be employed to study the potential interaction of CLCC1 with EMC subunits. Biochemical assays following the experimental procedures used by Chitwood et al [243] would be instrumental to determine whether EMC inserts CLCC1 in the ER membrane.

CLCC1 homozygous knockout in fish and mouse were embryonically lethal, while the heterozygous knockout was viable, indicating that *CLCC1* is necessary during early development. Therefore, zebrafish or mouse neuronal primary culture from embryos could be used to identify developmental pathways in which CLCC1 is implicated, and if CLCC1 expression is necessary for the development of other organs. The use of neuronal primary culture from heterozygous and homozygous animals could also be employed to verify if CLCC1, as it is present in the axonal ER, is implicated in axon guidance; for example if CLCC1 mediates calcium signalling at the growth cone.

CHAPTER 5

GENETIC SPECTRUM OF INHERITED EYE DYSTROPHIES IN PAKISTAN

CHAPTER 5 GENETIC SPECTRUM OF INHERITED RETINAL DYSTROPHIES IN PAKISTAN

5.1 Introduction

Inherited retinal dystrophies (IRD) are a clinically and genetically heterogeneous group of ocular conditions, characterised by progressive degeneration of the retina, leading to visual impairment and even blindness [303]. Variants in 269 genes have been identified to date in association with IRD encompassing either non-syndromic or syndromic forms of the condition. Prevalence of each subtype of IRD in Pakistan has not been extensively reported and even though several papers explore the recurrence of gene alteration, differences between reports might underlie the heterogeneity of the Pakistani population. A systematic review, carried out in 2015 [166], on the cause of IRDs in South Asia (Pakistan, India, and Bangladesh) involving 66 families, showed that mutations in *TULP1*, *PRPF31* and *CRB1* were the most common. Moreover, the 95% of causes of disease were autosomal recessive, consistent with geographical constraints and marriage patterns within communities which often give rise to genetic isolates with a higher frequency of certain disease-associated founder alterations [167] [169, 304, 305]. Similarly, an extensive study using homozygosity mapping on 144 consanguineous Punjabi families [169] affected by non-syndromic IRDs showed that the most commonly altered genes were *RPE65* (6.9% of families), *TULP1* (6.9%), *RP1* (4.9%) which is most commonly mutated in Saudi Arabians [240], *PDE6A* (4.9%) and *USH2A* (3.5%). Homozygosity mapping failed in identifying the pathological variant underlying the disease in the 27.8% of families, a proportion in line with studies in other populations. Another review on Pakistani population [304] identified 103 non-syndromic IRD families, with arRP encompassing for the 59% of cases,

followed by arLCA (19%), arCRD (10%), and arCSNB (9%). Syndromic IRD were found in 52 families with Usher syndrome and BBS the most common (36% and 33% respectively). Amongst the non-syndromic IRDs *AIPL1, CRB1, TULP1*, and *RPGRIP1* were the most common genes mutated, while amongst the syndromic IRDs *CDH23, TMEM67* and *BBS10* were the most prevalent.

This chapter describes the genetic bases of syndromic and non-syndromic IRDs 27 families from Pakistan, and presents a review of all pathogenic gene variants associated with IRD in the Pakistani population, to generate a database of all gene variant found in this population and to highlight provinces where the specific gene alteration or disease are more prevalent [240].

5.2 Results

In order to learn more about the nature, spectrum, and frequencies of IRD in Pakistan we undertook genomic studies in 27 families from Pakistan with individuals with a preliminary clinical diagnosis of IRD, nystagmus and congenital cataracts, as part of an ongoing international collaboration. A total of 16 families (families 1 to 4, 6, 7, 9, 11 to 19) were recruited through the Exeter (IBCS) collaborator consortium while 11 families were investigated at the National Eye Institute (NEI), USA (families 5, 8, 10, 20 to 27). When possible detailed family history, geographical localisation, and clinical information were collected by local clinicians, and collated by Dr. Siying Lin (IBCS). IBCS families were investigated with WES or with Illumina Trusight One clinical exome sequencing panel, while NEI families were investigated with linkage analysis followed by WES/WGS and Sanger sequencing. Table 5.1 summarise the clinical and genetic findings of these families.

Table 4.1 **Variants segregating with inherited retinal diseases identified in this study** *Abbreviations: ar, autosomal recessive; BBS, Bardet Biedl syndrome, gnomAD, genome aggregation database; MAF, minor allele frequency; NA, not available; SAS, South Asian; KPK, Khyber Paktunkhwa; RP; Retinitis pigmentosa; IRD, inherited retinal dystrophy; (-) indicates absence of additional clinical information. Variants in shaded rows are interpreted as being of uncertain clinical significance due to the clinical and genetic evidence below.*

Family	Region, province (Caste)	Initial clinical diagnosis	Ocular findings	Genotyping	Previously reported	gnomAD MAF all/SAS (homozygous count)	Clinvar (Accession)	Revised diagnosis	Additional clinical findings post molecular diagnosis
1	Swabi,KPK (Pashtoon, Yousafzai)	Congenital nystagmus	Congenital nystagmus, visual impairment, strabismus	***CNGA3*** c.955T>C/c.955T>C; p.(Cys319Arg)/p.(Cys319Arg)	[306-308]	0.00001767/ 0.0001307 (not present)	Not listed	IRD	-
2	Jatoi, Muzaffargarh, Punjab	Cone dystrophy	Severe photophobia, visual impairment, congenital nystagmus and strabismus	***CNGA3*** c.1556T>C/c.1556T>C; p.(Met519Thr)/p.(Met519Thr)	[309]	Absent	Not listed	IRD	-
3	Sargodha, Punjab	Achromatopsia	Visual impairment, impaired colour vision photophobia, strabismus, nystagmus, normal fundus appearance	***CNGA3*** c.1600G>A/c.1600G>A; p.(Gly534Arg)/p.(Gly534Arg)	No	Absent	Not listed	IRD	-
4	Peshawar, KPK	Nystagmus	-	***CNGA3*** c.1443dup/c.1443dup p.Ile482Hisfs*6/p.Ile482Hisfs*6	[310]	Absent	Not listed	IRD	-
5	NA	IRD	-	***CNGA3*** c.1641C>A /c.1641C>A p.Phe547Leu/p.Phe547Leu	[311]	0.0001592/ 0.0007186	Likely pathogenic (VCV000009478)	IRD	-

6	Lahore, Punjab (Mughal)	RP	-	***TULP1*** c.855dupC/c.855dupC p.(Val286Argfs*98)/p.(Val286Argfs*98)	[312]	Absent	Likely pathogenic (VCV000505327)	arRP	-
7	Kohat Dist., KPK	RP	Visual impairment, photophobia, nystagmus	***TULP1*** c.238C>T/c.238C>T p.(Gln80Lys)/p.(Gln80Lys)	No	Absent	Not listed	arRP	Fundus examination: pigmentary retinopathy, optic disc pallor, attenuated vessels
7	Kohat Dist., KPK	IRD	-	***PDE6C*** c. 480delG/c.480delG p.(Asn161Thrfs*33)/p.(Asn161Thrfs*33)	No	Absent	Not listed	IRD	Fundus examination: pigmentary maculooathy
8	NA	IRD	-	***PDE6C*** c.1A>G/c.1A>G p.(Met1*)/p.(Met1*)	No	0.00003184/ 0.00006479 (not present)	Not listed	IRD	-
9	Pishin, Baluchistan (Syed, Pashtoon)	Nystagmus	Visual impairment, nystagmus, strabismus	***RPGRIP1*** c.2789dup/c.2789dup p.(Pro931Thrfs*3)/p.(Pro931Thrfs*3)	No	Absent	Not listed	IRD	-
10	NA	IRD	-	***RPGRIP1*** c.2710G>A/c.2710G>A p.(Gly904Ser)/p.(Gly904Ser)	No	Absent	Not listed	IRD	-
11	KPK (Pakhtun)	Oculocutaneous albinism	Visual impairment, photosensitivity, nystagmus, light skin and hair	***ABCA4*** c.3364G>A/ c.3364G>A p.(Glu1122Lys)/p.(Glu1122Lys)	[313]	0.00002829/ 0.00006533 (not present)	Pathogenic/ Likely pathogenic (VCV000030218)	IRD	-

12	Quetta, Balochistan (Tajik, Afghan)	Nystagmus	Visual impairment, nystagmus, myopia	***BBS4*** c.221-1G>A/c.221-1G>A	No	Absent	Not listed	arBBS	Polydactyly, intellectual disability, obesity, myopia, retinitis pigmentosa
13	Borewala Punjab, (Dogar)	RP	-	***CRB1*** c.3735delA/c.3735delA; p.(Gly1246Glufs*36)/p.(Gly1246Glufs*36)	No	Absent	Not listed	arRP	-
14	KPK	Congenital cataract	-	***GUCY2D*** c.3056A>C/ c.3056A>C p.His1019Pro/p.His1019Pro	[314]	0.000004077/ 0.00003347 (not present)	Not listed	IRD	-
15	Lahore, Punjab (Rajpoot)	RP	-	***TTC8*** c.768+5G>A/c.768+5G>A	No	Absent	Not listed	arRP	-
16	Mastung, Baluchistan (Ababki, Bravi)	Nystagmus	Nystagmus and visual impairment.	***CACNA1F*** c.2254G>A/c.2254G>A; p.(Val752Met)/p.(Val752Met)	No	Absent	Not listed	IRD	-
17	Karak Dist., KPK	Usher syndrome	Visual impairment, hearing loss	***USH2A*** c.7334C>T/c.7334G>A; p.(Ser2445Phe)/p.(Ser2445Phe)	[315]	0.0008410/ 0.006435 (2)	Uncertain significance/ Benign (VCV000048581)	Usher syndrome	Audiogram: sensorineural hearing loss Fundus examination pigmentary retinopathy, optic disc pallor, attenuated vessels, maculopathy, cataract, epiretinal membrane

18	Raiwind, Punjab (Chohan)	RP	-	***CNGB1*** c.852_874+25del/c.852_874+25del p.(Ile286Aspfs*9)/p.(Ile286Aspfs*9)	No	Absent	Not listed	arRP	-
19	Rawalpindi, Punjab	RP	Visual impairment, strabismus	***LRAT*** c.196G>C/c.196G>C; p.(Gly66Arg)/p.(Gly66Arg)	No	Absent	Not listed	arRP	-
20	NA	IRD	-	***CLCC1*** c.75C>A/c.75C>A; p.(Asp25Glu)/p.(Asp25Glu)	[316]	0.00004778/ 0.0003924 (not present)	Not listed	IRD	-
20	NA	IRD	-	***CDH23*** c.1595C>T/c.1595C>T; p.(Thr532Met)/p.(Thr532Met)	[317, 318]	Absent	Not listed	IRD	-
21	NA	IRD	-	***LCA5*** c.1550_1551delGA/ c.1550_1551delGA; p.(Arg517Ilefs*3)/p.(Arg517Ilefs*3)	No	0.000007978/ 0.00006534 (not present)	Not listed	IRD	-
22	NA	IRD	-	***RPGR*** c.310+1G>C/c.310+1G>C	[319, 320]	Absent	Not provided (VCV0000987 79)	IRD	-
23	NA	IRD	-	***PDE6B*** c.12_15delAGTG/c.12_15delAGTG p.(Ser4Argfs*23)/p.(Ser4Argfs*23)	[321]	Absent	Not listed	IRD	-
24	NA	IRD	-	***RDH5*** c.838C>G/c.838C>G p.(Arg280Gly)/p.(Arg280Gly)	No	Absent	Not listed	IRD	-

25	NA	IRD	-	***MERTK*** c.2194C>T/c.2194C>T; p.(Arg732*)/p.(Arg732*)	[322]	0.000/0.000	Not listed	IRD	-
26	NA	IRD	-	***OAT*** c.722C>T/c.722C>T p.(Phe241Leu)/p.(Phe241Leu)	[308, 323]	0.00003579/ 0.0001633	Not listed	IRD	-
27	NA	IRD	-	***ARL6*** c.534A>G/c.534A>G p.(Gln178Gln)/p.(Gln178Gln)	No	Absent	Not listed	IRD	-

5.2.1 Sequence alterations in CNGA3 associated with IRD in five families

Family 1 (Fig. 5.1 (i)) was a large consanguineous family with four affected individuals presenting congenital nystagmus, visual impairment and strabismus. The family originated from Swabi, in the KPK region, and belonged to the Pashtoon tribe. Exome sequencing and co-segregation analysis revealed a variant in the gene *CNGA3* c.955T>C; p.(Cys319Arg). This variant has a MAF of 0.0001307 in South Asian population and 0.000007741 in the North-Western European population, no homozygous individuals have been reported on gnomAD. This variant has been reported as causative of juvenile CRD with maculopathy in a Pakistani family [306] and in other families of unknown ethnic origin [307, 308].

Family 2 (Fig. 5.1 (i)) was a large multigenerational family with individuals initially diagnosed with cone dystrophy. The five affected individuals showed severe photophobia, visual impairment, congenital nystagmus, and strabismus. The family originates from Jatoi, Muzzaffargarh, Punjab. Exome sequencing identified a candidate pathogenic homozygous missense variant in *CNGA3* gene, c.1556T>C, p.(Met519Thr), which co-segregates as appropriate in this family. This variant was previously reported by Huang et al. [309] in a Chinese family as a likely cause of CRD, and it was absent in gnomAD.

Family 3 (Fig. 5.1 (i)) originated from Sagodha, Punjab, and has four affected individuals which were diagnosed achromatopsia. They presented visual impairment, impaired colour vision, photophobia, strabismus, and fundus examination showed a normal appearance. Genetic analysis identified that affected family members were homozygous for a *CNGA3* c.1600G>A; p.(Gly534Arg) variant, which has not been reported previously and was also absent in gnomAD.

Family 4 (Fig. 5.1 (i)) was a small nuclear family originating from Peshwar, KPK. The two affected family members were diagnosed with nystagmus. Unfortunately, no other clinical information was available. Illumina Trusight One clinical exome sequencing panel identified a homozygous frameshift variant *CNGA3* c.1443dup; p.(Ile482Hisfs*6) as the likely cause of disease. This variant has been reported as disease causing in unknown ethnic groups [310], and it was absent from gnomAD.

In Family 5 (61421) (Fig. 5.1 (i)), the homozygous missense variant *CNGA3* c.1641C>A; p.(Phe547Leu) was found to co-segregate in the four affected (and other) family members, was identified as the likely cause. The variant has been already associated with IRDs [324-326], and has a MAF of 0.0007186 in South Asian population, and also present in European and Finnish populations.

All the *CNGA3* variants identified were highly conserved among vertebrates (Fig. 5.1 (ii)), and were located in functionally-relevant regions of the channel; Cys319 was in the ion channel transmembrane domain (Ion_trans), while Met519, Gly534, Phe547 are located in the cyclic nucleotide-binding domain (cNMP_binding). Residue Ile482 lies outside those domains.

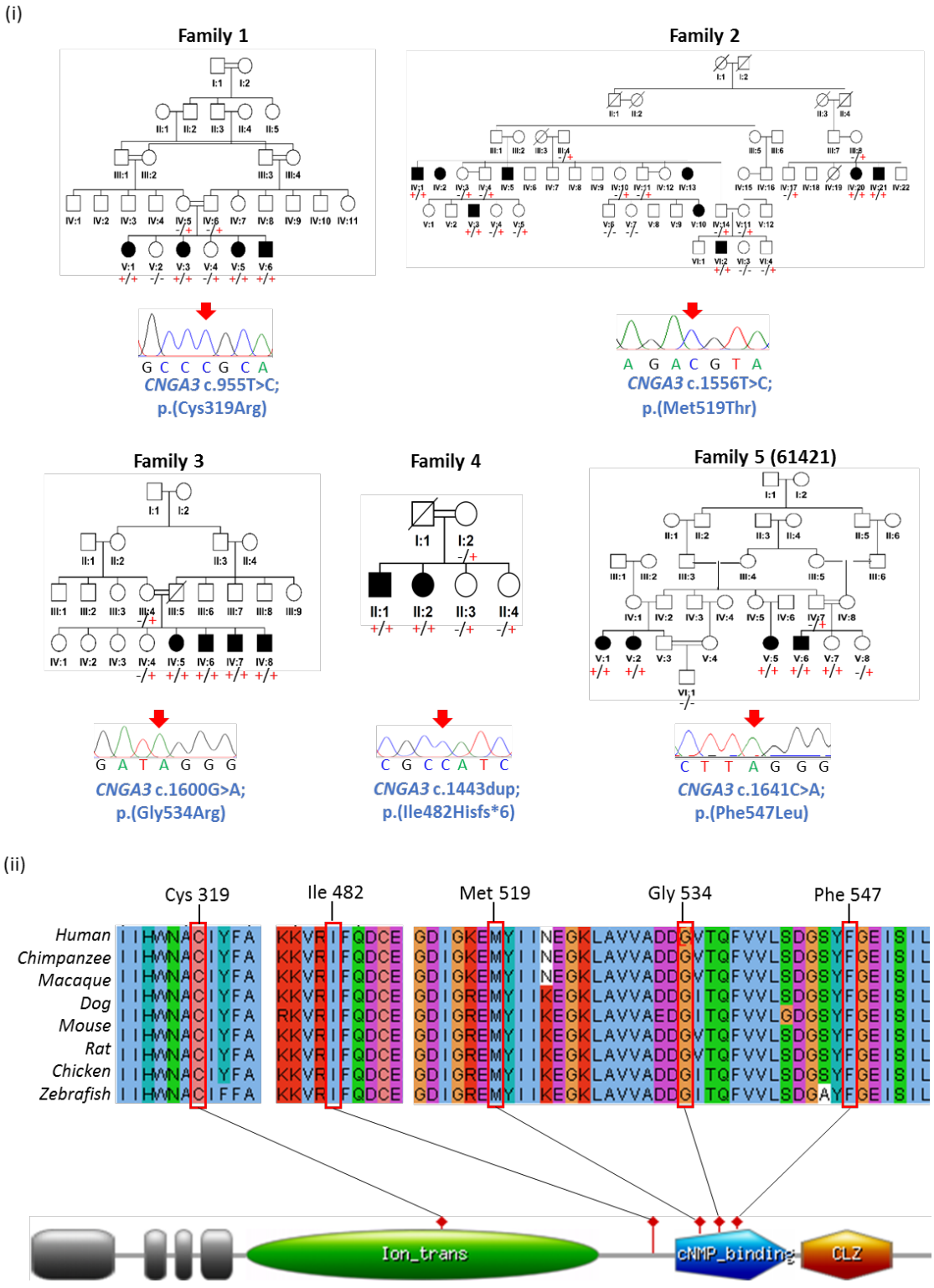

Figure 5.1 Families with CNGA3 alterations. ***(i)*** *Pedigrees and electropherograms for CNGA3 variants of families 1 to 5.* ***(ii)*** *Conservation in vertebrates of CNGA3 variants and protein domains to which they belong. Ion_trans= ion channel transmembrane domain; cNMP_binding= cyclic*

nucleotide-binding domain; CLZ= C-terminal leucine zipper domain of cyclic nucleotide-gated channels.

5.2.2 Sequence alterations in TULP1 and PDE6C identified in three families with RP

Family 6 (Fig. 5.2 (i)) was diagnosed with RP and originated from Lahore, Punjab; family members belonged to the Mughal tribe. Exome sequencing identified the homozygous duplication *TULP1* c.855dupC; p.(Val286Argfs*98), as the likely cause of the disease. This variant was absent in gnomAD and reported in a single individual of unknown origin in heterozygous state [312].

Family 7 (Fig. 5.2 (i)) was initially diagnosed with RP. The five affected individuals showed decreased vision with progressive deterioration, night blindness, photophobia, nystagmus. Fundus examination identified pigmentary retinopathy, optic disc pallor and attenuated vessels (Fig. 4.2 (ii), individual III:4). Individual III:2 also showed symptoms of bilateral maculopathy. This family originated from the Kohat district, KPK. Exome sequencing identified two possible pathogenic variants in *TULP1* c.238C>T, p.(Gln80Lys), and *PDE6C* c.480delG, p.(Asn161Thrfs*33). Two of the affected individuals (III:1 and III:3) were homozygous for both the variants, while III:4, III:5 were homozygous for the *TULP1* variant and heterozygous for the *PDE6C* variant. Individual III:2 was instead homozygous for *PDE6C* variant, and heterozygous for the *TULP1* variant. Therefore, in this family two potentially causative variants causing RP and CD were identified. None of these variants have been previously reported and were absent in gnomAD. Unfortunately, due to the lack of clinical

information, a definitive diagnosis of each affected member of the family was not possible to reach.

Family 8 (61401) (Fig. 5.2 (i)) comprised an extended family with four affected individuals. No clinical information were available however exome sequencing identified a novel homozygous variant *PDE6C* c.1A>G; p.(Met1*). This variant has a MAF of 0.00006479 in gnomAD, and no homozygous individual were present in the database.

Conservation (Fig. 5.2 (iii)) of *TULP1* showed conservation of Gln80 only amongst humans and monkeys, while *TULP1* Val286, *PDE6C* Met1, and Asn161 were conserved from humans to chicken. Both *TULP1* variants lied in the protein domains outside the coiled coil regions or Tub domains.

Interestingly, prior to this study, alterations in *PDE6C* have never been reported in Pakistan.

(i)

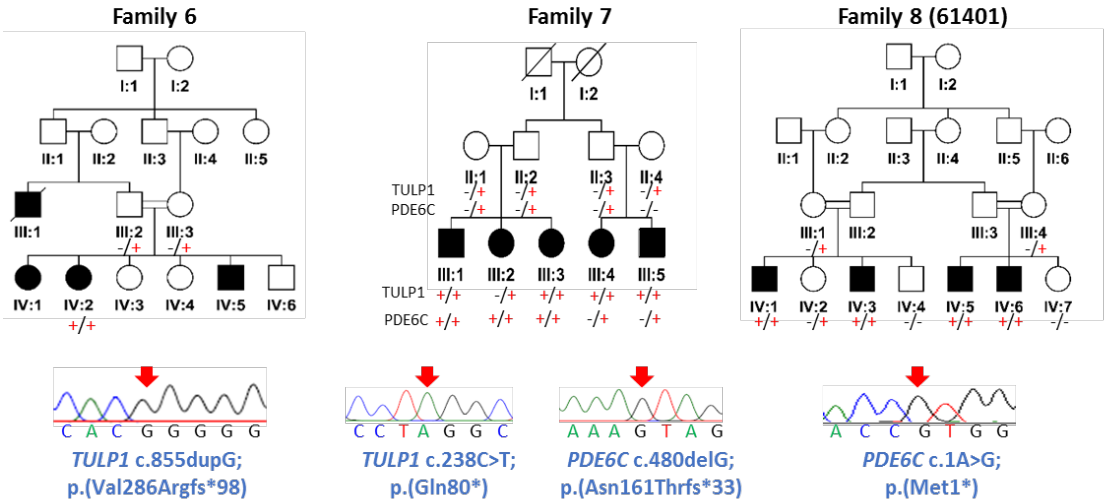
Family 6
Family 7
Family 8 (61401)
TULP1
PDE6C
C A C G G G G G
C C T A G G C
A A A G T A G
A C C G T G G
TULP1 c.855dupG; p.(Val286Argfs*98)
TULP1 c.238C>T; p.(Gln80*)
PDE6C c.480delG; p.(Asn161Thrfs*33)
PDE6C c.1A>G; p.(Met1*)

(ii)

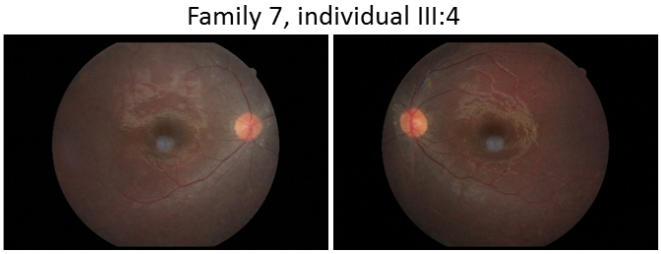
Family 7, individual III:4

(iii)

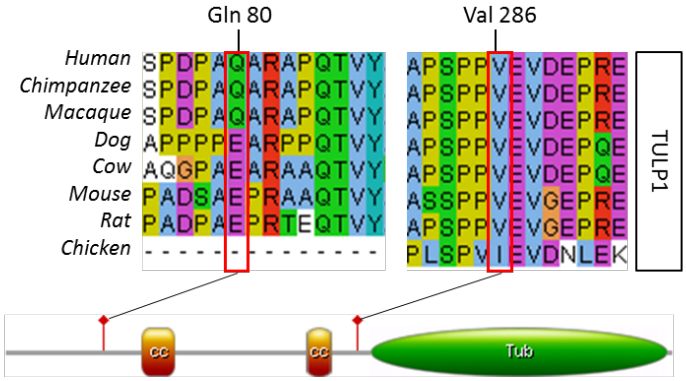
Gln 80
Val 286
Human
Chimpanzee
Macaque
Dog
Cow
Mouse
Rat
Chicken
TULP1
cc
cc
Tub

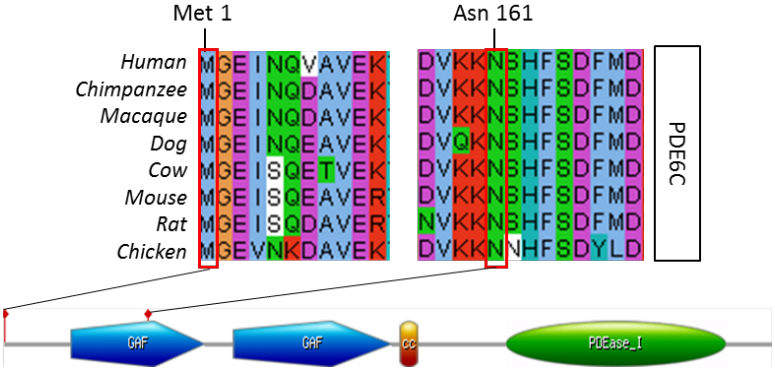
Met 1
Asn 161
Human
Chimpanzee
Macaque
Dog
Cow
Mouse
Rat
Chicken
PDE6C
GAF
GAF
cc
PDEase_I

Figure 5.2 TULP1 and PDE6C co-segregation analysis. (i) *Pedigrees of families 6, 7 and 8 and co-segregation of TULP1 and PDE6C.* ***(ii)*** *Fundus examination of individual III:4 of family 7, homozygous for the TULP1 p.(Gln80*) and heterozygous for PDE6C p.(Asn161Thrfs*33), showed attenuation of retinal vessels and optic disc pallor.* ***(iii)*** *Conservation analysis of the TULP1 and PDE6C variants. While TULP1 Val286, PDE6C Met1 and Asn161 were conserved amongst all the species examined, TULP1 Gln80 was conserved only amongst higher mammals. TULP1 has two coiled coil domains (cc), and a Tub domain. PDE6C has two GAF domains (cGMP-specific phosphodiesterases, adenylyl cyclases and FhlA), a cc domain and a PDEase I domain.*

5.2.3 RPGRIP1 sequence alterations in two families

Family 9 (Fig. 5.3 (i)) belonged to the Syed, Pashtoon tribe, and originated from Pishin, Baluchistan. Two affected individuals were diagnosed with nystagmus, visual impairment, and strabismus. Illumina Trusight One clinical exome sequencing panel identified a homozygous duplication *RPGRIP1* c.2789dup; p.(Pro931Thrfs*3), which has not been reported previously and is absent in gnomAD. This finding enabled a more precise diagnosis of the condition in this family, as affected by IRD.

Similarly, affected individuals of Family 10 (61007) (Fig. 5.3 (i)) were found to be homozygous for a previously unreported *RPGRIP1* variant c.2710G>A, p.(Gly904Ser).

Conservation (Fig. 5.3 (ii)) of the residues impacted by these alterations showed that the Gly904 was conserved from human to xenopus, while the Pro931 was

conserved only amongst higher mammals. *RPGRP1* protein has three coiled coils domains, two C2 domains, and a C-termini domain; the two gene variants we found to impact residues in proximity of the C2 domain.

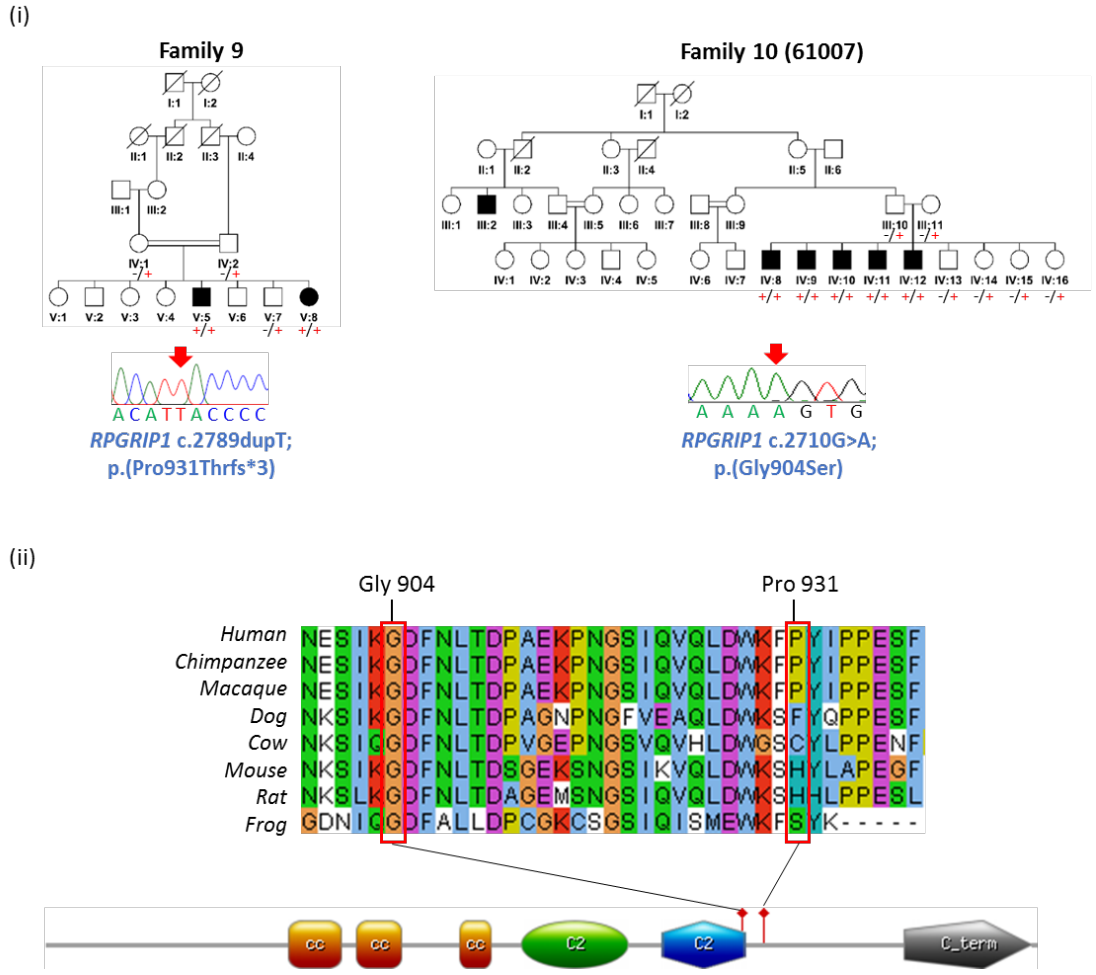

Figure 5.3 RPGRIP1 variants in Family 9 and 10. (i) *Pedigrees and electropherograms of family 9 having a the variant RPGRIP1 c.2789dupT; p.(Pro931Thrfs*3), while family 10 carried the variant c.2710G>A, p.(Gly904Ser).* ***(ii)*** *Conservation showed that Gly904 was a stringently conserved amino acid which resides in the C2 domain of the protein, while Pro931 is less stringently conserved and lies between the C2 and C-termini domain.*

5.2.4 Sequence alterations in other genes

Family 11 (Fig. 5.4) was initially diagnosed with oculocutaneous albinism, displaying signs of photosensitivity, visual impairment, nystagmus and light skin and hair. This family originated in KPK and belonged to the Paktoon tribe. Illumina Trusight One clinical exome sequencing panel identified a *ABCA4* c.3364G>A; p.(Glu1122Lys) variant, which has a MAF of 0.00006533 in the South Asian population. This variant has never been reported in the Pakistani population however, it has been reported in Europeans including British [313, 315, 327] and Han Chinese [56] populations, where it is known to be associated with Stargardt disease.

Family 12 (Fig. 5.4) originated from Quetta, Balochistan and belonged to the Tajik, Afghan tribe. The two affected members were firstly diagnosed with nystagmus however, visual impairment, nystagmus, and strabismus were also associated with polydactyly, intellectual disability, obesity, myopia and RP, all classical symptoms of Bardet-Biedl syndrome. Illumina Trusight One clinical exome sequencing panel identified a novel homozygous splice site missense variant c.221-1G>A in *BBS4* gene, which was absent from gnomAD. In Pakistan only one other *BBS4* variant has been reported (*BBS4* c.1463C>A; p.(Thr488Lys)), as affecting two siblings [328].

Family 13 (Fig. 5.4) belonged to the Dogar caste and originated from Borewala, Punjab. The three affected individuals were diagnosed with arRP and exome sequencing confirmed a novel homozygous deletion in *CRB1* c.3735delA; p.(Gly1246Glufs*36). *CRB1* variants have been associated with both arRP and arLCA in the Pakistani population previously.

Family 14 (Fig. 5.4) was diagnosed with congenital cataract and originated from KPK. Illumina Trusight One clinical exome sequencing panel identified a homozygous variant in *GUCY2D* c.3056A>C, p.(His1019Pro). The variant has been previously reported as pathogenic in two other Pakistani families affected by LCA [314] but not in other populations, and it had a MAF of 0.00003347 in the South Asian population.

Family 15 (Fig. 5.4) originated from Lahore, Punjab, with individuals diagnosed with RP. Exome sequencing identified the homozygous novel splice variant *TTC8* c.768 +5G>A, which was also absent from gnomAD, as the likely cause of disease. Alterations in *TTC8* have been associated with BBS and RP in the Pakistani population.

Family 16 (Fig. 5.5) was diagnosed with nystagmus and visual impairment, and originated from Mastung, in the Baluchistan province. This family belonged to the Ababki, Bravi caste. Illumina Trusight One clinical exome sequencing panel identified a novel missense variant in the gene *CACNA1F* c.2254G>A; p.(Val752Met). This variant was not present in gnomAD, and alterations in this gene have never been reported in the Pakistani population. This gene encodes for the voltage-dependent L-type calcium channel subunit alpha-1F, alterations are known to cause either fundus albipuntatus or cone-rod dystrophy however, lack of clinical information about this family did not allow us to provide a final diagnosis.

Family 17 (Fig. 5.5) has 3 affected individuals, 2 children and the mother. The family originated from the Karak district, in the KPK province, and was diagnosed with Usher syndrome. Audiogram performed to affected members showed hearing loss, and fundus examination showed pigmentary retinopathy,

optic disc pallor, attenuated retinal vessels, maculopathy, cataract, epiretinal membrane. Illumina Trusight One clinical exome sequencing panel identified the missense variant *USH2A* c.7334C>T; p.(Ser2445Phe), which has been ascertained in an individual of unknown origins in a compound heterozygous state [315] and present in gnomAD with a MAF of 0.006435. gnomAD also reported the presence of two homozygous individuals present in their cohort. Genetic analysis on this family confirmed the initial diagnosis of Usher syndrome.

Family 18 (Fig. 5.5) originated from Raiwind in Punjab and belonged to the Chohan caste. This family was diagnosed with RP, confirmed with exome sequencing which identified a novel deletion of 48 bp in the beta subunit of the cyclic nucleotide-gated channel *CNGB1* c.852_874+25del which resulted in the frameshift alteration p.(Ile286Aspfs*9). This has been associated only with RP, confirming the initial diagnosis for the affected individuals we examined.

Family 19 (Fig. 5.5) was an extended family which was diagnosed with RP, affected members showed signs of strabismus and visual impairment. WES identified a novel missense variant in the Lecithin retinol acyltransferase gene *LRAT* c.196G>C; p.(Gly66Arg) which confirmed the initial diagnosis. This family originated from Rawalpindi, Punjab.

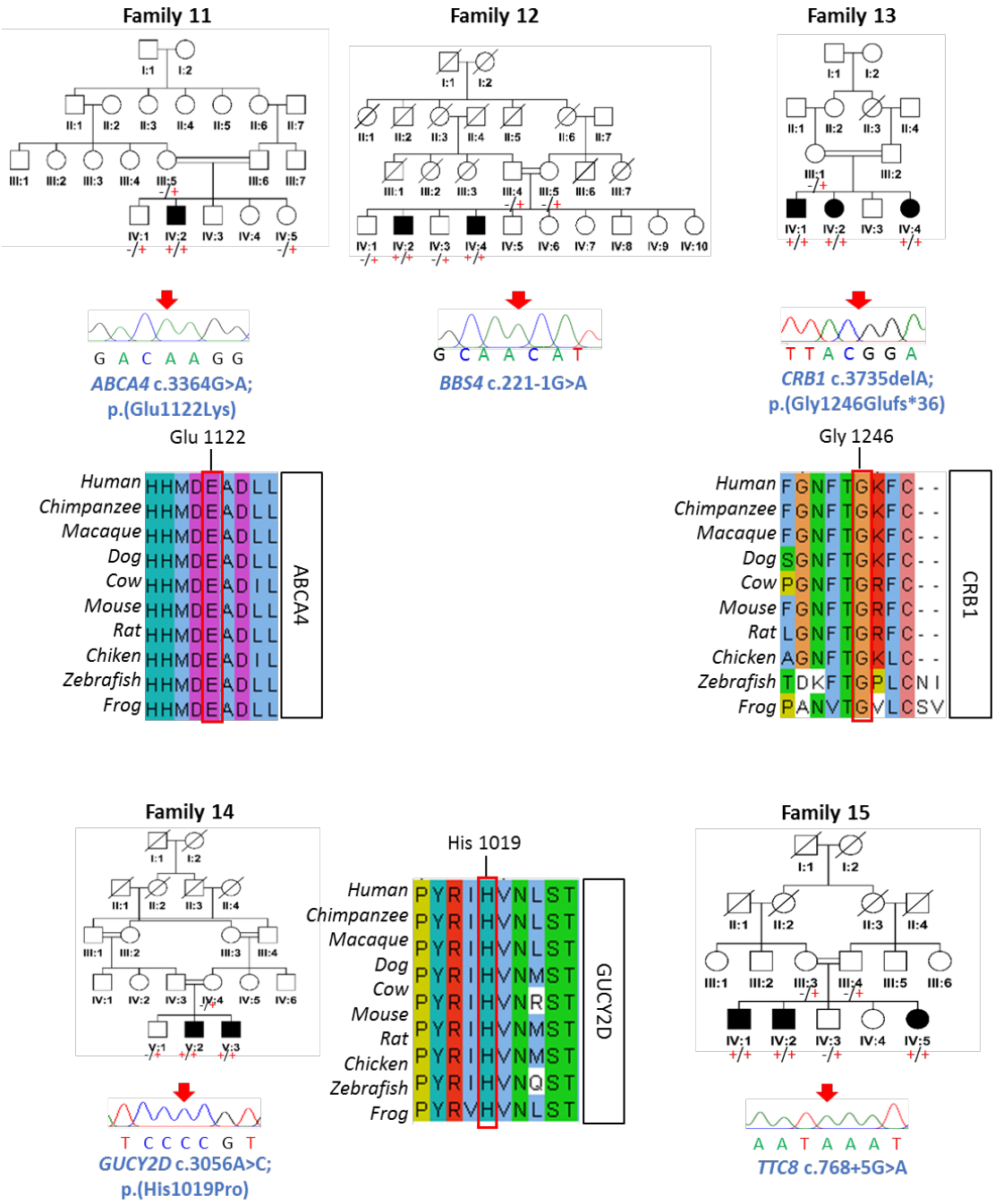

Figure 5.4 Pedigrees and electropherograms of families 11 to 15 and sequence alignments.

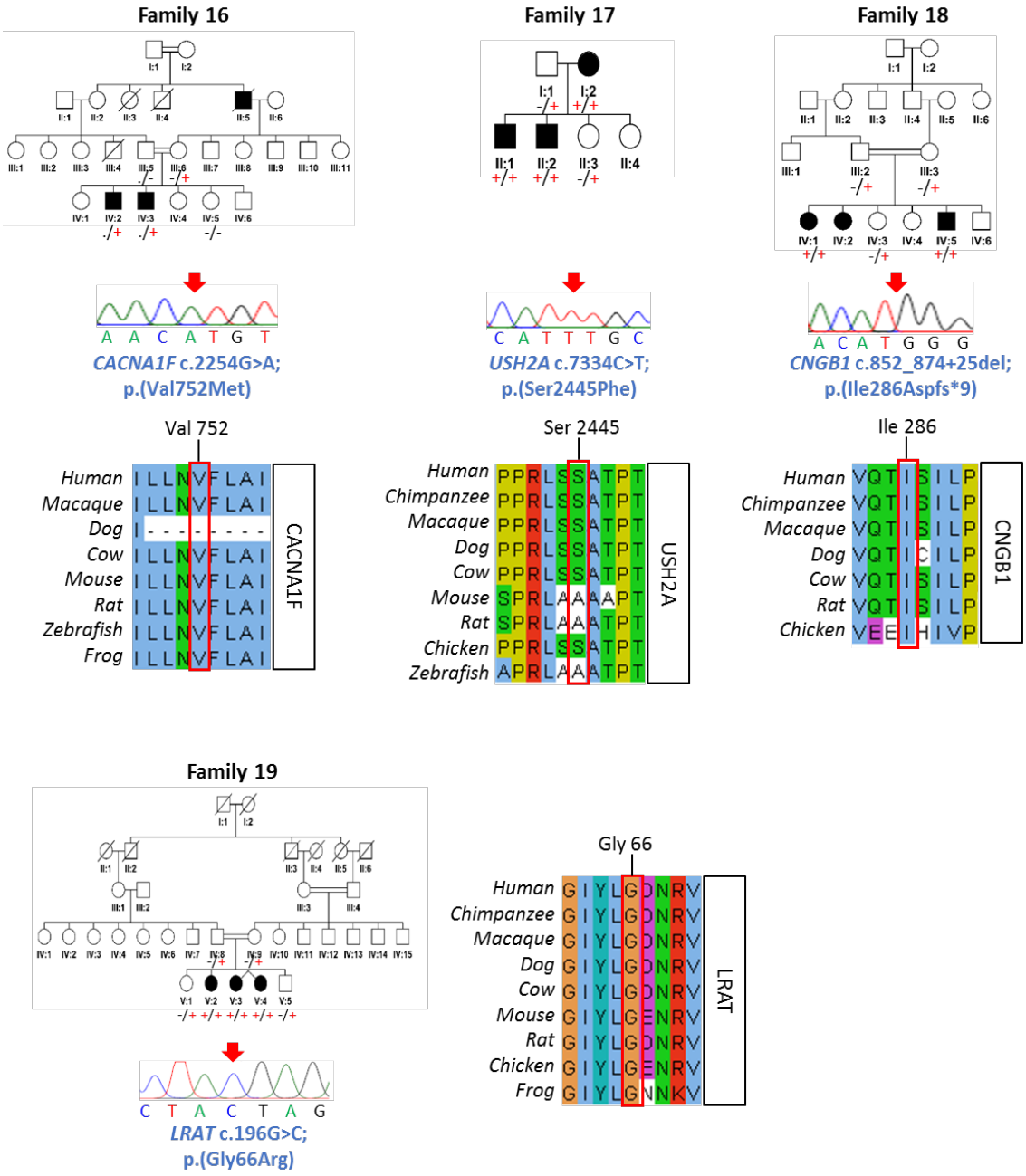

Figure 5.5 Pedigrees and electropherograms of families 16 to 19 and sequence alignments.

5.2.5 Sequence alterations identified in the NEI samples cohort

Family 20 (Fig. 5.6) had five members affected by IRD. Genotyping showed that in this families two variants in different genes segregated in the affected members, *CLCC1* c.75C>A; p.(Arg25Glu) and *CDH23* c.1595C>T; p.(Thr532Met). Affected individuals were either homozygous for at least one of these variants. *CLCC1* has been identified by our group as a founder alteration causing RP in the Pakistani population [316], while the *CDH23* variant has been identified in people of unknown ethnic origins [317, 318]. *CLCC1* c.75C>A has a MAF in the South Asian population of 0.0003924, while *CDH23* c.1595C>T was absent from the database.

In Family 21 (Fig. 5.6) affected individuals were homozygous for a *LCA5* c.1550_1551delGA; p.(Arg517Ilefs*3) variant. This variant has never been reported and only other three variants have been reported in the Pakistani population (see Appendix D).Investigations in family 22 (Fig. 5.6) showed the previously described splice variant *RPGR* c.310+1G>C, which was absent from gnomAD, but has been reported in a family in the USA [320] and in a family of unknown ethnic origins [319]. The three affected members of family 23 (Fig. 5.6) segregated with the variant *PDE6B* c.12_15delAGTG; p.(Ser4Argfs*23), this variant has already been reported in a Pakistani family as causative of RP [321].

Family 24 (Fig. 5.7) was homozygous for the novel homozygous variant *RDH5* c.838C>G; p.(Arg280Gly). Another four disease-causing variants for this gene have been reported exclusively in Pakistan. In Family 25 (Fig. 5.7), a homozygous *MERTK* variant c.2194C>T; p.(Arg732*) was identified as the likely cause, this variant has been already reported as disease causing in a family of unknown origin [322], and only another variant, *MERTK* c.718G>T,

p.(Glu240*) has been reported in two families in Pakistan [169, 329]. Affected members of family 26 (Fig. 5.7) were found to be homozygous for an *OAT* c.722C>T; p.(Pro241Leu) variant, which has been reported in German/Italian individuals [323];however, the *OAT* c.722C>T variant is the first to be identified in a Pakistani family. The *OAT* locus has been previously mapped in another Pakistani family [169]. In family 27 (Fig. 5.7), a *ARL6* variant c.534A>G; p.(Gln178Gln), previously reported in another Pakistani family with BBS [330], but not reported in other populations. Two other variants in the same gene have been reported in Pakistan, the c.281T>C [331] and c.123+1118del53985 [332].

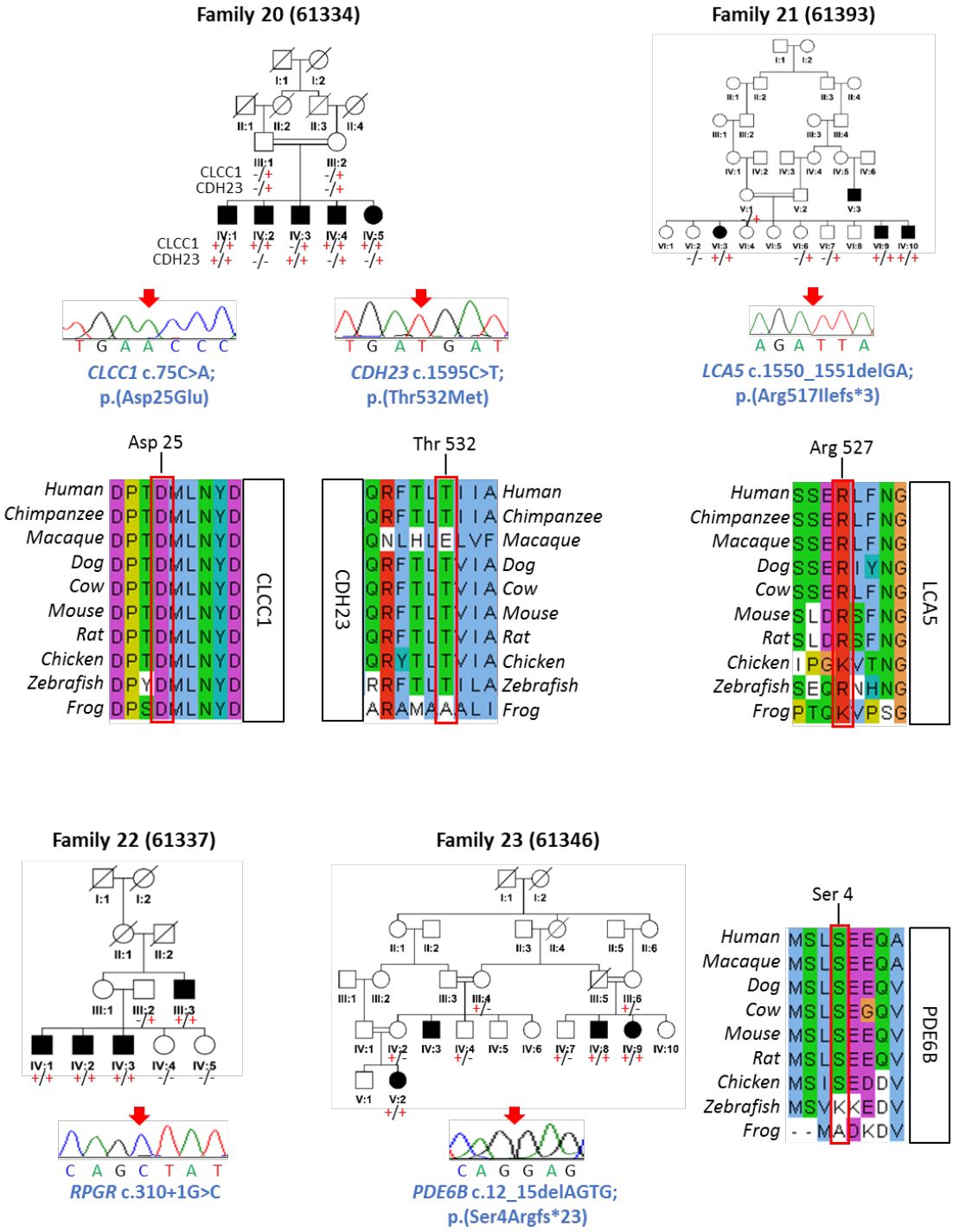

Figure 5.6 Pedigrees and sequence chromatograms of families 20 to 23.

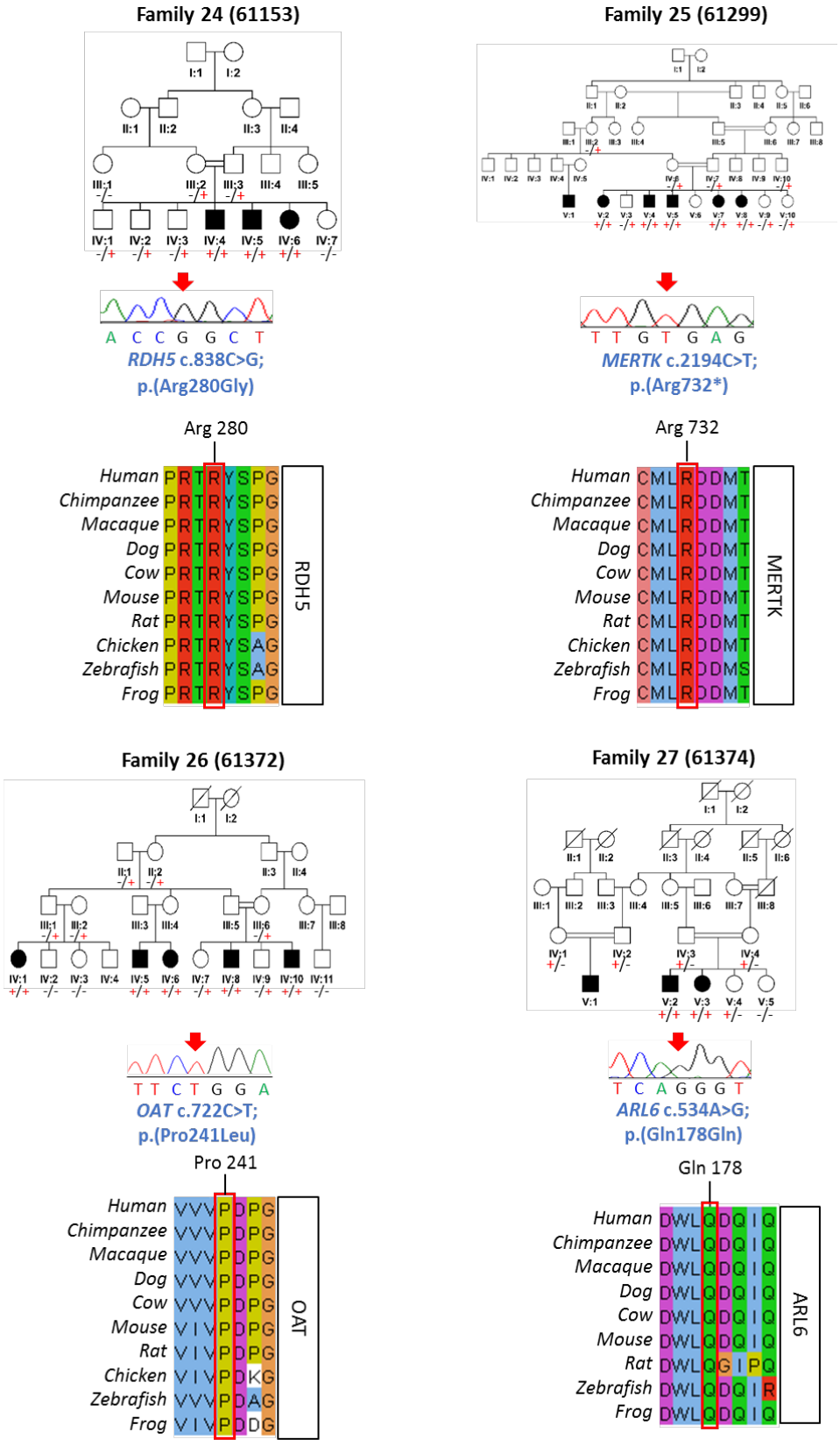

Figure 5.7 Pedigrees and sequence chromatograms of families 24 to 27.

5.2.6 Literature review of IRD causes in Pakistan

An overview of all genetic causes of IRD in Pakistan was undertaken to provide a more completed understanding of the causes of IRD in Pakistan. PubMed (https://www.ncbi.nlm.nih.gov/pubmed/) and Google Scholar (https://scholar.google.co.uk/) were used as platforms to search for publications. We explored the specific nucleotide and protein variants, phenotypes reported, the region in Pakistan where the affected families originate, the number of families and individuals affected by the alteration, the presence of the alteration in other ethnicities, and levels of confidence of causality according to the sub-categorisation within NCBI ClinVar (https://www.ncbi.nlm.nih.gov/clinvar/). Where the author has indicated that there may be some degree of doubt, or subsequent evidence has come to light in the literature, calling the deleterious nature of the variant into question [333], this was also noted. We identified a total of 519 families with candidate genetic variants in 118 genes or loci, creating the most comprehensive database on inherited retinal disorders population-specific (see Appendix D).

Alterations in *ABCA4* gene have been reported in 6 families (9 individuals) as causative of Stargardt disease, and in 2 families (7 individuals) as causative of IRD. Interestingly, the common pathogenic variant *ABCA4* c.5882G>A, widely reported in many ethnicities, has only been reported in two Pakistani families.

Bardet-Biedl syndrome has an estimated frequency of 1:100.000 in non-consanguineous populations however, the frequency may vary depending on the population analysed. We found that in literature 34 variants described in BBS genes (*ARL6, BBS1, BBS2, BBS4, BBS5, BBS7, BBS9, BBS10, BBS12, CEP19, CEP164, MKKS, TTC8, WDR60*) in the Pakistani population, affecting 44 families and a total of 97 individuals. Amongst the gene of which variants

have been associated with disease, variants in *BBS10* were the highest in number in Pakistani population, accounting for the 17% of them (Fig. 5.8 (i)) and affecting eight families. Alterations in genes *TRIM32, MKS1, WDPCP, SDCCAG8, LZTFL1, BBIP1,* and *IFT27* known to be associated with BBS, were not reported in the Pakistani population.

From this data, Usher syndrome seems to be the most prevalent syndromic retinal disorder in Pakistan as literature review identified 66 families (162 individuals) with the condition. Forty-nine variants were causative of the disease in this population, the most mutated genes being *MYO7A* (23 variants, 50% of total variants) and *CDH23* (15 variants, 33% of total variants) (Fig. 5.8 (ii)).

Other rare syndromic IRDs were found in the Pakistani population. Joubert syndrome (JBTS), is characterised by ocular features associated with developmental delay, hypoplasia of the cerebellar vermis, renal abnormalities and dysregulation of breathing pattern. Out of more than 30 genes associated with JBTS worldwide, six of them (*AHI1, ARL3, ARL13B, CC2D2A, CEP290, TCNT2*) have been reported as causing the disease in Pakistan. Meckel syndrome (MKS) is typically associated with kidney cysts, occipital encephalocele, polydactyly, and eye features. Six genes have been associated with this disease in the Pakistani population; *TMEM67* was the most common mutated with eight variants associated with this disease, three were present in Mirpur, in the Azad Kashmir province.

(i)

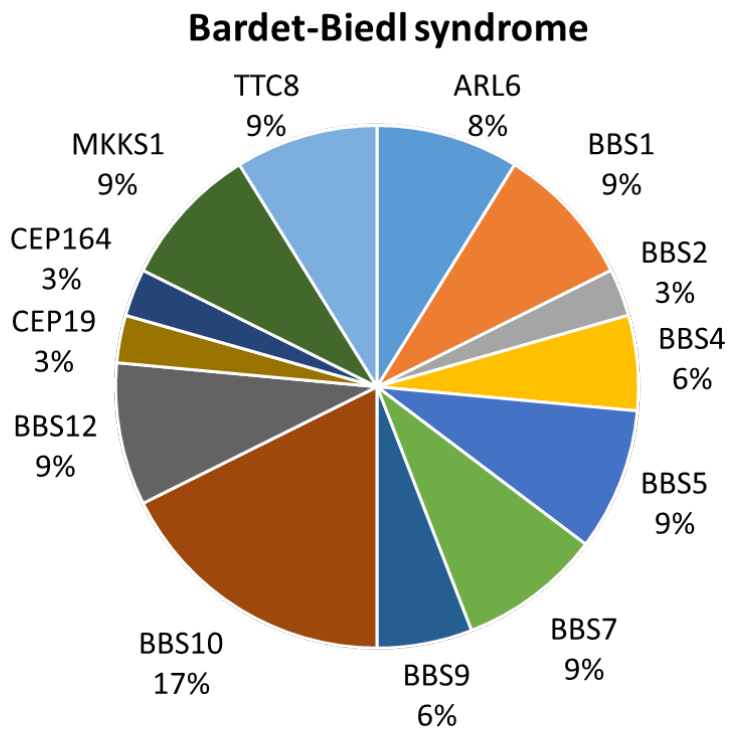

(ii)

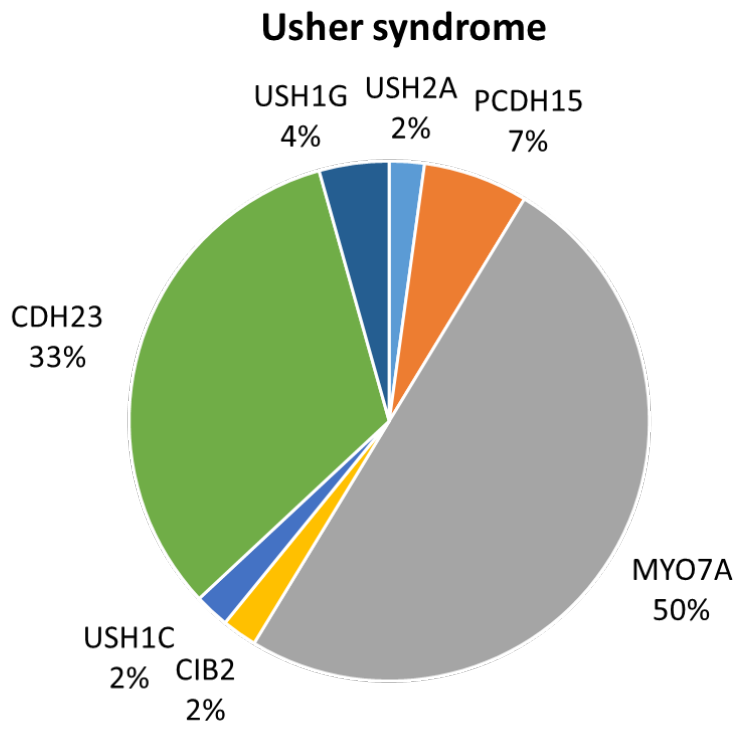

Fig 5.8 Proportion of variants associated with BBS and Usher syndrome in Pakistan.

Autosomal recessive RP was the most common non-syndromic retinal disorder in the Pakistani community, with *RP1* variants and *CRB1* variants making up the 16% and 15% of the total disease-associated variants present in the population (Fig. 5.9). *RP1* variants were identified in 14 families, with 6 of them originating from Punjab, while *CRB1* variants were described in 13 families with no clear clustering in any specific region due to a lack of information reported in literature. Amongst the most common variants causing arRP in Pakistan, *TULP1* c.1466A>G has been found in 15 families from Punjab, indicating that the variant was a founder alteration effect of that particular region. Similarly, the *CLCC1* c.75C>A variant was identified in 9 families from Punjab, and represents a founder alteration which arose in that region.

Regionalisation of disease-causing variants affecting high number of families was particularly observable for LCA where the variants *RPE65* c.1087C>A was found in 10 families from Punjab, *AIPL1* c.834G>A, p.(Trp278*), and 11 families in Northern Pakistan. The *LCA5* c.1151delC variant was found in six families from both Northern Pakistan and Punjab. While these variants represent just a single founder event occurred in a community, seven different alterations have been reported for the gene *RPGRIP1*, which constitutes the 25% of the variants causing dieses and the most commonly mutated in the Pakistani population (Fig 5.9 (ii)).

Northern Pakistan has also been flagged as hot spot for Alström syndrome (MIM 203800), characterised by progressive cone-rod dystrophy, sensorineural hearing loss, obesity, type 2 diabetes, dilated cardiomyopathy, renal failure and pulmonary, hepatic, and urological dysfunctions. We found seven variants reported as associated with this disease in Pakistan, five of them present in the Northern Pakistani population.

Not surprisingly, autosomal dominant IRDs have been reported only in for three variants harbouring in the same gene, *SEMA4A*. The variants c.1033G>C and c.1049T>G have been reported as causing adCRD, and the c.2138G>A variant reported as associated with adRP. All of them have been described in four families each however, no geographical localisation was reported. Such a low number of variants-causing dominant diseases was probably due by endogamy practises, making recessive disorders more common.

Non-progressive forms of retinal degeneration such as congenital stationary night blindness (CSNB), mainly rod-associated, has been found associated with *GNAT1, GRM6* and *SLC24A1* gene variants in a total of four families, while the cone-associated non-progressive achromatopsia (ACHM) has been found segregating in ten familes, with alterations in genes *ATF6, CNGA3, CNGB3,* and *PDE6H*.

(i)

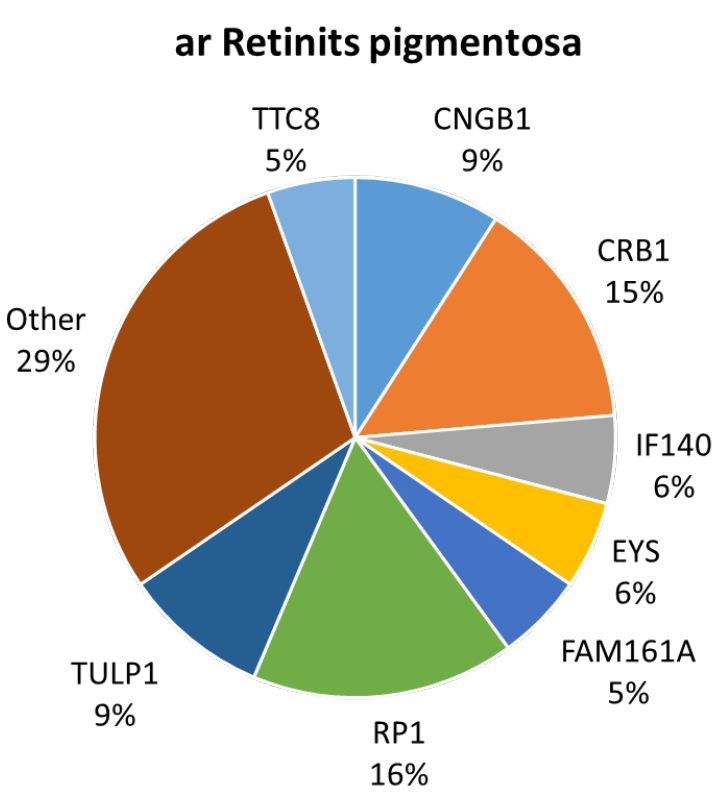

(ii)

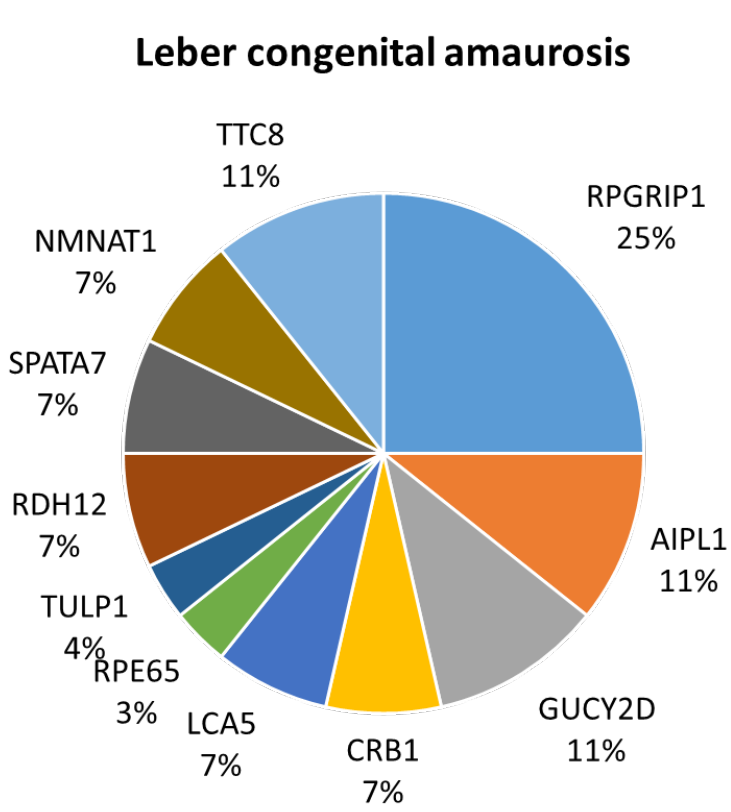

Figure 5.9 Percentage of variants per gene associated with AR retinitis pigmentosa and Leber congenital amaurosis.

5.3 Discussion

Our study entails the genetic analyses of 27 families of Pakistani descent, identifying a total of 29 likely disease-associated variants in 22 genes responsible for a range of IRDs in Pakistani communities. A previous study of 144 families identified *RPE65*, *TULP1*, *RP1*, *PDE6A*, *USH2A* and *RDH5* as the most common genes associated with autosomal recessive RP in Pakistan [169]. Our genetic studies, together with a comprehensive literature review, highlight other important genes commonly contributing to IRD in Pakistani communities, including *ABCA4*, *AIPL1*, *CDH23*, *CNGA3*, *CRB1*, *RPGRIP1* and *TMEM67*. Our findings also include the first report of *CACNA1F* and *PDE6C* variants as a cause of IRD in Pakistani families, as well as known disease-associated variants described for the first time in Pakistani families including *CNGA3* p.(Met519Thr), p.(Phe547Leu) and p.(Ile482Hisfs*6), *TULP1* p.(Val286Argfs*98), *ABCA4* p.(Glu1122Lys), *USH2A* p.(Ser2445Phe), *MERTK* p.(Arg732*), *RPGR* c.310+1G>C, *CDH23* p.(Thr532Met), and *OAT* p.(Pro241Leu), and 14 other novel variants in established disease genes.

Studies of IRD in Pakistan have mainly focused on families from the Punjab region, in which our literature review highlights *CNGA3* and *PDE6A* variants as a common cause of IRD in this region. Additionally, our findings also highlight *TMEM67* variants as a common cause of IRD in communities of the Kashmir region. As has been demonstrated for the *CLCC1* gene variant [316] many common gene variants likely stem from a single gene alteration event that occurred in a founder ancestor individual, which was transmitted to subsequent generations and accumulated to an increased frequency in particular communities and regions. This includes *AIPL1* p.(Trp278*) identified in 11 families from Northern Pakistan, and *RPE65* p.(Pro363Thr) in 10 families,

TULP1 p.(Lys489Arg) in 15 families, and *CLCC1* p.(Asp25Glu) in 9 families, all from Punjab. As such founder alterations often represent important causes of disease in a particular region, and knowledge of their presence and clinical outcomes is of importance when designing community-appropriate genetic testing and counselling protocols.

Further to regional founder alterations, recurrent ('hot spot') gene alterations also represent an important cause of disease globally. While a large spectrum of *ABCA4* sequence variants have been previously described in Stargardt disease, including founder variants associated with individuals of German [334], Spanish [335], Danish [336], Mexican [337], African-American [338] and South Asian descent [170]. Stargardt disease variants are generally found distributed throughout the *ABCA4* gene [339], although recurrent gene mutations have been described in populations of different ethnicities and geographical location [170]. The *ABCA4* p.(Glu1122Lys) variant identified in our study, for example, is well described and has been identified in compound heterozygous form in affected individuals from diverse ethnicities including European and Han Chinese [12, 13], likely indicating that it represents such a recurrent gene alteration. As with ancestral founder alterations, knowledge of recurrent gene alterations is of great utility in the development of disease-specific genetic testing strategies. Our studies also provide improved knowledge of the relative frequencies of other causes of IRD in Pakistan. *ARL6* and *TTC8* gene variants are an uncommon cause of Bardet-Biedl syndrome globally, accounting for 0.4% and 1% of all Bardet-Biedl syndrome cases respectively [340], whilst *LRAT* variants are an uncommon cause of Leber congenital amaurosis, estimated to account for only 1% of all cases [341]. However, our studies significantly expand knowledge of the molecular spectrum of disease-

associated variants in these genes and identifies them as being more commonly represented in the Pakistani population, with 4/20 (20%), 5/19 (26%) and 5/26 (19%) of all reported IRD-associated disease-causing variants in *ARL6*, *TTC8* and *LRAT* respectively identified in Pakistani families (Appendix D).

In geographically and culturally isolated communities such as those which may occur in Pakistan, an enrichment of disease-associated alleles may increase the probability of two distinct autosomal recessive causes of disease manifesting within the same family [171]. This is supported by the findings in our study, in which two of the 27 of families investigated (families 7 and 20) were found to segregate likely pathogenic genetic variants in two distinct genetic causes of IRD. In family 7, all affected individuals presented with progressive deterioration of visual acuity and were initially diagnosed with RP. There was however some variability noted in the clinical phenotype, with nyctalopia and typical fundus findings of RP being the main clinical features in individuals III:1, III:3, III:4 and III:5, whilst individual III:2 instead described severe photophobia with predominantly macular involvement on ophthalmic examination. Our genetic studies subsequently confirmed the segregation of two separate novel predicted loss of function variants in two established IRD genes; *TULP1* p.(Gln80*) and *PDE6C* p.(Asn161Thrfs*33) within this family, likely accounting for the phenotypic variability seen in affected individuals. Interesting, the two individuals who were homozygous for both *TULP1* and *PDE6C* variants (III:1 and III:3) did not appear to be more severely affected compared to individuals III:4 and III:5 who were homozygous for only the *TULP1* variant. Additionally, our studies identified two separate variants as segregating with disease in family 20; *CLCC1* p.(Asp25Glu) and *CDH23* p.(Thr532Met). *CLCC1* has only

recently been described in association with RP [316], and is likely to represent a founder alteration in the Punjab region in Pakistan (Appendix D). The same *CDH23* p.(Thr532Met) variant has been reported in only a single individual with Usher syndrome [317] and another individual with non-syndromic hearing loss [318], both in compound heterozygous form. However, as two homozygous individuals for this variant are present in the South Asian population in gnomAD, the clinical significance of this variant therefore remains unclear. The presence of >1 disease-associated variant in a family may give rise to atypical inheritance patterns or phenotypical outcomes, complicating clinical interpretation and patient counselling and management. This intra-familial locus heterogeneity is particularly relevant within isolated communities such as those which may occur in Pakistan, and has been demonstrated to occur in up to 15% of a cohort of Pakistani families with presumed autosomal recessive hearing loss [342]. Our findings underscore the value of knowledge of the specific molecular causes(s) of disease in each family, and highlights the importance of considering the possibility of multiple molecular diagnoses within the same family. These genomic evaluations also aided a revised and more precise clinical (and specific molecular) diagnosis to be provided for many other families in this study. This work also emphasises the considerable diagnostic difficulties encountered by clinicians in certain regions of Pakistan, in which access to specialised equipment for detailed and accurate ocular phenotyping may be limited.

Further benefits of genetic studies to aid diagnosis are provided by studies of family 18 in which an apparently autosomal dominant form of RP was segregating in an affected parent (III:3) and offspring (IV:1, IV:2 and IV:5). However, exome sequencing of parental individual III:3 failed to identify any

candidate heterozygous variants in known dominant IRD genes, although it did identify a heterozygous likely loss of function variant in *CNGB1* c.852_874+25del, p.(Ile286Aspfs*9), a gene known to be associated with autosomal recessive IRD; indeed, segregation analysis subsequently confirmed this variant as the likely cause of the disease in homozygous form in the offspring of this family. Subsequent ophthalmic examinations in the family confirmed the clinical diagnosis of RP in homozygous offspring and on re-evaluation the parental carrier (III:3) was found to have mature cataracts accounting for her decreased visual acuity, with no signs of RP noted. Our genomic evaluations also aided a revised and more precise clinical (and specific molecular) diagnosis to be provided for many other families in this study.

This study also provides further insights into the likely pathogenicity of a second gene variant in *USH2A* [c.7334C>T, p.(Ser2445Phe)], identified in family 17. Disease-causing variants in *USH2A* are the most common cause of Usher syndrome, accounting for 29% of all cases globally, and are also one of the most common causes of nonsyndromic autosomal recessive RP, accounting for 19–23% of all cases [16]. The *USH2A* variant [(c.7334C>T, p.(Ser2445Phe)] is predicted to be deleterious by *in silico* pathogenicity tools (SIFT, Polyphen and Provean) and was first reported by Carss KJ et al. [12] in a compound heterozygous form in a single individual with RP. However as with the *CDH23* variant discussed above, the clinical significance of this variant remains unclear due to the high allele frequency of the variant in genome databases (MAF of 0.006435 with 193 heterozygote carriers out of 15,308 individuals) including the presence of two homozygous individuals in the South Asian population (gnomAD v2.1.1). While this high allele frequency seems incompatible with

pathogenicity, our finding of the *USH2A* p.(Ser2445Phe) variant segregating with disease in five genotyped individuals in family 17 (including three affected individuals and two unaffected siblings) may indicate the variant has a role in disease perhaps in combination with other *USH2A* gene variants on the same founder haplotype, and/or other gene variants elsewhere in the genome. Further studies investigating the functional impact and potential pathogenic basis of this variant may be useful in clarifying any possible disease association.

Taken together our data highlight the value of using high-throughput genomic technologies to achieve an accurate molecular diagnosis, particularly where deep clinical phenotyping may be limited due to resource constraints, and a precise clinical diagnosis may be difficult to achieve. This has important implications for future therapeutic interventions, particularly given recent developments in the field of IRD, with Luxturna® (voretigene neparvovec), the first ever licensed gene replacement therapy for the treatment of a genetic disease in humans, approved for the treatment of patients with *RPE65*-associated retinal dystrophy [343]; there are also numerous other emerging therapies currently under development and in clinical trials [344]. We have compiled the most comprehensive and curated review of genes and variants associated with IRD in Pakistan, highlighting regional founder mutations, clarifying likely disease associations (including some previously reported variants that are now considered likely to be benign) and enabling an improved scientific and clinical understanding of the genomic architecture of IRD in Pakistan. This knowledge will facilitate the development of hierarchical strategies for rapid and cost-efficient genetic testing assays to enable an accurate disease diagnosis to be achieved more rapidly, thus aiding the

development of diagnostic and clinical care pathways and policies throughout Pakistan. Our findings, together with potential improvements in access to IRD therapies, will bring about direct clinical benefits for IRD patients in Pakistan, in the wider South Asian population, and worldwide.

CHAPTER 6

CONCLUDING COMMENTS

CHAPTER 6: CONCLUDING COMMENTS

The complexity of the origins of the Pakistani population, and specific cultural practices, have led to a higher risk of autosomal recessive inheritance of disease [166, 167]. The presence of numerous isolated rural communities, alongside limited freely available (and expensive private) healthcare provision and low literacy rate (http://uis.unesco.org/country/PK), provide significant healthcare limitations to many Pakistani communities.

Cataract and refractive errors entail the main causes of blindness and visual impairment in Pakistan, with a prevalence of 3.4% and 4.9% respectively [345-347]. Prevalence of inherited retinal diseases have not been reported, however a report on the Afghan refugee population in Hairpur and Ghazi in 1998 reported that the 12.5% of blindness in the Afghan refugee community was caused by retinal degeneration/dystrophy [348]. The field of ophthalmology often faces many challenges with the diagnosis of inherited eye disease. In particular, IRDs entail a highly heterogeneous group of diseases, in which variable phenotypic manifestation may occur within a family carrying the same pathogenic variant, and additionally distinct alterations in the same gene may give rise to different clinical outcomes. Such heterogeneity may lead to misdiagnosis of IRDs, particularly in poorly clinically-resourced countries such as Pakistan in which access to specialised equipment for detailed and accurate ocular phenotyping may be limited, representing a significant challenge.

The work detailed as part of this thesis involves genetic analyses in 27 families affected by a wide range of syndromic and non-syndromic IRDs. For some families, a definite diagnosis was not possible to reach, while for others genetic testing revealed that the initial diagnosis of cataract or nystagmus was incorrect,

enabling a new molecular diagnosis of (a specific) IRD to be provided. Moreover, in some other families the initial clinical diagnosis was instead confirmed by our molecular diagnosis. Using WES, new variants known genes associated with IRDs, as well as new variants in known genes never found in the Pakistan were reported, expanding knowledge of genetic ocular disease in the Pakistani population.

Alongside this, a literature review on IRD in Pakistani population was performed to build a community-relevant database of gene variants associated with IRDs. This was used to better define the extent of IRDs in Pakistan and which gene variants are the most common, their association with specific retinal dystrophy as well their regional prevalence. This work enabled the identification of regional founder mutations in IRD associated disease genes including: *AIPL1, TMEM67, RPE65, TULP1* and *CLCC1*, as well as the genes most often mutated to cause IRD in Pakistan. In turn this analysis will help clinicians to prioritise genes and specific gene variants for diagnostic evaluation to create a cost-effective and community-appropriate sequencing panel to be employed in those cases in which a clinical diagnosis is unclear. Other benefits of this work also relate to treatment as new therapies have been developed [158] for many retinal disorders. While unfortunately Pakistani families identified do not relate to genes for which these therapies are currently available, this will undoubtedly change in future years as new therapies and genetic disorders are identified. This again underlie the uniqueness of the genetic background of the Pakistani population.

Amongst the IRDs RP was found to be the most prevalent. Over 70 genes have been associated with RP, however in about 20-30% of cases a genetic cause of disease has not been identified [47]. The work described in this thesis entails

the identification of a new genetic cause of arRP, identified initially in eight Pakistani families and a British-Bangladeshi family. We show that the variant (c.75C>A, p.(Asp25Glu)) in *CLCC1* represents a founder mutation which arose in Punjab, and as such all families with the conditions descend from the same common ancestor,. Functional studies of CLCC1 found it to be important for retinal development, photoreceptors morphology, and function. As the function of CLCC1 was not known, functional studies were necessary, defining CLCC1 as an ER protein, although the functional significance of the Asp25Glu variant has not yet been defined. While this work defines a new molecular cause of RP, many questions about the mechanism of disease remain open and further studies will be necessary to define the role of CLCC1 within normal cells, and the functional outcome of the Asp25Glu variant.

Together the work presented in this thesis provides a greatly improved knowledge of the genetic causes of IRD in Pakistan. Targeted and cost-effective genetic testing for Pakistani populations, based on detailed knowledge of the prevalence of specific genetic alterations in geographically isolated communities and their clinical outcomes, will ultimately provide substantial healthcare improvements and enable a more efficient path for the diagnosis of inherited disease. Understanding the causes as well as the consequences of genetic alterations

APPENDIX A

Table 1 Genes reported in RetNet as related to Inherited Retinal Dystrophies.

Disease	*Type*	*Gene*	*Protein function*	*Clinical phenotype*	*Prevalence*	*MIM*
Non-syndromic IRDs-Rod dominant	**adRP**	*ADIPOR1*	Regulator of fatty acid catabolism and glucose levels	Night blindness, bone spicule, absent or undetectable ERG, tunnel vision, loss of central vision in late stages.	1 in 3000-1 in 7000	607945
		ARL3	Cilia signalling			604695
		BEST1	Forms calcium-sensitive chloride channels			607854
		CA4	Nitrogen metabolism			114760
		CRX	Transcription factor for photoreceptor-specific genes			602225
		FSCN2	Actin bundling protein			607643
		GUCA1B	Ca(2+)-sensitive regulation of guanylyl cyclase			602275
		HK1	Glucose metabolism			142600
		IMPDH1	Involved in de novo synthesis of guanine nucleotides			146690
		IMPG1	Proteoglycan involved in maintaining viability of photoreceptor cells and adhesion of the neural retina to the retinal pigment epithelium.			602870
		KLHL7	Proteins degradation			611119
		NR2E3	Transcriptional factor that activates rod development and repress cone development			604485
		NRL	Transcriptional activator of rod genes			162080
		PRPF3	Spliceosome assembly			607301
		PRPF4	Spliceosome assembly			607795
		PRPF6	Spliceosome component			613979
		PRPF8	Spliceosome assembly			607300
		PRPF31	Spliceosome component			606419

	PRPH2	Adhesion molecule involved in stabilization and compaction of outer segment discs	179605
	RDH12	Retinoids dehydrogenase/reductase	608830
	RHO	Rhodopsin	180380
	ROM1	Disc morphogenesis	180721
	RP1	Microtubule-associated protein regulating the stability and length of the microtubule-based axoneme of photoreceptors	603937
	RP9	pre-mRNA splicing	607331
	RPE65	Involved in the visual cycle	180069
	SAG	Visual arrestin	181031
	SEMA4A	Regulator of axon guidance	607292
	SNRNP200	Spliceosome assembly	601664
	SPP2	secreted phosphoprotein member of the cystatin superfamily	602637
	TOPORS	E3 ubiquitin-protein ligase	609507
arRP	*ABCA4*	ABC transporter	601691
	AGBL5	Metallocarboxypeptidase that mediates protein deglutamylation	615900
	AHR	Ligand-activated transcriptional activator	600253
	ARHGEF18	Guanine nucleotide exchange factor (GEF) for RhoA GTPases	616432
	ARL6	Regulator of intracellular trafficking to cilia	608845
	ARL2BP	Nuclear translocation, retention and transcriptional activity of STAT3	615407
	BBS1	Component of BBSome complex	209901
	BBS2	Component of BBSome complex	606151
	BEST1	Forms calcium-sensitive chloride channels	607854
	C2orf71	Normal photoreceptor cell maintenance and	613425

	vision	
C2orf37	Substrate receptor for CUL4-DDB1 E3 ubiquitin-protein ligase complex	612515
CERKL	Involved in autophagy and phagocytosis	608381
CLCC1	ER protein	617539
CLRN1	Ribbon synapse junctions	606397
CNGA1	Cyclic nucleotide-gated cation channel subunit	123825
CNGB1	Subunit of cyclic nucleotide-gated (CNG) channels,	600724
CRB1	Photoreceptor morphogenesis	604210
CYP4V2	Omega-hydroxylase	608614
DHDDS	Glycoproteins biosynthesis	608172
DHX38	Component of the spliceosome	605584
EMC1	Subunit of the endoplasmic reticulum membrane protein complex (EMC)	616846
EYS	Maintains the integrity of photoreceptor cells	612424
FAM161A	Ciliogenesis	613596
GPR125	Planar cell polarity pathway	612303
HGSNAT	Lysosomal acetyltransferase	610453
IDH3B	Enzyme related to pyruvate metabolism	604526
IFT140	Required for retrograde ciliary transport and entry into cilia of GPCR receptors	614620
IFT172	Maintenance and formation of cilia	607386
IMPG2	Chondroitin sulfate- and hyaluronan-binding proteoglycan	607056
KIAA1549	Unknown	613344
KIZ	Stabiliser the pericentriolar region prior to spindle formation	615757
LRAT	Catalyzes the esterification of all-trans-retinol into all-trans-retinyl ester	604863
MAK	Regulator of ciliary	154235

	length	
MERTK	Regulator of rod outer segments fragments phagocytosis	604705
MVK	Peroxisomal enzyme involved in sterol synthesis	251170
NEK2	Serine/threonine-protein kinase involved in mitotic regulation	604043
NEUROD1	Transcriptional activator	601724
NR2E3	Transcriptional factor that activates rod development and repress cone development	604485
NRL	Transcriptional activator of rod-specific genes	162080
PDE6A	Alpha subunit of phosphodiesterase	180071
PDE6B	Beta subunit of phosphodiesterase	180072
PDE6G	Gamma subunit of phosphodiesterase	180073
POMGNT1	Participates in O-mannosyl glycosylation	606822
PRCD	Photoreceptor disc component	610598
PROM1	Regulator of disk morphogenesis	604365
RBP3	IRBP shuttles 11-cis and all trans retinoids between the pigment epithelium and photoreceptor	180290
REEP6	Transport of receptors from the endoplasmic reticulum (ER) to the cell surface	609346
RGR	Receptor for all-*trans*- and 11-*cis*-retinal	600342
RHO	Rhodopsin	180380
RLBP1	Soluble retinoid carrier	180090
RP1	Microtubule-associated protein regulating the stability and length of the microtubule-based axoneme of photoreceptors	603937
RP1L1	Required for the differentiation of photoreceptor cells	608581

	RPE65	Involved in the visual cycle			180069
	SAG	Visual arrestin			181031
	SAMD11	May play a role in photoreceptor development			616765
	SLC7A14	Amino acid transporter protein			615720
	SPATA7	Recruits and localises RPGRIP1 in the cilium			609868
	TRNT1	CCA-adding enzyme			612907
	TTC8	Component of BBSome complex			608132
	TULP1	Required for normal development of photoreceptor synapses			602280
	USH2A	Maintenance of periciliary membrane complex			608400
	ZNF408	DNA binding protein			616454
	ZNF513	Transcriptional regulator			613598
X-linked RP	*RP2*	Trafficking between the Golgi and the ciliary membrane			
	RPGR	Regulates cilia formation by regulating actin stress filaments and cell contractility			312610
adLCA	*CRX*	Transcription factor for photoreceptor-specific genes	Severe visual impairment from birth, nystagmus, poor pupillary light responses, oculodigital sign, abnormal or undetectable ERG.	2-3 in 100,000	602225
	IMPDH1	Involved in de novo synthesis of guanine nucleotides			146690
	OTX2	Transcription factor			600037
arLCA	*AIPL1*	Chaperone of PDE6			604392
	CABP4	Calcium-binding protein			608965
	CCT2	Molecular chaperone			605139
	CEP290	Involved in early and late steps in cilia formation			610142
	CLUAP1	Cilia biogenesis			616787
	CRB1	Photoreceptor morphogenesis			604210
	CRX	Transcription factor for photoreceptor-specific genes			602225
	DTHD1	Death domain-containing proteins			616979
	GDF6	Growth factor that			601147

		controls proliferation and cellular differentiation in the retina			
	GUCY2D	Retinal guanylyl cyclase			600179
	IFT140	Required for retrograde ciliary transport and entry into cilia of GPCR receptors			614620
	IQCB1	Ciliogenesis			609237
	KCNJ13	Inwardly rectifying potassium channel			603208
	LCA5	Involved in intraflagellar protein (IFT) transport in photoreceptor cilia			611408
	LRAT	Catalyzes the esterification of all-trans-retinol into all-trans-retinyl ester			604863
	NMNAT1	Catalyse biosynthesis of NAD			608700
	PRPH2	Adhesion molecule involved in stabilization and compaction of outer segment discs			179605
	RD3	Regulates GUCY2D			180040
	RDH12	Retinoids dehydrogenase/reductase			608830
	RPE65	Involved in the visual cycle			180069
	RPGRIP1	Interacts with GTPase regulator protein. Required for normal location of RPGR at the connecting cilium of photoreceptor cells			605446
	SPATA7	Recruits and localises RPGRIP1 in the cilium			609868
	TULP1	Required for normal development of photoreceptor synapses			602280
adCSNB	*GNAT1*	Signal transducer for the rod photoreceptor RHO	Early onset stationary night blindness, decreased visual acuity, nystagmus, myopia, and strabismus.	unknown	139330
	PDE6B	Beta subunit of phosphodiesterase			180072
	RHO	Rhodopsin			180380
arCSNB	*CABP4*	Calcium-binding protein			608965
	GNAT1	Signal transducer			139330

			for the rod photoreceptor RHO			
		GNB3	Heterotrimeric G protein subunit			139130
		GPR179	Member of the glutamate receptor subfamily			614515
		GRK1	Rhodopsin kinase			180381
		GRM6	Glutamate receptor			604096
		LRIT3	localise TRPM1 at dendrite tips in ON-bipolar cells			615004
		RHD5	Catalyzes the oxidation of cis-isomers of retinol			601617
	(Oguchi disease)	*SAG*	Visual arrestin			181031
		SLC24A1	Controls calcium concentration of outer segments			603617
		TRPM1	Cation channel essential for the depolarizing photoresponse of retinal ON bipolar cells.			603576
	X-linked CSNB	*CACNA1F*	voltage-dependent calcium channel			300110
		NYX	Forms complex with TRPM1			300278
Non-syndromic IRDs-Cone dominant	**adCD/CRD**	*AIPL1*	Chaperone of PDE6	Progressive cone degeneration, loss of visual acuity, photophobia, defective colour vision, decrease central vision.	1 in 30,000	604392
		CRX	Transcription factor for photoreceptor-specific genes			602225
		GUCA1A	Regulator of retinal guanylyl cyclase			600364
		GUCY2D	retinal guanylyl cyclase			600179
		PITPNM3	catalyzes the transfer of phosphatidylinositol and phosphatidylcholine between membranes			608921
		PROM1	Regulator of disk morphogenesis			604365
		PRPH2	Adhesion molecule involved in stabilization and compaction of outer segment discs			179605
		RIMS1	Regulator of synaptic vesicle exocytosis			606629

	SEMA4A	Regulator of axon guidance	607292
	UNC119	Involved in synaptic functions in photoreceptor cells	604011
arCD/CRD	*ABCA4*	ABC transporter	601691
	ADAM9	Disintegrin and metalloprotease	602713
	ATF6	Transcription factor	605537
	C8orf37	unknown	614477
	CACNA2D4	Voltage-dependent calcium channels	608171
	CFAP510	Cilia-associated protein	603191
	CDHR1	Cadherin involved in disc morphogenesis	609502
	CEP78	Ciliogenesis	617110
	CERKL	Involved in autophagy and phagocytosis	608381
	CNGA3	Cyclic nucleotide-gated cation channel	600053
	CNGB3	Cyclic nucleotide-gated ion channel	605080
	CNNM4	Metal transporter	607805
	GNAT2	Transducin	139340
	IFT81	Transport of tubulin within the cilium	605489
	KCNV2	Voltage-gated potassium channels.	607604
	PDE6C	Phosphodiesterase subunit.	600827
	PDE6H	Phosphodiesterase subunit.	601190
	POC1B	Centriole assembly and/or stability and ciliogenesis.	614784
	RAB28	Intracellular trafficking.	612994
	RAX2	Gene expression modulator in photoreceptors.	610362
	RDH5	Catalyzes the oxidation of cis-isomers of retinol.	601617
	RPGRIP1	Interacts with GTPase regulator protein. Required for normal location of RPGR at the connecting cilium of photoreceptor cells.	605446
	TTLL5	Polyglutamylase which preferentially modifies alpha-tubulin.	612268
X-linked	*RPGR*	Regulates cilia formation by	312610

	CD/CRD		regulating actin stress filaments and cell contractility.			
	arACHM	*ATF6*	Transcription factor			605537
		CNGA3	Cyclic nucleotide-gated cation channel			600053
		CNGB1	Subunit of cyclic nucleotide-gated (CNG) channels,			600724
		GNAT2	Transducin			139340
		PDE6C	Phosphodiesterase subunit.			600827
		PDE6H	Phosphodiesterase subunit.			601190
Macular dystrophy	**Stargardt disease**	*ABCA4*	Inward-directed retinoid flipase	Macular atrophy, loss of central vision, and yellow-white flakes at the level of RPE	1:8000-1:10,000	601691
Syndromic IRDs-Usher syndrome	**arUSH**	*ABHD12*	Lysophosphatidylserine (LPS) lipase that mediates the hydrolysis of lysophosphatidylserine	Vestibular areflexia, deafness, retinitis pigmentosa.	1-4 per 25,000 people	613599
		ADGRV1	G-protein coupled receptor which has an essential role in the development of hearing and vision			602851
		ARSG	Lysosomal sulfatase			610008
		CDH23	Calcium-dependent cell adhesion proteins			605516
		CEP250	Centrosome cohesion during interphase			609689
		CEP78	Ciliogenesis			617110
		CIB2	Calcium-binding protein			605564
		CLRN1	Ribbon synapse junctions			606397
		DFNB31	Member of the USH2 complex			607928
		ESPN	Actin-bundling protein			606351
		HARS	Plays a role in axon guidance			142810
		MYO7A	Actin-based motor molecules			276903
		PCDH15	Calcium-dependent cell-adhesion protein			605514
		USH1C	Assembly of Usher protein complexes			605242
		USH1G	Anchoring/scaffoldi			607696

			ng protein			
		USH2A	Maintenance of periciliary membrane complex			608400
Syndromic IRDs-Ciliopathies	**arBBS**	*ADIPOR1*	Regulator of fatty acid catabolism and glucose levels	Retinitis pigmentosa, renal abnormalities, obesity, hypogonadism, polydactyly, learning disabilities.	1 in 100,00	607945
		ARL6	Regulator of intracellular trafficking to cilia			608845
		BBIP1	Component of BBSome complex			613605
		BBS1	Component of BBSome complex			209901
		BBS2	Component of BBSome complex			606151
		BBS4	Component of BBSome complex			600374
		BBS5	Component of BBSome complex			603650
		BBS7	Component of BBSome complex			607590
		BBS9	Component of BBSome complex			607968
		BBS10	Chaperone and component of BBSome complex			610148
		BBS12	Component of the chaperonin-containing T-complex (TRiC)			610683
		C8orf37	unknown			614477
		CEP19	Ciliogenesis initiator			615586
		CEP164	Centrosomal protein involved in microtubule organization, DNA damage response, and chromosome segregation			614848
		CEP290	Involved in early and late steps in cilia formation			610142
		IFT172	Maintenance and formation of cilia			607386
		IFT27	Small GTPase-like component of the intraflagellar transport (IFT) complex B that promotes the exit of the BBSome complex from cilia			615870
		INPP5E	Controls cilia growth			613037
		LZTFL1	Regulates ciliary localization of the			606568

		BBSome comple			
	MKKS	Chaperone, assembly of BBSome			604896
	MKS1	Component of the tectonic-like complex that prevents diffusion of transmembrane proteins between the cilia and plasma membranes.			609883
	SDCCAG8	Plays a role in the establishment of cell polarity and epithelial lumen formation			613524
	TRIM32	E3 ubiquitin ligase activity			602290
	TTC8	Component of BBSome complex			608132
	WDPCP	ciliogenesis and collective cell movements			613580
ALMS	*ALMS1*	Formation and maintenance of cilia	Sensorineural hearing loss, cone-rod dystrophy, nystagmus, photophobia, cardiomyopathy, insulin resistance and type 2 diabetes, progressive renal disease, and hypogonadism	1:1000,000	606844
JBTS	*AHI1*	Involved in vesicle trafficking and required for ciliogenesis	Mid-hindbrain malformation, hypotonia ataxia, intellectual disability, oculomotor apraxia, retinal dystrophy, renal disease, ocular colobomas, episodic tachypnea	1:80,000	608894
	ARL13B	Control the microtubule-based ciliary axoneme structure			608922
	B9D1	Component of the tectonic-like complex localised at the transition zone of primary cilia			614144
	B9D2	Component of the tectonic-like complex localised at the transition			611951

	zone of primary cilia	
C2CD3	Regulator of centriole elongation	615944
CC2D2A	Component of the tectonic-like complex localised at the transition zone of primary cilia	612013
CEP41	Required during ciliogenesis for tubulin glutamylation in cilium	610523
CEP104	Required for ciliogenesis and for structural integrity at the ciliary tip	616690
CEP120	Plays a role in the microtubule-dependent coupling of the nucleus and the centrosome	613446
CEP290	Involved in early and late steps in cilia formation	610142
CPLANE1	Involved in the establishment of cell polarity required for directional cell migration.	614571
CSPP1	Centrosome and spindle pole associated protein	611654
IFT172	Maintenance and formation of cilia	607386
INPP5E	Control cilia growth	613037
KIAA0556	Influence the stability of microtubules through interaction with the MT-severing katanin complex	616650
KIAA0586	Required for ciliogenesis and sonic hedgehog signalling pathway	610178
KIF7	Sonic hedgehog signalling pathway	611254
MKS1	Component of the tectonic-like complex that prevents diffusion of transmembrane proteins between the cilia and plasma membranes.	609883

NPHP1	Control of epithelial cell polarity	607100
OFD1	Component of the centrioles	300170
PDE6D	Phosphodiesterase subunit	602676
POC1B	Centriole assembly and/or stability and ciliogenesis	614784
RPGRIP1L	Localise to the basal body-centrosome complex or to primary cilia and centrosomes	610937
TCTN1	Component of the tectonic-like complex that prevents diffusion of transmembrane proteins between the cilia and plasma membranes.	609863
TCTN2	Component of the tectonic-like complex that prevents diffusion of transmembrane proteins	613846
TCTN3	Member of the tectonic gene family which functions in Hedgehog signal transduction and development of the neural tube	613847
TMEM67	Centriole migration to the apical membrane and formation of the primary cilium.	609884
TMEM107	Component of the primary cilia transition zone	616183
TMEM138	Ciliogenesis	614459
TMEM216	Part of the tectonic-like complex which is required for tissue-specific ciliogenesis and may regulate ciliary membrane composition	613277
TMEM231	Component of the tectonic-like complex that prevents diffusion of transmembrane proteins between the cilia and	614949

		plasma membranes.			
	TMEM237	Tetraspanin protein involved in WNT signalling			614423
	TTC21B	Component of the IFT complex A			612014
	ZNF423	Nuclear protein that belongs to the family of Kruppel-like C2H2 zinc finger proteins.			604557
MKS	*B9D1*	Component of the tectonic-like complex localised at the transition zone of primary cilia	Occipital encephalocele, cystic dysplastic kidneys, polydactyly, retinal dystrophy and other minor features	1:135,000	614144
	B9D2	Component of the tectonic-like complex localised at the transition zone of primary cilia			611951
	CPLANE1	Involved in the establishment of cell polarity required for directional cell migration.			614571
	CC2D2A	Component of the tectonic-like complex localised at the transition zone of primary cilia			612013
	CEP55	Plays a role in mitotic exit and cytokinesis			610000
	CEP290	Involved in early and late steps in cilia formation			610142
	CSPP1	Centrosome and spindle pole associated protein			611654
	KIF14	Vesicle transport, chromosome segregation, mitotic spindle formation, and cytokinesis			611279
	MKS1	Component of the tectonic-like complex that prevents diffusion of transmembrane proteins between the cilia and plasma membranes.			609883
	NPHP3	Required for normal ciliary development and			608002

		function.			
	RPGRIP1L	Localise to the basal body-centrosome complex or to primary cilia and centrosomes			610937
	TCTN2	Component of the tectonic-like complex that prevents diffusion of transmembrane proteins			613846
	TMEM67	Centriole migration to the apical membrane and formation of the primary cilium.			609884
	TMEM107	C omponent of the primary cilia transition zone			616183
	TMEM216	Part of the tectonic-like complex which is required for tissue-specific ciliogenesis and may regulate ciliary membrane composition.			613277
	TMEM231	Component of the tectonic-like complex that prevents diffusion of transmembrane proteins between the cilia and plasma membranes.			614949
	TXNDC15	Member of the thioredoxin superfamily			617778
SLS	*CEP164*	Centrosomal protein involved in microtubule organization, DNA damage response, and chromosome segregation	nephronophthisis and LCA	1:1,000,000	614848
	CEP290	Involved in early and late steps in cilia formation			610142
	IQCB1	Ciliogenesis			609237
	NPHP1	Control of epithelial cell polarity			607100
	NPHP3 locus				
	NPHP4	Involved in the organization of apical junctions			607215
	SDCCAG8	Plays a role in the establishment of			613524

	cell polarity and epithelial lumen formation	
TRAF31IP 1	Interacts with TNF receptor-associated factor 3 tethering it to cytoskeletal microtubules.	607380
WDR19	Component of the IFT complex A	608151

APPENDIX B

Table 1 Primary antibodies used in this study

Supplier	Cat #	Clone	Antigen	Application	Concentration	Dilution
Atlas	HPA013210		CLCC1	ICC WB Co-IP	0.3 mg/ml	1:100 1:1000 1:1000
Abcam	ab31290	AF18	Calnexin	ICC WB		1:100 1:500
Thermo fisher	PA3-900		Calreticulin Anti-rabbit	ICC WB Co-IP		1:100 1:1000 1:1000
Thermo fisher	MA5-15382	1G6A7	Calreticulin Anti-mouse	ICC	1 mg/ml	1:100
Atlas	HPA040890 4		EMC1	ICC WB	0.1 mg/ml	1:100 1:250
Sigma-Aldrich	F1804	M2	Flag tag	ICC WB Co-IP		1:100 1:1000 1:1000
Proteintech	11587-1-AP	AG2188	GPR-78	ICC WB	0.5 mg/ml	1:150 1:1000
Proteintech	60004-1-Ig	AG0766	GAPDH	WB	1 mg/ml	1:5000
Thermo fisher	A-11122		GFP tag	WB	2 mg/ml	1:1000
QED Bioscience	11076-200	10C3	KDEL	ICC		1:200
Abcam	Ab53852		SigmaR1 C-terminal	ICC WB	0.25 mg/ml	1:50 1:200
Santa cruz	Sc-137075	B-5	SigmaR1	ICC	0.2 mg/ml	
Novus	NBP2-44168		STIM1	ICC	1.12 mg/ml	1:100
Cell signaling	5589	D4F5	Rab11	ICC		1:50
abcam	Ab14748	15H4C4	ATPA5A	ICC	1 mg/ml	1:100
Cell Signaling	9664	5A1	Cleaved caspase-3 (Asp175)	ICC		1:50
Novus	NBP2-00812	OTI3F1	Tubulin beta 4	ICC		1:100

Table 2 Secondary antibodies and phalloidin used in this study

Supplier	Cat #	Target	Host	Conjugate	Application	Concentration	Dilution
Invitrogen	A-32723	Mouse IgG	Goat	AlexaFluor 488	ICC	2 mg/mL	1:400
Invitrogen	A-11034	Rabbit IgG	Goat	AlexaFluor 568	ICC	2 mg/mL	1:400
Invitrogen	A-11004	Mouse IgG	Goat	AlexaFluor 488	ICC	2 mg/mL	1:400
Invitrogen	A-11036	Rabbit IgG	Goat	AlexaFluor 568	ICC	2 mg/mL	1:400
Invitrogen	A-11015	Sheep IgG	Donkey	AlexaFluor 488	ICC	2 mg/mL	1:400
Invitrogen	A-21244	Rabbit IgG	Goat	AlexaFluor 647	ICC	2 mg/mL	1:400
Sigma	A9044	Mouse IgG	Rabbit	Horseradish peroxidase	WB		1:5000
Sigma	A0545	Rabbit IgG	Goat	Horseradish peroxidase	WB		1:5000
Thermo Fisher	A12380			Alexa Fluor 568 Phalloidin	ICC		1:200

APPENDIX C

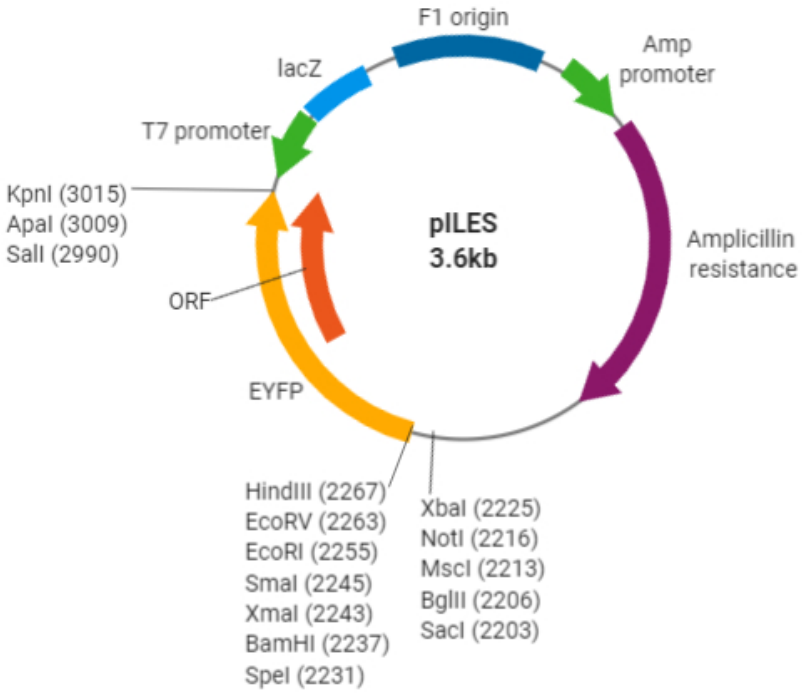

Figure 1 Schematics of pILES-EYFP vector. *Based upon pBluescript SK (+/-) phagemid with an additional polylinker which adds the sites XhoI, BglII, MscI into a multiple cloning site. Image made with BioRender.*

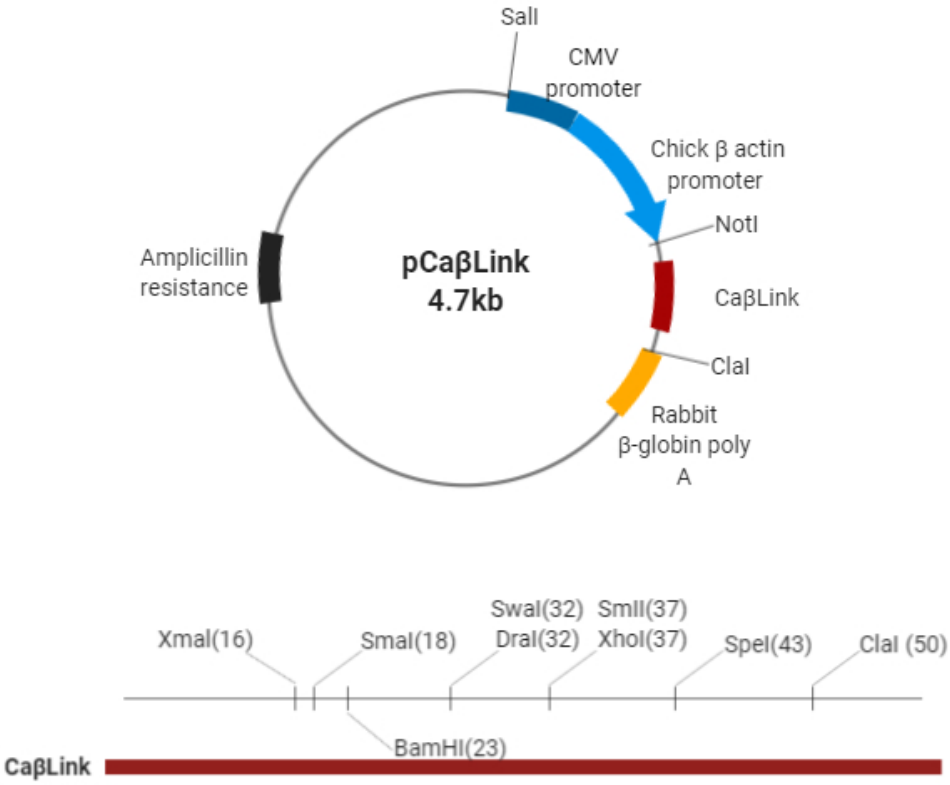

Figure 2 Schematics of the expression vector pCaβLink. *Based on pCAGGS expression vector which had the SV40 iri removed between two BamHI sites, which were filled and re-ligated. LacZ present between the chick β-actin and the rabbit β-globin poly was removed and CaβLink was inserted. Unique restriction sites for the CaβLink are reported in the bottom part of the image.Image created with BioRender.*

APPENDIX D

Table 1 Genetic variants and mapped loci previously associated with inherited retinal disease in Pakistani populations. *This includes a summary of ClinVar entries and PubMed reports defining possible pathogenicity of each variant, as well as other genetic information including the number of families and affected individuals reported in which each variant cosegregated.*

Gene	Nucleotide variant	Protein variant	Phenotype	Ref.	Region	Number affected families (number of affected individuals)	Families ID	Variant found in other countries or ethnicities	Clinvar (Accession)
1p13.3-p21.2	Mapped locus only; gene not identified	NA	Severe arRP	[195]	Punjab	1 (9)	61030	NA	Not listed
1p36	Mapped locus only; gene not identified	NA	arLCA	[349]	Punjab	1 (6)	LCA9	NA	Not listed
2p22.3-p24.1	Mapped locus only; gene not identified	NA	arRP	[196]	Punjab	1 (4)	PKRP115	NA	Not listed
11p11.2-q13.1	Mapped locus only; gene not identified	NA	arRP	[169]	NA	2	61103; 61167	NA	Not listed
11p11.2-q13.2	Mapped locus only; gene not identified	NA	arRP	[169]	NA	1	61061	NA	Not listed
15q24	Mapped locus only; gene not identified	NA	Tapetoretinal degeneration and mental retardation	[350]	Mirpur district, Azad Kashmir	1 (9)	No ID	NA	Not listed
17p13	Mapped locus only; gene not identified	NA	arLCA with keratoconus	[351]	NA	1 (4)	No ID	NA	Not listed
ABCA4	c.93T>C	p.(Trp31Arg)	Stargardt disease	[170]	NA	1 (1)	36	[327] NA [352] Caucasian	Not listed
ABCA4	c.2023G>A	p.(Val675Ile)	Stargardt disease	[170]	NA	1 (1)	23	[327] NA [339] Germany	Likely pathogenic/ Uncertain significance (VCV000288341)
ABCA4	c.3364G>A	p.(Glu1122Lys)	Stargardt disease/IRD	This study	KPK	1 (1)	Family 11	[313] European [353] NA [315] European [56] Han Chinese [354] NA [339] UK	Pathogenic/ Likely pathogenic (VCV000030218)
ABCA4	c.5243G>A	p.(Gly1748Glu)	Stargardt disease	[170]	NA	(1)	29	[355] Caucasian	Not listed
ABCA4	c.5646G>A	p.(Met1882Ile)	Stargardt disease	[170]	NA	(1)	23	[356] NA [354] NA [357] Chinese [358] NA	Likely pathogenic (VCV000377407)
ABCA4	c.5882G>A	p.(Gly1961Glu)	Stargardt disease/CRD	[170, 359]	NA	2 (3)	32, RF.RA.0812	[312, 353, 354, 360-375] NA [376] European, Somali, Jordanian [377] Southern Europe [378] Czech [379] Central Europe [380] USA, Japan, France, Germany, Holland, Spain, Italy, Sweden, UK, China, Australia, Switzerland [381] Italian [47] Spanish	Pathogenic/ Likely pathogenic (VCV000007888)

								[382] Dutch [383] Brazilian [384] Iraq [385] Somali [386] French, Italian, Austrian/Algerian, Algerian/Spanish [387] Polish [339] USA, France, Germany, UK [388] Denmark	
ABCA4	c.6098T>A	p.(Leu2033His)	Stargardt disease	[170]	NA	1 (1)	32	No	Not listed
ABCA4	c.6317G>A	p.(Arg2106His)	Stargardt disease	[170]	NA	1 (1)	29	[355] Caucasian [352] Hispanic	Likely pathogenic (VCV000377409)
ABCA4	c.6658C>T	p.(Gln2220*)	IRD	[389]	NA	1 (6)	RP03	[390] Germany/ The Netherlands [308, 371, 391] NA [315] South Asia	Pathogenic (VCV000099476)
ADAM9	c.766C>T	p.(Arg256*)	CRD	[392]	NA	1 (4)	MEP49	No	Pathogenic (VCV000006877)
ADAMTS18	c.1952G>A	p.(Arg651Gln)	CRD	[393]	NA	1 (1)	Family 3	No	Not listed
ADAMTS18	c.2159G>C	p.(Cys720Ser)	CRD	[393]	NA	1 (2)	Family 2	No	Not listed
AHI1	c.2367_2368insT	p.(Asn790*)	arJBTS	[394]	NA	1 (2)	F799	[395] NA	Pathogenic (VCV000002016)
AIPL1	c.116C>A	p.(Thr39Asn)	arLCA	[396]	NA	1 (6)	011LCA	No	Not listed
AIPL1	c.264G>A	p.(Trp88*)	arLCA	[397]	NA	2 (2)	Patient 4; Patient 5	[398] Bangladesh	Not provided (VCV000099793)
AIPL1	c.465G>T	p.(Gln155His)	IRD	[399]	Sindh	1 (6)	61227	[388] Denmark [400] NA	Uncertain significance (VCV000635994)
AIPL1	c.773G>C	p.(Arg258Pro)	IRD	[399]	Punjab	1 (7)	61032	No	Not listed
AIPL1	c.834G>A	p.(Trp278*)	EORP; arLCA w/o keratoconus	[389, 401-404]	Northern Pakistan	11 (38)	RP27; MD; MEP20; MEP21; MEP29; 3500; 3501; 3502; 3503; F1; F2;	[405] Italian [406] Australian [407] Indian [408] German [398] French, Spanish	Pathogenic (VCV000005565)
ALMS1 locus	Mapped locus only; variant not identified	NA	Alström syndrome	[409]	NA	3 (7)	No ID	NA	Not listed
ALMS1	c.4937C>A	p.(Ser1646*)	Alström syndrome	[410]	Northern Pakistan	1 (2)	Family D	No	Not listed
ALMS1	c.5248A>G	p.(Thr1750Ala)	IRD	[305]	Punjab	1 (3)	PKRD176	No	Likely benign (VCV000210128)
ALMS1	1444 bp, IVS8+895 incl. ex. 9		Alström syndrome + exudative retinopathy	[410, 411]	Northern Pakistan	2 (8)	Family B; No ID	No	Not listed
ALMS1	c.8008C>T	p.(Arg2670*)	Alström syndrome	[410]	Northern Pakistani/Caucasian	1 (1)	Family G	[412] NA [413] Arab Muslim [414] Iran	Pathogenic (VCV000529386)
ALMS1	c.9011_9021del	p.(Pro3004Hisfs*3)	Alström syndrome	[410]	Northern Pakistan	1 (4)	Family A	No	Not listed
ALMS1	c.9911_11550del	p.(Asn3306Lysfs*7)	Alström syndrome	[415, 416]	Haripur, KPK	2 (3)	SND12; No ID	[417] West Asia [418] NA	Not listed
ALMS1	c.10885C>T	p.(Arg3629*)	Alström syndrome	[410]	Northern Pakistani/ Caucasian	1 (1)	Family G	[419] Indian	Pathogenic (VCV000434136)
ARL3	c.446G>A	p.(Arg149His)	arJBTS	[420]	NA	1 (3)	Family 2	No	Uncertain significance (VCV000424963)
ARL6	c.123+1118del53985	p.(?)	arBBS	[332]	NA	1	61049	No	Not listed
ARL6	c.281T>C	p.(Ile94Thr)	arBBS	[331]	Remote regions	1 (7)	Family A	No	Likely pathogenic (VCV000438186)
ARL6	c.534A>G	p.(Gln178Gln)	arBBS/IRD	[330], this study	NA	2 (4)	F01; Family 27 (61374)	No	Not listed

ARL13B	c.223G>A	p.(Gly75Arg)	arJBTS	[421]	Baluchistan	2 (5)	Family A; Family B	No	Not listed
ARL13B	c.236G>A	p.(Arg79Gln)	arJBTS	[422]	NA	1 (2)	MTI-001	No	Pathogenic (VCV000001991)
ASRGL1	c.532G>A	p.(Gly178Arg)	EORD	[423]	NA	1 (6)	PKRD104	No	Not listed
ATF6	c.355dupG	p.(Glu119Glyfs*8)	arACHM	[75]	NA	1 (5)	MA28	No	Pathogenic (VCV000208171)
BBS1	c.47+1G>T	p.(?)	arBBS	[424]	Central Punjab	1 (2)	Family A	No	Not listed
BBS1	c.442G>A	p.(Asp148Asn)	arBBS	[424]	Central Punjab	1 (2)	Family B	[139] UK, USA	Likely pathogenic (VCV000645579)
BBS1	c.887delT	p.(Ile296Thrfs*7)	arBBS	[328]	NA	1 (1)	Family 47	No	Pathogenic (VCV000193740)
BBS2	c.1237C>T	p.(Arg413*)	arBBS/arRP	[425] [169, 332]	NA	3 (1)	PK1; A2002; 61014	[426] European	Pathogenic/ Likely pathogenic (VCV000370943)
BBS4	c.221-1G>A	p.(?)	arBBS	This study	Quetta, Balochistan	1 (2)	Family 12	No	Not listed
BBS4	c.1463C>A	p.(Thr488Lys)	arBBS	[328]	NA	1 (2)	24/56	No	Likely benign (VCV000462959)
BBS5	c.2T>A	p.(Met1Lys)	arBBS	[425]	NA	2 (2)	A2027; A2002	No	Not listed
BBS5	c.196delA	p.(Arg66Glufs*12)	arBBS	[427]	Bannu, KPK	1 (2)	Family 1	No	Not listed
BBS5	c.734_744del11	p.(Glu245Glyfs*18)	arBBS	[330]	NA	2 (3)	F02; F03	No	Not listed
BBS7	c.580_582delGCA	p.(Ala194del)	arBBS	[428]	KPK	1 (4)	Family A	No	Not listed
BBS7	c.719G>T	p.(Gly240Val)	arBBS	[429]	Peshwar city, KPK	1 (2)	No ID	No	Not listed
BBS7	c.1592_1597delTTCCAG	p.(Val531_Pro532del)	arBBS	[428]	Azad Jammu	1 (3)	Family B	No	Pathogenic (VCV000030680)
BBS9	c.299delC	p.(Ser100Leufs*24)	arBBS	[430, 431]	Rehmani-Khail village, Kirikhaisor village, D.I.Khan, KPK	3 (6)	No ID; Family A; Family B.	No	Not listed
BBS9	c.1789C>T	p.(Gln597*)	arBBS	[330]	NA	1 (1)	F04	[432] Latino	Not listed
BBS10	c.271dupT	p.(Cys91Leufs*5)	arBBS	[123, 428]	Azad Jammu	3 (6)	Family D; No ID; No ID	[315, 432] European [388] Denmark [122] Lebanese [419] Indian [433, 434] NA	Pathogenic (VCV000001328)
BBS10	c.1075C>T	p.(Gln359*)	arBBS	[331]	Remote regions	1 (5)	Family B	No	Not listed
BBS10	c.1091delA	p.(Asn364Thrfs*5)	arBBS	[123]	NA	1 (1)	No ID	[435] Caucasian	Pathogenic/ Likely pathogenic (VCV000166723)
BBS10	c.1958_1967del	p.(Ser653Ilefs*4)	arBBS	[436]	Punjab	1 (2)	MRQ19	No	Not listed
BBS10	c.2121dupT	p.(Lys708*)	arBBS	[123]	NA	1 (1)	No ID	No	Not listed
BBS10	c.2144A>G	p.(His715Arg)	arBBS	[328]	NA	1 (1)	Family 47	No	Uncertain significance (VCV000195378)
BBS12	c.1438delG	p.(Arg480Metfs*3)	arBBS	[328]	NA	1 (2)	24/56	No	Not listed
BBS12	c.1589T>C	p.(Leu530Pro)	arBBS	[425]	NA	2 (2)	A2003; A2015	No	Not listed
BBS12	c.1616G>T	p.(Gly539Val)	RP/IRD	[169]	NA	1	61247	No	Uncertain significance (VCV000555332)
BBS12	c.2102C>A	p.(Ser701*)	arBBS	[437]	NA	1 (3)	MR-10	No	Not listed
BEST1	c.418C>G	p.(Leu140Val)	arRP	[438]	NA	1 (3)	Family 5	[388] Denmark	Uncertain significance (VCV000002750)
C1QTNF4	c.902G>A	p.(Gly301Asp)	IRD	[439]	Punjab	1 (3)	PKRD320	No	Not listed
C8orf37	c.244-2A>C	p.(?)	arRP	[440]	Multan district, Punjab	1 (3)	MA48	No	Pathogenic (VCV000417787)
C8orf37	c.555G>A	p.(Trp185*)	arRP	[440]	NA	1 (2)	MA13	[441] Chinese	Pathogenic (VCV000417788)
CACNA1F	c.2254G>A	p.(Val752Met)	IRD	This study	MastungBaluchistan	1 (2)	Family 16	No	Not listed
CC2D2A	c.685_687delGAA	p.(Glu229del)	arMKS	[442]	NA	4	66 F1; 66 F2;	[395] NA	Benign/ Likely

							16; 17.		benign (VCV000056316)
CC2D2A	c.2338+1G>C	p.(?)	atJBTS	[193, 443]	Mianwali district, Punjab	2 (5)	No ID; PK1	No	Not listed
CC2D2A	c.3540delA	p.(Arg1180Serfs*7)	arMKS	[442]	NA	2 (2)	158; 180	No	Not listed
CDH3	c.353A>G	p.(Glu118Gly)	EEM	[444]	NA	1 (5)	Family 4	No	Not listed
CDH3	c.490dupA	p.(Thr164Asnfs*8)	Hypotrichosis with juvenile macular dystrophy	[444]	NA	1 (4)	Family 1	No	Not listed
CDH3	c.965A>T	p.(Asn322Ile)	EEM	[444]	NA	1 (2)	Family 5	[445] Danish	Pathogenic (VCV000017640)
CDH3	c.1425-1G>T	p.(?)	Hypotrichosis with juvenile macular dystrophy	[270, 444, 446, 447]	KPK (Pashtoon)	5 (33)	No ID; Family B; Family 2; Family 3; No ID	No	Not listed
CDH3	c.1796-2A>G	p.(?)	hypotrichosis with juvenile macular dystrophy	[447]	NA	1 (4)	Family A	[448] NA	Not listed
CDH23	c.1114C>T	p.(Gln372*)	arUSH type1	[449]	NA	1 (3)	PKDF176	No	Not listed
CDH23	c.1595C>T	p.(Thr532Met)	IRD	This study	NA	1 (5)	Family 20	[317]- NA [450]- NA	Uncertain significance/ Likely benign (VCV000194671)
CDH23	c.1702_1703del	p.(Gly568Cysfs*20)	arUSH type1	[451]	NA	1 (1)	DEM127	No	Not listed
CDH23	c.3106_3106+11delinsTGGT	p.(?)	arUSH type1	[449]	NA	1 (5)	PKDF218	No	Not listed
CDH23	c.3880C>T	p.(Gln1294*)	arUSH type1D	[92]	NA	1 (4)	PKZA56	No	Pathogenic (VCV000004921)
CDH23	c.6047-9G>A	p.(?)	arUSH type1	[451]	NA	1 (1)	DEM296	No	Not listed
CDH23	c.6049+1G>A	p.(?)	arUSH type1	[92]	NA	1 (4)	304	[452] NA	Pathogenic (VCV000045999)
CDH23	c.6050-1G>C	p.(?)	arUSH type1	[449]	NA	1 (5)	PKDF824	No	Not listed
CDH23	c.6050-9G>A	p.(?)	arUSH type1	[449]	NA	4 (13)	PKDF57a; PKDF177; PKDF266; PKDF464	[453] Germany/ Switzerland [454] NA [455] Spanish, French [456] France [457] Maghreb	Pathogenic (VCV000046001)
CDH23	c.6054_6074del	p.(Val2019_Val2025del)	arUSH type1	[449]	NA	1 (2)	PKDF097	No	Not listed
CDH23	c.6319C>T	p.(Arg2107*)	arUSH type1	[92, 458]	Sindh	2 (5)	USH05; 140	[458] Caucasian [459, 460] Japanese	Not listed
CDH23	c.6845delA	p.(Asn2282Thrfs*91)	arUSH type1	[449]	NA	1 (3)	PKDF522	No	Not listed
CDH23	c.7198C>T	p.(Pro2400Ser)	arUSH type1	[449]	NA	1 (4)	PKDF271	No	Not listed
CDH23	c.8150A>G	p.(Asp2717Gly)	arUSH type1	[449]	NA	1 (3)	PKDF151	No	Not listed
CDH23	c.8208_8209delAG	p.(Val2737Alafs*2)	arUSH type1	[449]	NA	2 (6)	PKDF532; PKDF629	No	Not listed
CDH23	c.8530C>T	p.(Pro2844Ser)	arUSH type1	[461]	NA	1 (3)	PKDF475	No	Not listed
CDHR1	c.1463delG	p.(Gly488Alafs*20)	arRP	[169, 462]	NA	3 (6)	61220; 61289; GC18832	[463] South Asian [464] Mauritius [465] NA	Pathogenic (VCV000438116)
CEP19	c.194dupA	p.(Tyr65*)	arBBS	[133]	Southern Punjab	1 (7)	No ID	No	Not listed
CEP164	c.277C>T	p.(Arg93Trp)	arBBS	[330]	NA	1 (2)	F05	[466] USA	Pathogenic (VCV000037296)
CEP290	c.148C>T	p.(His50Tyr)	EOIRD	[169]	NA	1 (3)	61166	[467] NA	Uncertain significance (VCV000236469)
CEP290	c.955delT	p.(Ser319Leufs*16)	arMKS	[442]	NA	1 (1)	292	No	Not listed
CEP290	c.1429C>T	p.(Arg477*)	arMKS	[442]	Mirpur, Azad Kashmir	1 (1)	39	[468] NA	Pathogenic/ Likely pathogenic (VCV000523768)
CEP290	c.5668G>T	p.(Gly1890*)	arJBTS	[469]	NA	1 (1)	A1188-	[354, 395,	Pathogenic

							21	470, 471] NA [472] The Netherlands [473] Caucasian [474] German [475] Arab	(VCV000001333)
CEP290	c.5743_5744insT	p.(Gly1915Valfs*2)	arMKS	[442]	NA	1 (1)	333	No	Not listed
CERKL	c.316C>A	p.(Arg106Ser)	arRP	[476]	Lahore	1 (3)	No ID	No	Likely pathogenic (VCV000438054)
CERKL	c.847C>T	p.(Arg283*)	arRP/IRD	[169, 389]	NA	3 (7)	RP48; 61219; 61373	[47, 477, 478] Spain [479] Qatar [315, 354, 366, 372] NA [480] Finland	Not listed
CHM	c.1695_1696delAT	p.(Tyr565*)	IRD	[481]	Punjab	1 (3)	PKRD168	No	Not listed
CIB2	c.192G>C	p.(Glu64Asp)	arUSH type1J	[95]	NA	1 (4)	PKDF117	No	Pathogenic (VCV000039688)
CLCC1	c.75C>A	p.(Asp25Glu)	arRP	[316], this study	Punjab	9 (41)	61030; 61031; 61328; 61244; 61224; Family 6; Family 7; Family 8; Family 20 (61334)	No	Not listed
CLRN1	c.92C>T	p.(Pro31Leu)	arRP	[482]	Punjab	1 (6)	RP18	No	Pathogenic (VCV000030575)
CLRN1	c.461T>G	p.(Leu154Trp)	arRP	[482]	Punjab	1 (5)	RP06	No	Pathogenic (VCV000030574)
CNGA1	c.626_627delTA	p.(Ile209Serfs*26)	arRP	[483]	Punjab	1 (7)	61039	No	Not listed
CNGA1	c.1091G>A	p.(Gly364Asp)	arRP	[304, 403]	NA	2 (6)	F08; No ID	No	Not listed
CNGA3	c.822G>T	p.(Arg274Ser)	arACHM	[484]	Punjab	1 (4)	RP26	No	Not listed
CNGA3	c.827A>G	p.(Asn276Ser)	arACHM	[485]	Punjab	2 (9)	Family 50; Family 74	No	Not listed
CNGA3	c.952G>A	p.(Ala318Thr)	IRD	[169]	NA	1 (3)	61086	No	Not listed
CNGA3	c.955T>C	p.(Cys319Arg)	juvenile CRD with maculopathy/IRD	[306] this study	Swabi, KPK	2 (10)	PKAB157; Family 1	[307, 308] NA	Not listed
CNGA3	c.991G>C	p.(Gly331Arg)	IRD/arACHM	[174]	Punjab	1 (3)	MA-69	No	Not listed
CNGA3	c.1306C>T	p.(Arg436Trp)	IRD/arACHM	[174, 486]	Punjab; KPK	2 (8)	MA-25; PKCN-02	[70] Germany, Greece [309] Chinese [326] NA	Pathogenic (VCV000009482)
CNGA3	c.1443dupC	p.(Ile482Hisfs*6)	IRD	This study	Peshawar, KPK	1 (2)	Family 4 (61421)	[310] NA	Not listed
CNGA3	c.1540G>A	p.(Asp514Asn)	arACHM	[486]	KPK	1 (4)	PKCN-07	No	Not listed
CNGA3	c.1556T>C	p.(Met519Thr)	IRD	This study	Jatoi,Muzaffargarh, Punjab	1 (5)	Family 2	[309] Chinese	Not listed
CNGA3	c.1600G>A	p.(Gly534Arg)	IRD	This study	Sargodha, Punjab	1 (4)	Family 3	No	Not listed
CNGA3	c.1641C>A	p.(Phe547Leu)	IRD	This study	NA	1 (4)	Family 5	[324-326] NA	Likely pathogenic (VCV000009478)
CNGB1	c.413-1G>A	p.(?)	IRD/RP	[174, 487]	Sindh	2 (2)	MA-97; RP12	No	Likely pathogenic (VCV000437976)
CNGB1	c.852_874+25del	p.(Ile286Aspfs*9)	arRP	This study	Raiwind, Punjab	1 (3)	Family 218	No	Not listed
CNGB1	c.2284C>T	p.(Arg762Cys)	arRP	[487]	Punjab	1	RP42	[488] NA	Not listed
CNGB1	c.2493-2A>G	p.(?)	arRP	[403]	NA	2 (18)	F09; No ID	No	Not listed
CNGB1	c.2493-2_2495delinsGGC	p.(Ser831Argfs*2)	arRP	[169, 305]	Punjab	3 (5)	PKRD142; 61142; 61032	No	Not listed
CNGB3	c.646C>T	p.(Arg216*)	IRD	[174]	Punjab	1 (3)	MA-94	[311] NA	Likely pathogenic (VCV000188844)

CNGB3	c.1148delC	p.(Thr383Ilefs*13)	arACHM/IRD	[169, 489]	NA	2 (8)	No ID; 61036	[490] Pingelap [308, 312, 491, 492] NA [315] European [405] Italian [493] Indian [478, 494] Spanish [388] Denmark [387] Polish	Pathogenic/ Uncertain significance (VCV000005225)
CNGB3	c.1208G>A	p.(Arg403Gln)	IRD	[169, 495]	NA	2 (6)	61221; No ID	[492, 496, 497] NA	Pathogenic/ Likely benign/ Benign (VCV000143154)
CNGB3	c.1825delG	p.(Val609Trpfs*9)	arACHM	[484]	KPK	1 (2)	RP44	No	Not listed
CORD8 locus 1q12-q24	Mapped locus only; variant not identified	NA	arCRD	[498]	NA	1 (6)	CORD8	No	Not listed
CRB1	c.107C>G	p.(Ser36*)	arLCA	[404]	Northern Pakistan	1 (10)	MEP53	No	Not listed
CRB1	c.433T>C	p.(Cys145Arg)	IRD	[169]	NA	1	61186	No	Not listed
CRB1	c.1459T>C	p.(Ser487Pro)	arRP	[377]	NA	1 (1)	Patient 7	No	Not listed
CRB1	c.2234C>T	p.(Thr745Met)	arRP	[403]	Punjab	2 (4)	F10	[499-502] NA [503] Chinese [504] Iranian [505] Saudi Arabia	Pathogenic (VCV000005733)
CRB1	c.2536G>A	p.(Gly846Arg)	arRP	[396, 506]	Kashmir	2 (8)	3330RP; No ID	[308, 500] NA	Not listed
CRB1	c.2966T>C	p.(Ile989Thr)	arLCA	[396]	NA	1 (8)	010LCA	No	Not listed
CRB1	c.3296C>A	p.(Thr1099Lys)	arRP	[487]	NA	1	RP04	No	Not listed
CRB1	c.3343_3352del	p.(Gly1115Ilefs*23)	arRP	[507]	NA	1 (9)	No ID	No	Not listed
CRB1	c.3347T>C	p.(Leu1071Pro)	arRP	[396]	NA	1 (7)	111RP	[499] NA	Not listed
CRB1	c.3735delA	p.(Gly1246Glufs*36)	arRP	This study	Borewala, Punjab	1 (3)	Family 13	No	Not listed
CRB1	c.3961G>C	p.(Cys1321Ser)	arRP	[507]	NA	1 (5)	No ID	[508] NA	Not listed
DHX38	c.971G>A	p.(Arg324Gln)	EORP	[509]	Bagh district, Azad Kashmir	2 (10)	MA88; MA157	No	Likely pathogenic (VCV000592160)
DHX38	c.995G>A	p.(Gly332Asp)	EORP w/ macular coloboma	[186]	KPK	1 (4)	Family A	No	Uncertain significance (VCV000140595)
DRAM2	c.140delG	p.(Gly47Valfs*3)	IRD with early macular involvement	[510]	NA	1 (9)	Family ES1	No	Pathogenic (VCV000192233)
ELOVL4	c.78C>G	p.(Tyr26*)	Neuro-ichthyotic disorder with maculopathy	[511]	Remote region	1 (3)	No ID	No	Not listed
EYS	c.6137G>A	p.(Trp2046*)	arRP	[169]	NA	1 (7)	61192	[467, 512] NA	Likely pathogenic (VCV000236448)
EYS	c.7187G>C	p.(Cys2396Ser)	arRP	[169]	NA	1 (2)	61016	[513] Indian	Not listed
EYS	c.8236G>T	p.(Asp2747Tyr)	arRP	[514]	Punjab	1 (6)	RP50	No	Not listed
ESPN	c.2369_2386del	p.(Arg790_Arg795del)	arUSH type1	[96]	NA	1 (13)	PKDF1051	No	Pathogenic (VCV000560535)
FAM161A	c.1139G>T	p.(Arg380Leu)	arRP	[169]	NA	1	61239	No	Not listed
FAM161A	c.1309A>T	p.(Arg437*)	arRP	[515]	NA	1 (2)	GC3796	[515] British [516] German [517] Dutch, Belgian [354, 366] NA	Pathogenic (VCV000000036)
FAM161A	c.1600A>T	p.(Lys534*)	arRP	[169, 305]	Punjab; -	2 (3)	61176; PKRD176	No	Not listed
FDFT1	c.930C>G	p.(Phe310Leu)	arIRD	[518]	NA	1 (2)	Family C	No	Not listed
GNAT1	c.386A>G	p.(Asp129Gly)	arCSNB	[169, 519]	Punjab	2 (4)	PKRP130; 61130	[520] Chinese [521] Hong Kong	Pathogenic (VCV000190968)
GNAT2	c.840_843insATGC	p.(His282Serfs*11)	arACHM/arCD	[72, 522]	NA	2 (11)	No ID; No ID	No	Not listed
GRM6	c.824G>A	p.(Gly275Asp)	IRD	[169]	NA	1 (4)	61155	[523] NA [524] South Asian	Not listed

GRM6	c.1336C>T	p.(Arg446*)	arCSNB	[169, 525]	Punjab	2 (7)	PKRP170; 61170	No	Not listed
GRM6	c.2267G>A	p.(Gly756Asp)	arCSNB	[169, 525]	Punjab	2 (6)	61172; PKRP172	No	Not listed
GRK1	c.55C>T	p.(Arg19*)	IRD	[169]	NA	1 (2)	61015	No	Not listed
GRK1	c.614C>A	p.(Ser205*)	IRD/Oguchi disease 2	[487, 526]	Punjab	1 (8)	RP19	No	Not listed
GRK1	c.827+623_883del	p.(?)	Oguchi disease 2	[527]	Punjab	1 (3)	61029	No	Not listed
GUCY2D	c.1573delC	p.(Gln525Argfs*38)	arLCA	[528]	Dera Ismail Khan, KPK	1 (4)	No ID	No	Not listed
GUYC2D	c.2189T>C	p.(Phe730Ser)	IRD	[169, 305]	Punjab	2 (3)	PKRD103; 61103	No	Not listed
GUCY2D	c.2283delG	p.(Ser762Alafs*22)	arLCA	[403]	NA	1 (2)	F3	No	Not listed
GUCY2D	c.2384G>A	p.(Arg795Gln)	IRD	[169, 305]	Punjab	2 (3)	PKRD077; 61077	[529] Italian	Uncertain significance (VCV000596790)
GUCY2D	c.3056A>C	p.(His1019Pro)	arLCA/IRD	[314]; This study	KPK	2 (3)	Family 56; Family 14	No	Not listed
HMX1	c.650A>C	p.(Gln217Pro)	Oculoauricolar syndrome	[530]	NA	1 (2)	No ID	No	Pathogenic (VCV000192315)
IFT43	c.100G>A	p.(Glu34Lys)	arIRD	[531]	NA	1 (9)	PKRD272	No	Likely pathogenic (VCV000489395)
IFT140	c.998G>A	p.(Cys333Tyr)	arRP	[532]	Punjab	1 (1)	Family 4	No	Likely pathogenic (VCV000438181)
IFT140	c.1451C>T	p.(Thr484Met)	arRP	[532]	Northern Pakistan and Punjab	1 (4)	Family 1	[533] Chinese	Pathogenic (VCV000446314)
IMPDH1	c.931G>A	p.(Asp311Asn)	arRP	[169, 534]	NA	2 (4)	61004; PKRP004	[535] NA [536] Spanish [537] Mexican	Pathogenic (VCV000014834)
IMPG2	c.1680T>A	p.(Tyr560*)	arRP	[538]	NA	1 (3)	RP-49	[315] South Asia	Pathogenic (VCV000437938)
INPP5E	c.1879C>T	p.(Gln627*)	MORM syndrome	[427, 539]	Khushab, Punjab	2 (9)	Family 2; No ID	No	Pathogenic (VCV000000396)
IQCB1	c.488-1G>A	p.(?)	arSLSN	[540]	NA	1 (1)	A364	[395] NA	Not listed
IQCB1	c.1363C>T	p.(Arg455*)	arSLSN	[541]	NA	1 (1)	N10	[312, 395, 542] NA	Pathogenic (VCV000504877)
IQCB1	c.1465C>T	p.(Arg489*)	arSLSN	[540]	NA	1 (1)	A389	[395, 543] NA [405] Italian [544] USA	Pathogenic (VCV000030778)
LCA5 locus	Mapped locus only; variant not identified	NA	arLCA	[545]	NA	1 (5)	No ID	No	Not listed
LCA5	c.643delC	p.(Leu215Tyrfs*11)	arLCA	[546]	remote area	1 (4)	BUIT-LA01	No	Not listed
LCA5	c.652C>G	p.(Arg218Gly)	EOIRD	[169]	NA	1 (4)	61058	No	Not listed
LCA5	c.1151delC	p.(Pro384Glnfs*18)	IRD/arLCA	[169, 305, 404, 547, 548]	Punjab; Northern Pakistan	6 (20)	PKRD078; 61078; MEP2; MEP4; MEP25; W12-2240	[548] Afgani	Pathogenic (VCV000000966)
LCA5	c.1550_1551delGA	p.(Arg517Ilefs*3)	arRP	This study	NA	1 (3)	Family 21 (61393)	No	Not listed
LCA9 locus	Mapped locus only; variant not identified	NA	IRD	[404]	Northern Pakistan	1 (9)	MEP34	No	Not listed
LRAT	c.196G>C	p.(Gly66Arg)	arRP	This study	Rawalpindi, Punjab	1 (3)	Family 19	No	Not listed
LRAT	c.418G>T	p.(Glu140*)	arRP	[169]	NA	1 (3)	61076	No	Not listed
LRAT	c.538A>T	p.(Lys180*)	arRP	[169]	NA	1	61120	No	Not listed
LRAT	c.541-15T>G	p.(?)	EOIRD	[549]	NA	1 (6)	61254	No	Not listed
LRP5	c.4268C>T	p.(Pro1423Leu)	IRD	[169]	NA	1 (2)	61169	No	Not listed
MERTK	c.718G>T	p.(Glu240*)	arRP	[169, 329]	Punjab	2 (4)	61173; PKRP173	No	Not listed
MERTK	c.2194C>T	p.(Arg732*)	IRD	This study	NA	1 (5)	Family 25 (61299)	[322] NA	Not listed
MKKS	c.119C>G	p.(Ser40*)	arBBS	[428]	Nawab Shah City, Sindh	1 (3)	Family E	No	Likely pathogenic (VCV000549478)
MKKS	c.287C>T	p.(Ala96Val)	arBBS	[550]	NA	1 (2)	Family B	No	Not listed
MKKS	c.775delA	p.(Thr259Leufs*21)	arBBS	[550]	NA	1 (2)	Family A	[551] NA	Not listed

MKS1	c.1450_1453dupGGCA	p.(Thr485Argfs*107)	arMKS	[442]	NA	4 (4)	102; 103; 244; 270	No	Not listed
MYO7A	c.252C>G	p.(Asn84Lys)	arUSH type1 B	[552]	NA	1	PKSK26	No	Not listed
MYO7A	c.397dupC	p.(His133Profs*7)	arUSH type 1	[342, 451]	NA	3 (5)	DEM289; DEM318; Family 5	[456] France [553, 554] Chinese [457] Maghreb	Likely pathogenic (VCV000043229)
MYO7A	c.399dupC	p.(Ile134Hisfs*6)	arUSH type1 B	[552]	NA	1	PKDF124	No	Not listed
MYO7A	c.471-1G>A	p.(?)	arUSH type1 B	[552]	NA	1	PKDF355	No	Likely pathogenic (VCV000557808)
MYO7A	c.496delG	p.(Glu166Argfs*5)	arUSH type1 B	[552]	NA	3	PKDF096; PKB01; PKDF189	[456] Italy	Pathogenic (VCV000043266)
MYO7A	c.640G>A	p.(Gly214Arg)	arUSH type1 B	[552]	NA	2	PKDF008; PKDF161	[456] France [555] NA [556] European [83] Morocco [557] Spain [558] North African Jewish	Pathogenic/ Likely pathogenic (VCV000043327)
MYO7A	c.721C>T	p.(Arg241Cys)	arUSH type1	[461]	NA	3 (26)	PKDF896 PKDF1079 PKDF1080	[553, 559] Chinese [560] England, Scotland	Likely pathogenic (VCV000438180)
MYO7A	c.745G>T	p.(Glu249*)	arUSH type 1	[451]	NA	1(1)	DEM279	No	Not listed
MYO7A	c.977T>A	p.(Leu326Gln)	arUSH type 1 B	[552]	NA	1	PKSR40A	[458] Indian	Likely pathogenic/ Uncertain significance (VCV000164664)
MYO7A	c.1309G>A	p.(Asp437Asn)	arUSH type1 B	[552]	NA	2	PKDF229; PKDF142	No	Not listed
MYO7A	c.1355T>C	p.(Leu452Pro)	arUSH type1 B	[461]	NA	1 (3)	PKDF803	No	Not listed
MYO7A	c.1591C>T	p.(Gln531*)	arUSH type 1 B	[552]	NA	1	PKDF137	No	Likely pathogenic (VCV000553105)
MYO7A	c.1935+1G>A	p.(?)	arUSH type 1 B	[552]	NA	1	PKDF290	No	Not listed
MYO7A	c.2476G>A	p.(Ala826Thr)	arUSH type 1 B	[552]	NA	1	PKDF140	[456] France [83] Algeria, Morocco [458] Caucasian [558] North African Jew	Uncertain significance (VCV000177732)
MYO7A	c.2695-9A>G	p.(?)	arUSH type 1 B	[461]	NA	1 (5)	PKDF771	[456] France [561] NA	Not listed
MYO7A	c.2914C>T	p.(Arg972*)	arUSH type 1 B	[552]	NA	1	PKDF164	[456] France, Spain [457] Maghreb [458] Iranian	Not listed
MYO7A	c.3136dupC	p.(Leu1046Profs*9)	arUSH type 1 B	[552]	NA	1	PKDF148	No	Not listed
MYO7A	c.3508G>A	p.(Glu1170Lys)	arUSH type 1 B	[552]	NA	2	PKDF045; PKDF449	[456] Spain [562] NA	Pathogenic/ Likely pathogenic (VCV000043208)
MYO7A	c.3631delT	p.(Tyr1211Thrfs*21)	arUSH type 1 B	[552]	NA	1	PKDF257	No	Not listed
MYO7A	c.4838delA	p.(Asp1613Valfs*32)	arUSH type 1 B	[552]	NA	1	PKSK12	No	Pathogenic (VCV000438178)
MYO7A	c.5366+1G>A	p.(?)	arUSH type 1 B	[552]	NA	1	PKDF426	No	Not listed
MYO7A	c.5899C>T	p.(Arg1967*)	arUSH type 1 B	[461]	NA	1 (4)	PKDF788	[456] NA	Pathogenic/ Likely pathogenic (VCV000178495)
MYO7A	c.5944G>A	p.(Gly1982Arg)	arUSH type 1 B	[552]	NA	2	PKDF078; PKSR55A	[456] Spain, France [454, 555, 561] NA [458] Caucasian	Pathogenic (VCV000500416)
NPHP4	c.3272dupT	p.(Ser1092Valfs*11)	arSLSN	[469]	NA	1 (1)	F1132	[395] NA	Not listed
NR2E3	c.227G>A	p.(Arg76Gln)	arRP	[169]	NA	1 (3)	61150	[354, 563, 564] NA	Uncertain significance (VCV00000

									5530)
NMNAT 1	c.25G>A	p.(Val9Met)	arLCA	[565, 566]	NA	2 (7)	Family 047; No ID	No	Pathogenic (VCV000037140)
NMNAT 1	c.838T>C	p.(*280Gln)	arLCA	[567]	NA	1 (8)	LCA9	No	Pathogenic (VCV000037132)
OAT	c.722C>T	p.(Pro241Leu)	IRD	This study	NA	1 (5)	Family 26 (61327)	[308] NA [323] German/Italian	Likely pathogenic (VCV000000168)
OAT locus	Mapped locus only; variant not identified	NA	IRD	[169]	NA	1	61125	No	Not listed
PCDH15	c.7C>T	p.(Arg3*)	arUSH type1F	[568]	NA	1 (5)	PKSR17	[454] NA [456] Spain	Pathogenic/ Likely pathogenic (VCV000004931)
PCDH15	c.1927C>T	p.(Arg643*)	arUSH type1	[89]	NA	1 (3)	PKDF139	No	Pathogenic (VCV000177724)
PCDH15	c.3389-2A>G	p.(?)	arUSH type1F	[568]	NA	1 (3)	PKSR8b	No	Not listed
PDE6A	c.304C>A	p.(Arg102Ser)	arRP	[321, 403]	Punjab	2 (8)	F12; PKRP360	[488, 569] NA	Likely pathogenic/ Uncertain significance (VCV000193099)
PDE6A	c.769C>T	p.(Arg257*)	arRP	[169, 321, 570]	Punjab; Punjab	2 (6)	61019; PKRP345; 61124	No	Pathogenic (VCV000437984)
PDE6A	c.1408-2A>G	p.(?)	IRD/RP	[169, 305, 321, 570]	Punjab	4 (18)	MA-132; 61140; 61074; PRPK140	No	Not listed
PDE6A	c.1630C>T	p.(Arg544Trp)	IRD	[389]	NA	1 (3)	RP55	No	Likely pathogenic (VCV000437982)
PDE6A	c.2028-1G>A	p.(?)	arRP	[169, 305]	Punjab; -	2 (5)	PKRP133; 61133	No	Not listed
PDE6A	c.2098dupT	p.(Tyr700Leufs*21)	arRP	[570]	Punjab	1 (3)	61021	No	Not listed
PDE6A locus	Mapped locus only; variant not identified	NA	arRP	[570]	Punjab	1 (4)	61081	No	Not listed
PDE6B	c.12_15delTGAG	p.(Ser4Argfs*23)	arRP/IRD	[321], This study	Punjab	2 (9)	PKRP336; Family 23 (61346)	No	Not listed
PDE6B	c.243delG	p.(Arg82Alafs*68)	arRP	[321]	Punjab	1 (4)	PKRP264	No	Not listed
PDE6B	c.1160C>T	p.(Pro387Leu)	arRP	[169, 571]	NA	2 (6)	PKRP183; 61183	No	Not listed
PDE6B	c.1655G>A	p.(Arg552Gln)	arRP	[169, 571]	NA	2 (9)	61161; PKRP161	[354] NA [572] Spanish	Not listed
PDE6B	c.1722+1G>A	p.(?)	arRP	[487]	NA	1	RP23	No	Not listed
PDE6C	c.1A>G	p.(Met1*)	IRD	This study	NA	1 (4)	Family 8 (61401)	No	Not listed
PDE6C	c.480delG	p.(Asn161Thrfs*33)	IRD	This study	Kohat Dist., KPK	1 (5)	Family 7	No	Not listed
PDE6H	c.35C>G	p.(Ser12*)	Incomplete ACHM	[573]	NA	1 (2)	No ID	[77] Belgium, The Netherlands [574] NA	Likely pathogenic (VCV000037245)
PLK4	c.2811-5C>G	p.(?)	developmental disorder + retina degeneration	[575]	KPK	1 (5)	Family 1	No	Pathogenic (VCV000162400)
PRCD	c.2T>C	p.(Met1Thr)	arRP	[169]	NA	1	61376	[576] Chinese	Pathogenic/ Uncertain significance (VCV000143095)
PROM1	c.1726C>T	p.(Gln576*)	IRD	[577]	Punjab	1 (6)	61037	No	Not listed
PROM1	c.1946C>T	p.(Ser649Leu)	IRD	[169]	NA	2 (6)	61237; 61267	No	Not listed
RBP3	c.3353_3354delCT	p.(Ser1118Cysfs*3)	arRP	[169]	NA	1 (4)	61217	No	Not listed
RDH5	c.536A>G	p.(Lys179Arg)	FA	[169, 578]	NA	3 (20)	Pedigree 1; 61198; 61199	No	Uncertain significance (VCV000236445)
RHD5	c.602C>T	p.(Ser201Phe)	arRP	[377, 579]	Lower Dir district, KPK	2 (3)	No ID; Patient 24	No	Not listed
RDH5	c.758T>G	p.(Met253Arg)	FA	[169, 580]	NA	3 (18)	61035; 61126; Family B	No	Not listed
RDH5	c.838C>G	p.(Arg280Gly)	IRD	This study	NA	1 (3)	Family 24 (61153)	No	Not listed

RDH5	c.913_917delGTGCT	p.(Val305Hisfs*29)	FA	[580]	NA	1 (2)	Family A	No	Not listed
RDH12	c.506G>A	p.(Arg169Gln)	arLCA/EOIRD	[581]	NA	2 (2)	Family 21; Family 16	[354] NA [582] Chinese	Likely pathogenic (VCV000623219)
RDH12	c.609C>A	p.(Ser203Arg)	IRD	[169]	Punjab?	1 (4)	61065	[581] Afghani, Saudi Arabian, Caucasian	Pathogenic (VCV000663830)
RDH12	c.619A>G	p.(Asn207Asp)	arLCA/EOIRD	[581]	NA	1 (2)	Family 19	No	Not listed
RGS9BP	c.94_102delGACTCGCAG	p.(Asp32_Gln34del)	Bradyopsia	[583]	NA	1 (2)	No ID	No	Not listed
RHO	c.448G>A	p.(Glu150Lys)	arRP; IRD	[174, 487]	Sindh	3 (4)	MA-62; RP21; RP53	No	Pathogenic (VCV000013046)
RLBP1	c.346G>C	p.(Gly116Arg)	FA	[169, 584]	NA	2 (4)	61107; PKRP107	No	Likely pathogenic (VCV000636197)
RLBP1	c.466C>T	p.(Arg156*)	FA	[169, 584]	Punjab	2 (6)	61064; PKRP064	No	Not listed
RP1	11,117 bp incl entire gene	Gene deletion	arRP	[585]	NA	1 (4)	PKRP358	No	Not listed
RP1	c.551_552dupTA	(p.Gln185Tyrfs*4)	arRP	[585]	NA	1 (4)	PKRP344	No	Not listed
RP1	c.787+1G>A	p.(?)	arRP	[169, 585]	NA	2 (6)	PKRP262; 61262	No	Not listed
RP1	c.1118C>T	p.(Thr373Ile)	arRP	[586]	NA	2 (11)	442RP; 452RP	[366, 587, 588] NA [479] Qatar [589] Saudi Arabia	Benign/ Likely benign (VCV000005970)
RP1	c.1126C>T	p.(Arg376*)	arRP	[169]	NA	1 (3)	61113	No	Not listed
RP1	c.1458_1461dupTGAA	p.(Glu488*)	arRP	[586, 590]	Punjab	2 (9)	336RP; 61040	No	Pathogenic (VCV000005971)
RP1	c.3697delT	p.(Ser1233Profs*22)	arRP	[169, 585]	Punjab	2 (9)	PKRP117; 61117	No	Not listed
RP1	c.4555delA	p.(Arg1519Glufs*2)	arRP	[590]	Punjab	1 (5)	61006	No	Pathogenic (VCV000197271)
RP1	c.5252delA	p.(Asn1751Ilefs*4)	arRP	[590]	Punjab	1 (4)	61043	No	Not listed
RP29 locus 4q32-q34	Mapped locus only; no variant identified	NA	arRP	[591]	NA	1 (6)	No ID	No	Not listed
RPE65	c.95-1G>A	p.(?)	IRD	[169, 592]	Punjab	2 (4)	61020; PKRP020	No	Not listed
RPE65	c.119G>A	p.(Gly40Asp)	IRD	[169]	NA	1 (2)	61231	No	Not listed
RPE65	c.131G>A	p.(Arg44Gln)	EORP	[403]	NA	1 (3)	F06	[307, 593] NA	Likely pathogenic (VCV000098840)
RPE65	c.179T>C	p.(Leu60Pro)	IRD	[169, 592]	NA	2 (4)	61160; PKRP160	[594] NA	Not listed
RPE65	c.361delT	p.(Ser121Leufs*6)	EOIRD/ EORP	[169, 403, 592]	NA	3 (7)	61235; PKRP235; F07	[595] Portugal	Not listed
RPE65	c.746A>G	p.(Tyr249Cys)	IRD	[359]	NA	1 (2)	RF.RA.0812	[375, 594, 596] NA	Not listed
RPE65	c.751G>T	p.(Val251Phe)	arLCA	[404]	Northern Pakistan	1 (6)	MEP55	No	Not listed
RPE65	c.782T>C	p.(Leu261Pro)	IRD	[169]	NA	1	61116	No	Not listed
RPE65	c.963T>G	p.(Asn321Lys)	IRD	[169]	NA	1	61116	No	Benign (VCV000092860)
RPE65	c.1087C>A	p.(Pro363Thr)	IRD	[169, 305]	Punjab	10 (25)	PKRD281; PKRD282; PKRD283; PKRD284; PKRD285; 61281; 61282; 61283; 61284; 61285.	[597, 598] NA	Pathogenic (VCV000013117)
RPE65	c.1451G>A	p.(Gly484Asp)	IRD	[359]	NA	1 (2)	RF.RA.0812	[375, 598-600] NA	Likely pathogenic (VCV000098848)
RPGR	c.310+1G>C	p.(?)	IRD	This study	NA	1 (4)	Family 22 (61337)	[319] NA [320] USA	Not provided (VCV000098779)
RPGR	c.2426_2427delCA	p.(Glu809*)	X-linked RP	[403]	NA	1 (8)	F13	No	Pathogenic (VCV000636109)

RPGRIP 1	c.587+1G>C	p.(?)	arLCA	[404]	Northern Pakistan	1	MEP1	No	Not listed
RPGRIP 1	c.930+1G>A	p.(?)	arLCA	[403]	NA	1 (1)	F5	No	Not listed
RPGRIP 1	c.932delA	p.(Asn311Ilefs*5)	arLCA	[169]	NA	1 (3)	61312	No	Not listed
RPGRIP 1	c.1180C>T	p.(Gln394*)	arLCA	[404]	Northern Pakistan	1	MEP43	No	Not listed
RPGRIP 1	c.2480G>T	p.(Arg827Ieu)	CRD/arLCA	[404, 601]	Northern Pakistan	2 (8)	1CRD; MEP50	No	Pathogenic (VCV00000 4986)
RPGRIP 1	c.2656C>T	p.(Leu886Phe)	IRD	[174]	NA	1 (2)	MA-117	No	Not listed
RPGRIP 1	c.2710G>A	p.(Gly904Ser)	IRD	This study	NA	1 (5)	Family 10 (61007)	No	Not listed
RPGRIP 1	c.2789dupT	p.(Pro931Thrfs*3)	IRD	This study	Pishin, Baluchistan	1 (2)	Family 9	No	Not listed
RPGRIP 1	c.3565C>T	p.(Arg1189*)	arLCA	[403]	NA	1 (2)	F04	[240] Saudi Arabia [307, 602] NA	Pathogenic (VCV00038 1684)
RPGRIP 1	c.3620T>G	p.(Leu1207*)	arLCA	[404]	Northern Pakistan	1	MEP3	No	Not listed
RPGRIP 1L	c.466C>T	p. (Arg156Cys)	arMKS	[442]	Gujarat	2(2)	36; 36A	No	Not listed
RPGRIP 1L	c.1945C>T	p. (Arg649*)	arMKS	[442]	NA	2 (2)	336; 207	No	Pathogenic (VCV00065 1948)
SAG	c.874C>T	p.(Arg292*)	IRD	[169]	NA	1	61324	[603] Japanese [322] NA	Pathogenic (VCV00004 1897)
SAG	c.916G>T	p.(Glu306*)	Oguchi type 1	[604]	NA	1 (1)	No ID	No	Pathogenic (VCV00004 1898)
SAG locus	Mapped locus only; variant not identified	NA	IRD	[169]	NA	1	61129	No	Not listed
SEMA4 A	c.1033G>C	p.(Asp345His)	adCRD	[187]	NA	4 (4)	No ID	No	Pathogenic (VCV00000 3360)
SEMA4 A	c.1049T>G	p.(Phe350Cys)	adCRD	[187]	NA	4 (4)	No ID	No	Pathogenic (VCV00000 3361)
SEMA4 A	c.2138G>A	p.(Arg713Gln)	adRP	[187]	NA	4 (4)	No ID	[188, 588] NA [589] Saudi Arabia	Benign/ Likely benign (VCV00000 3362)
SLC24A 1	c.1613 _1614delTT	p.(Phe538Cysfs* 23)	arCSNB	[169, 605]	South Punjab	2 (5)	PKRP07 0; 61070	No	Not listed
SNRNP 200	c.3269G>A	p.(Arg1090Gln)	arIRD	[518]	NA	1 (2)	Family G	No	Pathogenic (VCV00003 9746)
SPATA7	c.253C>T	p.(Arg85*)	arLCA/arIR D	[606]	NA	2 (3)	Family 1; Family 2	[607] NA	Likely pathogenic (VCV00003 0806)
SPATA7	c.960dupA	p.(Pro321Thrfs*6)	arLCA/arIR D	[606]	NA	1 (6)	Family 4	[608] Middle Eastern	Pathogenic (VCV00000 1396)
TCTN2	c.1873C>T	p.(Gln625*)	arJBTS	[609]	NA	1 (4)	MR20	No	Pathogenic (VCV00021 8100)
TMEM6 7	c.274G>A	p.(Gly92Arg)	arMKS	[442]	NA	1 (1)	C28	[610] NA	Uncertain significance (VCV00021 9997)
TMEM6 7	c.648delA	p.(Val217Leufs*5)	arMKS	[442, 611]	NA	2 (3)	67FB; 67F	No	Not listed
TMEM6 7	c.870-2A>G	p.(?)	arMKS	[442, 611]	Mirpur, Azad Kashmir.	2 (2)	73; 51	No	Not listed
TMEM6 7	c.1127A>C	p.(Gln376Pro)	arMKS	[442, 611]	NA	3 (3)	P95; 40T; No ID	No	Not listed
TMEM6 7	c.1321C>T	p.(Arg441Cys)	arMKS	[442]	NA	1 (1)	347	[145, 612] NA	Not listed
TMEM6 7	c.1575+1G>A	p.(?)	arMKS	[442, 611]	Mirpur, Azad Kashmir.	4 (5)	77117; 76; 70; 29A; 33A	No	Not listed
TMEM6 7	c.1645C>T	p.(Arg549Cys)	arMKS	[442]	Mirpur, Azad Kashmir.	1	178	[613, 614] China [615] USA	Not listed
TMEM1 38	c.287A>G	p.(His96Arg)	arMKS	[442]	NA	2	42; 43	No	Likely pathogenic (VCV00003 1188)
TRNT1	c.569G>T	p.(Arg190Ile)	RP?	[616]	NA	1 (1)	P3	No	Pathogenic (VCV00015 7613)
TTC8	c.115-2A>G	p.(?)	arRP	[169, 617]	South Punjab	2 (4)	61179; PKRP17 9	No	Pathogenic (VCV00000 2532)
TTC8	c.235+1G>A	p.(?)	arBBS	[618]	NA	1 (2)	61/178	[619] NA	Not listed
TTC8	c.768+5G>A	p.(?)	IRD	This study	Lahore	1 (3)	Family 15	No	Not listed
TTC8	c.1019+2_1019+4de l	p.(?)	arBBS	[120, 425]	NA	2 (5)	A2827; BB12	No	Not listed

TTC8	c.1347G>C	p.(Gln449His)	arBBS	[428]	KPK	1 (3)	Family C	No	Pathogenic (VCV000235131)
TTPA locus	Mapped locus only; variant not identified	NA	IRD	[169]	NA	1	61147	No	Not listed
TULP1	c.238C>T	p.(Gln80*)	IRD	This study	Kohat Dist., KPK	1 (5)	Family 7	No	Not listed
TULP1	c.287_288delGA	p.(Glu96Glyfs*77)	IRD	[168]	NA	1 (6)	PKRP364	No	Not listed
TULP1	c.855dupC	p.(Val286Argfs*98)	arRP	This study	Lahore	1 (1)	Family 6	[312] NA	Likely pathogenic (VCV000505327)
TULP1	c.1138A>G	p.(Thr380Ala)	arRP/arLCA	[169, 404, 620, 621]	Northern Pakistan, Punjab	5 (32)	MEP51; 61206; 61063; PKRP063; FamilyA	No	Not listed
TULP1	c.1445G>A	p.(Arg482Gln)	arRP	[620]	NA	1 (6)	Family B	No	Not listed
TULP1	c.1466A>G	p.(Lys489Arg)	arRP/EORP	[168, 169, 403, 621]	Punjab	15 (40)	F11; PKRP301; PKRP309; PKRP356: PKRP367; 61084; 61111; 61122; 61171; 61301; 61309; PKRP122; PKRP171; PKRP111 PKRP084	[622] Sardinian	Not provided (VCV000099663)
TULP1	c.1495+4A>C	p.(?)	IRD	[168, 169]	NA	2 (4)	61268; PKRP268	No	Not listed
TULP1	c.1561C>T	p.(Pro521Ser)	arRP	[168, 169]	NA	2 (3)	61259; PKRP259	No	Not listed
USH1C	c.238dupC	p.(Arg80Profs*69)	arUSH type1C	[623, 624]	NA	2 (4)	No ID; Family 3	[456] France, Italy, Slovenia [457] Maghreb	Pathogenic (VCV000005141)
USH1G	c.163_164+13del	p.(?)	arUSH type1G	[625]	Sheikhupura, Punjab.	1 (4)	HLRB12	No	Not listed
USH1G	c.1373A>T	p.(Asp458Val)	arUSH type1G	[451]	NA	1 (1)	DEM74	[626] Turkish [312] NA	Likely pathogenic (VCV000048127)
USH1H locus 15q22-23	Mapped locus only; no variant identified	NA	arUSH type1H	[627]	Punjab	2 (9)	PKDF125; PKDF117	No	Not listed
USH1K locus 10p11.21-q21.1	Mapped locus only; no variant identified	NA	arUSH type1K	[628]	Punjab	2 (10)	PKDF231; PKDF608	No	Not listed
USH2A	c.4645C>T	p.(Arg1549*)	IRD	[169, 305]	Punjab	1 (3)	PKRD141; 61141	[47, 354, 629] NA [630] Northern Ireland [631] Han Chinese [456] Slovenia	Pathogenic (VCV000504513)
USH2A	c.5740C>T	p.(Gln1914*)	RP/IRD	[169]	NA	1 (8)	61191	No	Not listed
USH2A	c.7334C>T	p.(Ser2445Phe)	arUSH type 2A	This study	Karak Dist., KPK	1 (3)	Family 17	[315] NA	Uncertain significance/ Benign (VCV000048581)
USH2A	c.11473delC	p.(His3825Ilefs*10)	IRD	[169, 305]	Punjab	2 (5)	PKRD138; 61138	No	Not listed
USH2A	c.12523T>G	p.(Trp4175Gly)	IRD/RP	[169, 305]	Punjab	2 (5)	PKRP185; 61185	No	Not listed
USH2A locus	Mapped locus only; no variant identified	NA	RP/IRD	[169]	NA	1	61151	No	Not listed
WDR60	c.44delC	p.(Ala15Glufs*90)	retinal degeneration and postaxial polydactyly+ BBS	[632]	NA	1 (2)	No ID	No	Not listed
ZNF408	c.1304G>A	p.(Arg435Gln)	IRD	[439]	Punjab	1 (3)	PKRD320	No	Not listed

ZNF513	c.1015T>C	p.(Cys339Arg)	arRP	[192]	NA	1 (4)	61115	No	Uncertain significance (VCV000000028)

Abbreviations: ACHM, achromatopsia; ad, autosomal dominant; ar, autosomal recessive; BBS, Bardet-Biedl syndrome; CRD, cone-rod dystrophy; CSNB, Congenital stationary night blindness; Dist., District; EEM, Ectodermal dysplasia, ectrodactyly, and macular dystrophy; EOIRD, Early-onset inherited retinal dystrophy; EORP, Early-onset retinitis pigmentosa; FA, fundus albipunctatus; JBTS, Joubert syndrome; ID; identifier; IRD, inherited retinal dystrophies; LCA, Leber congenital amaurosis; MKS, Meckel syndrome; MORM, mental retardation, truncal obesity, retinal dystrophy, and micropenis; NA, not available; RP, Retinitis Pigmentosa; SLSN, Senior-Loken syndrome; UK, United Kingdom; USA, United States of America; USH, Usher syndrome; KPK, Khyber Pakhtunkhwa.

APPENDIX E

Media 1

Description: Time-lapse movie of wild type SH-SY5Y cell expressing mCherry-KDEL and EGFP-SigmaR1. Images were captured with a 63x oil immersion objective, for 100 frames, every 7 sec.

File name: control_SigmaR1_KDEL

Media 2

Description: Time-lapse movie of *CLCC1* $^{-/-}$ KO cell (SH-SY5Y) expressing mCherry-KDEL and EGFP-SigmaR1. Images were captured with a 63x oil immersion objective, for 80 frames, every 7 sec.

File name: CLCC1knockout_SigmaR1_KDEL

Media 3

Description: Time-lapse movie of wild type cell expressing mCherry-KDEL and EGFP-SigmaR1 and treated with DMSO for 30 min. Images were captured with a 63x oil immersion objective, for 80 frames, every 7 sec.

File name: Control_SigmaR1_KDEL_PRE084

Media 4

Description: Time-lapse movie of *CLCC1* $^{-/-}$ KO cell expressing mCherry-KDEL and EGFP-SigmaR1, and treated with PRE-084 for 30 min. Images were captured with a 63x oil immersion objective, for 80 frames, every 7 sec.

File name: CLCC1knockout_SigmaR1_KDEL_PRE084

Media 5

Description: Time-lapse movie of wild type cell expressing mCherry-KDEL and EGFP-SigmaR1, and treated with BD1047 for 30 min. Images were captured with a 63x oil immersion objective, for 80 frames, every 7 sec.

File name: Control_SigmaR1_KDEL_BD1047

Media 6

Description: Time-lapse movie of *CLCC1* $^{-/-}$ KO cell expressing mCherry-KDEL and EGFP-SigmaR1, and treated with BD1047 for 30 min. Images were captured with a 63x oil immersion objective, for #### frames, every 7 sec.

File name: CLCC1knockout_SigmaR1_KDEL_BD1047

APPENDIX F

Table of primers used for genotyping the families

Primer	Primer sequences
ABCA4 c.3364G>A	*For:* CTTGCGCACCAAGGTTAAGT *Rev:* TGAATTAGTTCCCTTGGGTTTT
BBS4 c.221-1G>A	*For:* TCTGACCCCAGGCTCCAT *Rev:* TGGACCTAGGAATGCATTTTACA
CACNA1F c.2254G>A	*For:* CCAGGGTGACTAGAGGCATC *Rev*: ATATGGTGGCCCCTTCTTCC
CNGA3 c.1443dup	*For:* CCAACAAGAAGACGGTGGAT *Rev:* TTGCCCTCGTTGATGATGTA
CNGA3 c.955T>C	*For:* GATGTGTTGTCCCTGGTCCC *Rev:* TCAATCTTGGCCTGGAACTCT
CNGA3 c.1556T>C	*For:* AAGGTTCGCATCTTCCAGGA *Rev:* TGCTCCCCTTGATGTTCAGA
CNGA3 c.1600G>A	*For:* ATCTTCCAGGACTGTGAGGC *Rev:* CTTTGAGAGGCAGAACAGGTC
CNGB1 c.852_874+25del	*For:* AGAGCATGGGGCTCTCTCAG *Rev:* CCCCACCTCAAATCCTTCAT
CRB1 c.3735delA	*For:* CCTGGATACACTGGTGTGAACT *Rev:* TCCCATCTGAACATGACCAA
GUCY2D c.3056A>C	*For:* CATCTCCACAGGTCCATGC *Rev:* GTCAGAAGGGTGAGCTGAGG
LRAT c.196G>C	*For:* AGAAGCTGCTCCTCATCTCC *Rev:* GATGCTGGCCACTTTGACAA
PDE6C c.480delG	*For:* TAGGTTGCTGGATGTCACCC Rev: GTGATCCTCTTCCCTGCCAC
RPGRIP1 c.2789dup	*For:* GGTGATTTTAACCTCACTGACC *Rev:* CTCCTTCAAATCTGCTCCATA
TTC8 c.768+5G>A	*For:* AAGCAGAAAAACAGTTTAAATCAGC *Rev*: GACAGTTACCCTCTATACGTTCTCA
TULP1 c.855dupC	*For:* CCACACTCCCTCCTCTGCT *Rev:* CTGCTCTAGCCAGCCTCTCT
TULP1 c.238C>T	*For:* CCAGCCCCTTCTCTCCTTAG *Rev:* AGTGTTGAAAGTGGAAACCCA
USH2A c.7334C>T	*For:* CCCAGCTGATAGAATGGACAA *Rev:* CAGGAGTTCAGGAATGAAAATG

APPENDIX G

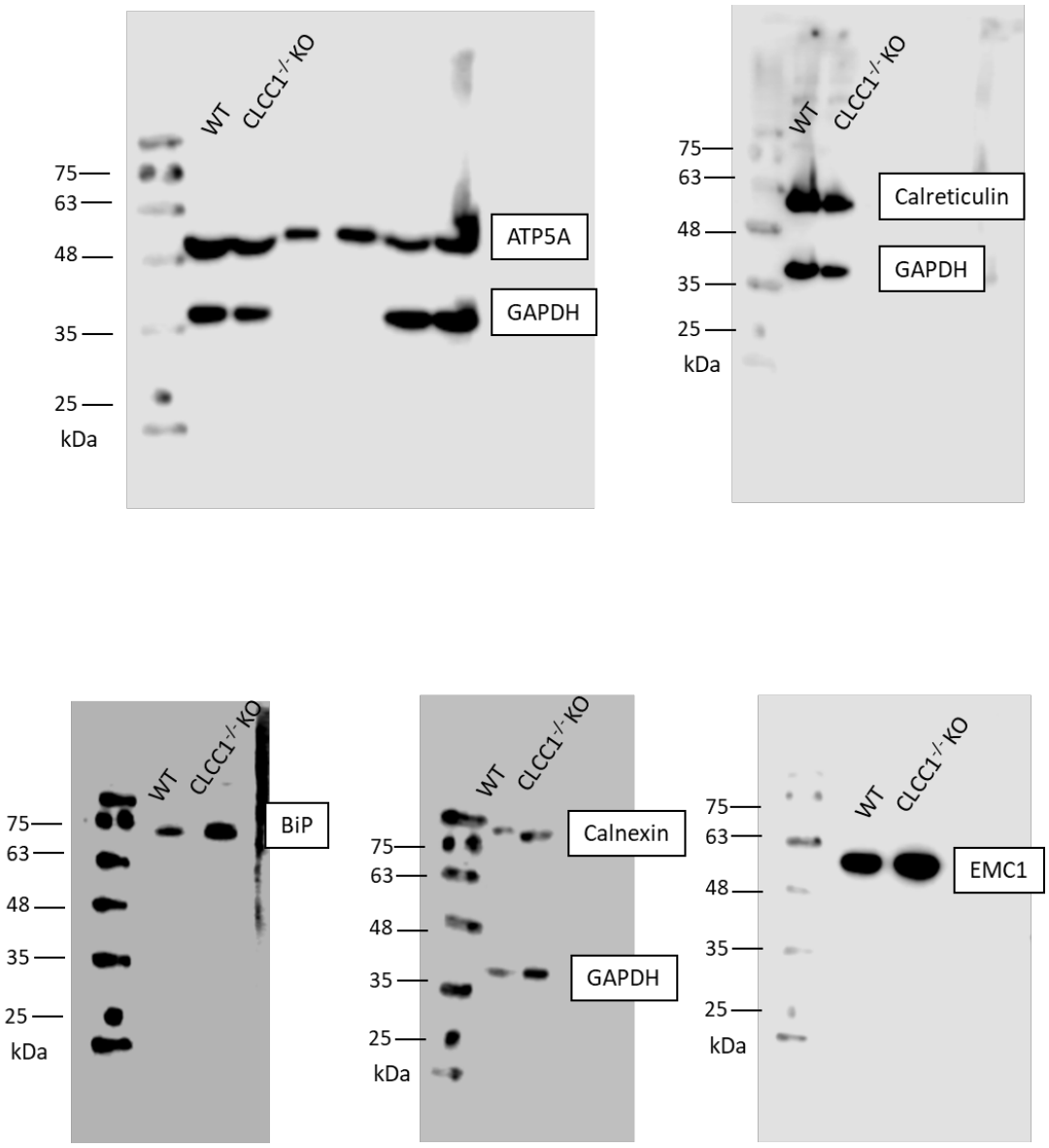

Figure 1 Whole western blots showing fractionation of ER proteins in WT and CLCC1$^{+/-}$ KO cells. *Cropped images are shown in Figure 4.39.*

REFERENCES

1. Yun, S., et al., *Lhx2 links the intrinsic and extrinsic factors that control optic cup formation.* Development, 2009. **136**(23): p. 3895-906.
2. Zagozewski, J.L., Q. Zhang, and D.D. Eisenstat, *Genetic regulation of vertebrate eye development.* Clin Genet, 2014. **86**(5): p. 453-60.
3. Loosli, F., et al., *Loss of eyes in zebrafish caused by mutation of chokh/rx3.* EMBO Rep, 2003. **4**(9): p. 894-9.
4. Voronina, V.A., et al., *Mutations in the human RAX homeobox gene in a patient with anophthalmia and sclerocornea.* Hum Mol Genet, 2004. **13**(3): p. 315-22.
5. Heavner, W. and L. Pevny, *Eye development and retinogenesis.* Cold Spring Harb Perspect Biol, 2012. **4**(12).
6. Fuhrmann, S., *Eye morphogenesis and patterning of the optic vesicle.* Curr Top Dev Biol, 2010. **93**: p. 61-84.
7. Cavodeassi, F., *Dynamic Tissue Rearrangements during Vertebrate Eye Morphogenesis: Insights from Fish Models.* J Dev Biol, 2018. **6**(1).
8. Amram, B., et al., *The retinal pigmented epithelium - from basic developmental biology research to translational approaches.* Int J Dev Biol, 2017. **61**(3-4-5): p. 225-234.
9. Nguyen, M. and H. Arnheiter, *Signaling and transcriptional regulation in early mammalian eye development: a link between FGF and MITF.* Development, 2000. **127**(16): p. 3581-91.
10. Pittack, C., G.B. Grunwald, and T.A. Reh, *Fibroblast growth factors are necessary for neural retina but not pigmented epithelium differentiation in chick embryos.* Development, 1997. **124**(4): p. 805-16.
11. Livesey, F.J. and C.L. Cepko, *Vertebrate neural cell-fate determination: lessons from the retina.* Nat Rev Neurosci, 2001. **2**(2): p. 109-18.
12. Boije, H., R.B. MacDonald, and W.A. Harris, *Reconciling competence and transcriptional hierarchies with stochasticity in retinal lineages.* Curr Opin Neurobiol, 2014. **27**: p. 68-74.
13. Lamb, T.D., *Why rods and cones?* Eye (Lond), 2016. **30**(2): p. 179-85.
14. Amini, R., M. Rocha-Martins, and C. Norden, *Neuronal Migration and Lamination in the Vertebrate Retina.* Front Neurosci, 2017. **11**: p. 742.
15. Masland, R.H., *The neuronal organization of the retina.* Neuron, 2012. **76**(2): p. 266-80.
16. Reese, B.E., *Development of the retina and optic pathway.* Vision Res, 2011. **51**(7): p. 613-32.
17. Helmstaedter, M., et al., *Connectomic reconstruction of the inner plexiform layer in the mouse retina.* Nature, 2013. **500**(7461): p. 168-74.
18. Wallace, V.A., *Concise review: making a retina--from the building blocks to clinical applications.* Stem Cells, 2011. **29**(3): p. 412-7.
19. Zhang, C., et al., *Establishing Wiring Specificity in Visual System Circuits: From the Retina to the Brain.* Annu Rev Neurosci, 2017. **40**: p. 395-424.
20. Sung, C.H. and J.Z. Chuang, *The cell biology of vision.* J Cell Biol, 2010. **190**(6): p. 953-63.
21. Curcio, C.A., et al., *Human photoreceptor topography.* J Comp Neurol, 1990. **292**(4): p. 497-523.

22. Shichida, Y. and T. Matsuyama, *Evolution of opsins and phototransduction.* Philos Trans R Soc Lond B Biol Sci, 2009. **364**(1531): p. 2881-95.
23. Chen, C.K., et al., *Abnormal photoresponses and light-induced apoptosis in rods lacking rhodopsin kinase.* Proc Natl Acad Sci U S A, 1999. **96**(7): p. 3718-22.
24. Xu, J., et al., *Prolonged photoresponses in transgenic mouse rods lacking arrestin.* Nature, 1997. **389**(6650): p. 505-9.
25. Kawamura, S. and S. Tachibanaki, *Rod and cone photoreceptors: molecular basis of the difference in their physiology.* Comp Biochem Physiol A Mol Integr Physiol, 2008. **150**(4): p. 369-77.
26. Liu, J., et al., *The biosynthesis of A2E, a fluorophore of aging retina, involves the formation of the precursor, A2-PE, in the photoreceptor outer segment membrane.* J Biol Chem, 2000. **275**(38): p. 29354-60.
27. Haeseleer, F., et al., *Molecular characterization of a novel short-chain dehydrogenase/reductase that reduces all-trans-retinal.* J Biol Chem, 1998. **273**(34): p. 21790-9.
28. Wu, Q., et al., *Interphotoreceptor retinoid-binding protein is the physiologically relevant carrier that removes retinol from rod photoreceptor outer segments.* Biochemistry, 2007. **46**(29): p. 8669-79.
29. Bunt-Milam, A.H. and J.C. Saari, *Immunocytochemical localization of two retinoid-binding proteins in vertebrate retina.* J Cell Biol, 1983. **97**(3): p. 703-12.
30. Okajima, T.I., et al., *Retinoid processing in retinal pigment epithelium of toad (Bufo marinus).* J Biol Chem, 1994. **269**(35): p. 21983-9.
31. Ala-Laurila, P., et al., *Visual cycle: Dependence of retinol production and removal on photoproduct decay and cell morphology.* J Gen Physiol, 2006. **128**(2): p. 153-69.
32. Saari, J.C., L. Bredberg, and G.G. Garwin, *Identification of the endogenous retinoids associated with three cellular retinoid-binding proteins from bovine retina and retinal pigment epithelium.* J Biol Chem, 1982. **257**(22): p. 13329-33.
33. Saari, J.C. and D.L. Bredberg, *Lecithin:retinol acyltransferase in retinal pigment epithelial microsomes.* J Biol Chem, 1989. **264**(15): p. 8636-40.
34. Deigner, P.S., et al., *Membranes as the energy source in the endergonic transformation of vitamin A to 11-cis-retinol.* Science, 1989. **244**(4907): p. 968-71.
35. Redmond, T.M., et al., *Rpe65 is necessary for production of 11-cis-vitamin A in the retinal visual cycle.* Nat Genet, 1998. **20**(4): p. 344-51.
36. Mata, N.L., et al., *Rpe65 is a retinyl ester binding protein that presents insoluble substrate to the isomerase in retinal pigment epithelial cells.* J Biol Chem, 2004. **279**(1): p. 635-43.
37. Jin, M., et al., *Rpe65 is the retinoid isomerase in bovine retinal pigment epithelium.* Cell, 2005. **122**(3): p. 449-59.
38. Saari, J.C., et al., *Visual cycle impairment in cellular retinaldehyde binding protein (CRALBP) knockout mice results in delayed dark adaptation.* Neuron, 2001. **29**(3): p. 739-48.
39. Simon, A., et al., *The retinal pigment epithelial-specific 11-cis retinol dehydrogenase belongs to the family of short chain alcohol dehydrogenases.* J Biol Chem, 1995. **270**(3): p. 1107-12.

40. Driessen, C.A., et al., *Cloning and expression of a cDNA encoding bovine retinal pigment epithelial 11-cis retinol dehydrogenase.* Invest Ophthalmol Vis Sci, 1995. **36**(10): p. 1988-96.
41. Crouch, R.K., et al., *Interphotoreceptor retinoid-binding protein and alpha-tocopherol preserve the isomeric and oxidation state of retinol.* Photochem Photobiol, 1992. **56**(2): p. 251-5.
42. Jones, G.J., et al., *Retinoid Requirements for Recovery of Sensitivity after Visual-Pigment Bleaching in Isolated Photoreceptors.* Proceedings of the National Academy of Sciences of the United States of America, 1989. **86**(23): p. 9606-9610.
43. Broadgate, S., et al., *Unravelling the genetics of inherited retinal dystrophies: Past, present and future.* Prog Retin Eye Res, 2017. **59**: p. 53-96.
44. Hartong, D.T., E.L. Berson, and T.P. Dryja, *Retinitis pigmentosa.* Lancet, 2006. **368**(9549): p. 1795-809.
45. Karali, M. and S. Banfi, *Inherited Retinal Dystrophies: the role of gene expression regulators.* Int J Biochem Cell Biol, 2015. **61**: p. 115-9.
46. Ding, H.J., et al., *Hydroxychloroquine-related retinal toxicity.* Rheumatology (Oxford), 2016. **55**(6): p. 957-67.
47. Bravo-Gil, N., et al., *Unravelling the genetic basis of simplex Retinitis Pigmentosa cases.* Sci Rep, 2017. **7**: p. 41937.
48. Li, Z.Y., D.E. Possin, and A.H. Milam, *Histopathology of bone spicule pigmentation in retinitis pigmentosa.* Ophthalmology, 1995. **102**(5): p. 805-16.
49. Daiger, S.P., L.S. Sullivan, and S.J. Bowne, *Genes and mutations causing retinitis pigmentosa.* Clin Genet, 2013. **84**(2): p. 132-41.
50. Farrar, G.J., et al., *Autosomal dominant retinitis pigmentosa: absence of the rhodopsin proline----histidine substitution (codon 23) in pedigrees from Europe.* Am J Hum Genet, 1990. **47**(6): p. 941-5.
51. Sullivan, L.S., et al., *Prevalence of disease-causing mutations in families with autosomal dominant retinitis pigmentosa: a screen of known genes in 200 families.* Invest Ophthalmol Vis Sci, 2006. **47**(7): p. 3052-64.
52. Athanasiou, D., et al., *The molecular and cellular basis of rhodopsin retinitis pigmentosa reveals potential strategies for therapy.* Prog Retin Eye Res, 2018. **62**: p. 1-23.
53. Ferrari, S., et al., *Retinitis pigmentosa: genes and disease mechanisms.* Curr Genomics, 2011. **12**(4): p. 238-49.
54. Sullivan, L.S., et al., *Prevalence of mutations in eyeGENE probands with a diagnosis of autosomal dominant retinitis pigmentosa.* Invest Ophthalmol Vis Sci, 2013. **54**(9): p. 6255-61.
55. Xu, Y., et al., *Mutations of 60 known causative genes in 157 families with retinitis pigmentosa based on exome sequencing.* Hum Genet, 2014. **133**(10): p. 1255-71.
56. Huang, L., et al., *Mutation screening in genes known to be responsible for Retinitis Pigmentosa in 98 Small Han Chinese Families.* Sci Rep, 2017. **7**(1): p. 1948.
57. Sharon, D. and E. Banin, *Nonsyndromic retinitis pigmentosa is highly prevalent in the Jerusalem region with a high frequency of founder mutations.* Mol Vis, 2015. **21**: p. 783-92.
58. Chiang, J.P.W., et al., *Development of High-Throughput Clinical Testing of RPGR ORF15 Using a Large Inherited Retinal Dystrophy Cohort.* Invest Ophthalmol Vis Sci, 2018. **59**(11): p. 4434-4440.

59. Kajiwara, K., E.L. Berson, and T.P. Dryja, *Digenic retinitis pigmentosa due to mutations at the unlinked peripherin/RDS and ROM1 loci.* Science, 1994. **264**(5165): p. 1604-8.
60. Perrault, I., et al., *Spectrum of NPHP6/CEP290 mutations in Leber congenital amaurosis and delineation of the associated phenotype.* Hum Mutat, 2007. **28**(4): p. 416.
61. Wan, L., et al., *A new novel nonsense mutation in AIPL1 in a LCA4 family.* Ophthalmic Genet, 2019. **40**(4): p. 380-384.
62. Kumaran, N., et al., *Leber congenital amaurosis/early-onset severe retinal dystrophy: clinical features, molecular genetics and therapeutic interventions.* Br J Ophthalmol, 2017. **101**(9): p. 1147-1154.
63. Yucel-Yilmaz, D., et al., *Genome-wide homozygosity mapping in families with leber congenital amaurosis identifies mutations in AIPL1 and RDH12 genes.* DNA Cell Biol, 2014. **33**(12): p. 876-83.
64. Chacon-Camacho, O.F. and J.C. Zenteno, *Review and update on the molecular basis of Leber congenital amaurosis.* World J Clin Cases, 2015. **3**(2): p. 112-24.
65. Zeitz, C., A.G. Robson, and I. Audo, *Congenital stationary night blindness: an analysis and update of genotype-phenotype correlations and pathogenic mechanisms.* Prog Retin Eye Res, 2015. **45**: p. 58-110.
66. He, S., et al., *Retinitis Pigmentosa GTPase Regulator (RPGR) protein isoforms in mammalian retina: insights into X-linked Retinitis Pigmentosa and associated ciliopathies.* Vision Res, 2008. **48**(3): p. 366-76.
67. Mavlyutov, T.A., H. Zhao, and P.A. Ferreira, *Species-specific subcellular localization of RPGR and RPGRIP isoforms: implications for the phenotypic variability of congenital retinopathies among species.* Hum Mol Genet, 2002. **11**(16): p. 1899-907.
68. Hamel, C.P., *Cone rod dystrophies.* Orphanet J Rare Dis, 2007. **2**: p. 7.
69. Kohl, S., et al., *Mutations in the CNGB3 gene encoding the beta-subunit of the cone photoreceptor cGMP-gated channel are responsible for achromatopsia (ACHM3) linked to chromosome 8q21.* Hum Mol Genet, 2000. **9**(14): p. 2107-16.
70. Wissinger, B., et al., *CNGA3 mutations in hereditary cone photoreceptor disorders.* Am J Hum Genet, 2001. **69**(4): p. 722-37.
71. Kohl, S., et al., *Mutations in the cone photoreceptor G-protein alpha-subunit gene GNAT2 in patients with achromatopsia.* Am J Hum Genet, 2002. **71**(2): p. 422-5.
72. Aligianis, I.A., et al., *Mapping of a novel locus for achromatopsia (ACHM4) to 1p and identification of a germline mutation in the alpha subunit of cone transducin (GNAT2).* J Med Genet, 2002. **39**(9): p. 656-60.
73. Xu, M., et al., *ATF6 Is Mutated in Early Onset Photoreceptor Degeneration With Macular Involvement.* Invest Ophthalmol Vis Sci, 2015. **56**(6): p. 3889-95.
74. Kohl, S., et al., *Mutations in the unfolded protein response regulator ATF6 cause the cone dysfunction disorder achromatopsia.* Nat Genet, 2015. **47**(7): p. 757-65.
75. Ansar, M., et al., *Mutation of ATF6 causes autosomal recessive achromatopsia.* Hum Genet, 2015. **134**(9): p. 941-50.
76. Thiadens, A.A., et al., *Homozygosity mapping reveals PDE6C mutations in patients with early-onset cone photoreceptor disorders.* Am J Hum Genet, 2009. **85**(2): p. 240-7.

77. Kohl, S., et al., *A nonsense mutation in PDE6H causes autosomal-recessive incomplete achromatopsia.* Am J Hum Genet, 2012. **91**(3): p. 527-32.
78. Tanna, P., et al., *Stargardt disease: clinical features, molecular genetics, animal models and therapeutic options.* Br J Ophthalmol, 2017. **101**(1): p. 25-30.
79. Boughman, J.A., M. Vernon, and K.A. Shaver, *Usher syndrome: definition and estimate of prevalence from two high-risk populations.* J Chronic Dis, 1983. **36**(8): p. 595-603.
80. Kimberling, W.J., et al., *Frequency of Usher syndrome in two pediatric populations: Implications for genetic screening of deaf and hard of hearing children.* Genet Med, 2010. **12**(8): p. 512-6.
81. Kimberling, W.J., et al., *Linkage of Usher syndrome type I gene (USH1B) to the long arm of chromosome 11.* Genomics, 1992. **14**(4): p. 988-94.
82. Smith, R.J., et al., *Localization of two genes for Usher syndrome type I to chromosome 11.* Genomics, 1992. **14**(4): p. 995-1002.
83. Adato, A., et al., *Mutation profile of all 49 exons of the human myosin VIIA gene, and haplotype analysis, in Usher 1B families from diverse origins.* Am J Hum Genet, 1997. **61**(4): p. 813-21.
84. Ouyang, X.M., et al., *Mutations in the alternatively spliced exons of USH1C cause non-syndromic recessive deafness.* Hum Genet, 2002. **111**(1): p. 26-30.
85. Ahmed, Z.M., et al., *Nonsyndromic recessive deafness DFNB18 and Usher syndrome type IC are allelic mutations of USHIC.* Hum Genet, 2002. **110**(6): p. 527-31.
86. Verpy, E., et al., *A defect in harmonin, a PDZ domain-containing protein expressed in the inner ear sensory hair cells, underlies Usher syndrome type 1C.* Nat Genet, 2000. **26**(1): p. 51-5.
87. Alagramam, K.N., et al., *The mouse Ames waltzer hearing-loss mutant is caused by mutation of Pcdh15, a novel protocadherin gene.* Nat Genet, 2001. **27**(1): p. 99-102.
88. Alagramam, K.N., et al., *Mutations in the novel protocadherin PCDH15 cause Usher syndrome type 1F.* Hum Mol Genet, 2001. **10**(16): p. 1709-18.
89. Ahmed, Z.M., et al., *PCDH15 is expressed in the neurosensory epithelium of the eye and ear and mutant alleles are responsible for both USH1F and DFNB23.* Hum Mol Genet, 2003. **12**(24): p. 3215-23.
90. Wayne, S., et al., *Localization of the Usher syndrome type ID gene (Ush1D) to chromosome 10.* Hum Mol Genet, 1996. **5**(10): p. 1689-92.
91. Bolz, H., et al., *Mutation of CDH23, encoding a new member of the cadherin gene family, causes Usher syndrome type 1D.* Nat Genet, 2001. **27**(1): p. 108-12.
92. Bork, J.M., et al., *Usher syndrome 1D and nonsyndromic autosomal recessive deafness DFNB12 are caused by allelic mutations of the novel cadherin-like gene CDH23.* Am J Hum Genet, 2001. **68**(1): p. 26-37.
93. Mustapha, M., et al., *A novel locus for Usher syndrome type I, USH1G, maps to chromosome 17q24-25.* Hum Genet, 2002. **110**(4): p. 348-50.
94. Weil, D., et al., *Usher syndrome type I G (USH1G) is caused by mutations in the gene encoding SANS, a protein that associates with the USH1C protein, harmonin.* Hum Mol Genet, 2003. **12**(5): p. 463-71.

95. Riazuddin, S., et al., *Alterations of the CIB2 calcium- and integrin-binding protein cause Usher syndrome type 1J and nonsyndromic deafness DFNB48.* Nat Genet, 2012. **44**(11): p. 1265-71.
96. Ahmed, Z.M., et al., *Inframe deletion of human ESPN is associated with deafness, vestibulopathy and vision impairment.* J Med Genet, 2018. **55**(7): p. 479-488.
97. Kimberling, W.J., et al., *Localization of Usher syndrome type II to chromosome 1q.* Genomics, 1990. **7**(2): p. 245-9.
98. Eudy, J.D., et al., *Mutation of a gene encoding a protein with extracellular matrix motifs in Usher syndrome type IIa.* Science, 1998. **280**(5370): p. 1753-7.
99. Weston, M.D., et al., *Genomic structure and identification of novel mutations in usherin, the gene responsible for Usher syndrome type IIa.* Am J Hum Genet, 2000. **66**(4): p. 1199-210.
100. Weston, M.D., et al., *Mutations in the VLGR1 gene implicate G-protein signaling in the pathogenesis of Usher syndrome type II.* Am J Hum Genet, 2004. **74**(2): p. 357-66.
101. Ebermann, I., et al., *A novel gene for Usher syndrome type 2: mutations in the long isoform of whirlin are associated with retinitis pigmentosa and sensorineural hearing loss.* Hum Genet, 2007. **121**(2): p. 203-11.
102. Mathur, P. and J. Yang, *Usher syndrome: Hearing loss, retinal degeneration and associated abnormalities.* Biochim Biophys Acta, 2015. **1852**(3): p. 406-20.
103. Joensuu, T., et al., *Mutations in a novel gene with transmembrane domains underlie Usher syndrome type 3.* Am J Hum Genet, 2001. **69**(4): p. 673-84.
104. Puffenberger, E.G., et al., *Genetic mapping and exome sequencing identify variants associated with five novel diseases.* PLoS One, 2012. **7**(1): p. e28936.
105. Eisenberger, T., et al., *Targeted next-generation sequencing identifies a homozygous nonsense mutation in ABHD12, the gene underlying PHARC, in a family clinically diagnosed with Usher syndrome type 3.* Orphanet J Rare Dis, 2012. **7**: p. 59.
106. Fiskerstrand, T., et al., *Mutations in ABHD12 cause the neurodegenerative disease PHARC: An inborn error of endocannabinoid metabolism.* Am J Hum Genet, 2010. **87**(3): p. 410-7.
107. Khateb, S., et al., *A homozygous nonsense CEP250 mutation combined with a heterozygous nonsense C2orf71 mutation is associated with atypical Usher syndrome.* J Med Genet, 2014. **51**(7): p. 460-9.
108. Nikopoulos, K., et al., *Mutations in CEP78 Cause Cone-Rod Dystrophy and Hearing Loss Associated with Primary-Cilia Defects.* Am J Hum Genet, 2016. **99**(3): p. 770-776.
109. Leppert, M., et al., *Bardet-Biedl syndrome is linked to DNA markers on chromosome 11q and is genetically heterogeneous.* Nat Genet, 1994. **7**(1): p. 108-12.
110. Nishimura, D.Y., et al., *Positional cloning of a novel gene on chromosome 16q causing Bardet-Biedl syndrome (BBS2).* Hum Mol Genet, 2001. **10**(8): p. 865-74.
111. Beales, P.L., et al., *Bardet-Biedl syndrome: a molecular and phenotypic study of 18 families.* J Med Genet, 1997. **34**(2): p. 92-8.

112. Fan, Y., et al., *Mutations in a member of the Ras superfamily of small GTP-binding proteins causes Bardet-Biedl syndrome.* Nat Genet, 2004. **36**(9): p. 989-93.
113. Chiang, A.P., et al., *Comparative genomic analysis identifies an ADP-ribosylation factor-like gene as the cause of Bardet-Biedl syndrome (BBS3).* Am J Hum Genet, 2004. **75**(3): p. 475-84.
114. Mykytyn, K., et al., *Identification of the gene that, when mutated, causes the human obesity syndrome BBS4.* Nat Genet, 2001. **28**(2): p. 188-91.
115. Young, T.L., et al., *A fifth locus for Bardet-Biedl syndrome maps to chromosome 2q31.* Am J Hum Genet, 1999. **64**(3): p. 900-4.
116. Li, J.B., et al., *Comparative genomics identifies a flagellar and basal body proteome that includes the BBS5 human disease gene.* Cell, 2004. **117**(4): p. 541-52.
117. Katsanis, N., et al., *Mutations in MKKS cause obesity, retinal dystrophy and renal malformations associated with Bardet-Biedl syndrome.* Nat Genet, 2000. **26**(1): p. 67-70.
118. Slavotinek, A.M., et al., *Mutations in MKKS cause Bardet-Biedl syndrome.* Nat Genet, 2000. **26**(1): p. 15-6.
119. Badano, J.L., et al., *Identification of a novel Bardet-Biedl syndrome protein, BBS7, that shares structural features with BBS1 and BBS2.* Am J Hum Genet, 2003. **72**(3): p. 650-8.
120. Ansley, S.J., et al., *Basal body dysfunction is a likely cause of pleiotropic Bardet-Biedl syndrome.* Nature, 2003. **425**(6958): p. 628-33.
121. Nishimura, D.Y., et al., *Comparative genomics and gene expression analysis identifies BBS9, a new Bardet-Biedl syndrome gene.* Am J Hum Genet, 2005. **77**(6): p. 1021-33.
122. Stoetzel, C., et al., *BBS10 encodes a vertebrate-specific chaperonin-like protein and is a major BBS locus.* Nat Genet, 2006. **38**(5): p. 521-4.
123. White, D.R., et al., *Autozygosity mapping of Bardet-Biedl syndrome to 12q21.2 and confirmation of FLJ23560 as BBS10.* Eur J Hum Genet, 2007. **15**(2): p. 173-8.
124. Chiang, A.P., et al., *Homozygosity mapping with SNP arrays identifies TRIM32, an E3 ubiquitin ligase, as a Bardet-Biedl syndrome gene (BBS11).* Proc Natl Acad Sci U S A, 2006. **103**(16): p. 6287-92.
125. Stoetzel, C., et al., *Identification of a novel BBS gene (BBS12) highlights the major role of a vertebrate-specific branch of chaperonin-related proteins in Bardet-Biedl syndrome.* Am J Hum Genet, 2007. **80**(1): p. 1-11.
126. Leitch, C.C., et al., *Hypomorphic mutations in syndromic encephalocele genes are associated with Bardet-Biedl syndrome.* Nat Genet, 2008. **40**(4): p. 443-8.
127. Kim, S.K., et al., *Planar cell polarity acts through septins to control collective cell movement and ciliogenesis.* Science, 2010. **329**(5997): p. 1337-40.
128. Otto, E.A., et al., *Candidate exome capture identifies mutation of SDCCAG8 as the cause of a retinal-renal ciliopathy.* Nat Genet, 2010. **42**(10): p. 840-50.
129. Marion, V., et al., *Exome sequencing identifies mutations in LZTFL1, a BBSome and smoothened trafficking regulator, in a family with Bardet--Biedl syndrome with situs inversus and insertional polydactyly.* J Med Genet, 2012. **49**(5): p. 317-21.

130. Scheidecker, S., et al., *Exome sequencing of Bardet-Biedl syndrome patient identifies a null mutation in the BBSome subunit BBIP1 (BBS18).* J Med Genet, 2014. **51**(2): p. 132-6.
131. Aldahmesh, M.A., et al., *IFT27, encoding a small GTPase component of IFT particles, is mutated in a consanguineous family with Bardet-Biedl syndrome.* Hum Mol Genet, 2014. **23**(12): p. 3307-15.
132. Bujakowska, K.M., et al., *Mutations in IFT172 cause isolated retinal degeneration and Bardet-Biedl syndrome.* Hum Mol Genet, 2015. **24**(1): p. 230-42.
133. Yildiz Bolukbasi, E., et al., *Homozygous mutation in CEP19, a gene mutated in morbid obesity, in Bardet-Biedl syndrome with predominant postaxial polydactyly.* J Med Genet, 2018. **55**(3): p. 189-197.
134. Heon, E., et al., *Mutations in C8ORF37 cause Bardet Biedl syndrome (BBS21).* Hum Mol Genet, 2016. **25**(11): p. 2283-2294.
135. Khan, A.O., et al., *C8orf37 is mutated in Bardet-Biedl syndrome and constitutes a locus allelic to non-syndromic retinal dystrophies.* Ophthalmic Genet, 2016. **37**(3): p. 290-3.
136. Jin, H. and M.V. Nachury, *The BBSome.* Curr Biol, 2009. **19**(12): p. R472-3.
137. Katsanis, N., et al., *BBS4 is a minor contributor to Bardet-Biedl syndrome and may also participate in triallelic inheritance.* Am J Hum Genet, 2002. **71**(1): p. 22-9.
138. Katsanis, N., et al., *Triallelic inheritance in Bardet-Biedl syndrome, a Mendelian recessive disorder.* Science, 2001. **293**(5538): p. 2256-9.
139. Beales, P.L., et al., *Genetic interaction of BBS1 mutations with alleles at other BBS loci can result in non-Mendelian Bardet-Biedl syndrome.* Am J Hum Genet, 2003. **72**(5): p. 1187-99.
140. Badano, J.L., et al., *Heterozygous mutations in BBS1, BBS2 and BBS6 have a potential epistatic effect on Bardet-Biedl patients with two mutations at a second BBS locus.* Hum Mol Genet, 2003. **12**(14): p. 1651-9.
141. Badano, J.L., et al., *Dissection of epistasis in oligogenic Bardet-Biedl syndrome.* Nature, 2006. **439**(7074): p. 326-30.
142. Alvarez-Satta, M., S. Castro-Sanchez, and D. Valverde, *Alstrom syndrome: current perspectives.* Appl Clin Genet, 2015. **8**: p. 171-9.
143. Marshall, J.D., et al., *Alstrom syndrome: genetics and clinical overview.* Curr Genomics, 2011. **12**(3): p. 225-35.
144. Brancati, F., B. Dallapiccola, and E.M. Valente, *Joubert Syndrome and related disorders.* Orphanet J Rare Dis, 2010. **5**: p. 20.
145. Bachmann-Gagescu, R., et al., *Joubert syndrome: a model for untangling recessive disorders with extreme genetic heterogeneity.* J Med Genet, 2015. **52**(8): p. 514-22.
146. Hartill, V., et al., *Meckel-Gruber Syndrome: An Update on Diagnosis, Clinical Management, and Research Advances.* Front Pediatr, 2017. **5**: p. 244.
147. Weihbrecht, K., et al., *Keeping an Eye on Bardet-Biedl Syndrome: A Comprehensive Review of the Role of Bardet-Biedl Syndrome Genes in the Eye.* Med Res Arch, 2017. **5**(9).
148. Tsang, S.H., A.R.P. Aycinena, and T. Sharma, *Ciliopathy: Senior-Loken Syndrome.* Adv Exp Med Biol, 2018. **1085**: p. 175-178.
149. Ng, Y.S. and D.M. Turnbull, *Mitochondrial disease: genetics and management.* J Neurol, 2016. **263**(1): p. 179-91.

150. Yu-Wai-Man, P. and N.J. Newman, *Inherited eye-related disorders due to mitochondrial dysfunction.* Hum Mol Genet, 2017. **26**(R1): p. R12-R20.
151. Acland, G.M., et al., *Gene therapy restores vision in a canine model of childhood blindness.* Nat Genet, 2001. **28**(1): p. 92-5.
152. Russell, S., et al., *Efficacy and safety of voretigene neparvovec (AAV2-hRPE65v2) in patients with RPE65-mediated inherited retinal dystrophy: a randomised, controlled, open-label, phase 3 trial.* Lancet, 2017. **390**(10097): p. 849-860.
153. Dulla, K., et al., *Splice-Modulating Oligonucleotide QR-110 Restores CEP290 mRNA and Function in Human c.2991+1655A>G LCA10 Models.* Mol Ther Nucleic Acids, 2018. **12**: p. 730-740.
154. Parfitt, D.A., et al., *Identification and Correction of Mechanisms Underlying Inherited Blindness in Human iPSC-Derived Optic Cups.* Cell Stem Cell, 2016. **18**(6): p. 769-81.
155. Ben M'Barek, K. and C. Monville, *Cell Therapy for Retinal Dystrophies: From Cell Suspension Formulation to Complex Retinal Tissue Bioengineering.* Stem Cells International, 2019. **2019**.
156. Schwartz, S.D., et al., *Human embryonic stem cell-derived retinal pigment epithelium in patients with age-related macular degeneration and Stargardt's macular dystrophy: follow-up of two open-label phase 1/2 studies.* Lancet, 2015. **385**(9967): p. 509-16.
157. Mehat, M.S., et al., *Transplantation of Human Embryonic Stem Cell-Derived Retinal Pigment Epithelial Cells in Macular Degeneration.* Ophthalmology, 2018. **125**(11): p. 1765-1775.
158. Dias, M.F., et al., *Molecular genetics and emerging therapies for retinitis pigmentosa: Basic research and clinical perspectives.* Prog Retin Eye Res, 2018. **63**: p. 107-131.
159. Brito-Garcia, N., et al., *Effectiveness and safety of nutritional supplements in the treatment of hereditary retinal dystrophies: a systematic review.* Eye (Lond), 2017. **31**(2): p. 273-285.
160. Collins, F.S. and V.A. McKusick, *Implications of the Human Genome Project for medical science.* JAMA, 2001. **285**(5): p. 540-4.
161. Alkuraya, F.S., *The application of next-generation sequencing in the autozygosity mapping of human recessive diseases.* Hum Genet, 2013. **132**(11): p. 1197-211.
162. Carr, I.M., et al., *Autozygosity mapping with exome sequence data.* Hum Mutat, 2013. **34**(1): p. 50-6.
163. Majewski, J., et al., *What can exome sequencing do for you?* J Med Genet, 2011. **48**(9): p. 580-9.
164. Petersen, B.S., et al., *Opportunities and challenges of whole-genome and -exome sequencing.* BMC Genet, 2017. **18**(1): p. 14.
165. Sen, P., et al., *Prevalence of retinitis pigmentosa in South Indian population aged above 40 years.* Ophthalmic Epidemiol, 2008. **15**(4): p. 279-81.
166. Zafar, S., et al., *Retinitis pigmentosa genes implicated in South Asian populations: a systematic review.* J Pak Med Assoc, 2017. **67**(11): p. 1734-1739.
167. Hussain, R. and A.H. Bittles, *The prevalence and demographic characteristics of consanguineous marriages in Pakistan.* J Biosoc Sci, 1998. **30**(2): p. 261-75.

168. Ullah, I., et al., *Pathogenic mutations in TULP1 responsible for retinitis pigmentosa identified in consanguineous familial cases.* Mol Vis, 2016. **22**: p. 797-815.
169. Li, L., et al., *Homozygosity Mapping and Genetic Analysis of Autosomal Recessive Retinal Dystrophies in 144 Consanguineous Pakistani Families.* Invest Ophthalmol Vis Sci, 2017. **58**(4): p. 2218-2238.
170. Lee, W., et al., *Genotypic spectrum and phenotype correlations of ABCA4-associated disease in patients of south Asian descent.* Eur J Hum Genet, 2017. **25**(6): p. 735-743.
171. Lal, D., et al., *Increased Probability of Co-Occurrence of Two Rare Diseases in Consanguineous Families and Resolution of a Complex Phenotype by Next Generation Sequencing.* PLoS One, 2016. **11**(1): p. e0146040.
172. Katagiri, S., et al., *Compound heterozygous splice site variants in the SCLT1 gene highlight an additional candidate locus for Senior-Loken syndrome.* Sci Rep, 2018. **8**(1): p. 16733.
173. Wang, M., et al., *Novel compound heterozygous mutations in CNGA1in a Chinese family affected with autosomal recessive retinitis pigmentosa by targeted sequencing.* BMC Ophthalmol, 2016. **16**: p. 101.
174. Saqib, M.A., et al., *Homozygosity mapping reveals novel and known mutations in Pakistani families with inherited retinal dystrophies.* Sci Rep, 2015. **5**: p. 9965.
175. Nishiguchi, K.M. and C. Rivolta, *Genes associated with retinitis pigmentosa and allied diseases are frequently mutated in the general population.* PLoS One, 2012. **7**(7): p. e41902.
176. O'Gorman, L., et al., *A small gene sequencing panel realises a high diagnostic rate in patients with congenital nystagmus following basic phenotyping.* Sci Rep, 2019. **9**(1): p. 13229.
177. Li, H. and R. Durbin, *Fast and accurate short read alignment with Burrows-Wheeler transform.* Bioinformatics, 2009. **25**(14): p. 1754-60.
178. Li, H. and R. Durbin, *Fast and accurate long-read alignment with Burrows-Wheeler transform.* Bioinformatics, 2010. **26**(5): p. 589-95.
179. Hamburger, V. and H.L. Hamilton, *A series of normal stages in the development of the chick embryo. 1951.* Dev Dyn, 1992. **195**(4): p. 231-72.
180. Schindelin, J., et al., *Fiji: an open-source platform for biological-image analysis.* Nat Methods, 2012. **9**(7): p. 676-82.
181. Bales, K.L. and A.K. Gross, *Aberrant protein trafficking in retinal degenerations: The initial phase of retinal remodeling.* Exp Eye Res, 2016. **150**: p. 71-80.
182. Arno, G., et al., *Mutations in REEP6 Cause Autosomal-Recessive Retinitis Pigmentosa.* Am J Hum Genet, 2016. **99**(6): p. 1305-1315.
183. Agrawal, S.A., et al., *REEP6 deficiency leads to retinal degeneration through disruption of ER homeostasis and protein trafficking.* Hum Mol Genet, 2017. **26**(14): p. 2667-2677.
184. Maita, H., et al., *PAP-1, the mutated gene underlying the RP9 form of dominant retinitis pigmentosa, is a splicing factor.* Exp Cell Res, 2004. **300**(2): p. 283-96.
185. Lv, J.N., et al., *Targeted RP9 ablation and mutagenesis in mouse photoreceptor cells by CRISPR-Cas9.* Sci Rep, 2017. **7**: p. 43062.

186. Ajmal, M., et al., *A missense mutation in the splicing factor gene DHX38 is associated with early-onset retinitis pigmentosa with macular coloboma.* J Med Genet, 2014. **51**(7): p. 444-8.
187. Abid, A., et al., *Identification of novel mutations in the SEMA4A gene associated with retinal degenerative diseases.* J Med Genet, 2006. **43**(4): p. 378-81.
188. Bryant, L., et al., *On variants and disease-causing mutations: Case studies of a SEMA4A variant identified in inherited blindness.* Ophthalmic Genet, 2018. **39**(1): p. 144-146.
189. Rice, D.S., et al., *Severe retinal degeneration associated with disruption of semaphorin 4A.* Invest Ophthalmol Vis Sci, 2004. **45**(8): p. 2767-77.
190. Nojima, S., et al., *A point mutation in Semaphorin 4A associates with defective endosomal sorting and causes retinal degeneration.* Nat Commun, 2013. **4**: p. 1406.
191. Tsuruma, K., et al., *SEMA4A mutations lead to susceptibility to light irradiation, oxidative stress, and ER stress in retinal pigment epithelial cells.* Invest Ophthalmol Vis Sci, 2012. **53**(10): p. 6729-37.
192. Li, L., et al., *A mutation in ZNF513, a putative regulator of photoreceptor development, causes autosomal-recessive retinitis pigmentosa.* Am J Hum Genet, 2010. **87**(3): p. 400-9.
193. Noor, A., et al., *CC2D2A, encoding a coiled-coil and C2 domain protein, causes autosomal-recessive mental retardation with retinitis pigmentosa.* Am J Hum Genet, 2008. **82**(4): p. 1011-8.
194. Ojeda Naharros, I., et al., *Loss-of-function of the ciliopathy protein Cc2d2a disorganizes the vesicle fusion machinery at the periciliary membrane and indirectly affects Rab8-trafficking in zebrafish photoreceptors.* PLoS Genet, 2017. **13**(12): p. e1007150.
195. Zhang, Q., et al., *Severe autosomal recessive retinitis pigmentosa maps to chromosome 1p13.3-p21.2 between D1S2896 and D1S457 but outside ABCA4.* Hum Genet, 2005. **118**(3-4): p. 356-65.
196. Naz, S., et al., *A novel locus for autosomal recessive retinitis pigmentosa in a consanguineous Pakistani family maps to chromosome 2p.* Am J Ophthalmol, 2010. **149**(5): p. 861-6.
197. Meunier, I., et al., *Spectral-Domain Optical Coherence Tomography in Hereditary Retinal Dystrophies*, in *Inherited Chorioretinal Dystrophies*. 2012, Springer, Berlin, Heidelberg.
198. Karczewski, K.J., et al., *Variation across 141,456 human exomes and genomes reveals the spectrum of loss-of-function intolerance across human protein-coding genes.* bioRxiv, 2019: p. 531210.
199. Dajani, R., et al., *CNV Analysis Associates AKNAD1 with Type-2 Diabetes in Jordan Subpopulations.* Sci Rep, 2015. **5**: p. 13391.
200. Kannan, M., et al., *WD40-repeat 47, a microtubule-associated protein, is essential for brain development and autophagy.* Proc Natl Acad Sci U S A, 2017. **114**(44): p. E9308-E9317.
201. Sun, S.C., et al., *Mutations in C1orf194, encoding a calcium regulator, cause dominant Charcot-Marie-Tooth disease.* Brain, 2019. **142**(8): p. 2215-2229.
202. Tawamie, H., et al., *Hypomorphic Pathogenic Variants in TAF13 Are Associated with Autosomal-Recessive Intellectual Disability and Microcephaly.* Am J Hum Genet, 2017. **100**(3): p. 555-561.

203. Mauriac, S.A., et al., *Defective Gpsm2/Galphai3 signalling disrupts stereocilia development and growth cone actin dynamics in Chudley-McCullough syndrome.* Nat Commun, 2017. **8**: p. 14907.
204. Holthuis, J.C. and G.J. Martens, *The neuroendocrine proteins secretogranin II and III are regionally conserved and coordinately expressed with proopiomelanocortin in Xenopus intermediate pituitary.* J Neurochem, 1996. **66**(6): p. 2248-56.
205. Nagasawa, M., et al., *Identification of a novel chloride channel expressed in the endoplasmic reticulum, golgi apparatus, and nucleus.* J Biol Chem, 2001. **276**(23): p. 20413-8.
206. Jia, Y., et al., *Loss of Clcc1 results in ER stress, misfolded protein accumulation, and neurodegeneration.* J Neurosci, 2015. **35**(7): p. 3001-9.
207. Okkenhaug, H., et al., *The human ClC-4 protein, a member of the CLC chloride channel/transporter family, is localized to the endoplasmic reticulum by its N-terminus.* FASEB J, 2006. **20**(13): p. 2390-2.
208. Morier, N. and R. Sauve, *Analysis of a novel double-barreled anion channel from rat liver rough endoplasmic reticulum.* Biophys J, 1994. **67**(2): p. 590-602.
209. Schmid, A., et al., *Anion channels in giant liposomes made of endoplasmic reticulum vesicles from rat exocrine pancreas.* J Membr Biol, 1988. **104**(3): p. 275-82.
210. Rapoport, T.A., L. Li, and E. Park, *Structural and Mechanistic Insights into Protein Translocation.* Annual Review of Cell and Developmental Biology, Vol 33, 2017. **33**: p. 369-390.
211. Olzmann, J.A., R.R. Kopito, and J.C. Christianson, *The mammalian endoplasmic reticulum-associated degradation system.* Cold Spring Harb Perspect Biol, 2013. **5**(9).
212. Ron, D. and H.P. Harding, *Protein-folding homeostasis in the endoplasmic reticulum and nutritional regulation.* Cold Spring Harb Perspect Biol, 2012. **4**(12).
213. Kroeger, H., et al., *ER stress and unfolded protein response in ocular health and disease.* FEBS J, 2019. **286**(2): p. 399-412.
214. Griciuc, A., L. Aron, and M. Ueffing, *ER stress in retinal degeneration: a target for rational therapy?* Trends Mol Med, 2011. **17**(8): p. 442-51.
215. Chiang, W.C., et al., *Robust Endoplasmic Reticulum-Associated Degradation of Rhodopsin Precedes Retinal Degeneration.* Mol Neurobiol, 2015. **52**(1): p. 679-95.
216. Cox, J.S., C.E. Shamu, and P. Walter, *Transcriptional induction of genes encoding endoplasmic reticulum resident proteins requires a transmembrane protein kinase.* Cell, 1993. **73**(6): p. 1197-206.
217. Mori, K., et al., *A transmembrane protein with a cdc2+/CDC28-related kinase activity is required for signaling from the ER to the nucleus.* Cell, 1993. **74**(4): p. 743-56.
218. Harding, H.P., Y. Zhang, and D. Ron, *Protein translation and folding are coupled by an endoplasmic-reticulum-resident kinase.* Nature, 1999. **397**(6716): p. 271-4.
219. Haze, K., et al., *Mammalian transcription factor ATF6 is synthesized as a transmembrane protein and activated by proteolysis in response to endoplasmic reticulum stress.* Mol Biol Cell, 1999. **10**(11): p. 3787-99.

220. Adams, C.J., et al., *Structure and Molecular Mechanism of ER Stress Signaling by the Unfolded Protein Response Signal Activator IRE1.* Front Mol Biosci, 2019. **6**: p. 11.
221. Almanza, A., et al., *Endoplasmic reticulum stress signalling - from basic mechanisms to clinical applications.* FEBS J, 2019. **286**(2): p. 241-278.
222. Cerella, C., M. Diederich, and L. Ghibelli, *The dual role of calcium as messenger and stressor in cell damage, death, and survival.* Int J Cell Biol, 2010. **2010**: p. 546163.
223. Michalak, M. and M. Opas, *Endoplasmic and sarcoplasmic reticulum in the heart.* Trends Cell Biol, 2009. **19**(6): p. 253-9.
224. Raffaello, A., et al., *Calcium at the Center of Cell Signaling: Interplay between Endoplasmic Reticulum, Mitochondria, and Lysosomes.* Trends Biochem Sci, 2016. **41**(12): p. 1035-1049.
225. Lipskaia, L., J.S. Hulot, and A.M. Lompre, *Role of sarco/endoplasmic reticulum calcium content and calcium ATPase activity in the control of cell growth and proliferation.* Pflugers Arch, 2009. **457**(3): p. 673-85.
226. Nakamura, K., et al., *Functional specialization of calreticulin domains.* J Cell Biol, 2001. **154**(5): p. 961-72.
227. Coe, H. and M. Michalak, *Calcium binding chaperones of the endoplasmic reticulum.* Gen Physiol Biophys, 2009. **28 Spec No Focus**: p. F96-F103.
228. Williams, D.B., *Beyond lectins: the calnexin/calreticulin chaperone system of the endoplasmic reticulum.* J Cell Sci, 2006. **119**(Pt 4): p. 615-23.
229. Llewellyn, D.H. and H.L. Roderick, *Overexpression of calreticulin fails to abolish its induction by perturbation of normal ER function.* Biochem Cell Biol, 1998. **76**(5): p. 875-80.
230. Lievremont, J.P., et al., *BiP, a major chaperone protein of the endoplasmic reticulum lumen, plays a direct and important role in the storage of the rapidly exchanging pool of Ca2+.* J Biol Chem, 1997. **272**(49): p. 30873-9.
231. Prins, D. and M. Michalak, *Organellar calcium buffers.* Cold Spring Harb Perspect Biol, 2011. **3**(3).
232. Stathopulos, P.B., et al., *STIM1/Orai1 coiled-coil interplay in the regulation of store-operated calcium entry.* Nat Commun, 2013. **4**: p. 2963.
233. Gomez-Navarro, N. and E. Miller, *Protein sorting at the ER-Golgi interface.* J Cell Biol, 2016. **215**(6): p. 769-778.
234. Olzmann, J.A. and P. Carvalho, *Dynamics and functions of lipid droplets.* Nature Reviews Molecular Cell Biology, 2019. **20**(3): p. 137-155.
235. Lewis, M.J. and H.R. Pelham, *Ligand-induced redistribution of a human KDEL receptor from the Golgi complex to the endoplasmic reticulum.* Cell, 1992. **68**(2): p. 353-64.
236. Zurek, N., L. Sparks, and G. Voeltz, *Reticulon short hairpin transmembrane domains are used to shape ER tubules.* Traffic, 2011. **12**(1): p. 28-41.
237. Freund, A., et al., *Proteostatic control of telomerase function through TRiC-mediated folding of TCAB1.* Cell, 2014. **159**(6): p. 1389-403.
238. Seo, S., et al., *BBS6, BBS10, and BBS12 form a complex with CCT/TRiC family chaperonins and mediate BBSome assembly.* Proc Natl Acad Sci U S A, 2010. **107**(4): p. 1488-93.

239. Harel, T., et al., *Monoallelic and Biallelic Variants in EMC1 Identified in Individuals with Global Developmental Delay, Hypotonia, Scoliosis, and Cerebellar Atrophy.* Am J Hum Genet, 2016. **98**(3): p. 562-570.
240. Abu-Safieh, L., et al., *Autozygome-guided exome sequencing in retinal dystrophy patients reveals pathogenetic mutations and novel candidate disease genes.* Genome Res, 2013. **23**(2): p. 236-47.
241. Guna, A., et al., *The ER membrane protein complex is a transmembrane domain insertase.* Science, 2018. **359**(6374): p. 470-473.
242. Shurtleff, M.J., et al., *The ER membrane protein complex interacts cotranslationally to enable biogenesis of multipass membrane proteins.* Elife, 2018. **7**.
243. Chitwood, P.J., et al., *EMC Is Required to Initiate Accurate Membrane Protein Topogenesis.* Cell, 2018. **175**(6): p. 1507-1519 e16.
244. Volkmar, N., et al., *The ER membrane protein complex promotes biogenesis of sterol-related enzymes maintaining cholesterol homeostasis.* J Cell Sci, 2019. **132**(2).
245. Satoh, T., et al., *dPob/EMC is essential for biosynthesis of rhodopsin and other multi-pass membrane proteins in Drosophila photoreceptors.* Elife, 2015. **4**.
246. Al-Saif, A., F. Al-Mohanna, and S. Bohlega, *A mutation in sigma-1 receptor causes juvenile amyotrophic lateral sclerosis.* Annals of Neurology, 2011. **70**(6): p. 913-919.
247. Gregianin, E., et al., *Loss-of-function mutations in the SIGMAR1 gene cause distal hereditary motor neuropathy by impairing ER-mitochondria tethering and Ca2+ signalling.* Human Molecular Genetics, 2016. **25**(17): p. 3741-3753.
248. Mavlyutov, T.A., M. Epstein, and L.W. Guo, *Subcellular localization of the sigma-1 receptor in retinal neurons - an electron microscopy study.* Sci Rep, 2015. **5**: p. 10689.
249. Hayashi, T. and T.P. Su, *Sigma-1 receptor chaperones at the ER-mitochondrion interface regulate Ca(2+) signaling and cell survival.* Cell, 2007. **131**(3): p. 596-610.
250. Srivats, S., et al., *Sigmal receptors inhibit store-operated Ca2+ entry by attenuating coupling of STIM1 to Orail.* Journal of Cell Biology, 2016. **213**(1): p. 65-79.
251. Dudek, J., et al., *Functions and pathologies of BiP and its interaction partners.* Cell Mol Life Sci, 2009. **66**(9): p. 1556-69.
252. Otero, J.H., B. Lizak, and L.M. Hendershot, *Life and death of a BiP substrate.* Semin Cell Dev Biol, 2010. **21**(5): p. 472-8.
253. Pincus, D. and P. Walter, *A first line of defense against ER stress.* J Cell Biol, 2012. **198**(3): p. 277-9.
254. Lamriben, L., et al., *N-Glycan-based ER Molecular Chaperone and Protein Quality Control System: The Calnexin Binding Cycle.* Traffic, 2016. **17**(4): p. 308-326.
255. Roderick, H.L., J.D. Lechleiter, and P. Camacho, *Cytosolic phosphorylation of calnexin controls intracellular Ca(2+) oscillations via an interaction with SERCA2b.* J Cell Biol, 2000. **149**(6): p. 1235-48.
256. Yeung, T., et al., *Receptor activation alters inner surface potential during phagocytosis.* Science, 2006. **313**(5785): p. 347-51.
257. Hayashi, T. and T.P. Su, *Cholesterol at the endoplasmic reticulum: roles of the sigma-1 receptor chaperone and implications thereof in human diseases.* Subcell Biochem, 2010. **51**: p. 381-98.

258. Zhang, D., et al., *2-Deoxy-D-glucose targeting of glucose metabolism in cancer cells as a potential therapy.* Cancer Lett, 2014. **355**(2): p. 176-83.
259. Bhutia, Y.D., E. Babu, and V. Ganapathy, *Re-programming tumour cell metabolism to treat cancer: no lone target for lonidamine.* Biochem J, 2016. **473**(11): p. 1503-6.
260. Wang, H., et al., *Effects of treatment with an Hsp90 inhibitor in tumors based on 15 phase II clinical trials.* Mol Clin Oncol, 2016. **5**(3): p. 326-334.
261. Mendes, H.F. and M.E. Cheetham, *Pharmacological manipulation of gain-of-function and dominant-negative mechanisms in rhodopsin retinitis pigmentosa.* Hum Mol Genet, 2008. **17**(19): p. 3043-54.
262. Han, J. and R.J. Kaufman, *Measurement of the unfolded protein response to investigate its role in adipogenesis and obesity.* Methods Enzymol, 2014. **538**: p. 135-50.
263. McIlwain, D.R., T. Berger, and T.W. Mak, *Caspase functions in cell death and disease.* Cold Spring Harb Perspect Biol, 2013. **5**(4): p. a008656.
264. Vithana, E.N., et al., *A human homolog of yeast pre-mRNA splicing gene, PRP31, underlies autosomal dominant retinitis pigmentosa on chromosome 19q13.4 (RP11).* Mol Cell, 2001. **8**(2): p. 375-81.
265. McKie, A.B., et al., *Mutations in the pre-mRNA splicing factor gene PRPC8 in autosomal dominant retinitis pigmentosa (RP13).* Hum Mol Genet, 2001. **10**(15): p. 1555-62.
266. Chakarova, C.F., et al., *Mutations in HPRP3, a third member of pre-mRNA splicing factor genes, implicated in autosomal dominant retinitis pigmentosa.* Hum Mol Genet, 2002. **11**(1): p. 87-92.
267. Zhao, C., et al., *Autosomal-dominant retinitis pigmentosa caused by a mutation in SNRNP200, a gene required for unwinding of U4/U6 snRNAs.* Am J Hum Genet, 2009. **85**(5): p. 617-27.
268. Tanackovic, G., et al., *A missense mutation in PRPF6 causes impairment of pre-mRNA splicing and autosomal-dominant retinitis pigmentosa.* Am J Hum Genet, 2011. **88**(5): p. 643-9.
269. Chen, X., et al., *PRPF4 mutations cause autosomal dominant retinitis pigmentosa.* Hum Mol Genet, 2014. **23**(11): p. 2926-39.
270. Kamran-ul-Hassan Naqvi, S., et al., *A novel splice-acceptor site mutation in CDH3 gene in a consanguineous family exhibiting hypotrichosis with juvenile macular dystrophy.* Arch Dermatol Res, 2010. **302**(9): p. 701-3.
271. McMains, E., et al., *Expression and localization of CLC chloride transport proteins in the avian retina.* PLoS One, 2011. **6**(3): p. e17647.
272. !!! INVALID CITATION !!! {}.
273. Baens, M., et al., *The dark side of EGFP: defective polyubiquitination.* PLoS One, 2006. **1**: p. e54.
274. Agbulut, O., et al., *Green fluorescent protein impairs actin-myosin interactions by binding to the actin-binding site of myosin.* J Biol Chem, 2007. **282**(14): p. 10465-71.
275. Aliye, N., et al., *Engineering color variants of green fluorescent protein (GFP) for thermostability, pH-sensitivity, and improved folding kinetics.* Appl Microbiol Biotechnol, 2015. **99**(3): p. 1205-16.
276. Schwarz, D.S. and M.D. Blower, *The endoplasmic reticulum: structure, function and response to cellular signaling.* Cellular and Molecular Life Sciences, 2016. **73**(1): p. 79-94.

277. Shibata, Y., et al., *The reticulon and DP1/Yop1p proteins form immobile oligomers in the tubular endoplasmic reticulum.* Journal of Biological Chemistry, 2008. **283**(27): p. 18892-18904.
278. Shibata, Y., et al., *Mechanisms Determining the Morphology of the Peripheral ER.* Cell, 2010. **143**(5): p. 774-788.
279. Bantscheff, M., et al., *Quantitative mass spectrometry in proteomics: a critical review.* Anal Bioanal Chem, 2007. **389**(4): p. 1017-31.
280. Liu, R., et al., *Novel interacting proteins identified by tandem affinity purification coupled to nano LC-MS/MS interact with ribosomal S6 protein kinase 4 (RSK4) and its variant protein (RSK4m).* Int J Biol Macromol, 2017. **96**: p. 421-428.
281. Li, Y., et al., *Escherichia coli condensin MukB stimulates topoisomerase IV activity by a direct physical interaction.* Proc Natl Acad Sci U S A, 2010. **107**(44): p. 18832-7.
282. Del Mar Masdeu, M., et al., *Identification of novel Ack1-interacting proteins and Ack1 phosphorylated sites in mouse brain by mass spectrometry.* Oncotarget, 2017. **8**(60): p. 101146-101157.
283. Costello, J.L., et al., *ACBD5 and VAPB mediate membrane associations between peroxisomes and the ER.* J Cell Biol, 2017. **216**(2): p. 331-342.
284. English, A.R. and G.K. Voeltz, *Endoplasmic Reticulum Structure and Interconnections with Other Organelles.* Cold Spring Harbor Perspectives in Biology, 2013. **5**(4).
285. Trinkle-Mulcahy, L., et al., *Identifying specific protein interaction partners using quantitative mass spectrometry and bead proteomes.* J Cell Biol, 2008. **183**(2): p. 223-39.
286. Lam, C., et al., *Prospective phenotyping of NGLY1-CDDG, the first congenital disorder of deglycosylation.* Genetics in Medicine, 2017. **19**(2): p. 160-168.
287. Taylor, R.L., et al., *Association of Steroid 5 alpha-Reductase Type 3 Congenital Disorder of Glycosylation With Early-Onset Retinal Dystrophy.* Jama Ophthalmology, 2017. **135**(4): p. 339-347.
288. Caramelo, J.J. and A.J. Parodi, *A sweet code for glycoprotein folding.* FEBS Lett, 2015. **589**(22): p. 3379-87.
289. Cherepanova, N., S. Shrimal, and R. Gilmore, *N-linked glycosylation and homeostasis of the endoplasmic reticulum.* Curr Opin Cell Biol, 2016. **41**: p. 57-65.
290. Tian, S., et al., *Proteomic Analysis Identifies Membrane Proteins Dependent on the ER Membrane Protein Complex.* Cell Rep, 2019. **28**(10): p. 2517-2526 e5.
291. Chitwood, P.J. and R.S. Hegde, *The Role of EMC during Membrane Protein Biogenesis.* Trends Cell Biol, 2019. **29**(5): p. 371-384.
292. Lynes, E.M., et al., *Palmitoylation is the switch that assigns calnexin to quality control or ER Ca2+ signaling.* J Cell Sci, 2013. **126**(Pt 17): p. 3893-903.
293. Kourrich, S., et al., *The sigma-1 receptor: roles in neuronal plasticity and disease.* Trends Neurosci, 2012. **35**(12): p. 762-71.
294. Chu, Q., et al., *Regulation of the ER stress response by a mitochondrial microprotein.* Nat Commun, 2019. **10**(1): p. 4883.
295. Rosengren, V., et al., *Thapsigargin down-regulates protein levels of GRP78/BiP in INS-1E cells.* J Cell Biochem, 2012. **113**(5): p. 1635-44.

296. Janyou, A., et al., *Suppression effects of O-demethyldemethoxycurcumin on thapsigargin triggered on endoplasmic reticulum stress in SK-N-SH cells.* Neurotoxicology, 2015. **50**: p. 92-100.
297. Leveillard, T. and J.A. Sahel, *Metabolic and redox signaling in the retina.* Cell Mol Life Sci, 2017. **74**(20): p. 3649-3665.
298. Chichagova, V., et al., *Human iPSC disease modelling reveals functional and structural defects in retinal pigment epithelial cells harbouring the m.3243A > G mitochondrial DNA mutation.* Sci Rep, 2017. **7**(1): p. 12320.
299. Guo, Y., et al., *Modeling Retinitis Pigmentosa: Retinal Organoids Generated From the iPSCs of a Patient With the USH2A Mutation Show Early Developmental Abnormalities.* Front Cell Neurosci, 2019. **13**: p. 361.
300. Buskin, A., et al., *Disrupted alternative splicing for genes implicated in splicing and ciliogenesis causes PRPF31 retinitis pigmentosa.* Nat Commun, 2018. **9**(1): p. 4234.
301. Cieri, D., et al., *SPLICS: a split green fluorescent protein-based contact site sensor for narrow and wide heterotypic organelle juxtaposition.* Cell Death Differ, 2018. **25**(6): p. 1131-1145.
302. Weng, T.Y., S.A. Tsai, and T.P. Su, *Roles of sigma-1 receptors on mitochondrial functions relevant to neurodegenerative diseases.* J Biomed Sci, 2017. **24**(1): p. 74.
303. Werdich, X.Q., et al., *A clinical, radiologic, and immunopathologic study of five periorbital intraosseous cavernous vascular malformations.* Am J Ophthalmol, 2014. **158**(4): p. 816-826 e1.
304. Khan, M.I., et al., *The molecular basis of retinal dystrophies in pakistan.* Genes (Basel), 2014. **5**(1): p. 176-95.
305. Maranhao, B., et al., *Investigating the Molecular Basis of Retinal Degeneration in a Familial Cohort of Pakistani Decent by Exome Sequencing.* PLoS One, 2015. **10**(9): p. e0136561.
306. Shaikh, R.S., et al., *Homozygous missense variant in the human CNGA3 channel causes cone-rod dystrophy.* Eur J Hum Genet, 2015. **23**(4): p. 473-80.
307. Patel, N., et al., *Expanding the clinical, allelic, and locus heterogeneity of retinal dystrophies.* Genet Med, 2016. **18**(6): p. 554-62.
308. Taylor, R.L., et al., *Panel-Based Clinical Genetic Testing in 85 Children with Inherited Retinal Disease.* Ophthalmology, 2017. **124**(7): p. 985-991.
309. Huang, L., et al., *Molecular genetics of cone-rod dystrophy in Chinese patients: New data from 61 probands and mutation overview of 163 probands.* Exp Eye Res, 2016. **146**: p. 252-8.
310. Johnson, S., et al., *Achromatopsia caused by novel mutations in both CNGA3 and CNGB3.* J Med Genet, 2004. **41**(2): p. e20.
311. Kohl, S., et al., *CNGB3 mutations account for 50% of all cases with autosomal recessive achromatopsia.* Eur J Hum Genet, 2005. **13**(3): p. 302-8.
312. Ceyhan-Birsoy, O., et al., *Interpretation of Genomic Sequencing Results in Healthy and Ill Newborns: Results from the BabySeq Project.* Am J Hum Genet, 2019. **104**(1): p. 76-93.
313. Lewis, R.A., et al., *Genotype/Phenotype analysis of a photoreceptor-specific ATP-binding cassette transporter gene, ABCR, in Stargardt disease.* Am J Hum Genet, 1999. **64**(2): p. 422-34.

314. Perrault, I., et al., *Spectrum of retGC1 mutations in Leber's congenital amaurosis.* Eur J Hum Genet, 2000. **8**(8): p. 578-82.
315. Carss, K.J., et al., *Comprehensive Rare Variant Analysis via Whole-Genome Sequencing to Determine the Molecular Pathology of Inherited Retinal Disease.* Am J Hum Genet, 2017. **100**(1): p. 75-90.
316. Li, L., et al., *Mutation in the intracellular chloride channel CLCC1 associated with autosomal recessive retinitis pigmentosa.* PLoS Genet, 2018. **14**(8): p. e1007504.
317. Sloan-Heggen, C.M., et al., *Comprehensive genetic testing in the clinical evaluation of 1119 patients with hearing loss.* Hum Genet, 2016. **135**(4): p. 441-450.
318. Vanniya, S.P., et al., *Recurrence of reported CDH23 mutations causing DFNB12 in a special cohort of South Indian hearing impaired assortative mating families - an evaluation.* Ann Hum Genet, 2018. **82**(2): p. 119-126.
319. Sharon, D., et al., *X-linked retinitis pigmentosa: mutation spectrum of the RPGR and RP2 genes and correlation with visual function.* Invest Ophthalmol Vis Sci, 2000. **41**(9): p. 2712-21.
320. Breuer, D.K., et al., *A comprehensive mutation analysis of RP2 and RPGR in a North American cohort of families with X-linked retinitis pigmentosa.* Am J Hum Genet, 2002. **70**(6): p. 1545-54.
321. Ullah, I., et al., *Mutations in phosphodiesterase 6 identified in familial cases of retinitis pigmentosa.* Hum Genome Var, 2016. **3**: p. 16036.
322. O'Sullivan, J., et al., *A paradigm shift in the delivery of services for diagnosis of inherited retinal disease.* J Med Genet, 2012. **49**(5): p. 322-6.
323. Brody, L.C., et al., *Ornithine delta-aminotransferase mutations in gyrate atrophy. Allelic heterogeneity and functional consequences.* J Biol Chem, 1992. **267**(5): p. 3302-7.
324. Fahim, A.T., et al., *Diagnostic fundus autofluorescence patterns in achromatopsia.* Am J Ophthalmol, 2013. **156**(6): p. 1211-1219 e2.
325. Kohl, S., et al., *Total colourblindness is caused by mutations in the gene encoding the alpha-subunit of the cone photoreceptor cGMP-gated cation channel.* Nat Genet, 1998. **19**(3): p. 257-9.
326. Georgiou, M., et al., *Adaptive Optics Retinal Imaging in CNGA3-Associated Achromatopsia: Retinal Characterization, Interocular Symmetry, and Intrafamilial Variability.* Invest Ophthalmol Vis Sci, 2019. **60**(1): p. 383-396.
327. Fujinami, K., et al., *A longitudinal study of Stargardt disease: quantitative assessment of fundus autofluorescence, progression, and genotype correlations.* Invest Ophthalmol Vis Sci, 2013. **54**(13): p. 8181-90.
328. Billingsley, G., et al., *Mutations in chaperonin-like BBS genes are a major contributor to disease development in a multiethnic Bardet-Biedl syndrome patient population.* J Med Genet, 2010. **47**(7): p. 453-63.
329. Shahzadi, A., et al., *Nonsense mutation in MERTK causes autosomal recessive retinitis pigmentosa in a consanguineous Pakistani family.* Br J Ophthalmol, 2010. **94**(8): p. 1094-9.
330. Maria, M., et al., *Genetic and clinical characterization of Pakistani families with Bardet-Biedl syndrome extends the genetic and phenotypic spectrum.* Sci Rep, 2016. **6**: p. 34764.
331. Khan, S., et al., *Novel homozygous mutations in the genes ARL6 and BBS10 underlying Bardet-Biedl syndrome.* Gene, 2013. **515**(1): p. 84-8.

332. Chen, J., et al., *Molecular analysis of Bardet-Biedl syndrome families: report of 21 novel mutations in 10 genes.* Invest Ophthalmol Vis Sci, 2011. **52**(8): p. 5317-24.
333. Stenson, P.D., et al., *Human Gene Mutation Database (HGMD): 2003 update.* Hum Mutat, 2003. **21**(6): p. 577-81.
334. Rivera, A., et al., *A comprehensive survey of sequence variation in the ABCA4 (ABCR) gene in Stargardt disease and age-related macular degeneration.* Am J Hum Genet, 2000. **67**(4): p. 800-13.
335. Valverde, D., et al., *Microarray-based mutation analysis of the ABCA4 gene in Spanish patients with Stargardt disease: evidence of a prevalent mutated allele.* Mol Vis, 2006. **12**: p. 902-8.
336. Rosenberg, T., et al., *N965S is a common ABCA4 variant in Stargardt-related retinopathies in the Danish population.* Mol Vis, 2007. **13**: p. 1962-9.
337. Chacon-Camacho, O.F., et al., *ABCA4 mutational spectrum in Mexican patients with Stargardt disease: Identification of 12 novel mutations and evidence of a founder effect for the common p.A1773V mutation.* Exp Eye Res, 2013. **109**: p. 77-82.
338. Zernant, J., et al., *Genetic and clinical analysis of ABCA4-associated disease in African American patients.* Hum Mutat, 2014. **35**(10): p. 1187-94.
339. Fujinami, K., et al., *Detailed genetic characteristics of an international large cohort of patients with Stargardt disease: ProgStar study report 8.* Br J Ophthalmol, 2019. **103**(3): p. 390-397.
340. Forsythe, E. and P.L. Beales, *Bardet–Biedl syndrome.* European journal of human genetics, 2013. **21**(1): p. 8.
341. Sweeney, M.O., et al., *Low prevalence of lecithin retinol acyltransferase mutations in patients with Leber congenital amaurosis and autosomal recessive retinitis pigmentosa.* Mol Vis, 2007. **13**: p. 588-93.
342. Rehman, A.U., et al., *Challenges and solutions for gene identification in the presence of familial locus heterogeneity.* Eur J Hum Genet, 2015. **23**(9): p. 1207-15.
343. Miraldi Utz, V., et al., *Gene therapy for RPE65-related retinal disease.* Ophthalmic Genet, 2018. **39**(6): p. 671-677.
344. Smith, J., et al., *New and emerging technologies for the treatment of inherited retinal diseases: a horizon scanning review.* Eye (Lond), 2015. **29**(9): p. 1131-40.
345. Dineen, B., et al., *Causes of blindness and visual impairment in Pakistan. The Pakistan national blindness and visual impairment survey.* Br J Ophthalmol, 2007. **91**(8): p. 1005-10.
346. Jadoon, M.Z., et al., *Prevalence of blindness and visual impairment in Pakistan: the Pakistan National Blindness and Visual Impairment Survey.* Invest Ophthalmol Vis Sci, 2006. **47**(11): p. 4749-55.
347. Hassan, B., et al., *A comprehensive study capturing vision loss burden in Pakistan (1990-2025): Findings from the Global Burden of Disease (GBD) 2017 study.* PLoS One, 2019. **14**(5): p. e0216492.
348. Awan, H.R. and T. Ihsan, *Prevalence of visual impairment and eye diseases in Afghan refugees in Pakistan*. 1998.
349. Keen, T.J., et al., *Identification of a locus (LCA9) for Leber's congenital amaurosis on chromosome 1p36.* Eur J Hum Genet, 2003. **11**(5): p. 420-3.

350. Mitchell, S.J., et al., *A syndrome of severe mental retardation, spasticity, and tapetoretinal degeneration linked to chromosome 15q24.* Am J Hum Genet, 1998. **62**(5): p. 1070-6.
351. Hameed, A., et al., *A novel locus for Leber congenital amaurosis (LCA4) with anterior keratoconus mapping to chromosome 17p13.* Invest Ophthalmol Vis Sci, 2000. **41**(3): p. 629-33.
352. Tanaka, K., et al., *The Rapid-Onset Chorioretinopathy Phenotype of ABCA4 Disease.* Ophthalmology, 2018. **125**(1): p. 89-99.
353. Alapati, A., et al., *Molecular diagnostic testing by eyeGENE: analysis of patients with hereditary retinal dystrophy phenotypes involving central vision loss.* Invest Ophthalmol Vis Sci, 2014. **55**(9): p. 5510-21.
354. Stone, E.M., et al., *Clinically Focused Molecular Investigation of 1000 Consecutive Families with Inherited Retinal Disease.* Ophthalmology, 2017. **124**(9): p. 1314-1331.
355. Paavo, M., et al., *Mutations in GPR143/OA1 and ABCA4 Inform Interpretations of Short-Wavelength and Near-Infrared Fundus Autofluorescence.* Invest Ophthalmol Vis Sci, 2018. **59**(6): p. 2459-2469.
356. Schindler, E.I., et al., *Deducing the pathogenic contribution of recessive ABCA4 alleles in an outbred population.* Hum Mol Genet, 2010. **19**(19): p. 3693-701.
357. Zhang, J., et al., *Novel compound heterozygous mutations in ABCA4 in a Chinese pedigree with Stargardt disease.* Mol Vis, 2016. **22**: p. 1514-1521.
358. Zernant, J., et al., *Analysis of the ABCA4 gene by next-generation sequencing.* Invest Ophthalmol Vis Sci, 2011. **52**(11): p. 8479-87.
359. Biswas, P., et al., *Genetic analysis of 10 pedigrees with inherited retinal degeneration by exome sequencing and phenotype-genotype association.* Physiol Genomics, 2017. **49**(4): p. 216-229.
360. Allikmets, R., et al., *Mutation of the Stargardt disease gene (ABCR) in age-related macular degeneration.* Science, 1997. **277**(5333): p. 1805-7.
361. Wiszniewski, W., et al., *ABCA4 mutations causing mislocalization are found frequently in patients with severe retinal dystrophies.* Hum Mol Genet, 2005. **14**(19): p. 2769-78.
362. Cella, W., et al., *G1961E mutant allele in the Stargardt disease gene ABCA4 causes bull's eye maculopathy.* Exp Eye Res, 2009. **89**(1): p. 16-24.
363. Song, J., et al., *High-throughput retina-array for screening 93 genes involved in inherited retinal dystrophy.* Invest Ophthalmol Vis Sci, 2011. **52**(12): p. 9053-60.
364. Parodi, M.B., et al., *Bilateral choroidal neovascularization associated with bilateral ABCA4 gene mutation.* European Journal of Ophthalmology, 2012. **22**(3): p. 485-487.
365. Tabor, H.K., et al., *Pathogenic variants for Mendelian and complex traits in exomes of 6,517 European and African Americans: implications for the return of incidental results.* Am J Hum Genet, 2014. **95**(2): p. 183-93.
366. Wang, J., et al., *Dependable and efficient clinical utility of target capture-based deep sequencing in molecular diagnosis of retinitis pigmentosa.* Invest Ophthalmol Vis Sci, 2014. **55**(10): p. 6213-23.
367. Song, H., et al., *Cone and rod loss in Stargardt disease revealed by adaptive optics scanning light ophthalmoscopy.* JAMA Ophthalmol, 2015. **133**(10): p. 1198-203.

368. Aukrust, I., et al., *The intronic ABCA4 c.5461-10T>C variant, frequently seen in patients with Stargardt disease, causes splice defects and reduced ABCA4 protein level.* Acta Ophthalmol, 2017. **95**(3): p. 240-246.
369. Kaway, C.S., et al., *A Novel ABCA4 Mutation Associated with a Late-Onset Stargardt Disease Phenotype: A Hypomorphic Allele?* Case Rep Ophthalmol, 2017. **8**(1): p. 180-184.
370. Riera, M., et al., *Whole exome sequencing using Ion Proton system enables reliable genetic diagnosis of inherited retinal dystrophies.* Sci Rep, 2017. **7**: p. 42078.
371. Schulz, H.L., et al., *Mutation Spectrum of the ABCA4 Gene in 335 Stargardt Disease Patients From a Multicenter German Cohort-Impact of Selected Deep Intronic Variants and Common SNPs.* Investigative Ophthalmology & Visual Science, 2017. **58**(1): p. 394-403.
372. Birtel, J., et al., *Clinical and genetic characteristics of 251 consecutive patients with macular and cone/cone-rod dystrophy.* Sci Rep, 2018. **8**(1): p. 4824.
373. Garces, F., et al., *Correlating the Expression and Functional Activity of ABCA4 Disease Variants With the Phenotype of Patients With Stargardt Disease.* Invest Ophthalmol Vis Sci, 2018. **59**(6): p. 2305-2315.
374. Zuazo, F. and A.V. Dumitrescu, *The uncommon occurrence of two common inherited disorders in a single patient: a mini case series.* Ophthalmic Genet, 2018. **39**(5): p. 631-636.
375. Foote, K.G., et al., *Cone Spacing Correlates With Retinal Thickness and Microperimetry in Patients With Inherited Retinal Degenerations.* Invest Ophthalmol Vis Sci, 2019. **60**(4): p. 1234-1243.
376. Burke, T.R., et al., *Retinal phenotypes in patients homozygous for the G1961E mutation in the ABCA4 gene.* Invest Ophthalmol Vis Sci, 2012. **53**(8): p. 4458-67.
377. Eisenberger, T., et al., *Increasing the yield in targeted next-generation sequencing by implicating CNV analysis, non-coding exons and the overall variant load: the example of retinal dystrophies.* PLoS One, 2013. **8**(11): p. e78496.
378. Kousal, B., et al., *[The molecular genetic and clinical findings in two probands with Stargardt disease].* Cesk Slov Oftalmol, 2014. **70**(6): p. 228-33.
379. Sciezynska, A., et al., *Next-generation sequencing of ABCA4: High frequency of complex alleles and novel mutations in patients with retinal dystrophies from Central Europe.* Exp Eye Res, 2016. **145**: p. 93-99.
380. Zhang, R., et al., *Associations of the G1961E and D2177N variants in ABCA4 and the risk of age-related macular degeneration.* Gene, 2015. **567**(1): p. 51-7.
381. Passerini, I., et al., *Novel mutations in of the ABCR gene in Italian patients with Stargardt disease.* Eye (Lond), 2010. **24**(1): p. 158-64.
382. Haer-Wigman, L., et al., *Diagnostic exome sequencing in 266 Dutch patients with visual impairment.* Eur J Hum Genet, 2017. **25**(5): p. 591-599.
383. Salles, M.V., et al., *Novel Complex ABCA4 Alleles in Brazilian Patients With Stargardt Disease: Genotype-Phenotype Correlation.* Invest Ophthalmol Vis Sci, 2017. **58**(13): p. 5723-5730.
384. Sallevelt, S., et al., *A comprehensive strategy for exome-based preconception carrier screening.* Genet Med, 2017. **19**(5): p. 583-592.

385. Mahroo, O.A., et al., *Retinal findings in a patient with mutations in ABCC6 and ABCA4.* Eye (Lond), 2018. **32**(9): p. 1542-1543.
386. Nassisi, M., et al., *Expanding the Mutation Spectrum in ABCA4: Sixty Novel Disease Causing Variants and Their Associated Phenotype in a Large French Stargardt Cohort.* Int J Mol Sci, 2018. **19**(8).
387. Wawrocka, A., et al., *Novel variants identified with next-generation sequencing in Polish patients with cone-rod dystrophy.* Mol Vis, 2018. **24**: p. 326-339.
388. Jespersgaard, C., et al., *Molecular genetic analysis using targeted NGS analysis of 677 individuals with retinal dystrophy.* Sci Rep, 2019. **9**(1): p. 1219.
389. Khan, M.I., et al., *Homozygosity mapping identifies genetic defects in four consanguineous families with retinal dystrophy from Pakistan.* Clin Genet, 2013. **84**(3): p. 290-3.
390. Maugeri, A., et al., *Mutations in the ABCA4 (ABCR) gene are the major cause of autosomal recessive cone-rod dystrophy.* Am J Hum Genet, 2000. **67**(4): p. 960-6.
391. Shanks, M.E., et al., *Next-generation sequencing (NGS) as a diagnostic tool for retinal degeneration reveals a much higher detection rate in early-onset disease.* Eur J Hum Genet, 2013. **21**(3): p. 274-80.
392. Parry, D.A., et al., *Loss of the metalloprotease ADAM9 leads to cone-rod dystrophy in humans and retinal degeneration in mice.* Am J Hum Genet, 2009. **84**(5): p. 683-91.
393. Chandra, A., et al., *Expansion of ocular phenotypic features associated with mutations in ADAMTS18.* JAMA Ophthalmol, 2014. **132**(8): p. 996-1001.
394. Utsch, B., et al., *Identification of the first AHI1 gene mutations in nephronophthisis-associated Joubert syndrome.* Pediatr Nephrol, 2006. **21**(1): p. 32-5.
395. Chaki, M., et al., *Genotype-phenotype correlation in 440 patients with NPHP-related ciliopathies.* Kidney Int, 2011. **80**(11): p. 1239-45.
396. Khaliq, S., et al., *Mutation screening of Pakistani families with congenital eye disorders.* Exp Eye Res, 2003. **76**(3): p. 343-8.
397. Tan, M.H., et al., *Leber congenital amaurosis associated with AIPL1: challenges in ascribing disease causation, clinical findings, and implications for gene therapy.* PLoS One, 2012. **7**(3): p. e32330.
398. Sohocki, M.M., et al., *Prevalence of AIPL1 mutations in inherited retinal degenerative disease.* Mol Genet Metab, 2000. **70**(2): p. 142-50.
399. Li, D., et al., *AIPL1 implicated in the pathogenesis of two cases of autosomal recessive retinal degeneration.* Mol Vis, 2014. **20**: p. 1-14.
400. Bellingham, J., et al., *Investigation of Aberrant Splicing Induced by AIPL1 Variations as a Cause of Leber Congenital Amaurosis.* Invest Ophthalmol Vis Sci, 2015. **56**(13): p. 7784-7793.
401. Damji, K.F., et al., *Leber's congenital amaurosis with anterior keratoconus in Pakistani families is caused by the Trp278X mutation in the AIPL1 gene on 17p.* Can J Ophthalmol, 2001. **36**(5): p. 252-9.
402. Sohocki, M.M., et al., *Mutations in a new photoreceptor-pineal gene on 17p cause Leber congenital amaurosis.* Nat Genet, 2000. **24**(1): p. 79-83.
403. Maria, M., et al., *Homozygosity mapping and targeted sanger sequencing reveal genetic defects underlying inherited retinal disease in families from pakistan.* PLoS One, 2015. **10**(3): p. e0119806.

404. McKibbin, M., et al., *Genotype-phenotype correlation for leber congenital amaurosis in Northern Pakistan.* Arch Ophthalmol, 2010. **128**(1): p. 107-13.
405. Di Iorio, V., et al., *Clinical and Genetic Evaluation of a Cohort of Pediatric Patients with Severe Inherited Retinal Dystrophies.* Genes (Basel), 2017. **8**(10).
406. Thompson, J.A., et al., *The genetic profile of Leber congenital amaurosis in an Australian cohort.* Mol Genet Genomic Med, 2017. **5**(6): p. 652-667.
407. Srikrupa, N.N., et al., *Genetic profile and mutation spectrum of Leber congenital amaurosis in a larger Indian cohort using high throughput targeted re-sequencing.* Clin Genet, 2018. **93**(2): p. 329-339.
408. Weisschuh, N., et al., *Molecular and clinical analysis of 27 German patients with Leber congenital amaurosis.* PLoS One, 2018. **13**(12): p. e0205380.
409. Deeble, V.J., et al., *The continuing failure to recognise Alstrom syndrome and further evidence of genetic homogeneity.* J Med Genet, 2000. **37**(3): p. 219.
410. Bond, J., et al., *The importance of seeking ALMS1 mutations in infants with dilated cardiomyopathy.* J Med Genet, 2005. **42**(2): p. e10.
411. Gogi, D., et al., *Exudative retinopathy in a girl with Alstrom syndrome due to a novel mutation.* Br J Ophthalmol, 2007. **91**(7): p. 983-4.
412. Sinha, S.K., et al., *Effect of metformin and rosiglitazone in a prepubertal boy with Alstrom syndrome.* J Pediatr Endocrinol Metab, 2007. **20**(9): p. 1045-52.
413. Mahamid, J., et al., *Extreme clinical variability of dilated cardiomyopathy in two siblings with Alstrom syndrome.* Pediatr Cardiol, 2013. **34**(2): p. 455-8.
414. Castro-Sanchez, S., et al., *Whole exome sequencing as a diagnostic tool for patients with ciliopathy-like phenotypes.* PLoS One, 2017. **12**(8): p. e0183081.
415. Nikopoulos, K., et al., *A large multiexonic genomic deletion within the ALMS1 gene causes Alstrom syndrome in a consanguineous Pakistani family.* Clin Genet, 2016. **89**(4): p. 510-511.
416. Monzó, C., et al., *Alström syndrome caused by deletion in ALMS1 gene fixed in a Northern Pakistan recurrent haplotype.*
417. Marshall, J.D., et al., *Alstrom Syndrome: Mutation Spectrum of ALMS1.* Hum Mutat, 2015. **36**(7): p. 660-8.
418. Aradhya, S., et al., *Exon-level array CGH in a large clinical cohort demonstrates increased sensitivity of diagnostic testing for Mendelian disorders.* Genet Med, 2012. **14**(6): p. 594-603.
419. Sathya Priya, C., et al., *Mutation spectrum in BBS genes guided by homozygosity mapping in an Indian cohort.* Clin Genet, 2015. **87**(2): p. 161-6.
420. Alkanderi, S., et al., *ARL3 Mutations Cause Joubert Syndrome by Disrupting Ciliary Protein Composition.* Am J Hum Genet, 2018. **103**(4): p. 612-620.
421. Rafiullah, R., et al., *A novel homozygous ARL13B variant in patients with Joubert syndrome impairs its guanine nucleotide-exchange factor activity.* Eur J Hum Genet, 2017. **25**(12): p. 1324-1334.
422. Cantagrel, V., et al., *Mutations in the cilia gene ARL13B lead to the classical form of Joubert syndrome.* Am J Hum Genet, 2008. **83**(2): p. 170-9.

423. Biswas, P., et al., *A missense mutation in ASRGL1 is involved in causing autosomal recessive retinal degeneration.* Hum Mol Genet, 2016. **25**(12): p. 2483-2497.
424. Ajmal, M., et al., *Exome sequencing identifies a novel and a recurrent BBS1 mutation in Pakistani families with Bardet-Biedl syndrome.* Mol Vis, 2013. **19**: p. 644-53.
425. Harville, H.M., et al., *Identification of 11 novel mutations in eight BBS genes by high-resolution homozygosity mapping.* J Med Genet, 2010. **47**(4): p. 262-7.
426. Fauser, S., M. Munz, and D. Besch, *Further support for digenic inheritance in Bardet-Biedl syndrome.* J Med Genet, 2003. **40**(8): p. e104.
427. Khan, S., et al., *BBS5 and INPP5E mutations associated with ciliopathy disorders in families from Pakistan.* Ann Hum Genet, 2019.
428. Ullah, A., et al., *Sequence variants in four genes underlying Bardet-Biedl syndrome in consanguineous families.* Mol Vis, 2017. **23**: p. 482-494.
429. Hayat, A., et al., *A novel missense variant in the BBS7 gene underlying Bardet-Biedl syndrome in a consanguineous Pakistani family.* Clin Dysmorphol, 2019.
430. Khan, M.A., et al., *Homozygosity mapping identified a novel protein truncating mutation (p.Ser100Leufs*24) of the BBS9 gene in a consanguineous Pakistani family with Bardet Biedl syndrome.* BMC Med Genet, 2016. **17**: p. 10.
431. Muzammal, M., et al., *Exome sequence analysis in consanguineous Pakistani families inheriting Bardet-Biedle syndrome determined founder effect of mutation c.299delC (p.Ser100Leufs*24) in BBS9 gene.* Mol Genet Genomic Med, 2019. **7**(8): p. e834.
432. Lindstrand, A., et al., *Recurrent CNVs and SNVs at the NPHP1 locus contribute pathogenic alleles to Bardet-Biedl syndrome.* Am J Hum Genet, 2014. **94**(5): p. 745-54.
433. Stals, K.L., et al., *Diagnosis of lethal or prenatal-onset autosomal recessive disorders by parental exome sequencing.* Prenat Diagn, 2018. **38**(1): p. 33-43.
434. Shahi, R.B., et al., *Identification of candidate cancer predisposing variants by performing whole-exome sequencing on index patients from BRCA1 and BRCA2-negative breast cancer families.* BMC Cancer, 2019. **19**(1): p. 313.
435. Muller, J., et al., *Identification of 28 novel mutations in the Bardet-Biedl syndrome genes: the burden of private mutations in an extensively heterogeneous disease.* Hum Genet, 2010. **127**(5): p. 583-93.
436. Agha, Z., et al., *A novel homozygous 10 nucleotide deletion in BBS10 causes Bardet-Biedl syndrome in a Pakistani family.* Gene, 2013. **519**(1): p. 177-81.
437. Pawlik, B., et al., *A Novel Familial BBS12 Mutation Associated with a Mild Phenotype: Implications for Clinical and Molecular Diagnostic Strategies.* Mol Syndromol, 2010. **1**(1): p. 27-34.
438. Davidson, A.E., et al., *Missense mutations in a retinal pigment epithelium protein, bestrophin-1, cause retinitis pigmentosa.* Am J Hum Genet, 2009. **85**(5): p. 581-92.
439. Biswas, P., et al., *Whole-Exome Sequencing Identifies Novel Variants that Co-segregates with Autosomal Recessive Retinal Degeneration in a Pakistani Pedigree.* Adv Exp Med Biol, 2018. **1074**: p. 219-228.

440. Ravesh, Z., et al., *Novel C8orf37 mutations cause retinitis pigmentosa in consanguineous families of Pakistani origin.* Mol Vis, 2015. **21**: p. 236-43.
441. Chen, X., et al., *Distinct mutations with different inheritance mode caused similar retinal dystrophies in one family: a demonstration of the importance of genetic annotations in complicated pedigrees.* J Transl Med, 2018. **16**(1): p. 145.
442. Szymanska, K., et al., *Founder mutations and genotype-phenotype correlations in Meckel-Gruber syndrome and associated ciliopathies.* Cilia, 2012. **1**(1): p. 18.
443. Harripaul, R., et al., *Mapping autosomal recessive intellectual disability: combined microarray and exome sequencing identifies 26 novel candidate genes in 192 consanguineous families.* Mol Psychiatry, 2018. **23**(4): p. 973-984.
444. Shimomura, Y., et al., *P-cadherin is a p63 target gene with a crucial role in the developing human limb bud and hair follicle.* Development, 2008. **135**(4): p. 743-53.
445. Kjaer, K.W., et al., *Distinct CDH3 mutations cause ectodermal dysplasia, ectrodactyly, macular dystrophy (EEM syndrome).* J Med Genet, 2005. **42**(4): p. 292-8.
446. Jelani, M., M. Salman Chishti, and W. Ahmad, *A novel splice-site mutation in the CDH3 gene in hypotrichosis with juvenile macular dystrophy.* Clin Exp Dermatol, 2009. **34**(1): p. 68-73.
447. Shimomura, Y., et al., *Splice site mutations in the P-cadherin gene underlie hypotrichosis with juvenile macular dystrophy.* Dermatology, 2010. **220**(3): p. 208-12.
448. Singh, M.S., et al., *Hypotrichosis and juvenile macular dystrophy caused by CDH3 mutation: A candidate disease for retinal gene therapy.* Sci Rep, 2016. **6**: p. 23674.
449. Schultz, J.M., et al., *Allelic hierarchy of CDH23 mutations causing non-syndromic deafness DFNB12 or Usher syndrome USH1D in compound heterozygotes.* J Med Genet, 2011. **48**(11): p. 767-75.
450. Vanniya, S.P., et al., *Recurrence of reported CDH23 mutations causing DFNB12 in a special cohort of South Indian hearing impaired assortative mating families - an evaluation.* Annals of Human Genetics, 2018. **82**(2): p. 119-126.
451. Neuhaus, C., et al., *Next-generation sequencing reveals the mutational landscape of clinically diagnosed Usher syndrome: copy number variations, phenocopies, a predominant target for translational read-through, and PEX26 mutated in Heimler syndrome.* Mol Genet Genomic Med, 2017. **5**(5): p. 531-552.
452. Cremers, F.P., et al., *Development of a genotyping microarray for Usher syndrome.* J Med Genet, 2007. **44**(2): p. 153-60.
453. von Brederlow, B., et al., *Identification and in vitro expression of novel CDH23 mutations of patients with Usher syndrome type 1D.* Hum Mutat, 2002. **19**(3): p. 268-73.
454. Aparisi, M.J., et al., *Targeted next generation sequencing for molecular diagnosis of Usher syndrome.* Orphanet J Rare Dis, 2014. **9**: p. 168.
455. Besnard, T., et al., *Experience of targeted Usher exome sequencing as a clinical test.* Mol Genet Genomic Med, 2014. **2**(1): p. 30-43.

456. Bonnet, C., et al., *An innovative strategy for the molecular diagnosis of Usher syndrome identifies causal biallelic mutations in 93% of European patients.* Eur J Hum Genet, 2016. **24**(12): p. 1730-1738.
457. Bonnet, C., et al., *Complete exon sequencing of all known Usher syndrome genes greatly improves molecular diagnosis.* Orphanet J Rare Dis, 2011. **6**: p. 21.
458. Le Quesne Stabej, P., et al., *Comprehensive sequence analysis of nine Usher syndrome genes in the UK National Collaborative Usher Study.* J Med Genet, 2012. **49**(1): p. 27-36.
459. Nakanishi, H., et al., *Mutation analysis of the MYO7A and CDH23 genes in Japanese patients with Usher syndrome type 1.* J Hum Genet, 2010. **55**(12): p. 796-800.
460. Yoshimura, H., et al., *Massively parallel DNA sequencing facilitates diagnosis of patients with Usher syndrome type 1.* PLoS One, 2014. **9**(3): p. e90688.
461. Shahzad, M., et al., *Genetic analysis through OtoSeq of Pakistani families segregating prelingual hearing loss.* Otolaryngol Head Neck Surg, 2013. **149**(3): p. 478-87.
462. Ba-Abbad, R., et al., *Clinical characteristics of early retinal disease due to CDHR1 mutation.* Mol Vis, 2013. **19**: p. 2250-9.
463. Henderson, R.H., et al., *Biallelic mutation of protocadherin-21 (PCDH21) causes retinal degeneration in humans.* Mol Vis, 2010. **16**: p. 46-52.
464. Arno, G., et al., *Reevaluation of the Retinal Dystrophy Due to Recessive Alleles of RGR With the Discovery of a Cis-Acting Mutation in CDHR1.* Invest Ophthalmol Vis Sci, 2016. **57**(11): p. 4806-13.
465. Rego, S., et al., *High-frequency actionable pathogenic exome variants in an average-risk cohort.* Cold Spring Harb Mol Case Stud, 2018. **4**(6).
466. Chaki, M., et al., *Exome capture reveals ZNF423 and CEP164 mutations, linking renal ciliopathies to DNA damage response signaling.* Cell, 2012. **150**(3): p. 533-48.
467. Ellingford, J.M., et al., *Molecular findings from 537 individuals with inherited retinal disease.* J Med Genet, 2016. **53**(11): p. 761-767.
468. Wiszniewski, W., et al., *Potential involvement of more than one locus in trait manifestation for individuals with Leber congenital amaurosis.* Hum Genet, 2011. **129**(3): p. 319-27.
469. Otto, E.A., et al., *Mutation analysis of 18 nephronophthisis associated ciliopathy disease genes using a DNA pooling and next generation sequencing strategy.* J Med Genet, 2011. **48**(2): p. 105-16.
470. Sonmez, F., et al., *Development of end-stage renal disease at a young age in two cases with Joubert syndrome.* Turk J Pediatr, 2014. **56**(4): p. 458-61.
471. Migliavacca, E., et al., *A Potential Contributory Role for Ciliary Dysfunction in the 16p11.2 600 kb BP4-BP5 Pathology.* Am J Hum Genet, 2015. **96**(5): p. 784-96.
472. Yzer, S., et al., *Ocular and extra-ocular features of patients with Leber congenital amaurosis and mutations in CEP290.* Mol Vis, 2012. **18**: p. 412-25.
473. Molin, A., et al., *12q21 Microdeletion in a fetus with Meckel syndrome involving CEP290/MKS4.* Eur J Med Genet, 2013. **56**(10): p. 580-3.
474. Glockle, N., et al., *Panel-based next generation sequencing as a reliable and efficient technique to detect mutations in unselected patients with retinal dystrophies.* Eur J Hum Genet, 2014. **22**(1): p. 99-104.

475. Maddirevula, S., et al., *Expanding the phenome and variome of skeletal dysplasia.* Genet Med, 2018. **20**(12): p. 1609-1616.
476. Ali, M., et al., *A missense mutation in the nuclear localization signal sequence of CERKL (p.R106S) causes autosomal recessive retinal degeneration.* Mol Vis, 2008. **14**: p. 1960-4.
477. Tuson, M., G. Marfany, and R. Gonzalez-Duarte, *Mutation of CERKL, a novel human ceramide kinase gene, causes autosomal recessive retinitis pigmentosa (RP26).* Am J Hum Genet, 2004. **74**(1): p. 128-38.
478. Ezquerra-Inchausti, M., et al., *A new approach based on targeted pooled DNA sequencing identifies novel mutations in patients with Inherited Retinal Dystrophies.* Sci Rep, 2018. **8**(1): p. 15457.
479. Rodriguez-Flores, J.L., et al., *Exome sequencing identifies potential risk variants for Mendelian disorders at high prevalence in Qatar.* Hum Mutat, 2014. **35**(1): p. 105-16.
480. Avela, K., et al., *A founder mutation in CERKL is a major cause of retinal dystrophy in Finland.* Acta Ophthalmol, 2018. **96**(2): p. 183-191.
481. Branham, K., et al., *Identification of Novel Deletions as the Underlying Cause of Retinal Degeneration in Two Pedigrees.* Adv Exp Med Biol, 2018. **1074**: p. 229-236.
482. Khan, M.I., et al., *CLRN1 mutations cause nonsyndromic retinitis pigmentosa.* Ophthalmology, 2011. **118**(7): p. 1444-8.
483. Zhang, Q., et al., *Autosomal recessive retinitis pigmentosa in a Pakistani family mapped to CNGA1 with identification of a novel mutation.* Mol Vis, 2004. **10**: p. 884-9.
484. Azam, M., et al., *Novel CNGA3 and CNGB3 mutations in two Pakistani families with achromatopsia.* Mol Vis, 2010. **16**: p. 774-81.
485. Saqib, M.A., et al., *Genetic analysis of four Pakistani families with achromatopsia and a novel S4 motif mutation of CNGA3.* Jpn J Ophthalmol, 2011. **55**(6): p. 676-80.
486. Arshad, M.W., et al., *Identification of Novel Mutation in CNGA3 gene by Whole-Exome Sequencing and In-Silico Analyses for Genotype-Phenotype Assessment with Autosomal Recessive Achromatopsia in Pakistani families.* J Pak Med Assoc, 2019. **69**(2): p. 183-189.
487. Azam, M., et al., *Identification of novel mutations in Pakistani families with autosomal recessive retinitis pigmentosa.* Arch Ophthalmol, 2011. **129**(10): p. 1377-8.
488. Bocquet, B., et al., *Homozygosity mapping in autosomal recessive retinitis pigmentosa families detects novel mutations.* Mol Vis, 2013. **19**: p. 2487-500.
489. Maguire, J., et al., *CNGB3 mutations cause severe rod dysfunction.* Ophthalmic Genet, 2018. **39**(1): p. 108-114.
490. Sundin, O.H., et al., *Genetic basis of total colourblindness among the Pingelapese islanders.* Nat Genet, 2000. **25**(3): p. 289-93.
491. Thiadens, A.A., et al., *Comprehensive analysis of the achromatopsia genes CNGA3 and CNGB3 in progressive cone dystrophy.* Ophthalmology, 2010. **117**(4): p. 825-30 e1.
492. Lazarin, G.A., et al., *An empirical estimate of carrier frequencies for 400+ causal Mendelian variants: results from an ethnically diverse clinical sample of 23,453 individuals.* Genet Med, 2013. **15**(3): p. 178-86.
493. Gupta, S., et al., *Whole exome sequencing unveils a frameshift mutation in CNGB3 for cone dystrophy: A case report of an Indian family.* Medicine (Baltimore), 2017. **96**(30): p. e7490.

494. Gonzalez-Del Pozo, M., et al., *Searching the second hit in patients with inherited retinal dystrophies and monoallelic variants in ABCA4, USH2A and CEP290 by whole-gene targeted sequencing.* Sci Rep, 2018. **8**(1): p. 13312.
495. Michaelides, M., et al., *Progressive cone dystrophy associated with mutation in CNGB3.* Invest Ophthalmol Vis Sci, 2004. **45**(6): p. 1975-82.
496. Greenberg, J.P., et al., *Spectral-domain optical coherence tomography staging and autofluorescence imaging in achromatopsia.* JAMA Ophthalmol, 2014. **132**(4): p. 437-45.
497. Lee, H., et al., *Clinical exome sequencing for genetic identification of rare Mendelian disorders.* JAMA, 2014. **312**(18): p. 1880-7.
498. Ismail, M., et al., *Refinement of the locus for autosomal recessive cone-rod dystrophy (CORD8) linked to chromosome 1q23-q24 in a Pakistani family and exclusion of candidate genes.* J Hum Genet, 2006. **51**(9): p. 827-31.
499. den Hollander, A.I., et al., *Mutations in a human homologue of Drosophila crumbs cause retinitis pigmentosa (RP12).* Nat Genet, 1999. **23**(2): p. 217-21.
500. Henderson, R.H., et al., *Phenotypic variability in patients with retinal dystrophies due to mutations in CRB1.* Br J Ophthalmol, 2011. **95**(6): p. 811-7.
501. Talib, M., et al., *Genotypic and Phenotypic Characteristics of CRB1-Associated Retinal Dystrophies: A Long-Term Follow-up Study.* Ophthalmology, 2017. **124**(6): p. 884-895.
502. Mucciolo, D.P., et al., *Long-term follow-up of a CRB1-associated maculopathy.* Ophthalmic Genet, 2018. **39**(4): p. 522-525.
503. Yang, L., et al., *Novel mutations of CRB1 in Chinese families presenting with retinal dystrophies.* Mol Vis, 2014. **20**: p. 359-67.
504. Ghofrani, M., et al., *Homozygosity Mapping and Targeted Sanger Sequencing Identifies Three Novel CRB1 (Crumbs homologue 1) Mutations in Iranian Retinal Degeneration Families.* Iran Biomed J, 2017. **21**(5): p. 294-302.
505. Monies, D., et al., *The landscape of genetic diseases in Saudi Arabia based on the first 1000 diagnostic panels and exomes.* Hum Genet, 2017. **136**(8): p. 921-939.
506. Latif, Z., et al., *A Homozygous c.2536G>A Mutation in CRB1 Gene Manifesting Autosomal Recessive Retinitis Pigmentosa in a Large Consanguineous Kashmiri Family.* Pakistan Journal of Zoology, 2017. **49**(6): p. 2313-2317.
507. Lotery, A.J., et al., *CRB1 mutations may result in retinitis pigmentosa without para-arteriolar RPE preservation.* Ophthalmic Genet, 2001. **22**(3): p. 163-9.
508. Hanein, S., et al., *Leber congenital amaurosis: comprehensive survey of the genetic heterogeneity, refinement of the clinical definition, and genotype-phenotype correlations as a strategy for molecular diagnosis.* Hum Mutat, 2004. **23**(4): p. 306-17.
509. Latif, Z., et al., *Confirmation of the Role of DHX38 in the Etiology of Early-Onset Retinitis Pigmentosa.* Invest Ophthalmol Vis Sci, 2018. **59**(11): p. 4552-4557.
510. El-Asrag, M.E., et al., *Biallelic mutations in the autophagy regulator DRAM2 cause retinal dystrophy with early macular involvement.* Am J Hum Genet, 2015. **96**(6): p. 948-54.

511. Mir, H., et al., *A novel recessive mutation in the gene ELOVL4 causes a neuro-ichthyotic disorder with variable expressivity.* BMC Med Genet, 2014. **15**: p. 25.
512. Wang, X., et al., *Applying next generation sequencing with microdroplet PCR to determine the disease-causing mutations in retinal dystrophies.* BMC Ophthalmol, 2017. **17**(1): p. 157.
513. Di, Y., et al., *Whole-exome Sequencing Analysis Identifies Mutations in the EYS Gene in Retinitis Pigmentosa in the Indian Population.* Sci Rep, 2016. **6**: p. 19432.
514. Khan, M.I., et al., *Missense mutations at homologous positions in the fourth and fifth laminin A G-like domains of eyes shut homolog cause autosomal recessive retinitis pigmentosa.* Mol Vis, 2010. **16**: p. 2753-9.
515. Rose, A.M., et al., *Diverse clinical phenotypes associated with a nonsense mutation in FAM161A.* Eye, 2015. **29**(9): p. 1226-1232.
516. Langmann, T., et al., *Nonsense mutations in FAM161A cause RP28-associated recessive retinitis pigmentosa.* Am J Hum Genet, 2010. **87**(3): p. 376-81.
517. Van Schil, K., et al., *A Nonsense Mutation in FAM161A Is a Recurrent Founder Allele in Dutch and Belgian Individuals With Autosomal Recessive Retinitis Pigmentosa.* Invest Ophthalmol Vis Sci, 2015. **56**(12): p. 7418-26.
518. Astuti, G.D.N., et al., *Identification of Inherited Retinal Disease-Associated Genetic Variants in 11 Candidate Genes.* Genes (Basel), 2018. **9**(1).
519. Naeem, M.A., et al., *GNAT1 associated with autosomal recessive congenital stationary night blindness.* Invest Ophthalmol Vis Sci, 2012. **53**(3): p. 1353-61.
520. Marmor, M.F. and C. Zeitz, *Riggs-type dominant congenital stationary night blindness: ERG findings, a new GNAT1 mutation and a systemic association.* Doc Ophthalmol, 2018. **137**(1): p. 57-62.
521. Zeitz, C., et al., *A Novel Heterozygous Missense Mutation in GNAT1 Leads to Autosomal Dominant Riggs Type of Congenital Stationary Night Blindness.* Biomed Res Int, 2018. **2018**: p. 7694801.
522. Michaelides, M., et al., *Cone dystrophy phenotype associated with a frameshift mutation (M280fsX291) in the alpha-subunit of cone specific transducin (GNAT2).* Br J Ophthalmol, 2003. **87**(11): p. 1317-20.
523. Zeitz, C., et al., *Genotyping microarray for CSNB-associated genes.* Invest Ophthalmol Vis Sci, 2009. **50**(12): p. 5919-26.
524. Sergouniotis, P.I., et al., *A phenotypic study of congenital stationary night blindness (CSNB) associated with mutations in the GRM6 gene.* Acta Ophthalmol, 2012. **90**(3): p. e192-7.
525. Naeem, M.A., et al., *Mutations in GRM6 identified in consanguineous Pakistani families with congenital stationary night blindness.* Mol Vis, 2015. **21**: p. 1261-71.
526. Azam, M., et al., *A novel mutation in GRK1 causes Oguchi disease in a consanguineous Pakistani family.* Mol Vis, 2009. **15**: p. 1788-93.
527. Zhang, Q., et al., *A variant form of Oguchi disease mapped to 13q34 associated with partial deletion of GRK1 gene.* Mol Vis, 2005. **11**: p. 977-85.
528. Khan, M.A., et al., *Genetic analysis of a consanguineous Pakistani family with Leber congenital amaurosis identifies a novel mutation in GUCY2D gene.* J Genet, 2014. **93**(2): p. 527-30.

529. Simonelli, F., et al., *Clinical and molecular genetics of Leber's congenital amaurosis: a multicenter study of Italian patients.* Invest Ophthalmol Vis Sci, 2007. **48**(9): p. 4284-90.
530. Gillespie, R.L., et al., *Abrogation of HMX1 function causes rare oculoauricular syndrome associated with congenital cataract, anterior segment dysgenesis, and retinal dystrophy.* Invest Ophthalmol Vis Sci, 2015. **56**(2): p. 883-91.
531. Biswas, P., et al., *A mutation in IFT43 causes non-syndromic recessive retinal degeneration.* Hum Mol Genet, 2017. **26**(23): p. 4741-4751.
532. Hull, S., et al., *Nonsyndromic Retinal Dystrophy due to Bi-Allelic Mutations in the Ciliary Transport Gene IFT140.* Invest Ophthalmol Vis Sci, 2016. **57**(3): p. 1053-62.
533. Xu, M., et al., *Mutations in human IFT140 cause non-syndromic retinal degeneration.* Hum Genet, 2015. **134**(10): p. 1069-78.
534. Ali, S., et al., *Phenotypic variability associated with the D226N allele of IMPDH1.* Ophthalmology, 2015. **122**(2): p. 429-31.
535. Bowne, S.J., et al., *Mutations in the inosine monophosphate dehydrogenase 1 gene (IMPDH1) cause the RP10 form of autosomal dominant retinitis pigmentosa.* Hum Mol Genet, 2002. **11**(5): p. 559-68.
536. Martin-Merida, I., et al., *Toward the Mutational Landscape of Autosomal Dominant Retinitis Pigmentosa: A Comprehensive Analysis of 258 Spanish Families.* Invest Ophthalmol Vis Sci, 2018. **59**(6): p. 2345-2354.
537. Villanueva, A., et al., *Identification of the genetic determinants responsible for retinal degeneration in families of Mexican descent.* Ophthalmic Genet, 2018. **39**(1): p. 73-79.
538. Bandah-Rozenfeld, D., et al., *Mutations in IMPG2, encoding interphotoreceptor matrix proteoglycan 2, cause autosomal-recessive retinitis pigmentosa.* Am J Hum Genet, 2010. **87**(2): p. 199-208.
539. Jacoby, M., et al., *INPP5E mutations cause primary cilium signaling defects, ciliary instability and ciliopathies in human and mouse.* Nat Genet, 2009. **41**(9): p. 1027-31.
540. Otto, E.A., et al., *Mutation analysis in nephronophthisis using a combined approach of homozygosity mapping, CEL I endonuclease cleavage, and direct sequencing.* Hum Mutat, 2008. **29**(3): p. 418-26.
541. Hussain, S., et al., *Molecular Study of Nephronophthisis in 7 Unrelated Pakistani Families.* Iran J Kidney Dis, 2018. **12**(4): p. 240-242.
542. Stone, E.M., et al., *Variations in NPHP5 in patients with nonsyndromic leber congenital amaurosis and Senior-Loken syndrome.* Arch Ophthalmol, 2011. **129**(1): p. 81-7.
543. Wang, X., et al., *Comprehensive molecular diagnosis of 179 Leber congenital amaurosis and juvenile retinitis pigmentosa patients by targeted next generation sequencing.* J Med Genet, 2013. **50**(10): p. 674-88.
544. Estrada-Cuzcano, A., et al., *IQCB1 mutations in patients with leber congenital amaurosis.* Invest Ophthalmol Vis Sci, 2011. **52**(2): p. 834-9.
545. Mohamed, M.D., et al., *Progression of phenotype in Leber's congenital amaurosis with a mutation at the LCA5 locus.* Br J Ophthalmol, 2003. **87**(4): p. 473-5.
546. Ahmad, A., et al., *Identification of a novel LCA5 mutation in a Pakistani family with Leber congenital amaurosis and cataracts.* Mol Vis, 2011. **17**: p. 1940-5.

547. den Hollander, A.I., et al., *Mutations in LCA5, encoding the ciliary protein lebercilin, cause Leber congenital amaurosis.* Nat Genet, 2007. **39**(7): p. 889-95.
548. Mackay, D.S., et al., *Screening of a large cohort of leber congenital amaurosis and retinitis pigmentosa patients identifies novel LCA5 mutations and new genotype-phenotype correlations.* Hum Mutat, 2013. **34**(11): p. 1537-1546.
549. Chen, Y., et al., *A novel LRAT mutation affecting splicing in a family with early onset retinitis pigmentosa.* Hum Genomics, 2018. **12**(1): p. 35.
550. Ullah, A., et al., *Novel sequence variants in the MKKS gene cause Bardet-Biedl syndrome with intra- and inter-familial variable phenotypes.* Congenit Anom (Kyoto), 2018. **58**(5): p. 173-175.
551. Denniston, A.K., et al., *Evaluation of visual function and needs in adult patients with bardet-biedl syndrome.* Retina, 2014. **34**(11): p. 2282-9.
552. Riazuddin, S., et al., *Mutation spectrum of MYO7A and evaluation of a novel nonsyndromic deafness DFNB2 allele with residual function.* Hum Mutat, 2008. **29**(4): p. 502-11.
553. Jiang, L., et al., *Comprehensive molecular diagnosis of 67 Chinese Usher syndrome probands: high rate of ethnicity specific mutations in Chinese USH patients.* Orphanet J Rare Dis, 2015. **10**: p. 110.
554. Wei, X., et al., *Next-generation sequencing identifies a novel compound heterozygous mutation in MYO7A in a Chinese patient with Usher Syndrome 1B.* Clin Chim Acta, 2012. **413**(23-24): p. 1866-71.
555. Roux, A.F., et al., *Four-year follow-up of diagnostic service in USH1 patients.* Invest Ophthalmol Vis Sci, 2011. **52**(7): p. 4063-71.
556. Bujakowska, K.M., et al., *Targeted exon sequencing in Usher syndrome type I.* Invest Ophthalmol Vis Sci, 2014. **55**(12): p. 8488-96.
557. Jaijo, T., et al., *Mutation profile of the MYO7A gene in Spanish patients with Usher syndrome type I.* Hum Mutat, 2006. **27**(3): p. 290-1.
558. Khalaileh, A., et al., *The Genetics of Usher Syndrome in the Israeli and Palestinian Populations.* Invest Ophthalmol Vis Sci, 2018. **59**(2): p. 1095-1104.
559. Zhai, W., et al., *Phenotype of Usher syndrome type II assosiated with compound missense mutations of c.721 C>T and c.1969 C>T in MYO7A in a Chinese Usher syndrome family.* Int J Ophthalmol, 2015. **8**(4): p. 670-4.
560. Bharadwaj, A.K., et al., *Evaluation of the myosin VIIA gene and visual function in patients with Usher syndrome type I.* Exp Eye Res, 2000. **71**(2): p. 173-81.
561. Le Guedard-Mereuze, S., et al., *Ex vivo splicing assays of mutations at noncanonical positions of splice sites in USHER genes.* Hum Mutat, 2010. **31**(3): p. 347-55.
562. Pennings, R.J., et al., *Evaluation of visual impairment in Usher syndrome 1b and Usher syndrome 2a.* Acta Ophthalmol Scand, 2004. **82**(2): p. 131-9.
563. Haider, N.B., et al., *Mutation of a nuclear receptor gene, NR2E3, causes enhanced S cone syndrome, a disorder of retinal cell fate.* Nat Genet, 2000. **24**(2): p. 127-31.
564. Murro, V., et al., *Novel clinical findings in autosomal recessive NR2E3-related retinal dystrophy.* Graefes Arch Clin Exp Ophthalmol, 2019. **257**(1): p. 9-22.

565. Falk, M.J., et al., *NMNAT1 mutations cause Leber congenital amaurosis.* Nat Genet, 2012. **44**(9): p. 1040-5.
566. Hedergott, A., et al., *Clinical and genetic findings in a family with NMNAT1-associated Leber congenital amaurosis: case report and review of the literature.* Graefes Arch Clin Exp Ophthalmol, 2015. **253**(12): p. 2239-46.
567. Koenekoop, R.K., et al., *Mutations in NMNAT1 cause Leber congenital amaurosis and identify a new disease pathway for retinal degeneration.* Nat Genet, 2012. **44**(9): p. 1035-9.
568. Ahmed, Z.M., et al., *Mutations of the protocadherin gene PCDH15 cause Usher syndrome type 1F.* American Journal of Human Genetics, 2001. **69**(1): p. 25-34.
569. Dryja, T.P., et al., *Frequency of mutations in the gene encoding the alpha subunit of rod cGMP-phosphodiesterase in autosomal recessive retinitis pigmentosa.* Invest Ophthalmol Vis Sci, 1999. **40**(8): p. 1859-65.
570. Riazuddin, S.A., et al., *Mutations in the gene encoding the alpha-subunit of rod phosphodiesterase in consanguineous Pakistani families.* Mol Vis, 2006. **12**: p. 1283-91.
571. Ali, S., et al., *Mutations in the beta-subunit of rod phosphodiesterase identified in consanguineous Pakistani families with autosomal recessive retinitis pigmentosa.* Mol Vis, 2011. **17**: p. 1373-80.
572. Valverde, D., et al., *Identification of a novel R552O mutation in exon 13 of the beta-subunit of rod phosphodiesterase gene in a Spanish family with autosomal recessive retinitis pigmentosa.* Hum Mutat, 1996. **8**(4): p. 393-4.
573. Pedurupillay, C.R., et al., *Segregation of Incomplete Achromatopsia and Alopecia Due to PDE6H and LPAR6 Variants in a Consanguineous Family from Pakistan.* Genes (Basel), 2016. **7**(8).
574. Langlo, C.S., et al., *Residual Foveal Cone Structure in CNGB3-Associated Achromatopsia.* Invest Ophthalmol Vis Sci, 2016. **57**(10): p. 3984-95.
575. Martin, C.A., et al., *Mutations in PLK4, encoding a master regulator of centriole biogenesis, cause microcephaly, growth failure and retinopathy.* Nat Genet, 2014. **46**(12): p. 1283-1292.
576. Fu, Q., et al., *Next-generation sequencing-based molecular diagnosis of a Chinese patient cohort with autosomal recessive retinitis pigmentosa.* Invest Ophthalmol Vis Sci, 2013. **54**(6): p. 4158-66.
577. Zhang, Q., et al., *Severe retinitis pigmentosa mapped to 4p15 and associated with a novel mutation in the PROM1 gene.* Hum Genet, 2007. **122**(3-4): p. 293-9.
578. Maranhao, B., et al., *exomeSuite: Whole exome sequence variant filtering tool for rapid identification of putative disease causing SNVs/indels.* Genomics, 2014. **103**(2-3): p. 169-76.
579. Sultan, N., et al., *A novel mutation in RDH5 gene causes retinitis pigmentosa in consanguineous Pakistani family.* Genes Genomics, 2018. **40**(5): p. 553-559.
580. Ajmal, M., et al., *Novel mutations in RDH5 cause fundus albipunctatus in two consanguineous Pakistani families.* Molecular Vision, 2012. **18**(157-61): p. 1558-1571.
581. Mackay, D.S., et al., *RDH12 retinopathy: novel mutations and phenotypic description.* Mol Vis, 2011. **17**: p. 2706-16.

582. Zou, X., et al., *Phenotypic Variability of Recessive Rdh12-Associated Retinal Dystrophy.* Retina, 2018.
583. Michaelides, M., et al., *Novel mutations and electrophysiologic findings in RGS9- and R9AP-associated retinal dysfunction (Bradyopsia).* Ophthalmology, 2010. **117**(1): p. 120-127 e1.
584. Naz, S., et al., *Mutations in RLBP1 associated with fundus albipunctatus in consanguineous Pakistani families.* British Journal of Ophthalmology, 2011. **95**(7): p. 1019-1024.
585. Kabir, F., et al., *Loss of function mutations in RP1 are responsible for retinitis pigmentosa in consanguineous familial cases.* Mol Vis, 2016. **22**: p. 610-25.
586. Khaliq, S., et al., *Novel association of RP1 gene mutations with autosomal recessive retinitis pigmentosa.* J Med Genet, 2005. **42**(5): p. 436-8.
587. Berson, E.L., et al., *Clinical features and mutations in patients with dominant retinitis pigmentosa-1 (RP1).* Invest Ophthalmol Vis Sci, 2001. **42**(10): p. 2217-24.
588. Freudenberg-Hua, Y., et al., *Disease variants in genomes of 44 centenarians.* Mol Genet Genomic Med, 2014. **2**(5): p. 438-50.
589. Abouelhoda, M., et al., *Revisiting the morbid genome of Mendelian disorders.* Genome Biol, 2016. **17**(1): p. 235.
590. Riazuddin, S.A., et al., *Autosomal recessive retinitis pigmentosa is associated with mutations in RP1 in three consanguineous Pakistani families.* Invest Ophthalmol Vis Sci, 2005. **46**(7): p. 2264-70.
591. Hameed, A., et al., *A new locus for autosomal recessive RP (RP29) mapping to chromosome 4q32-q34 in a Pakistani family.* Invest Ophthalmol Vis Sci, 2001. **42**(7): p. 1436-8.
592. Kabir, F., et al., *Novel mutations in RPE65 identified in consanguineous Pakistani families with retinal dystrophy.* Mol Vis, 2013. **19**: p. 1554-64.
593. Simovich, M.J., et al., *Four novel mutations in the RPE65 gene in patients with Leber congenital amaurosis.* Hum Mutat, 2001. **18**(2): p. 164.
594. Henderson, R.H., et al., *An assessment of the apex microarray technology in genotyping patients with Leber congenital amaurosis and early-onset severe retinal dystrophy.* Invest Ophthalmol Vis Sci, 2007. **48**(12): p. 5684-9.
595. Coppieters, F., et al., *Genetic screening of LCA in Belgium: predominance of CEP290 and identification of potential modifier alleles in AHI1 of CEP290-related phenotypes.* Hum Mutat, 2010. **31**(10): p. E1709-66.
596. Hull, S., et al., *Preserved visual function in retinal dystrophy due to hypomorphic RPE65 mutations.* Br J Ophthalmol, 2016. **100**(11): p. 1499-1505.
597. Gu, S.M., et al., *Mutations in RPE65 cause autosomal recessive childhood-onset severe retinal dystrophy.* Nat Genet, 1997. **17**(2): p. 194-7.
598. Kumaran, N., et al., *Severe Loss of Tritan Color Discrimination in RPE65 Associated Leber Congenital Amaurosis.* Invest Ophthalmol Vis Sci, 2018. **59**(1): p. 85-93.
599. Weleber, R.G., et al., *The phenotype of Severe Early Childhood Onset Retinal Dystrophy (SECORD) from mutation of RPE65 and differentiation*

from Leber congenital amaurosis. Invest Ophthalmol Vis Sci, 2011. **52**(1): p. 292-302.
600. Chung, D.C., et al., *The Natural History of Inherited Retinal Dystrophy Due to Biallelic Mutations in the RPE65 Gene.* Am J Ophthalmol, 2019. **199**: p. 58-70.
601. Hameed, A., et al., *Evidence of RPGRIP1 gene mutations associated with recessive cone-rod dystrophy.* J Med Genet, 2003. **40**(8): p. 616-9.
602. Neveling, K., et al., *A post-hoc comparison of the utility of sanger sequencing and exome sequencing for the diagnosis of heterogeneous diseases.* Hum Mutat, 2013. **34**(12): p. 1721-6.
603. Nakamura, M., et al., *Novel mutations in the arrestin gene and associated clinical features in Japanese patients with Oguchi's disease.* Ophthalmology, 2004. **111**(7): p. 1410-4.
604. Waheed, N.K., et al., *A nonsense mutation in S-antigen (p.Glu306*) causes Oguchi disease.* Mol Vis, 2012. **18**: p. 1253-9.
605. Riazuddin, S.A., et al., *A mutation in SLC24A1 implicated in autosomal-recessive congenital stationary night blindness.* Am J Hum Genet, 2010. **87**(4): p. 523-31.
606. Mackay, D.S., et al., *Screening of SPATA7 in patients with Leber congenital amaurosis and severe childhood-onset retinal dystrophy reveals disease-causing mutations.* Invest Ophthalmol Vis Sci, 2011. **52**(6): p. 3032-8.
607. Avila-Fernandez, A., et al., *Late onset retinitis pigmentosa.* Ophthalmology, 2011. **118**(12): p. 2523-4.
608. Wang, H., et al., *Mutations in SPATA7 cause Leber congenital amaurosis and juvenile retinitis pigmentosa.* Am J Hum Genet, 2009. **84**(3): p. 380-7.
609. Sang, L., et al., *Mapping the NPHP-JBTS-MKS protein network reveals ciliopathy disease genes and pathways.* Cell, 2011. **145**(4): p. 513-28.
610. Kang, H.G., et al., *Targeted exome sequencing resolves allelic and the genetic heterogeneity in the genetic diagnosis of nephronophthisis-related ciliopathy.* Exp Mol Med, 2016. **48**: p. e251.
611. Smith, U.M., et al., *The transmembrane protein meckelin (MKS3) is mutated in Meckel-Gruber syndrome and the wpk rat.* Nat Genet, 2006. **38**(2): p. 191-6.
612. Doherty, D., et al., *Mutations in 3 genes (MKS3, CC2D2A and RPGRIP1L) cause COACH syndrome (Joubert syndrome with congenital hepatic fibrosis).* J Med Genet, 2010. **47**(1): p. 8-21.
613. Zhang, M., et al., *A missense mutation in TMEM67 causes Meckel-Gruber syndrome type 3 (MKS3): a family from China.* Int J Clin Exp Pathol, 2015. **8**(5): p. 5379-86.
614. Lu, Y., et al., *Preimplantation genetic diagnosis for a Chinese family with autosomal recessive Meckel-Gruber syndrome type 3 (MKS3).* PLoS One, 2013. **8**(9): p. e73245.
615. Hopp, K., et al., *B9D1 is revealed as a novel Meckel syndrome (MKS) gene by targeted exon-enriched next-generation sequencing and deletion analysis.* Hum Mol Genet, 2011. **20**(13): p. 2524-34.
616. Wedatilake, Y., et al., *TRNT1 deficiency: clinical, biochemical and molecular genetic features.* Orphanet J Rare Dis, 2016. **11**(1): p. 90.
617. Riazuddin, S.A., et al., *A splice-site mutation in a retina-specific exon of BBS8 causes nonsyndromic retinitis pigmentosa.* Am J Hum Genet, 2010. **86**(5): p. 805-12.

618. Deveault, C., et al., *BBS genotype-phenotype assessment of a multiethnic patient cohort calls for a revision of the disease definition.* Hum Mutat, 2011. **32**(6): p. 610-9.
619. Janssen, S., et al., *Mutation analysis in Bardet-Biedl syndrome by DNA pooling and massively parallel resequencing in 105 individuals.* Hum Genet, 2011. **129**(1): p. 79-90.
620. Ajmal, M., et al., *Identification of recurrent and novel mutations in TULP1 in Pakistani families with early-onset retinitis pigmentosa.* Mol Vis, 2012. **18**: p. 1226-37.
621. Iqbal, M., et al., *Association of pathogenic mutations in TULP1 with retinitis pigmentosa in consanguineous Pakistani families.* Arch Ophthalmol, 2011. **129**(10): p. 1351-7.
622. Gu, S., et al., *Tubby-like protein-1 mutations in autosomal recessive retinitis pigmentosa.* Lancet, 1998. **351**(9109): p. 1103-4.
623. Ouyang, X.M., et al., *Characterization of Usher syndrome type I gene mutations in an Usher syndrome patient population.* Hum Genet, 2005. **116**(4): p. 292-9.
624. Bitner-Glindzicz, M., et al., *A recessive contiguous gene deletion causing infantile hyperinsulinism, enteropathy and deafness identifies the Usher type 1C gene.* Nat Genet, 2000. **26**(1): p. 56-60.
625. Bashir, R., A. Fatima, and S. Naz, *A frameshift mutation in SANS results in atypical Usher syndrome.* Clin Genet, 2010. **78**(6): p. 601-3.
626. Kalay, E., et al., *A novel D458V mutation in the SANS PDZ binding motif causes atypical Usher syndrome.* J Mol Med (Berl), 2005. **83**(12): p. 1025-32.
627. Ahmed, Z.M., et al., *USH1H, a novel locus for type I Usher syndrome, maps to chromosome 15q22-23.* Clin Genet, 2009. **75**(1): p. 86-91.
628. Jaworek, T.J., et al., *USH1K, a novel locus for type I Usher syndrome, maps to chromosome 10p11.21-q21.1.* J Hum Genet, 2012. **57**(10): p. 633-7.
629. Baux, D., et al., *Molecular and in silico analyses of the full-length isoform of usherin identify new pathogenic alleles in Usher type II patients.* Hum Mutat, 2007. **28**(8): p. 781-9.
630. Zhao, L., et al., *Next-generation sequencing-based molecular diagnosis of 82 retinitis pigmentosa probands from Northern Ireland.* Hum Genet, 2015. **134**(2): p. 217-30.
631. Huang, L., et al., *Mutation screening of the USH2A gene in retinitis pigmentosa and USHER patients in a Han Chinese population.* Eye (Lond), 2018. **32**(10): p. 1608-1614.
632. Kakar, N., et al., *Expanding the phenotype associated with biallelic WDR60 mutations: Siblings with retinal degeneration and polydactyly lacking other features of short rib thoracic dystrophies.* Am J Med Genet A, 2018. **176**(2): p. 438-442.